RÔMULO MARÇAL GANDIA

# EVALUATION OF PRESSURES IN SLENDER CYLINDRICAL SILOS: EXPERIMENTAL AND NUMERICAL STUDY

**LAVRAS - MG**
**2022**

RÔMULO MARÇAL GANDIA

# EVALUATION OF PRESSURES IN SLENDER CYLINDRICAL SILOS: EXPERIMENTAL AND NUMERICAL STUDY

Tese apresentada à Universidade Federal de Lavras, como parte das exigências do Programa de Pós-Graduação em Engenharia Agrícola, área de concentração em Construções e Ambiência, para a obtenção do título de Doutor.

Orientador
Dr. Francisco Carlos Gomes

Coorientador
Dr. Pedro José Aguado Rodriguez

**LAVRAS - MG**

**2022**

**Ficha catalográfica elaborada pelo Sistema de Geração de Ficha Catalográfica da Biblioteca Universitária da UFLA, com dados informados pelo(a) próprio(a) autor(a).**

Gandia, Rômulo Marçal.
Evaluation of pressures in slender cylindrical silos: experimental and numerical study / Rômulo Marçal Gandia. - 2022.
192 p. : il.

Orientador(a): Francisco Carlos Gomes.
Coorientador(a): Pedro José Aguado Rodriguez.
Tese (doutorado) - Universidade Federal de Lavras, 2022.
Bibliografia.

1. Silo pressures. 2. Flow pattern. 3. Finite Element Model. I. Gomes, Francisco Carlos. II. Rodriguez, Pedro José Aguado. III. Título.

RÔMULO MARÇAL GANDIA

# EVALUATION OF PRESSURES IN SLENDER CYLINDRICAL SILOS: EXPERIMENTAL AND NUMERICAL STUDY

# AVALIAÇÃO DE PRESSÕES EM SILOS CILÍNDRICOS ESBELTOS: ESTUDOS EXPERIMENTAIS E NUMÉRICO

Tese apresentada à Universidade Federal de Lavras, como parte das exigências do Programa de Pós-Graduação em Engenharia Agrícola, área de concentração em Construções e Ambiência, para a obtenção do título de Doutor.

APROVADA em 07 de março de 2022

| | |
|---|---|
| Dr. Francisco Carlos Gomes | Universidade Federal de Lavras |
| Dr. Pedro José Aguado Rodríguez | Universidad de León |
| Dr. Francisco Ayuga Telles | Universidad Politécnica de Madrid |
| Dr. Carlito Calil Junior | Universidade de São Paulo |
| Dr. José Wallace Barbosa do Nascimento | Universidade Federal de Campina Grande |
| Dr. Andrés Batista Cheung | Universidade Federal do Mato Grosso do Sul |

Dr. Francisco Carlos Gomes
Orientador

Dr. Pedro José Aguado Rodriguez
Coorientador

**LAVRAS - MG**
**2022**

*Dedico este trabalho à minha família, minha base, meu tudo.*
*Albany Lourenço Godoy Gandia, meu pai, que me **estrutura**,*
*Marta Lúcia Perujo Marçal Gandia, minha mãe, que me **ilumina**, e*
*Rodrigo Marçal Gandia, meu irmão a quem me **espelho**.*

**AGRADECIMENTOS**

Agradeço a Deus, presente em todos os momentos. Onipresente nos momentos mais difíceis.

Sobre ombro de Gigantes, a metáfora dos anões em latim: *nanos gigantum humeris incidentes*. Expressa o significado de "descobrir a verdade a partir das descobertas anteriores".

Agradeço meu professor, que hoje é um grande amigo, meu orientador, Dr. Francisco Carlos Gomes, que está comigo desde o início de minha trajetória acadêmica, que acreditou e me ensinou que era possível.

Ao meu professor, meu amigo, meu coorientador, Dr. Pedro José Aguado Rodriguez, a quem tive a sorte de cruzar minha trajetória acadêmica, que me ajudou na Espanha, que me ensinou e que tornou essa tese possível.

Ao professor Dr. José Wallace Barbosa do Nascimento pelos conselhos, pela parceria e pelos ensinamos. Ao professor Dr. Andrés Batista Cheung por me ajudar e ensinar. Ao professor Dr. Tadayuki Yanagi Junior por sempre lapidar meus trabalhos. Aos professores catedráticos Dr. Carlito Calil Junior e Dr. Francisco Ayuga Telles por serem a base teórica de minha tese. Ao professor e grande amigo Dr. Wisner Coimbra de Paula por estar comigo desde o início dessa jornada.

Aos meus grandes amigos que contribuíram diretamente nessa tese, meus braços direitos, a equipe de trabalho do Centro de Processamento e Pesquisa dos Produtos Armazenados, Estácio Antunes de Oliveira Júnior, Luiz Felipe Souza, Simone Mancini, Luiz Gustavo Cherfen e Ricardo Perdigão.

A todos que sempre estiveram comigo, meus amigos, meus parentes, meus professores. Todos que de alguma maneira serviram de guia, mentor e conselheiro em minha vida profissional e pessoal.

A Universidade Federal de Lavras, minha casa. A *Universidad de León*, minha segunda casa. Nessas casas, a todos que indiretamente fez ser possível, ao pessoal da limpeza, pessoal da vigilância, aos técnicos, aos servidores, ao pessoal da secretaria, meu muito obrigado.

Gostaria de reforçar meu muito obrigado ao professor Dr. Carlito Calil Junior por, literalmente possibilitar essa investigação, diante da doação da estação experimental, principal equipamento utilizado na pesquisa.

Por fim, reforço o maior agradecimento a meus pais pelo incentivo, por possibilitar, por acreditar, pelo carinho, pela dedicação e pelo sacrifício durante toda a minha vida na busca por conhecimento. A meu irmão por me incentivar e ser meu exemplo de vida.

O presente trabalho foi realizado com apoio da Coordenação de Aperfeiçoamento de Pessoal de Nível Superior – Brasil (CAPES).

**ABSTRACT**

The main objective of this work is to understand the actions, mainly the pressures on the walls, in slender silos. For this, slender cylindrical silos were studied experimentally and by numerical simulation. This thesis allowed the experimental validation of a slender silo model. Based on this model, analyzes were performed with different configurations to understand the static and dynamic pressures in slender silos. Thus, the articles, "Static and dynamic pressure measurements of maize grain in silos under different conditions", published in the scientific journal Biosystems Engineering 209 (2021) 180-199, "Evaluation of pressures in slender silos varying hopper angle and silo slenderness", published in the scientific journal Powder Technology 394 (2021) 478-495, "Experimental pressures exerted by maize in slender cylindrical silo: comparison with ISO 11697", published in the scientific journal Engenharia Agrícola 41 (2021) 576-590 correspond to the validation of the composite station by a pilot silo, a bucket elevator and a storage silo. The first article describes the complete instrumentation of the pilot silo, the subsequent calibration with water and the final validation using maize as a stored product. In addition, interesting findings were found due to the slenderness of the silo. The second article, continuing the first results of the investigation, evaluated the variables hopper angle and slender (height / diameter ratio). In this article, static and dynamic pressures were evaluated at all stages of the test. In addition, the types of flow were also evaluated, presenting unprecedented results. The third, continuing the experimental studies "Effect of the hopper angle of a silo on the vertical stress at the cylinder-to-hopper transition", published in the scientific journal Agronomy 12 (2022) 830-844, presents static and dynamic results of the vertical force in the silo/hopper transition, analyzing the different flows and different hopper angles using h/d = 3.6 ratio. The fourth article, continuing the first results of the investigation, evaluated the angle of the hopper. In this article, static and dynamic pressures were evaluated and compared with the ISO standard. The fifth article, "Influence of specific weight and wall friction coefficient on normal pressures in silos using the Finite Element Method", published in the scientific journal Engenharia na Agricultura-REVENG 29 (2021) 192-203 evaluates numerical simulation in silos, using finite elements models to evaluate the normal pressures on the wall with different simulations of specific weights and coefficient of friction with the wall, since these two variables have a direct influence on the silo flows and pressures. This article deals with an initial model, presenting the first validations of these parameters in slender cylindrical silos. The sixth, "The influence of flow pattern and hopper angle on static and dynamic pressures in slender silos", in process to be submitted to Powder Technology journal, presents static and dynamic results of horizontal and friction pressures, K coefficient, analyzes the maximum pressures, comparing with Eurocode 1, part 4, analyzing the types of flows and five different angles of hoppers using h/d 3.6 ratio. The installation used for the experimental tests is based on the model by Pieper and Schütz (1980), providing the basis for the DIN 1055-6 standard (DIN, 2005). The experimental station is modular and proved to be versatile, allowing numerous configuration possibilities due to its instrumentation and structural independence.

Keywords: Silo pressures; Free-flowing product; Concentric hopper; Flow pattern; Slender silo; Finite Element Model.

**RESUMO**

O objetivo principal deste trabalho é compreender as ações, principalmente as pressões nas paredes, em silos esbeltos cilíndricos. Para isso, esses silos foram estudados experimentalmente e por simulação numérica. Esta tese permitiu a validação experimental de um modelo de silo esbelto. Com base neste modelo, foram realizadas análises com diferentes configurações para entender as pressões estáticas e dinâmicas. Assim, os artigos, "Static and dynamic pressure measurements of maize grain in silos under different conditions", publicado na revista científica Biosystems Engineering 209 (2021) 180-199, "Evaluation of pressures in slender silos varying hopper angle and silo slenderness", publicado na revista científica Powder Technology 394 (2021) 478-495, "Experimental pressures exerted by maize in slender cylindrical silo: comparison with ISO 11697", publicado na revista científica Engenharia Agrícola 41 (2021) 576-590 correspondem à validação da estação composta por um silo piloto, um elevador de canecas e um silo de armazenamento. O primeiro artigo descreve a instrumentação completa do silo piloto, a posterior calibração com água e a validação final utilizando milho como produto armazenado. Além disso, foram encontradas descobertas interessantes devido à esbelteza do silo. O segundo artigo, dando continuidade aos primeiros resultados da investigação, avaliou as variáveis ângulo da tremonha e esbeltes (relação entre altura e diâmetro). Neste artigo, as pressões estáticas e dinâmicas foram avaliadas em todas as etapas do teste. Além disso, os tipos de fluxo também foram avaliados, apresentando resultados inéditos. O terceiro, dando continuidade aos estudos experimentais "Effect of the hopper angle of a silo on the vertical stress at the cylinder-to-hopper transition", publicado na revista Agronomy 12 (2022) 830-844 apresenta resultados estáticos e dinâmicos da força vertical na transição silo/tremonha, analisando os tipos de fluxos e diferentes ângulos de tremonhas utilizando relação h/d = 3,6. O quarto artigo, dando continuidade aos primeiros resultados da investigação, avaliou o ângulo da tremonha. Neste artigo, as pressões estáticas e dinâmicas foram avaliadas e comparadas com a norma ISO. O quinto artigo, "Influence of specific weight and wall friction coefficient on normal pressures in silos using the Finite Element Method", publicado na revista científica Engenharia na Agricultura-REVENG 29 (2021) 192-203 trata da simulação numérica em silos, utilizando modelos de elementos finitos para avaliar as pressões normais à parede com diferentes simulações de pesos específicos e coeficiente de atrito com a parede, uma vez que essas duas variáveis têm influência direta nas pressões do silo. Este artigo trata de um modelo inicial, apresentando as primeiras validações desses parâmetros em silos cilíndricos esbeltos. O sexto, "The influence of flow pattern and hopper angle on static and dynamic pressures in slender silos", em tramitação para ser submetido à revista Powder Technology apresenta resultados estáticos e dinâmicos das pressões horizontais e de atrito, coeficiente K, análise das pressões máximas, comparando com a Eurocode 1 parte 4, analisando os tipos de fluxos em cinco diferentes ângulos de tremonhas, utilizando relação h/d 3,6. Por fim, a instalação utilizada para os testes experimentais é baseada no modelo de Pieper e Schütz (1980), dando embasamento à norma DIN 1055-6 (DIN, 2005). A estação experimental é modular e mostrou-se versatilidade, permitindo inúmeras possibilidades de configurações devido sua instrumentação e independência estrutural.

Palavras-chave: Pressões em silo; Produto de fluxo livre; Tremonha concêntrica; Padrão de fluxo; Silo esbelto; Método dos Elementos Finitos.

**FIGURE LIST**

Figure 1 - Difference between liquids and solids in pressure distribution. ..... 20
Figure 2 - Elevated silo geometry and active pressures. ..... 21
Figure 3 - Jenike's shear cell. ..... 23
Figure 4 - Main types of flow. ..... 25
Figure 5 - Funnel flow, channels. ..... 26
Figure 6 - Mixed funnel flow. ..... 26
Figure 7 - Obtaining the type of flow. ..... 27
Figure 8 - Arcing at hopper outlet. ..... 28
Figure 9 - Hopper geometry. ..... 30
Figure 10 - Flow classification diagram ..... 31
Figure 11 – Distribution of pressures in the silo. ..... 32
Figure 12 – Stress field in silos (mass flow). ..... 33
Figure 13 - Medium-sized, full-scale silo. ..... 35
Figure 14 - Medium-sized, full-scale silo. ..... 36
Figure 15 – Geometry and location of the pressure cells of the metallic prismatic test silo. ..... 37
Figure 16 - ETSIA/Spain experimental station. ..... 38
Figure 17 – Representation of the arrangement of pressure cells along the silo. ..... 39
Figure 18 - Conical hopper inclination as a function of flow pattern. ..... 41
Figure 19 – Wedge hopper slope as a function of flow pattern. ..... 42
Figure 20 - Loads in the hopper. ..... 43
Figure 21 – Additional load. ..... 45
Figure 22 - Representation of the limit eccentricity of silos. ..... 46
Figure 23 - Filling pressures in hoppers. ..... 47
Figure 24 - Discharge pressures in hoppers. ..... 49
Figure 25 – Alternative way of decomposing pressures. ..... 51
Figure 26 – Horizontal pressures in concentric (a) and eccentric (b) hoppers according to FEM and some existing standards. ..... 54
Figure 27 – Normal pressures to the walls of a silo with centered hopper (a), 60% eccentric hopper (b) and 100% eccentric hopper (c), variation of the internal friction angle of the product ($ø_i$). ..... 55
Figure 28 – Comparison of normal pressures on the silo wall for filling (a) and discharge (b). ..... 56

**TABLE LIST**

Table 1 – Classification of silos in terms of slenderness..... 19
Table 2 - Characterization of stored products related to the flow function (FF)..... 29

# SUMMARY

**FIRST PART** ..... **13**
**General Summary** ..... **13**
**1. INTRODUCTION** ..... **15**
**2. THEORETICAL REFERENCE** ..... **18**
2.1. Silos ..... 18
2.3. Stored product properties ..... 22
2.4. Flow pattern ..... 24
2.5. Hoppers ..... 29
2.6. Pressures on the walls and bottom of slender silos ..... 31
2.7. Pressure measurements in silos ..... 33
2.8. International standards for silo design ..... 40
2.8.1. *International Organization for Standardization* - ISO 11697 (2012) ..... 41
2.8.2. *European Committee of Standardization* - EN 1991-4 (2006) ..... 47
2.9. Finite Element Method in silos ..... 53
**3. GENERAL CONSIDERATIONS** ..... **58**
**REFERENCES** ..... **59**
**SECOND PART** ..... **66**
**Article 1 – Static and dynamic pressure measurements of maize grain in silos under different conditions - Biosystems Engineering journal (published version)** ..... **66**
**Article 2 – Evaluation of pressures in slender silos varying hopper angle and silo slenderness - Powder Technology journal (published version)** ..... **87**
**Article 3 – Effect of the hopper angle of a silo on the vertical stress at the cylinder-to-hopper transition - Agronomy journal (published version)** ..... **106**
**Article 4 – Experimental pressures exerted by maize in slender cylindrical silo: comparison with ISO 11697 - Engenharia Agrícola journal (published version)** ..... **121**
**Article 5 – Influence of specific weight and wall friction coefficient on normal pressures in silos using the Finite Element Method - Engenharia na Agricultura journal (published version)** ..... **137**
**Article 6 – The influence of flow pattern and hopper angle on static and dynamic pressures in slender silos - Powder Technology journal (preliminary version)** ..... **150**
**Final considerations** ..... **190**
**Future research** ..... **191**
**Team of researchers** ..... **192**

# FIRST PART

## General Summary

The main objective of this work is to understand the actions, mainly the pressures on the walls, in slender cylindrical silos. For this, such silos were studied experimentally and by numerical simulation. This thesis allowed the validation of the proposed experimental station. Based on this model, analyse were performed with different configurations to understand the actions, static and dynamic pressures and flows in slender cylindrical silos.

Thus, the article, “Static and dynamic pressure measurements of maize grain in silos under different conditions”, published in the scientific journal Biosystems Engineering 209 (2021) 180-199, corresponds to the validation of the station consisting of a pilot silo, a bucket elevator, and a storage silo.

The first article describes the complete instrumentation of the pilot silo, the subsequent calibration with water and the final validation using maize as a stored product. In addition, interesting findings were found due to the slenderness of the silo.

The second article, “Evaluation of pressures in slender silos varying hopper angle and silo slenderness”, published in the scientific journal Powder Technology 394 (2021) 478-495, continuing the first research results, evaluated the hopper angle and slender variables (relation between height and diameter). In this article, static and dynamic pressures were evaluated at all stages during the tests. In addition, the types of flow were also evaluated, presenting results.

The third article, “Effect of the hopper angle of a silo on the vertical stress at the cylinder-to-hopper transition”, published in the scientific journal Agronomy 12 (2022) 830-844, presents static and dynamic experimental results of the vertical force in the silo/hopper transition, analyzing the types of flows and different angles of hoppers using h/d 3.6 ratio.

The fourth article, “Experimental pressures exerted by maize in slender cylindrical silo: comparison with ISO 11697”, published in the scientific journal Engenharia Agrícola 41 (2021) 576-590, continuing the experimental results of the investigation, evaluated the hopper angle. In this article, static and dynamic pressures were evaluated and compared with the ISO standard.

The fifth article, “Influence of specific weight and wall friction coefficient on normal pressures in silos using the Finite Element Method”, published in the scientific journal Engenharia na Agricultura-REVENG 29 (2021) 192-203 deals with numerical simulation in silos, using models of finite elements to evaluate the normal pressures to the wall with different simulations of specific weights and coefficient of friction with the wall, since these two variables have a direct influence on the silo pressures. This article deals with an initial model, presenting the first validations of these parameters in slender cylindrical silos.

The sixth article, “The influence of flow pattern and hopper angle on static and dynamic pressures in slender silos”, submitted to the scientific journal Powder Technology, presents static and dynamic experimental results of horizontal and frictional pressures, coefficient K, analyzes the maximum pressures, always comparing with Eurocode, analyzing the types of flows and five different angles of hoppers using h/d ratio 3.6.

The installation used for the experimental tests is based on the model by Pieper and Schütz (1980), providing the basis for the DIN 1055-6 standard (DIN, 2005). The experimental station is modular and proved to be versatile, allowing numerous configuretion possibilities due to its instrumentation and structural independence.

# 1. INTRODUCTION

Brazil is a continental country with a climate and topography suitable for agricultural production. Therefore, the agricultural sector in Brazil grows considerably. The estimated grain production for the 2021/2022 harvest is 284.4 million tons (CONAB - COMPANHIA NACIONAL DE ABASTECIMENTO, 2022). Of this total, 87 million tons (25%) correspond to corn. Motivated by the future market, stock control, logistics or cooperatives, most agricultural products are stored. In 1980, the Brazilian storage capacity was 40.45 million tons of grain. In less than 4 decades (2019), Brazil has more than quadrupled its static capacity (177.7 million tons of grains), with 86.6 million (49%) being in silos (DPE - DIRETORIA DE PESQUISA E COORDENAÇÃO AGROPECUÁRIA, 2019). In addition, corn is also a leading product in the international market, for example, in Spain, with a production of 4.1 million tons (MINISTÉRIO DA AGRICULTURA PESCA Y ALIMENTACIÓN, 2020), with León being the Spanish province with the highest production. , 0.9 million (AGRICULTURA Y GANADERIA DE CASTILLA Y LEÓN, 2020).

However, despite the aforementioned data, Brazil still does not have its own standard for silo design. Currently, there is a study commission to discuss and enable the creation of the Brazilian standard (CE-203:020.001 – *Comissão de Estudo de Máquinas e Equipamentos para Sistemas de Armazenagem e Beneficiamento de Grãos Vegetais*). The importance of a proper standard becomes important for the calculations and structures, however, in addition, it is about the history of particularities of the properties of the products stored in the country and the properties of the constructive materials of the silo, in addition to cultural and operational factors in the storage, weather conditions, financial condition and quality of life index.

The study of the behavior of products stored in silos dates back to 1895 by Janssen (JANSSEN, 1895). Since then, other theories have been developed (WALKER, 1967) (WALTERS, 1973a, 1973b) (JENIKE; JOHANSON; CARSON, 1973a) supporting international standards (CEN, 2006; DIN, 2005). JENIKE (1964) developed an internationally known apparatus capable of determining the flow properties of stored products (Jenike Shear Tester), later improved by a group (Working Party on the Mechanics of Particulate Solids) of the European Federal of Chemical Engineers, renamed for “Standart Shear Testing Technique for Particulate Solids Using the Jenike

Shear Cell" (WPMPS, 1989). This device, in addition to supporting international standards, is capable of obtaining reliable parameters for calculating projects in silos.

In view of several studies reporting failures and collapses in silos (AYUGA, 2008; BYWALSKI; KAMIŃSKI, 2019; GUTIÉRREZ et al., 2015; CALIL; PALMA; CHEUNG, 2009; DOGANGUN et al., 2009; SUN; MORÁN et al., 2006; WANG, 2012; TENG; ZHAO; LAM, 2001; TENG, 1994; TENG; ROTTER, 1989, 1991), notes that the main causes refer to design errors; on pressures (normal and friction, on the wall and in the hopper) of the product stored in the structure; excess moisture in the stored product (causing unexpected pressure behaviors); product discharge step (maximum pressures in the silo, generally in the silo-hopper transition); discharge eccentricity; temperature variation in the product due to silo location and imperfections in the structural material.

The pilot scale test station proposed by Pieper and Schütz in 1980 (PIEPER; SCHÜTZ, 1980) supported DIN 1055-6: Basis of design and actions on structures – Part 6 (DIN, 2005) allows obtaining numerous variables that directly influence in the behavior of pressures in the silo (SONG; TENG, 2003; ZEGZULKA, 2013), being: use of any product as long as the maximum diameter of the product is less than 1.7 centimeters (to be allowed proportional values to the real scale) (BROWN; NIELSEN, 1998; PIEPER; SCHÜTZ, 1980); three walls with different roughness (varying the coefficient of friction between the product and the wall); twelve height/diameter ratios; 8 bottoms (1 flat bottom, 4 concentric hoppers (β: 60 to 15°) and three 100% eccentric hoppers with (β: 45 to 15°) and other possible test procedure variables. The test station was developed and studied at the University of São Paulo (CALIL; CHEUNG, 2007; CHEUNG, 2007) later, in partnership, the test station was studied at the Federal University of Lavras (GANDIA et al., 2021a).

The experimental model of real-scale silos provides proximity to real values, enabling confidence in the data and making it possible to understand the pressures in the silos. In the world, the number of full-scale experimental silo stations for investigating pressures is relatively small (BROWN; LAHLOUH; ROTTER, 2000; COUTO; RUIZ; AGUADO, 2012; GANDIA et al., 2021a; HÄRTL et al., 2008; RAMÍREZ; NIELSEN; AYUGA, 2010a; SCHURICHT; FURLL; EENSTAD, 2001; SCHWAB et al., 1994; SUN et al., 2020; TENG; LIN, 2005; TENG; ZHAO; LAM, 2001; ZHAO; TENG, 2004; ZHONG; OOI; ROTTER, 2001) due to the cost of construction, instrumentation and operations. In addition, the scale factor is extremely important for confidence in the

data (BROWN; NIELSEN, 1998). Furthermore, the study of experimental pressures in silo allows the advancement of numerical studies as a form of validation and comparisons in order to make the models reliable.

It can be said that due to the advancement of engineering combined with computational development today, engineering is supported by a tripod: theoretical model, experimental model and numerical model. These three models, not isolated, but in consortium, improve and advance studies in any area of engineering. Therefore, in recent years, investigations using the finite element method (FEM) in silos have increased significantly (JOFRIET, 1992; HOLST et al., 1999; AYUGA et al., 2006; GALLEGO et al., 2010; GALLEGO; RUIZ; AGUADO, 2015; PARDIKAR; ZAHID; RHEE et al., 2020; WASSGREN, 2020; ZHAO; GANDIA et al., 2021b), mainly due to the quality of the responses and the relative reduction in time and cost compared to full-scale experimental models . However, the numerical study needs to be validated with theories and experimental analyses.

Therefore, this work aims to advance in the scientific area relating pressures, flow, slender and angles of the hoppers using free flow stored product evaluated experimentally (real scale). In addition, a computational study was started using the Finite Element Method (FEM) to optimize the responses, allowing for a deeper understanding of the theory.

# 2. THEORETICAL REFERENCE

As with any area of study, we are supported on the shoulders of giants, so the investigation in silos, evaluating the behavior of the stored product, dates back to 1895 (JANSSEN, 1895). After that, the interest and need in the search for answers increased (AYUGA, 2008; AYUGA et al., 2001; BUTTERFIELD, 1969; CALIL; CHEUNG, 2007; DE PAULA et al., 2020; DEUTSH; SCHMIDT, 1985; FANK et al., 2018; GALLEGO; RUIZ; AGUADO, 2015; GOMES; CALIL, 2005; GONZÁLEZ-MONTELLANO et al., 2011; JA. B LVIN, 1971; JENIKE, 1964; NASCIMENTO; LOPES NETO; MONTROSS, 2013; RUIZ; COUTO; AGUADO, 2012; SADOWSKI; MICHAEL ROTTER; NIELSEN, 2020; WALKER, 1967; WENZEL, 1973).

## 2.1. Silos

The word silo originates from the Greek “sirus” (dark cavernous place). Currently, the use of the silo has several advantages in the storage of products such as: space (area), labor and transport cost savings, as well as the possibility of conservation of the stored product.

Silos can be divided into categories according to their structural material, their position in relation to the ground and geometric shape (CALIL; CHEUNG, 2007).

The silo geometry is a parameter for the classification of silos, being mainly influenced by the slenderness, directly interfering in the behavior of pressures due to the stored product (GANDIA et al., 2021c), being its relation between height of cylinder (H) and diameter (D) considered for such, as shown in Table 1 (CALIL; CHEUNG, 2007).

Table 1 – Classification of silos in terms of slenderness.

| Standards | Low silos | Medium slender silos | Slender silos |
|---|---|---|---|
| Australian (AS 3774:1996) | H/D <1,0 | 1,0≤ H/D ≤ 3,0 | H/D > 3,0 |
| European (EN 1991-4:2006) (DIN 1055-06:2005) | 0,4≤ H/D ≤ 1,0 | 1,0≤ H/D ≤ 2,0 | H/D ≥ 2,0 |
| International (ISO 11697:2012) | H/D <1,0 | 1,0≤ H/D ≤ 1,5 | H/D > 1,5 |

H is the height of the silo,
D is the silo diameter.

Source: Adapted from Calil and Cheung (CALIL; CHEUNG, 2007).

Still referring to the aforementioned authors, the first tall silos were built from 1870 onwards, a time when calculators believed that stored products behaved like liquids, designing the structures to resist pressures equivalent to hydrostatics.

According to Roberts (1884 apud PALMA, 2005), after carrying out tests on small-scale models, he found that grains differed in their behavior in relation to liquids. In their observations, it was found that the vertical pressures on the silo walls increased linearly with height up to a certain point, after which the behavior changed and was no longer proportional to height.

In this way, the aforementioned author concluded that a portion of the weight of the stored product was transferred to the walls through product-wall friction. Thus, the pressures on the bottom and walls, in the lowest part of a silo, are lower than those exerted by a liquid (Figure 1).

Figure 1 - Difference between liquids and solids in pressure distribution.

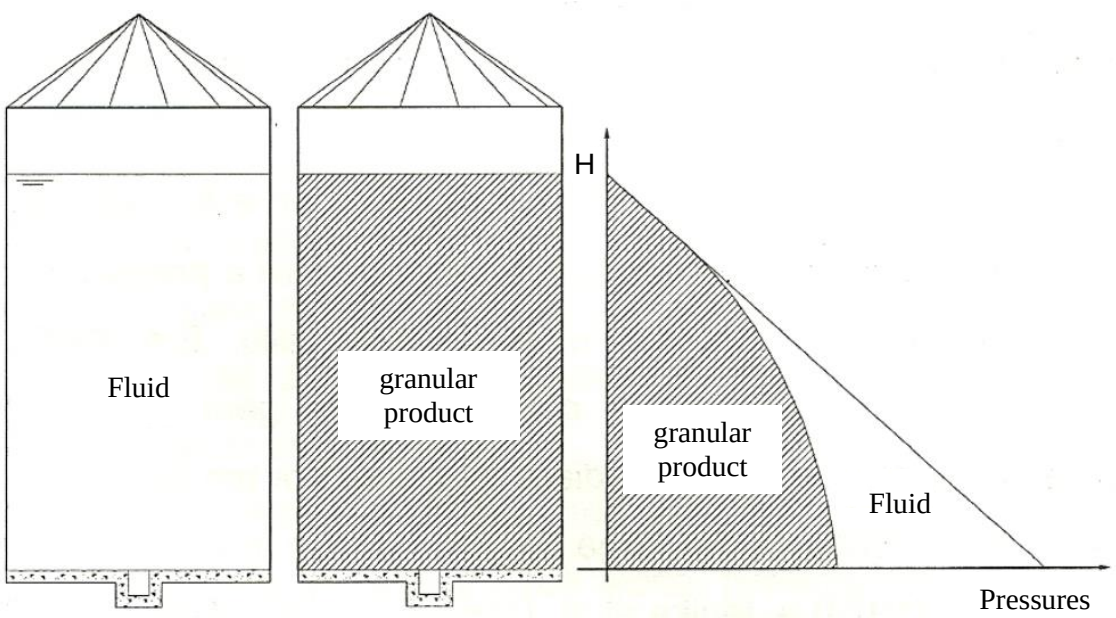


Source: CALIL; CHEUNG (2007).

Janssen (1895) pioneered the establishment of a theory for calculating the pressures occurring in silos. His study was based on square wooden silo in which, through the analysis of an infinitesimal part of the stored product, pressures were obtained via balance of forces. However, this study considered the condition of static filling and, it is known today, that in conditions of filling and discharge of the silo, higher pressures occur.

As with other constructions, the structural analysis of a silo takes place considering the active actions, which can be classified as permanent, variable and exceptional.

The permanent actions acting on the silo are its own weight and the weight of the fixed equipment that is supported on the silo. The variable loads are constituted by the stored products, structural elements that present vibration and that are fixed in the silo (such as conveyor belts, for example), wind forces, etc. Vehicle impacts and internal gas explosions in the silos are already exceptional actions.

Therefore, in a full silo, the main pressures to be considered are those from the stored products, which are illustrated in Figure 2, in filling, storage and discharge situations, defined by:

- Horizontal pressure in the silo cylinder ($p_h$);
- Vertical pressure ($p_v$);
- Friction pressure of the product with the silo cylinder wall ($p_w$);
- Friction pressure of the product with the hopper wall ($p_t$);
- Normal pressure to the hopper wall ($p_n$).

Figure 2 - Elevated silo geometry and active pressures.

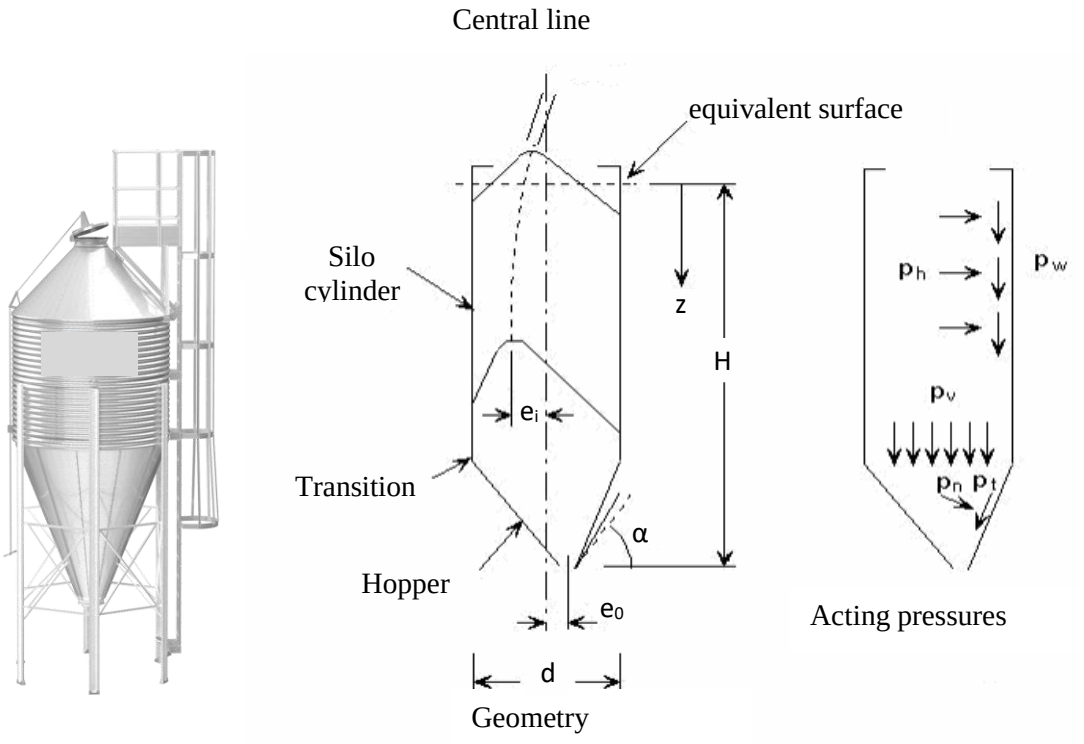


That means:

α = angle of the hopper with the horizontal;

$e_0$ = eccentricity of the discharge outlet;

$e_i$ = maximum eccentricity of filling at the top of the surface;

z = ordinate based on equivalent surface;

H = effective silo height;

d = silo diameter.

Source: Adapted from Palma (2005).

During filling and storage (prior to the start of discharge), the granular product is subjected to a state of stress called the active state. This is identified by presenting the maximum main stress in the vertical direction, coincident with the silo axis, and the

minimum stress in the horizontal direction. From the moment the silo product is discharged, this stress configuration changes, since the highest principal stress starts to act in the horizontal direction and the lowest principal stress, in the vertical direction. This situation is named the passive stress state and is characterized by vertical expansion of the product and horizontal compression (plastic deformation).

## 2.3. Stored product properties

As stated, the characteristics of granular and powdery products are different from liquids, making the design of silos more complex in relation to continuous flows and as economic and safe structures and, for this to occur, it is essential that loads are not underestimated or overrated.

During the processing of products stored in silos with gravity discharge, it is essential that the filling and discharge of the silos occur in an effective and efficient way, requiring knowledge of the relevant physical and flow properties of the stored products (MILANI, 1993).

For the safety and economy of a structure, it is important that loads are not specified as greater than strictly necessary. The safety of the structure can only be determined by the knowledge of the possible types and modes of collapses that may occur in it. The discharge characteristics of the stored material, the type of segregation, the formation of dead zones, the complete discharge of the silo, the pressure distributions on the walls and foundations, the integrity and the cost of the construction can be determined, directly or indirectly, by the type of flow (mass, funnel or transition). Therefore, the way the stored material will flow in the discharge must be determined while the silo is being designed and/or when changes in its structures are foreseen (CALIL, 1990).

The first step in the design of flow and structures of vertical silos is the determination of the physical properties of stored products, using the most severe conditions that can occur in the silo (CALIL; NASCIMENTO; ARAUJO, 1997).

The physical properties of stored products are important for calculation and estimation in stored systems in the filling and discharge stages. During filling, compaction and segregation can occur and, in discharge, the formation of stable vaults over the discharge outlet can occur, causing serious flow problems and structural problems in the installation. The subsequent fall of these vaults gives rise to very high

pressures on the walls of the silos and hoppers. On the other hand, the formation of the discharge duct, when the funnel flow occurs, causes serious segregation and damages in the mechanical elements of discharge (RAVENET, 1983).

Regarding the determination of physical and flow properties of bulk stored products, Jenike (1964) developed a study proposing the use of a direct shear device, suitable for stored products, called “Jenike Shear Cell” or Jenike shear cell (Figure 3a), currently used (DESHMUKH et al., 2019; LOPES NETO; NASCIMENTO; FANK, 2014; SALEHI et al., 2020).

In the aforementioned device, the product sample is subjected to shear, sliding over a plate (of the same material and geometry of the silo), under specific conditions, obtaining the friction angles.

Figure 3 - Jenike's shear cell.

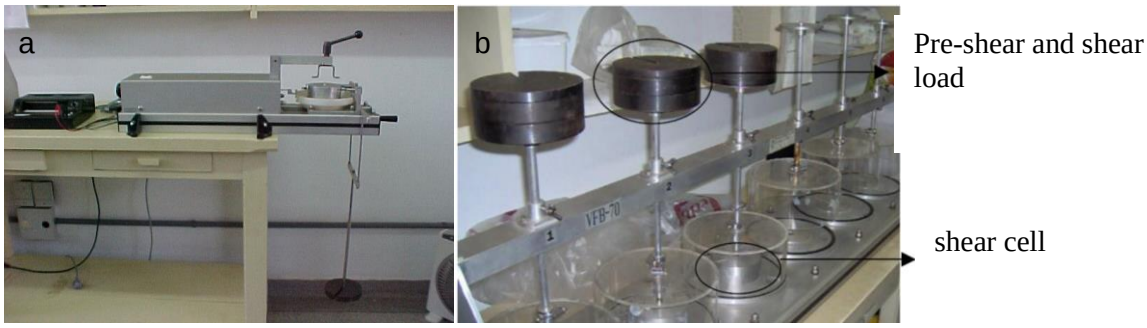


Source: Teixeira and Gomes (2003).

With the parameters determined, it is possible to calculate and predict the pressures in the silo, as well as the flow. The estimation of the consolidation effect is another parameter that can be reproduced in the Jenike shear cell, estimating the storage conditions with time. To determine the effect of the consolidation time of stored products, a consolidation bench associated with the shear device is used (Figure 3b).

The cells of the shear apparatus remain for a predetermined time, under the action of a static vertical force, supported by a hanging weight with loads. During consolidation, the cells are placed inside an airtight box that preserves the moisture contained in the sample under analysis.

The influence of the compressibility of solids stored in silos occurs in most granular and powdery products, making it difficult to obtain the design parameters.

Therefore, compressibility, which by many calculation methods is not considered, must be evaluated for projects in silos.

The physical properties of the stored products must be known or determined to carry out a project, for this, the method and equipment developed by Jenike (SCHWEDES, 1983) makes this determination possible. Therefore, the main measurable properties of granular and powdery products are (GAYLORD; GAYLORD, 1984):

- angle of repose
- internal friction angle ($\varphi_i$)
- effective angle of internal friction ($\varphi_e$)
- angle and coefficient of friction with the wall ($\varphi_w$)
- specific weight depending on the state of consolidation
- material moisture ($\chi$)
- granulometry.

## 2.4. Flow pattern

The behavior of pressures in a silo is influenced by the flow pattern, and the two parameters that directly influence it are the hopper angle and the friction angle between the material and the hopper wall. There are two possible flow patterns, mass flow and funnel flow. (CEN, 2006), directly influencing the magnitude and distribution of forces acting on the silo (JENIKE; JOHANSON; CARSON, 1973a).

Mass flow is characterized by the movement of all stored material at the same speed, a flow pattern that is usually achieved in silos with smooth-walled hoppers, where flowing material generates high dynamic pressures on the walls (particularly in the silo/hopper transition ). Hopper flow is characterized by a first-in-last out sequence with areas of static material, reducing silo capacity. This pattern is suitable for free-flowing materials. Wall pressures during discharge are slightly higher than during filling (WÓJCIK; TEJCHMAN; ENSTAD, 2012).

A third flow pattern, transition flow, is characterized by a distinct change in flow at a position that depends on the filling height (BENINK, 1989). It is possible to predict the flow pattern in bulk solids, where the hopper angle and the hopper wall friction angle are the two most influential parameters (CEN, 2006; INTERNACIONAL ORGANIZATION FOR STANDARDIZATION, 2012; JENIKE, 1964). However, flow

pressure is still poorly understood (CHEN et al., 2007; COUTO; RUIZ; AGUADO, 2013; NIELSEN, 1998; SADOWSKI; ROTTER, 2012).

The discharge of the material by gravity can occur as shown in the Figure 4.

Figure 4 - Main types of flow.

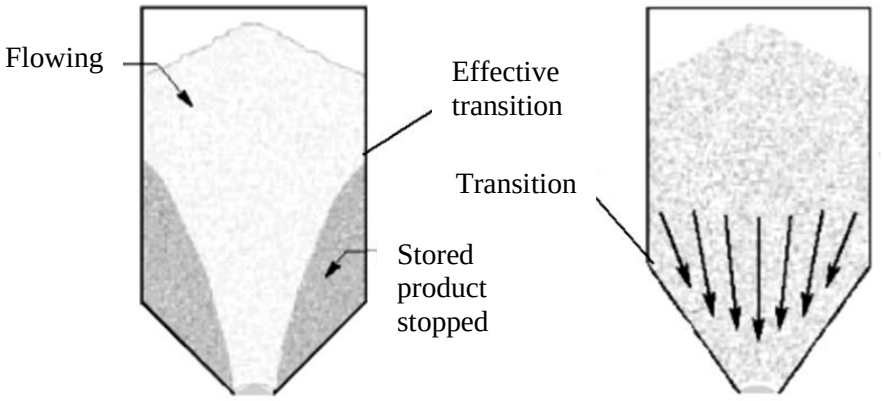


Source:Palma (2005).

The type of flow that will occur will depend on the physical properties of the product, as well as the geometry and roughness of the hopper surface.

The funnel flow is characterized by the formation of a flow channel, aligned with the discharge outlet, surrounded by a zone in which the product remains static, while the mass flow is characterized by the movement of all particles of the stored product. during the discharge operation.

According to (CALIL, 1990), the type of flow characterizes the discharge of the product, the type of segregation, the formation of product zones without movement and the possible total emptying. It also determines the distribution of pressures on the silo walls and foundation and the integrity and cost of the construction.

The formation of the discharge channels causes a decrease in pressures on the side walls due to the stagnant zone. However, in the effective transition region there is a marked increase in these pressures (region where the flow channel meets the silo wall).

Various patterns of flow channels can form, depending on the type of product stored, hopper geometry and placement, among other factors (Figure 5).

There are also situations in which the flow pattern in the silo is undetermined, and mass and funnel flow may occur partially, as shown in Figure 6.

Figure 5 - Funnel flow, channels.

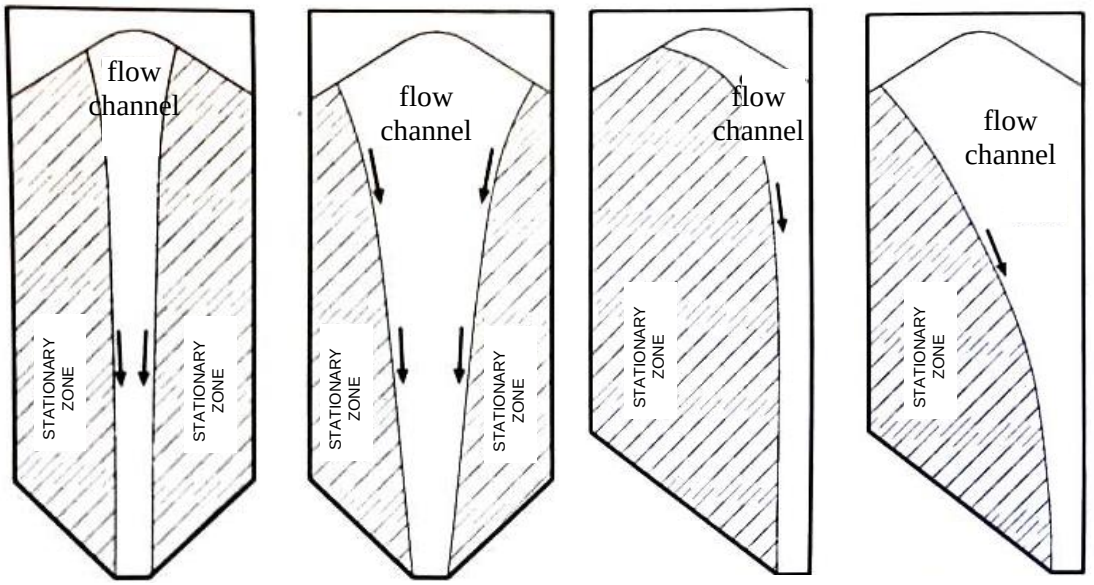


Concentric Parallel Internal | concentric inclined internal | Eccentric parallel internal | Interno inclinado excêntrico

Source: Calil and Cheung (2007).

Figure 6 - Mixed funnel flow.

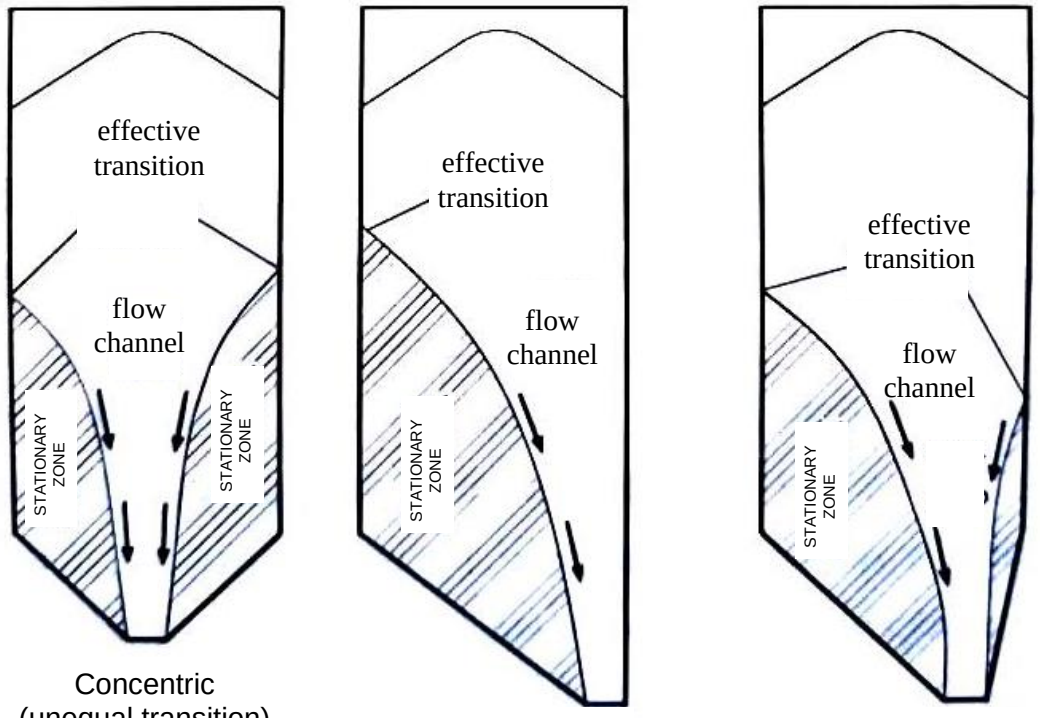


Concentric (unequal transition) | completely eccentric | partially eccentric

Source:Calil and Cheung (2007).

To determine the type of flow, the European international standard (CEN, 2006) determines through graphs that involve some variables (Figure 7). The graphs predict the type of flow as a function of the angle of the hopper or the coefficient of friction of the stored product with the wall, the slope of the hopper walls and their geometry (generally conical or pyramidal, concentric).

Figure 7 - Obtaining the type of flow.

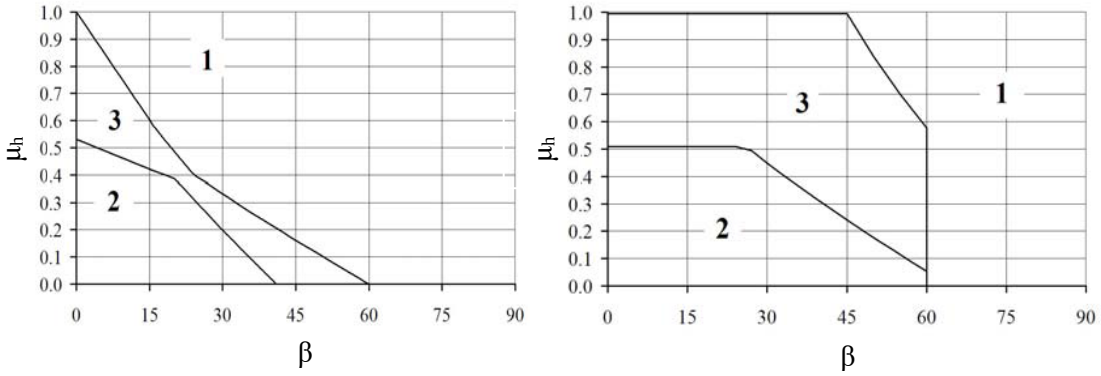


a) conical hopper b) wedge hopper

Where:
1 = Funnel Flow;
2 = Mass flow;
3 = Mass flow or funnel;
$\beta$ = Hopper inclination angle;
$\mu_h$ = Friction coefficient.

Source:Adaptado from EN 1991-4 (2006).

The ideal for a silo design is to ensure that the stored product will flow by gravity without obstructions to the flow. However, flow obstruction can occur and the two main types of obstruction are the cohesive mechanical arch, represented in Figure 8.

Figure 8 - Arcing at hopper outlet.

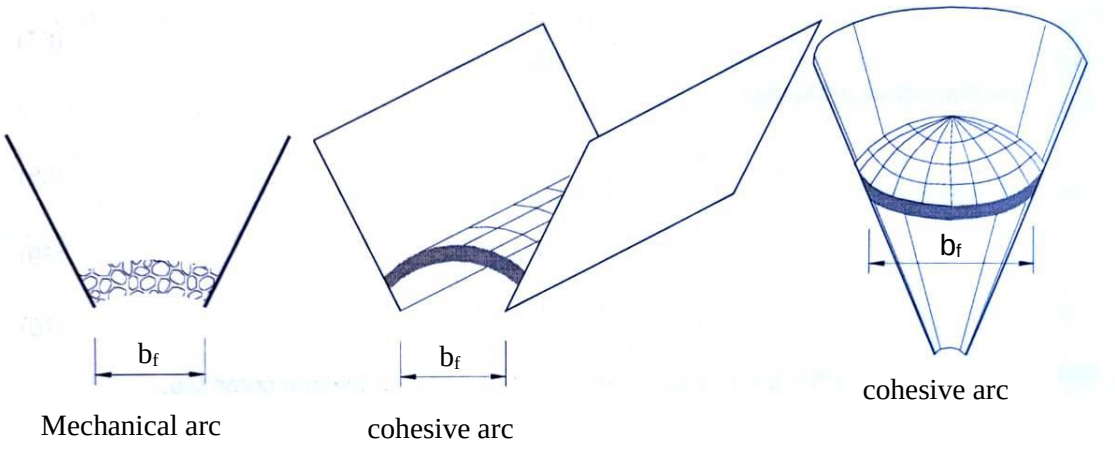


Source: Calil and Cheung (2007).

It is noted that the cohesive arc is formed due to the consolidation and resistance of the product stored by the influence of the cohesion of the product itself. The cohesive arc is distinguished from the mechanical arc because the meshing of solid particles occurs when the average particle size is large compared to the hopper outlet opening.

For the formation of a stable arc or channel, the stored product must acquire, within the contour of the storage cell, sufficient strength to support it. Resistance is a function of the degree of consolidation, as a "fluffy" solid has no resistance, but acquires it under compression (GOMES; CALIL, 2005).

The flow function (FF; dimensionless) is used to estimate the ability of solids to flow by gravity and is defined as the relationship between the principal consolidation stress ($\sigma_1$) versus the inconfined failure stress ($\sigma_{ic}$), shown in Equation 1, being an important property of the stored product for the evaluation of its flow capacity, since it describes its consolidation behavior.

$$FF = \frac{\sigma_1}{\sigma_{ic}} \tag{1}$$

The flow function is directly influenced by the storage time. However, the humidity and temperature of the solid interfere in the degree of consolidation and in the resistance of the flow function.

From the limits of the flow function (FF), evaluated according to Table 2, it is possible to characterize the flow using these índices (JENIKE, 1964).

Table 2 - Characterization of stored products related to the flow function (FF).

| FF limits | Characterization |
|---|---|
| FF < 2 | Cohesive |
| 2 < FF < 4 | Cohesive |
| 4 < FF < 10 | Easy flow |
| 10 < FF | Free flow |

Source: Adapted from Jenike (1964).

## 2.5. Hoppers

The hopper geometry (angle and size of the outlet opening) and the type of product stored (contact surface, roughness) used in the construction of the silo hopper define the type of flow, allowing to evaluate the behavior of the product inside the silo. Therefore, according to the characteristics of the products, various types of hoppers are used and chosen.

Figure 9 presents the main geometries that are used in vertical and horizontal silos (CALIL; CHEUNG, 2007).

Figure 9 - Hopper geometry.

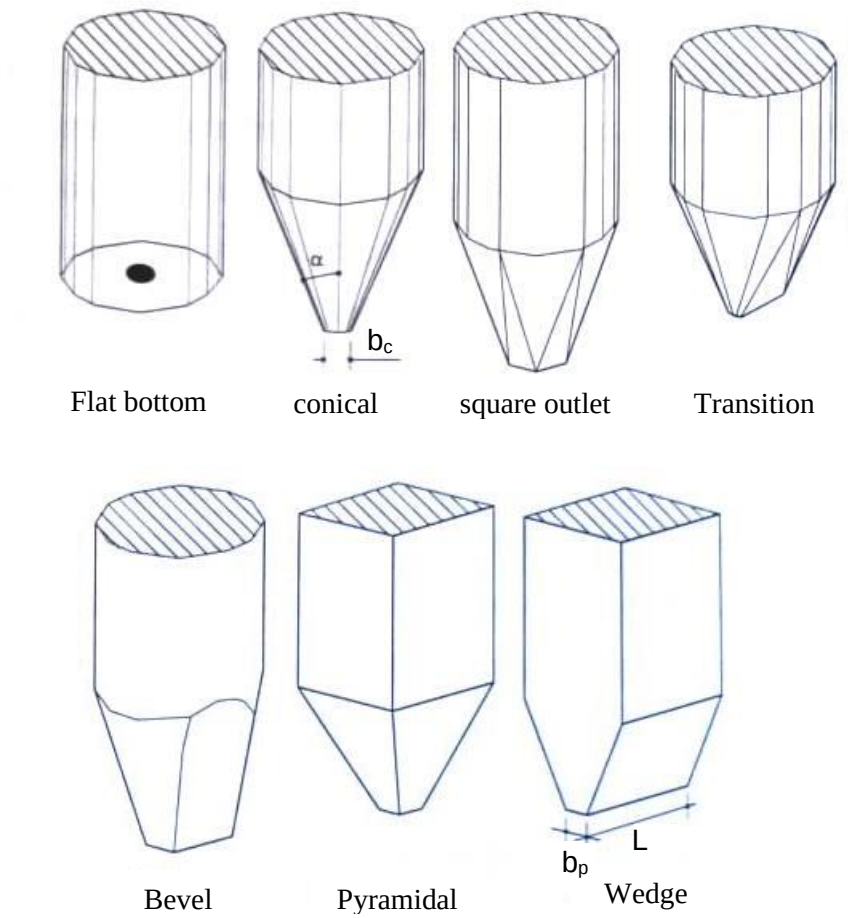


Source:Calil and Cheung (2007).

The prediction of the type of flow based on the friction angle of the product with the silo wall ($ø_w$) and on the internal friction angle of the stored product ($ø_e$) to define the hopper angle (α) has been a matter of investigation.

The definition of the angle of the wedge and conical hopper (Figure 10) was presented in diagrams by (Jenike (1964). Therefore, these diagrams allow the dimensioning of the structure, allowing the predictability of the type of flow (SCHULZE, 1996). Even so, as mentioned above, the rules based on the slope of the hopper also allow the prediction of the type of flow (ANSI - AMERICAN SOCIETY OF AGRICULTURAL AND BIOLOGICAL ENGINEERS, 2019; CEN, 2006; DIN, 2005; INTERNACIONAL ORGANIZATION FOR STANDARDIZATION, 2012).

Figure 10 - Flow classification diagram

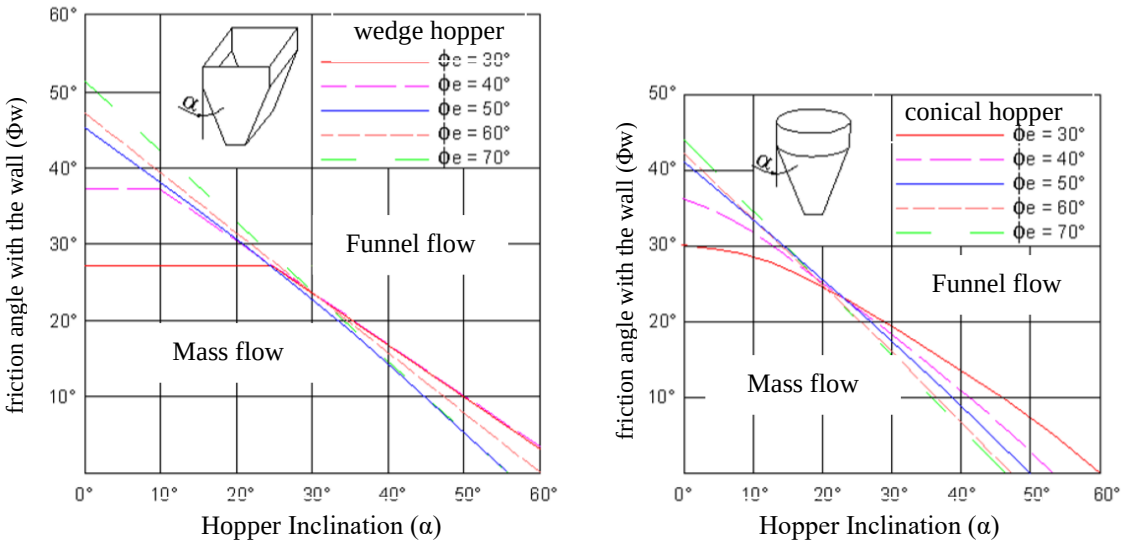


Source: Schulze (1996).

## 2.6. Pressures on the walls and bottom of slender silos

The estimation of horizontal pressures and friction on silo walls has been investigated by many authors (BARLETTA; POLETTO, 2013, 2019; CHEN et al., 2020; COUTO et al., 2013; COUTO; RUIZ; AGUADO, 2012, 2013; GANDIA et al., 2021a; GOODEY; BROWN; ROTTER, 2006; MOYA et al., 2002; NASCIMENTO; LOPES NETO; MONTROSS, 2013; RAMÍREZ et al., 2009; RAMÍREZ; NIELSEN; AYUGA, 2010b; WÓJCIK et al., 2017). Despite the many variables involved in this estimate, one statement is certain: the pressures exerted on the silo walls are directly related to the type of flow at the time of silo discharge.

The estimation of pressures in silos for funnel flow presents more uncertainties and variability than for mass flow (CALIL, 1985). Due to the complexity of the laws that govern the mechanical behavior of stored materials directly associated with the accuracy in the prediction of flow types, there is much to study about the geometric shapes of silos, filling and discharge configurations and types of hoppers (AYUGA, 2008; DOGANGUN et al., 2009; GANDIA et al., 2021d; NIELSEN, 2008).

The theoretical basis of the norms for estimating the overpressures in the silo walls are basically supported by two researchers: Janssen and Jenike in the theories: the theory of (JANSSEN, 1895), or the estimates of the initial loads or filling in the silo,

and the theories of Jenike (JENIKE, 1964; JENIKE; JOHANSON; CARSON, 1973a, 1973b), for the estimation of the flow (mass and funnel) in silos.

The procedures used by the standards in estimating wall pressures are quite variable. The standards use overpressure coefficients to ensure the effects during discharge (CEN, 2006; DIN, 2005; INTERNACIONAL ORGANIZATION FOR STANDARDIZATION, 2012).

The stored product exerts pressure on the silo structure: walls – horizontal and friction pressure; hopper – normal and friction pressure; transition (silo-hopper) vertical pressure. On the silo wall perpendicular forces act, causing horizontal pressures ($p_h$), and parallel forces due to friction of the product with the wall, causing friction pressures ($p_w$). In the silo transition (silo-hopper) vertical forces occur, causing the so-called vertical pressures ($p_v$). In the hopper, the normal forces and friction forces act from the vertical pressures that were decomposed into normal and tangential pressures to the hopper wall, represented by $p_n$ and $p_t$, respectively (Figure 11).

Figure 11 – Distribution of pressures in the silo.

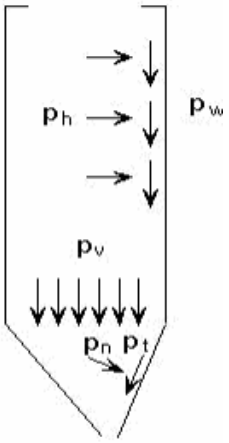


Source: Palma (2005).

The silo dynamics is defined by the silo filling, static phase and discharge. Pressures during filling present divergent discharge behaviors, these different situations occur the formation of maximum pressures (pressure peaks) due to the rapid change of state of the stored product, from passive to active (GANDIA et al., 2021c; PALMA, 2005; RUIZ; COUTO; AGUADO, 2012) (Figure 12). The percentage of increase in pressures (overpressures) in relation to the filling phase is still the subject of discussions and research.

Figure 12 – Stress field in silos (mass flow).

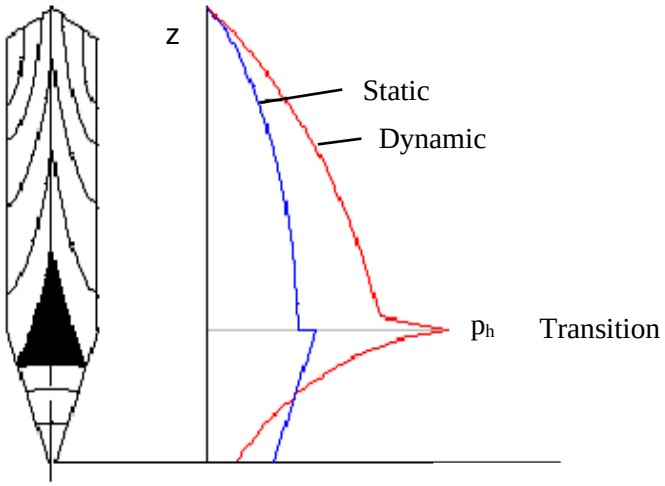


Source: Palma (2005).

At the beginning of discharge, the highest pressures in the silo occur, therefore, special attention is required. These pressures are located in the transition zone (silo/hopper), these overpressures usually occur within the first 10 seconds after the start of discharge (RUIZ; COUTO; AGUADO, 2012), however, due to the slenderness of the silo and the inclination of the hopper, this peak can exceed 10 seconds (GANDIA et al., 2021c).

The transition region that occurs the change from passive to active state, mentioned above, is called “switch”. This "peak" of pressure provided by the change of stress states has been studied by several researchers (JANSSEN, 1895; JENIKE; JOHANSON; CARSON, 1973a, 1973b; WALKER, 1967; WALTERS, 1973b, 1973a) developing theories and procedures, generating base for many studies.

## 2.7. Pressure measurements in silos

The measurement of pressures directly has been the subject of investigation during the last decades. Many tests were performed with the expectation of evaluating pressures through indirect methods and the use of reduced models, where the observed data could be extrapolated to the real-scale silos, however, the scale factor in experimental tests leads to uncertainties and uncertain values (BROWN; NIELSEN, 1998; COUTO; RUIZ; AGUADO, 2012; GANDIA et al., 2021a; NIELSEN; ASKEGAARD, 1977; RAMÍREZ; NIELSEN; AYUGA, 2010a; WÓJCIK et al., 2017).

In the tests conducted, the indirect methods correspond to the instrumentation of the silo wall material.

Full-scale experimental silo models provide proximity to real values, allowing confidence in the data and improving the understanding of pressures in silos Worldwide, the number of full-scale experimental silo stations is relatively small (BROWN; LAHLOUH; ROTTER, 2000; COUTO; RUIZ; AGUADO, 2012; HÄRTL et al., 2008; RAMÍREZ; NIELSEN; AYUGA, 2010a; SCHURICHT; FURLL; EENSTAD, 2001; SCHWAB et al., 1994; SUN et al., 2020; TENG; LIN, 2005; TENG; ZHAO; LAM, 2001; ZHAO; TENG, 2004; ZHONG; OOI; ROTTER, 2001) due to the cost of construction, instrumentation and operations.

However, the study of experimental pressures in silos brings advances in numerical studies as a form of validation and enables comparisons to be made for the construction of reliable models. Some experimental station studies for measuring pressures in silos are summarized below.

**Pilot silo test station - Pieper and Schutz**

The pilot silo was designed by Pieper and Schütz (1980). The pilot scale is considered by the classification ( (BROWN; NIELSEN, 1998), where:

- Class A: industrial silos;
- Class B: full-scale experimental stations;
- Class C: pilot models;
- Class D: small scale models;
- Class E: very small scale models (centrifugation).

The pilot silo is classified as C, defined by presenting the dimensions of the silo and the products stored at a scale with insignificant effects, as the dimensions are compatible with the real ones.

Therefore, the results obtained through the pilot silo can be used in the studies of real structures, and its behavior is considered identical in qualitative and quantitative terms at the 1:1 scale (full-scale).

The test station consists of the storage silo, bucket elevator and pilot silo. The pilot silo has its structure segmented into 12 independent rings and interchangeable hoppers. Along the silo, hopper and support pillars there are measurement cells that, by reading forces, stresses and pressures and using equations, allow obtaining the

horizontal, vertical and friction pressures present in the pilot silo (Figure 13). It is noteworthy that this test station was built in 2007 at the University of São Paulo at the School of Engineering (CHEUNG, 2007), later transferred to the Federal University of Lavras (GANDIA et al., 2021e).

Figure 13 - Medium-sized, full-scale silo.

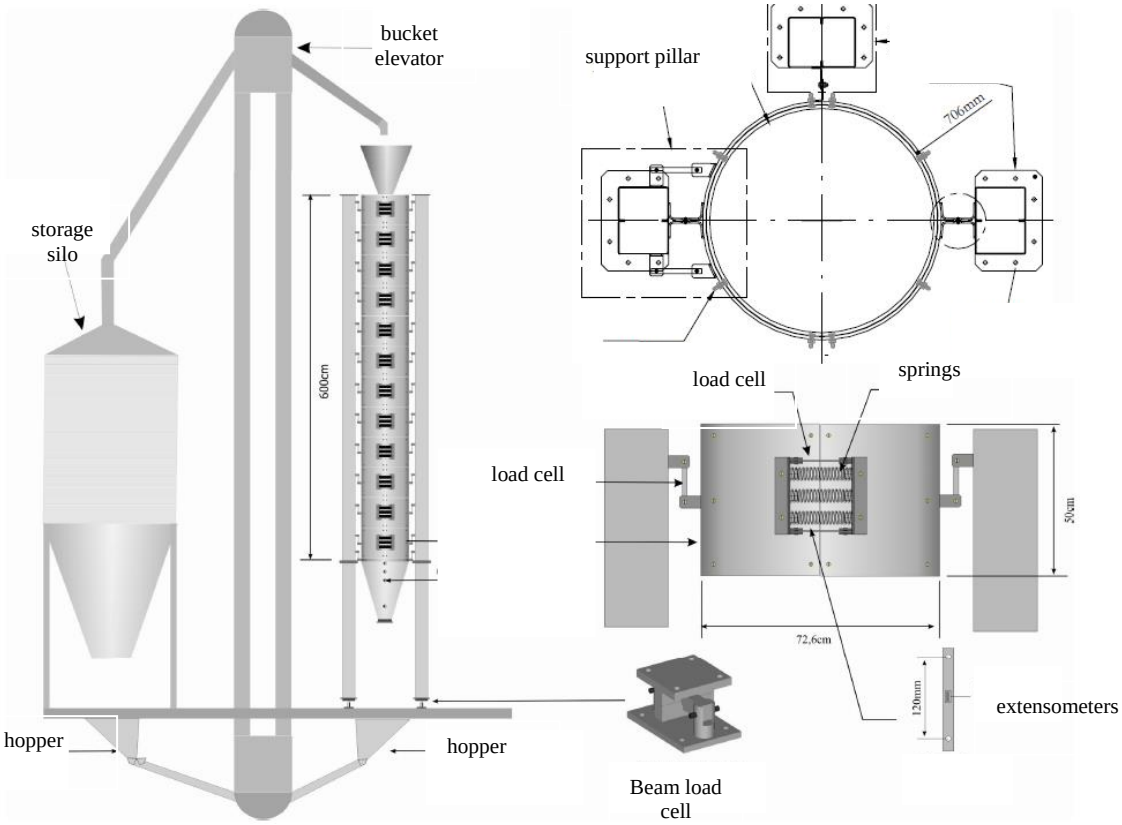


Subtitle: Components of the experimental station, dimensions and arrangement of the pilot silo sensors.

Source: Cheung (2007).

**Full-scale, medium-sized silo test station - Couto, Ruiz and Aguado**

Couto, Ruiz and Aguado (2012) developed at the University of León (Spain) a medium-sized, full-scale test station for dynamic measurements in silos under different conditions.

The station was instrumented and validated (RUIZ; COUTO; AGUADO, 2012). The instrumented silo is 2 meters high by 1 meter in diameter. This station made it possible to obtain the horizontal pressures on the silo walls according to the height, the

pressures in the transition zone (silo/hopper), the vertical pressures, the average friction pressure in the silo, and the coefficient of lateral pressures (K).

The station is versatile, being able to alternate the structure, such as: flat bottom and hoppers, both with discharges of different eccentricities; filling speed control; different height/diameter ratios (H/D) using a device that can apply pressure to the top of the silo, increasing its H/D ratio; storage of material with high humidity to calculate the pressure due to the expansion of the product. Figure 14 shows the silo and some measurement cells. The station allows various boundary conditions and using a real scale.

Figure 14 - Medium-sized, full-scale silo.

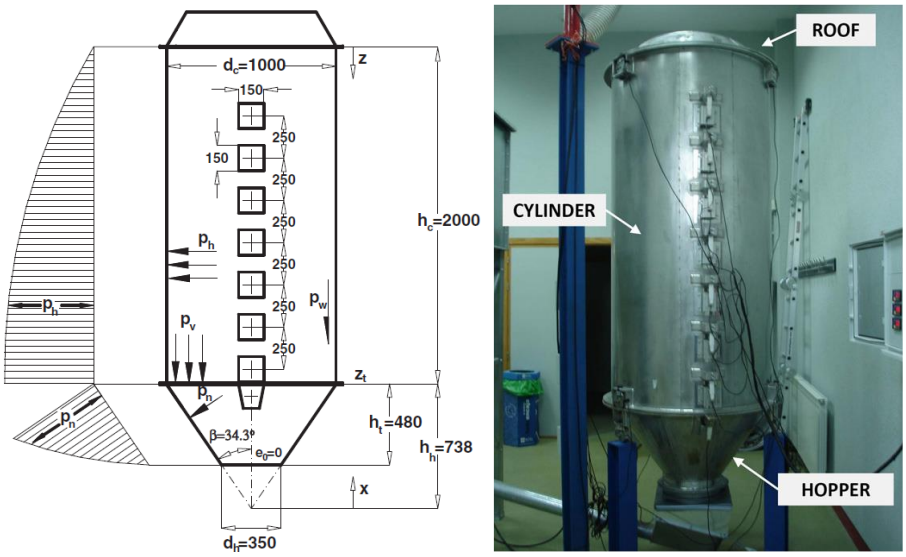


Source: Ruiz, Couto and Aguado (2012).

**Metallic prismatic silo test station - Brown e Lahlouh and Rotter**

Brown and Lahlouh e Rotter (2000) developed an experimental station to obtain pressures in prismatic silos at the Building Research Establishment laboratory in Garston (United Kingdom).

The dimensions used were chosen for a realistic approximation of pressure magnitudes and full-scale distribution. The height of the box (silo prism) is 2.5 meters and the cross section is 1.5 m, the prismatic hopper is 0.68 meters high (Figure 15). The thickness of the solid steel throughout the silo was 6 mm, with the silo prism welded at the four corners.

Figure 15 – Geometry and location of the pressure cells of the metallic prismatic test silo.

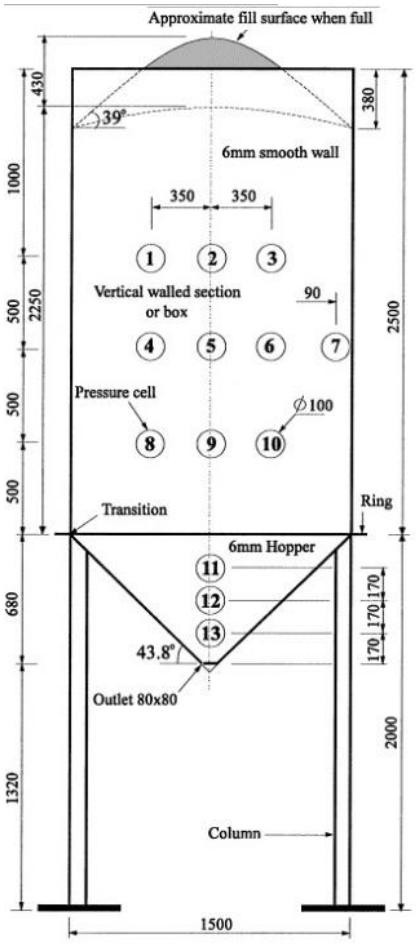


Source: Rotter, Brown and Lahlouh (2002).

The set features pressure cells distributed in vertical and horizontal positions in the silo and hopper. The studies evaluated that in prismatic silos the horizontal pressures at the same level vary due to the deformations of the thicknesses and rigidity of the silo structure plates, although Janssen's theory (JANSSEN, 1895) presents a good approximation for the pressure averages.

**Silos test station with eccentric hoppers - Ramírez, Nielsen and Ayuga**

Ramírez, Nielsen and Ayuga (2010a) designed an experimental station containing three instrumented silos supplied by a bucket elevator. The experimental station was built at the Higher Technical School of Agricultural Engineers (Escuela

Técnica Superior de Ingenieros Agrónomos - ETSIA) at the Polytechnic University of Madrid (Figure 16). The main objective of the station is to evaluate the pressures normal to the silo walls, both in the cylinder and in the hopper, and prioritizing the silo/hopper transition zone.

Figure 16 - ETSIA/Spain experimental station.

Source: Ramírez, Nielsen and Ayuga (2010a).

The silos have the same configurations, differing only by the geometry of the hopper, being: concentric, 50% eccentric and completely eccentric. The silo cylinder is 5.0 m high and 1.9 m in diameter with a height/diameter ratio of 2.63. The hoppers have an outlet of 0.32 m. Each silo is supported by four trussed steel pillars, stiffening rings were used in the cylinder and union of the silo with the hopper.

The system consists of 12 pressure measurement cells and was evaluated in two sets of measurements. In the first set the pressure cells were positioned only in the concentric silo along the height of the cylinder and the hopper. In the second set the pressure cells were positioned at three levels in height with four cells spaced at 90° per

level in each silo. The levels of both sets are shown in Figure 17. Still in the second set, three levels are located: silo cylinder, just before the silo/hopper transition zone, and just after the transition zone.

Figure 17 – Representation of the arrangement of pressure cells along the silo.

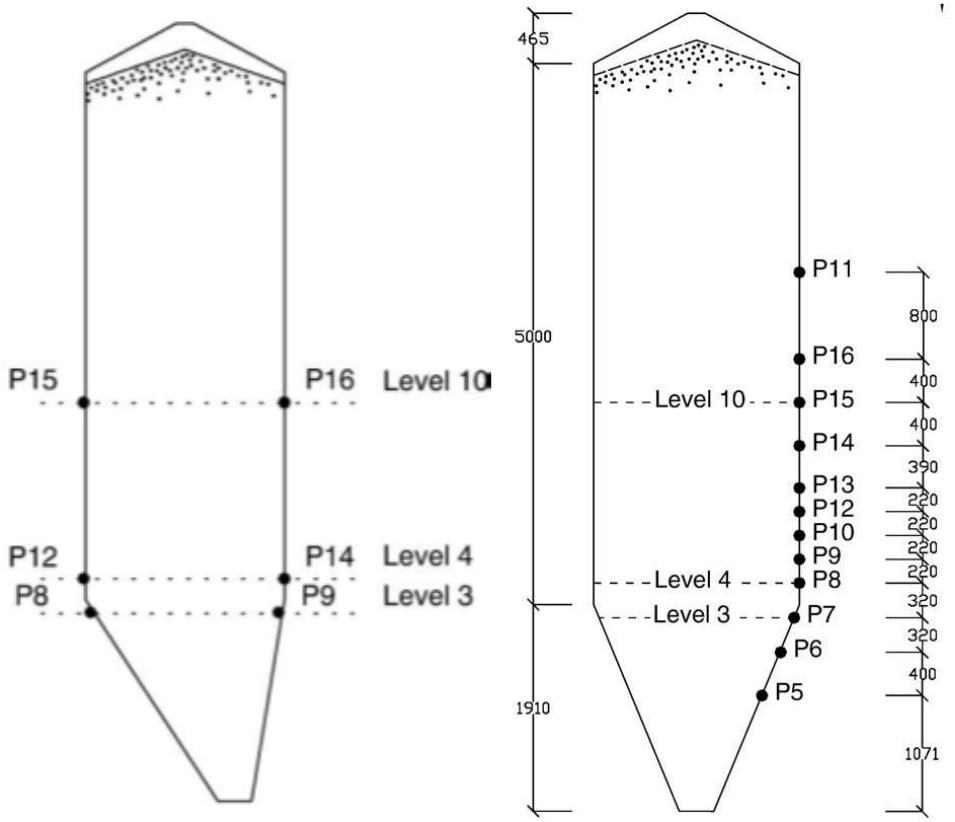


Source: Ramírez, Nielsen and Ayuga (2010a).

To set up evaluation settings, the station allows changing the stored product and the hopper, as well as evaluating the time of product consolidation in the silo and also changing the H/D ratio. In the study, filling and discharge using wheat and corn were evaluated.

The pressure curves of the second configuration were compared with theories (JANSSEN, 1895; WALKER, 1967), and the physical parameters to obtain the values were according to Eurocode 1, part 4 (CEN, 2006).

Therefore, in this work, in addition to confirming already known phenomena, it also presented new knowledge about the actions of pressures on the walls of the silos by non-symmetrical loads and eccentricity of hoppers using different stored products.

## 2.8. International standards for silo design

To determine the pressure exerted by the stored products on the side walls and on the bottom of silos, some international standards are worth mentioning:

- ANSI (ANSI, 2019);
- AS 3774 (AS, 1996).
- DIN (DIN, 2005);
- Eurocode 1, part 4 (CEN, 2006);
- ISO 11697 (ISO, 2012);

There are several discrepancies between the standards. The first concerns the classification in terms of geometry, addressing the relationship between the height/diameter (h/d) of structure, classifying the silos as slender, medium slender and low, as already shown in Table 1.

Regarding filling pressures, all adopt the formulation proposed by Janssen (1895) for the calculation of horizontal, vertical and wall friction pressures. The main variations occur in the calculation of vertical pressures at the base of flat bottom silos (slope $\leq 20^{o}$).

In relation to dynamic pressures, the standards generally adopt increase coefficients for static pressures. ISO 11697 (ISO, 2012) uses two overpressure coefficients, $C_w$ e $C_h$. These coefficients are 1.35 for slender silos, for the products listed in the table. For those not listed, it provides an equation for your calculation. AS 3774 (AS, 1996) recommends the use of an overpressure coefficient considering the type of discharge flow, symmetrical flow and planar flow, and makes considerations about the funnel flow. DIN 1055-6 (DIN, 2005) suggests the use of overpressure coefficients $C_w$ e $C_h$, relating the coefficients with the stored product through values listed in a proper table.

Normal hopper pressures are calculated by summing the hopper loads and those resulting from vertical overload directly above the transition. For mass flow silos, uniform normal pressure is applied in the transition region between the silo and the hopper. In the calculation of pressures, the standards suggest the application of different equations of their own.

Additional pressures must be considered, as their occurrence is inevitable. Even in silos with centered filling and symmetrical axis such pressures occur due to imperfections in the geometry of the hopper and silo walls. Also called asymmetric

pressures, these contribute to the occurrence of bending moments. ISO 11697 (ISO, 2012) considers additional pressures acting on any part of the silo wall and makes eccentric discharge considerations. EN 1991-4 (CEN, 2006) proposes an equation for the localized pressures acting on any part of the silo, during filling and discharge. For silos with a diameter smaller than 5.0m, this standard adopts simplifying equations. AS 3774 provides for the pressure increase in several situations, the most unfavorable situation being the eccentric discharge. DIN 1055-6 (DIN, 2005) uses the same procedure as EN 1991-4 (CEN, 2006), not mentioning the silo section and using different weighting coefficients.

### 2.8.1. *International Organization for Standardization* - ISO 11697 (2012)

The referred standard mentions that the flow pattern is dependent on some conditions, such as slope of the hopper wall and coefficient of friction with the wall. Therefore, it is proposed that the slope of the hopper (its geometric design) be defined through the following abacus (

Figure 18 e Figure 19), for conical and wedge hoppers, respectively, according to the type of flow expected to be obtained within the silo.

Figure 18 - Conical hopper inclination as a function of flow pattern.

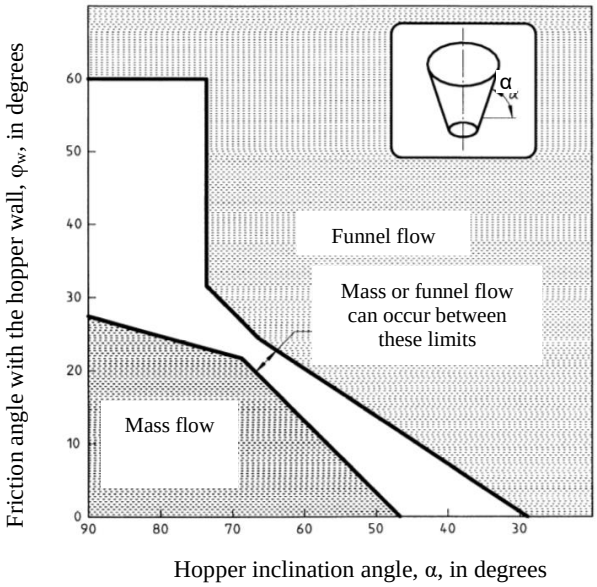


Source: ISO 11697 (2012).

Figure 19 – Wedge hopper slope as a function of flow pattern.

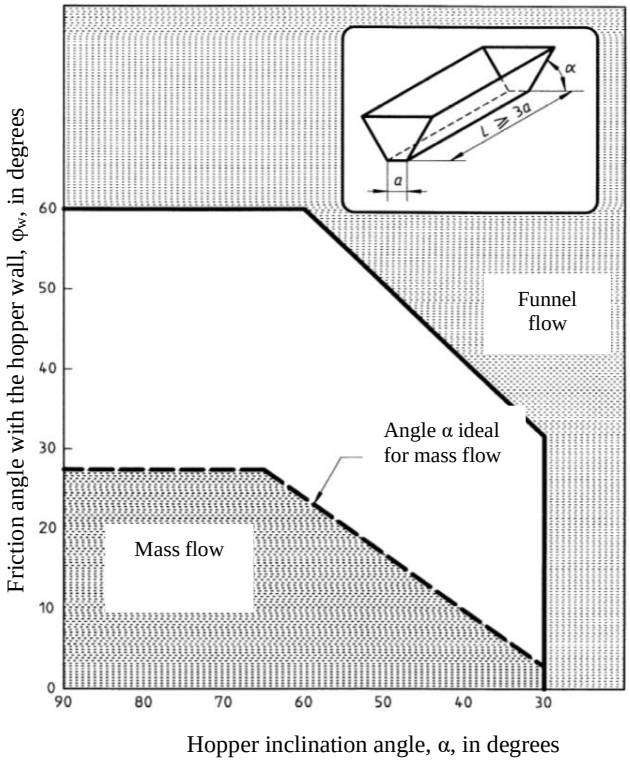


Source: ISO 11697 (2012).

The area between “mass flow” and “funnel flow”, shown on both abacus in Figure 18, configures the sizing situation where the flow pattern can change abruptly between mass and funnel flow. In this way, a discharge with unstable flow may occur, causing pressure fluctuations and, in this case, the silo must be designed for both types of flow, mass and funnel, in the worst condition of efforts and deformations.

The calculation of hopper pressures is performed in a similar way to EN 1991-4 (2006) and DIN 1055-6 (2005), not considering discharge in eccentric hoppers, that is, it is limited to cases where the eccentricity of the discharge is not exceeds 25% of the silo diameter.

The loads considered for calculating the pressure normal to the hopper wall, pn, are illustrated in Figure 20.

Figure 20 - Loads in the hopper.

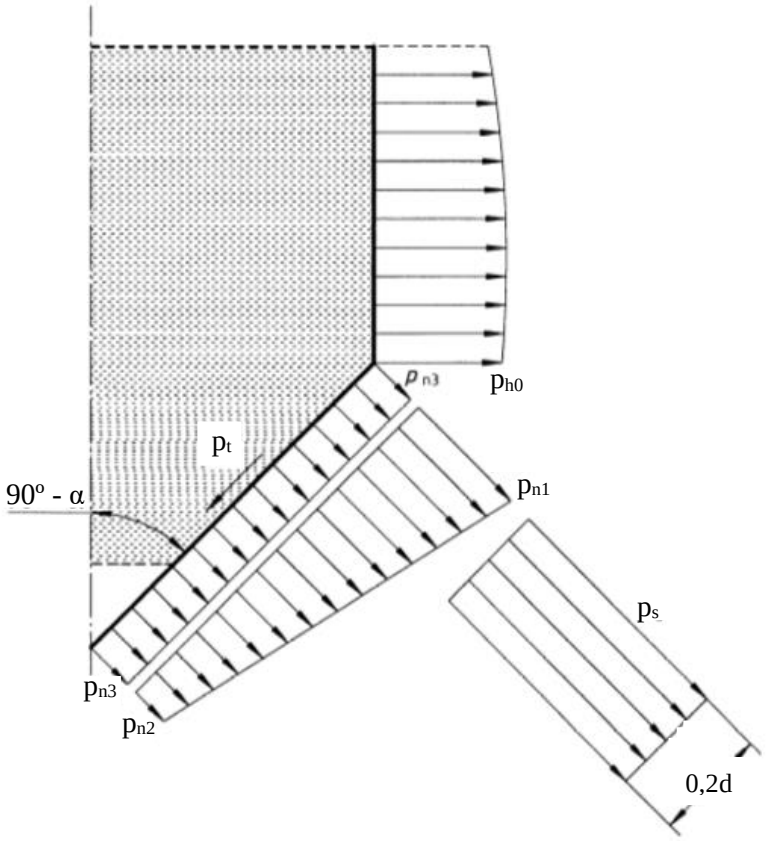


Source: ISO 11697 (2012).

For filling and discharge the silo, considering the inclination of the walls with the horizontal $\alpha \geq 20^{o}$, the normal pressure can be calculated by the sum of the loads during filling ($p_{n3}$) nd by those resulting from the vertical overloads above the transition ($p_{n1}$ and $p_{n2}$), according to the following equations:

$$p_n = p_{n1} + p_{n2} + p_{n3} \tag{2}$$

Where:

$$p_{n1} = 1,5\, p_{h0} \left( \frac{1}{\lambda} \cos^2 \alpha + sen^2 \alpha \right) \tag{3}$$

$$p_{n2} = \frac{1,5}{\lambda}\, p_{h0} \cos^2 \alpha \tag{4}$$

$$p_{n3} = 3,0 \frac{A}{U} \frac{\gamma\lambda}{\sqrt{\mu}} sen^2\alpha \quad (5)$$

Where:

$p_{h0}$ = horizontal pressure on the vertical wall of the silo, in the transition region with the hopper, kN.m$^{-2}$;

$\lambda$ = relationship between horizontal and vertical pressure, dimensionless;

$\alpha$ = angle of inclination of the hopper with the horizontal, in degrees;

$\mu$ = coefficient of friction between the silo wall and the stored product, dimensionless;

$A$ = cross-sectional area of the silo, in m²;

$U$ = perimeter of the silo cross section, in meters;

$\gamma$ = specific weight of the material, in kN.m$^{-3}$.

In the transition (silo/hopper), for mass flows, the normal pressure at the discharge considerably exceeds that which occurs during filling. In this case, the load acting on the hopper is added to a third component, $p_s$, given by:

$$p_s = 2.p_{h0} \quad (6)$$

This component of overload that occurs in the discharge of the silo is considered in a length equal to 0.2d in the hopper, starting from the transition region, with “d” being the measure of the internal diameter of the silo, as shown in Figure 20.

For shallow hopper angles ($\alpha \leq 20^o$), that is, hoppers with practically straight bottoms, the pressure normal to the wall will be the vertical pressure and must be estimated considering an increase factor of 1.35.

The friction pressure ($p_t$) acting on the hopper is given by Equation 7, the value of $p_n$ eing defined by the sum of the parcels $p_{n1}$, $p_{n2}$ and $p_{n3}$, as illustrated in Figure 20.

$$p_t = \mu.p_n \quad (7)$$

According to the standard, asymmetric pressures in the structure are unavoidable, even if the silo is filled concentrically, and these pressures cause bending moments in the walls and hopper. Therefore, an additional load equal to $0.2p_{he}$, must be considered, where $p_{he}$ is the value of the lateral pressure during discharge, acting on any

part of the silo wall over a square area with a length of $s = 0,8\,A/\mu$, as illustrated Figure 21. These pressures are dependent, in addition to the eccentricity of the discharge, on the characteristics of the stored product and its probabilistic heterogeneity, as well as on the geometric imperfections of the hopper and silo walls.

Figure 21 – Additional load.

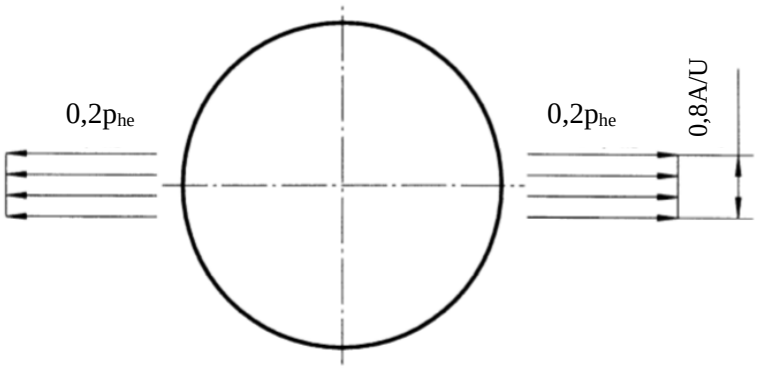


Source: ISO 11697 (2012).

ISO 11697 (2012) does not mention a calculation for silos with hoppers with large eccentricities, limiting that the discharge eccentricity (e) does not exceed 25% of the silo diameter (Figure 22). However, for silos with hoppers whose eccentricity is less than 0.25d, in the case of circular silos, or less than 0.25a, for rectangular silos, the additional load (Figure 21) must be increased by a factor β, given by Equation 8:

$$\beta = 1,0 + 4\frac{e}{d} \tag{8}$$

Where:

a = smallest side of the rectangular silo cross section, in meters;

e = eccentricity of the discharge outlet, in meters;

d = silo diameter, in meters.

Figure 22 - Representation of the limit eccentricity of silos.

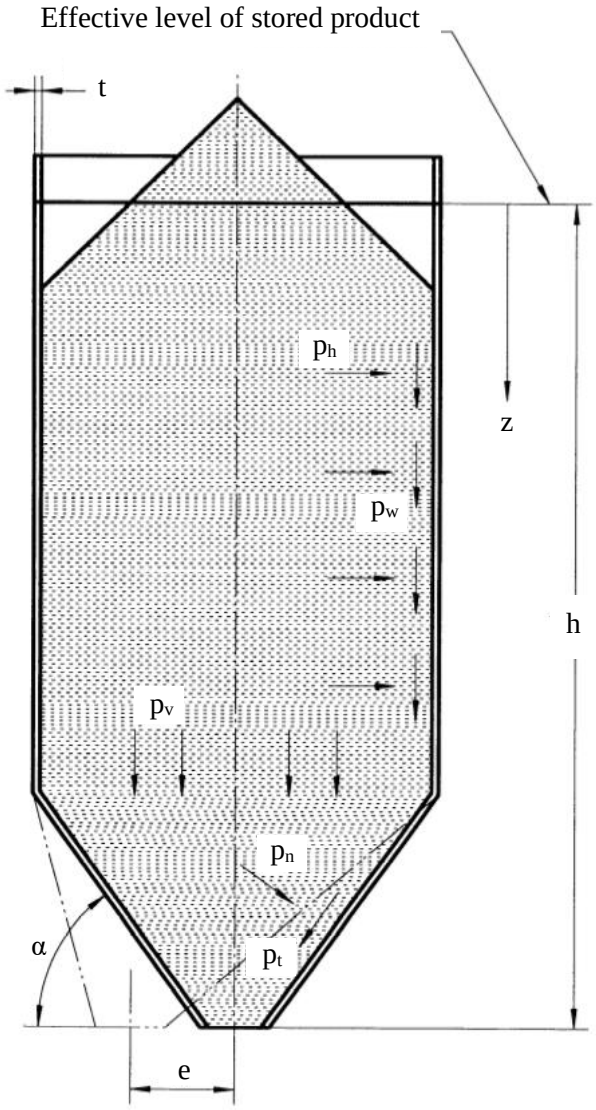


Where:
$p_v$ is the vertical pressure due to the storage material, in kN.m$^{-2}$;
$p_h$ is the lateral (horizontal) pressure due to the storage material, in kN.m$^{-2}$;
$p_w$ is the friction pressure of the product with the vertical wall of the silo, in kN.m$^{-2}$;
$p_n$ is the pressure normal to the hopper wall, in kN.m$^{-2}$;
$p_t$ is the friction pressure of the product with the hopper wall, in kN.m$^{-2}$;
α is the angle of inclination of the hopper wall with the horizontal, in degrees;
z is the ordinate below the equivalent surface of the solid for the maximum filling condition of the silo, in meters;
h is the total height of the silo, in meters;
e is the eccentricity of the discharge outlet, in meters.

Source: ISO 11697 (2012).

### 2.8.2. *European Committee of Standardization* - EN 1991-4 (2006)

For the evaluation of loads and stresses in the hoppers, EN 1991-4 (2006) distinguishes between silos with steep hoppers and silos with a flat bottom.

For hoppers with large slopes of their walls, under filling and discharge conditions, the coefficient of friction of the product storing with the wall is the smallest characteristic value of this parameter, being called $\mu_{heff}$.

According to this standard, the pressures acting on the hopper can be decomposed for calculation purposes, as shown in Figure 23.

Figure 23 - Filling pressures in hoppers.

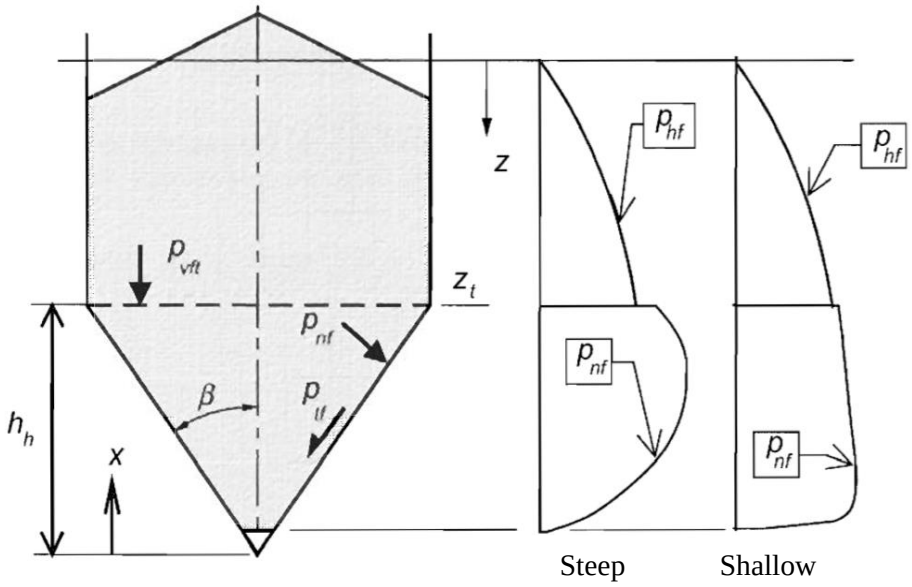


Where:
$p_{vft}$ is the average vertical pressure in the solid in the transition region, after filling the silo, in the condition of filling and storage, in $kN.m^{-2}$;
$p_{nf}$ is the pressure normal to the hopper wall, in the filling and storage condition, in $kN.m^{-2}$;
$p_{tf}$ is the friction pressure of the product with the hopper wall, in the filling and storage condition, in $kN.m^{-2}$;
β is the angle of inclination of the hopper with the vertical, in meters;
z is the ordinate below the equivalent surface of the solid for the maximum filling condition of the silo, in meters;
x is the ordinate from the vertex of the hopper, in meters;
ɣ the specific weight of the ensiled product, in $kN.m^{-3}$;
$h_h$ is the height of the hopper, measured from its apex to the transition zone, in meters.

Source: EN 1991-4 (2006).

During filling, the average vertical pressure, $p_v$, in the product stored at any level in the hopper is calculated by the equations shown below, with reference to Figure 23.

$$p_v = \left(\frac{\gamma . h_h}{n-1}\right)\left[\left(\frac{x}{h_h}\right) - \left(\frac{x}{h_h}\right)^n\right] + p_{vft}\left(\frac{x}{h_h}\right)^n \quad (9)$$

Where:

$$n = S\left(1-b\right)\mu_{heff}\cot\beta \quad (10)$$

$$F_f = 1 - \frac{b}{1+\frac{\tan\beta}{\mu_{heff}}} \quad (11)$$

Where:

S = hopper aspect ratio:

S = 2 for square conical and pyramidal hoppers (dimensionless);

S = 1 for wedge hoppers (dimensionless);

S = rectangular shaped hoppers, where “a” is defined as the length of the rectangular hopper and “b” as its width, both given in meters and parameter S is dimensionless;

*b* = 0.2 (empirical coefficient);

$\gamma$ = upper characteristic value of the specific weight of the ensiled material, in $kN.m^{-3}$;

$h_h$ = vertical height between the apex of the hopper and the transition region, in meters;

x = coordinate above the apex of the hopper, in meters;

$\mu_{heff}$ = coefficient of friction of the stored product with the hopper wall (dimensionless);

F = characteristic value of the ratio between the pressures in the hopper, being differentiated for the cases of filling ($F_f$) and discharge ($F_e$) of the silo (dimensionless);

$\beta$ = slope of the hopper wall with the vertical, in degrees;

$p_{vft}=p_v$ = average vertical pressure in the solid in the transition region, after filling the silo, in $kN.m^{-2}$.

The normal pressure, $p_{nf}$, and the wall friction pressure, $p_{tf}$, at any point in the hopper after filling are given by the following equations:

$$p_{nf} = F_f\, p_v \quad (12)$$

$$p_{tf} = \mu_{heff} F_f p_v \quad (13)$$

In silo discharge, the pressures in the structure are qualitatively illustrated in Figure 24.

Figure 24 - Discharge pressures in hoppers.

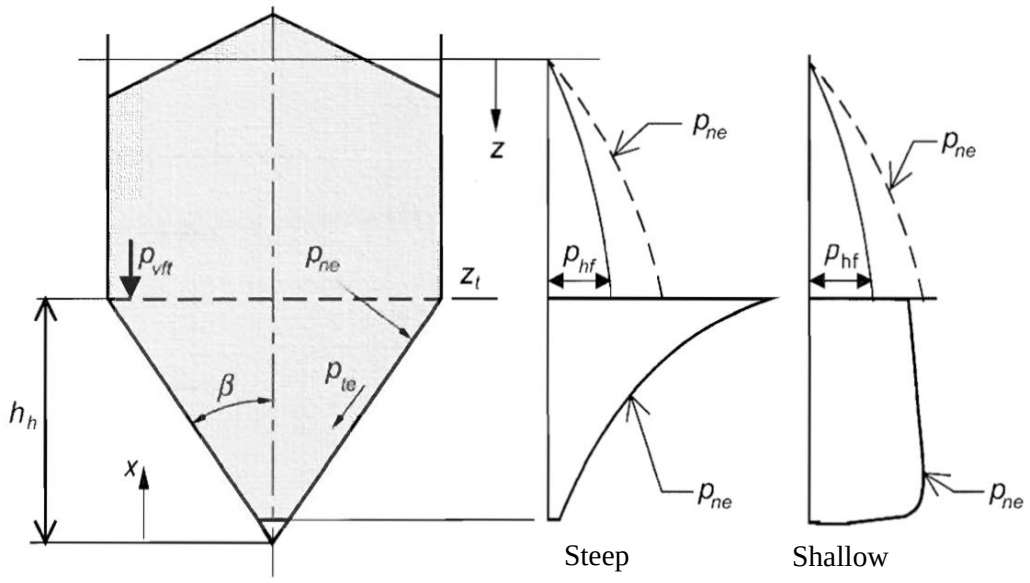


Where:
pvft is the average vertical pressure in the solid in the transition region, after filling the silo, in the condition of filling and storage, in kN.m-²;
$p_{ne}$ is the normal pressure to the hopper wall, at discharge, in kN.m$^{-2}$;
$p_{te}$ is the friction pressure of the product with the hopper wall, in the silo discharge condition, in kN.m$^{-2}$;
β is the angle of inclination of the hopper with the vertical, in meters;
z is the ordinate below the equivalent surface of the solid for the maximum filling condition of the silo, in meters;
x is the ordinate from the vertex of the hopper, in meters;
ɣ the specific weight of the ensiled product, in kN.m-³;
hh is the height of the hopper, measured from its apex to the transition zone, in meters.
Source: EN 1991-4 (2006).

In this situation, the average vertical pressure ($p_v$) of the product stored at any level in a steep hopper must also be determined by Equation 14, however, using the coefficient F = $F_e$, as shown below:

$$F_e = \frac{1 + sen\phi_i \cos\varepsilon}{1 - sen\phi_i \cos(2\beta + \varepsilon)} \quad (14)$$

Where:

$$\varepsilon = \phi_{wh} + sen^{-1}\left(\frac{sen\phi_{wh}}{sen\phi_i}\right) \quad (15)$$

$$\phi_{wh} = \tan^{-1}\mu_{heff} \quad (16)$$

Where:

β is the angle of inclination of the hopper with the vertical, in degrees;

$\mu_{heff}$ = coefficient of friction of the product with the hopper wall (dimensionless);

$ø_i$ = internal friction angle of the stored material, in degrees.

In silos that have shallow hoppers, the material wall friction is not fully mobilized, therefore, the effective coefficient of friction of the product with the hopper wall occurs by:

Also, for the silo discharge, the normal pressure, $p_{ne}$, and the wall friction pressure, $p_{te}$, at any point in the hopper, are given by:

$$p_{ne} = F_e p_v \quad (17)$$

$$p_{te} = \mu_{heff} F_e p_v \quad (18)$$

$$\mu_{heff} = \frac{1-K}{2\tan\beta} \quad (19)$$

where K is the lower characteristic value of the lateral pressure ratio.

Regarding the aforementioned K parameter, the standard defines it for some types of stored products, for silos with smooth or rough walls. For products not mentioned, it is suggested to determine the value of K experimentally or by the equation 20:

$$K = 1{,}1\left(1 - sen\phi_i\right) \quad (20)$$

Alternatively, to determine the values of filling pressures according to the EN 1991-4 (2006) standard, the value of the normal pressure to the hopper wall can be calculated from the portions decomposed into $p_{n1}$, $p_{n2}$, $p_{n3}$ and $p_s$, as shown in Figure 25.

Figure 25 – Alternative way of decomposing pressures.

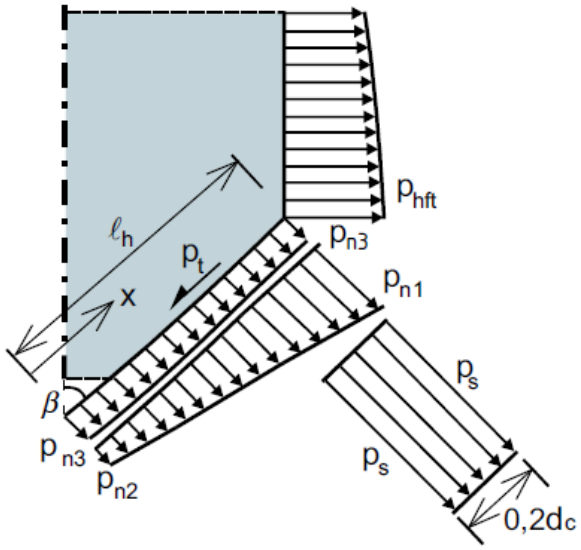


Source: EN 1991-4 (2006).

Therefore, for cases where the slope of the hopper walls with the horizontal is greater than 20º, the normal pressure on the surface can be calculated according to the following equations:

$$p_n = p_{n3} + p_{n2} + (p_{n1} - p_{n2})\frac{x}{l_h} \tag{21}$$

Where:

$$p_{n3} = 3,0\frac{A}{U}\frac{\gamma K}{\sqrt{\mu_h}}\cos^2\beta \tag{22}$$

$$p_{n2} = p_{vft}C_b\sin^2\beta \tag{23}$$

$$p_{n1} = p_{vft}(C_b\sin^2\beta + \cos^2\beta) \tag{24}$$

Where:

$\beta$ = slope of the hopper wall with the vertical, in degrees;

$l_h$ = length of the hopper wall, in meters;

x = relative height in the hopper between 0 and Ih, in meters;

$p_{n1}$ and $p_{n2}$ = define the hopper pressures due to the vertical pressure of the material stored in the transition region, in $kN.m^{-2}$;

$p_{n3}$ = pressure in the hopper due to the solid stored inside it, in $kN.m^{-2}$;

$p_{vft}$ = vertical pressure acting on the transition region after filling, in $kN.m^{-2}$;

$\mu_h$ = smallest characteristic value of the hopper wall friction coefficient (dimensionless);

k = lateral pressures ratio (dimensionless);

A = cross-sectional area of the silo cylinder, in $m^2$;

U = internal perimeter of the silo body cross section, in meters;

$C_b$ = augmentation coefficient = 1.3 (static state) or 1.6 (dynamic state).

Also, the value of friction pressure on the hopper wall is given by:

$$p_t = p_n \mu_h \tag{25}$$

where $p_n$ is calculated by Equation 6.

For flat bottom silos ($\beta \geq 70^o$), the discharge pressure ($p_{vfb}$) can be calculated using the following equation:

$$p_{vfb} = C_b p_{vf} \tag{26}$$

For funnel flow silos, the standard states that the discharge loads in the hoppers can be calculated using the orientation for filling loads, as shown in

Figure 25. In the case of silos with mass flow, an additional normal pressure is considered in the calculation, called $p_s$ (shown in the same figure). This load is applied along a length of 0.2dc below the hopper transition region and around the entire perimeter, defined by the following equation:

$$p_s = 2Kp_{vft} \tag{27}$$

where $p_{vft}$ é is the vertical pressure acting in the transition region after filling.

For the determination of the average vertical stress in the solid stored at any level in a steep hopper ($p_v$), the standard presents an alternative way to calculate the $F_e$

parameter (characteristic value of the ratio between the pressures in the hopper in the discharge situation), according to explained below:

$$F_e = \left( \frac{1}{1+\mu \cot \beta} \right) \left\{ 1+2 \left[ 1+ \left( \frac{sen\phi_i}{1+sen\phi_i} \right) \left( \frac{\cos \varepsilon sen(\varepsilon - \beta)}{sen\beta} \right) \right] \right\} \quad (28)$$

Where:

$$\varepsilon = \beta + \frac{1}{2} \left[ \phi_{wh} + sen^{-1} \left( \frac{sen\phi_{wh}}{sen\phi_i} \right) \right] \quad (29)$$

$$\phi_{wh} = \tan^{-1} \mu_h \quad (30)$$

Where:

$\mu_h$ = lower characteristic value of the wall friction coefficient in the hopper (dimensionless);

$ø_i$ = internal friction angle of the stored solid, in degrees.

## 2.9. Finite Element Method in silos

In view of advances in engineering and research in silos, allied to computational development, the modelling is based on a tripod: theoretical model (based on previous studies), experimental model (based on tests carried out experimentally) and numerical model (based on performing models as an example, the use of finite elements). The use of numerical methods has allowed advances in most areas of engineering.

The finite element method (FEM) is a numerical procedure for determining approximate solutions using differential equations in which the problem domain is subdivided into small parts, called elements. In recent years, studies using FEM in silos have increased significantly (JOFRIET, 1992; HOLST et al., 1999; AYUGA et al., 2006; GALLEGO et al., 2010; GALLEGO; RUIZ; AGUADO, 2015; PARDIKAR; ZAHID; RHEE et al., 2020; WASSGREN, 2020; ZHAO, 2004), mainly due to the quality of the results and the time and cost savings compared to full-scale experimental models. In the end, experimental testing is inevitable to validate finite element models,

but once validated they allow numerous analyzes to be performed quickly and at lower cost.

Yáñez, Femández and López (2001) performed a numerical study to evaluate the stresses in silos with eccentric discharge, validating their computational model with the geometry of a cylindrical silo with a centered hopper, whose structural behavior is known and well defined. Some results are seen in Figure 26.

Figure 26 – Horizontal pressures in concentric (a) and eccentric (b) hoppers according to FEM and some existing standards.

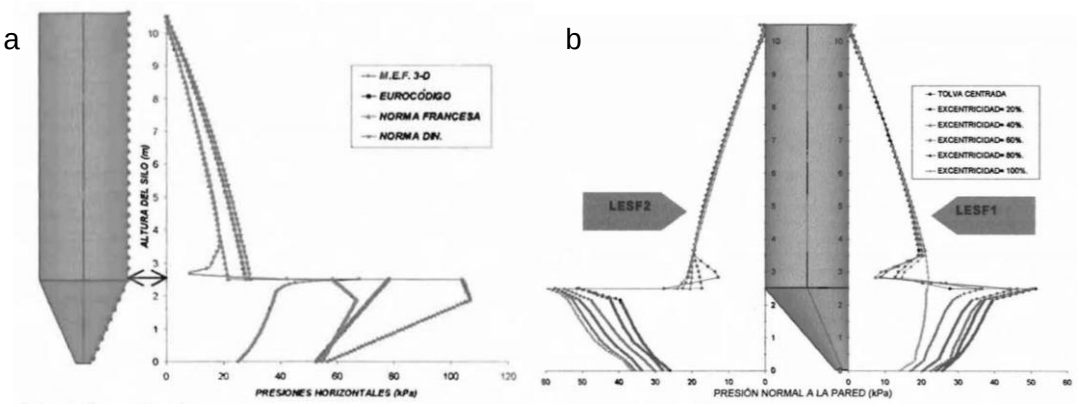


Source: Yáñez, Femández and López (2001).

The differences in horizontal pressures between the FEM and the calculation standards are observed (Figure 26) and the differences between horizontal pressures close to the transition and close to the outlet (discharge) (Figure 26). Therefore, the results were expected, demonstrating the applicability of this method in simulating the behavior of the product stored in the silo structure.

Using the FEM, the elastoplastic behavior was considered through the Drucker-Prager criterion (DRUCKER; PRAGER, 1952), demonstrating the variability of normal pressures on the walls of cylindrical silos with concentric and eccentric hoppers, in discharge (GUAITA; COUTO; AYUGA, 2003). In this work, the finite element "SOLID-45" from Ansys® software was used. The silo walls were considered rigid. Figure 27 illustrates the results of the work, observing the pressures increase on the side opposite the eccentricity of the discharge mouth (represented by L2). However, when the angles of internal friction are evaluated in the same silo configuration, the pressures normal to the wall increase with the decrease of this property of the product.

Figure 27 – Normal pressures to the walls of a silo with centered hopper (a), 60% eccentric hopper (b) and 100% eccentric hopper (c), variation of the internal friction angle of the product ($ø_i$).

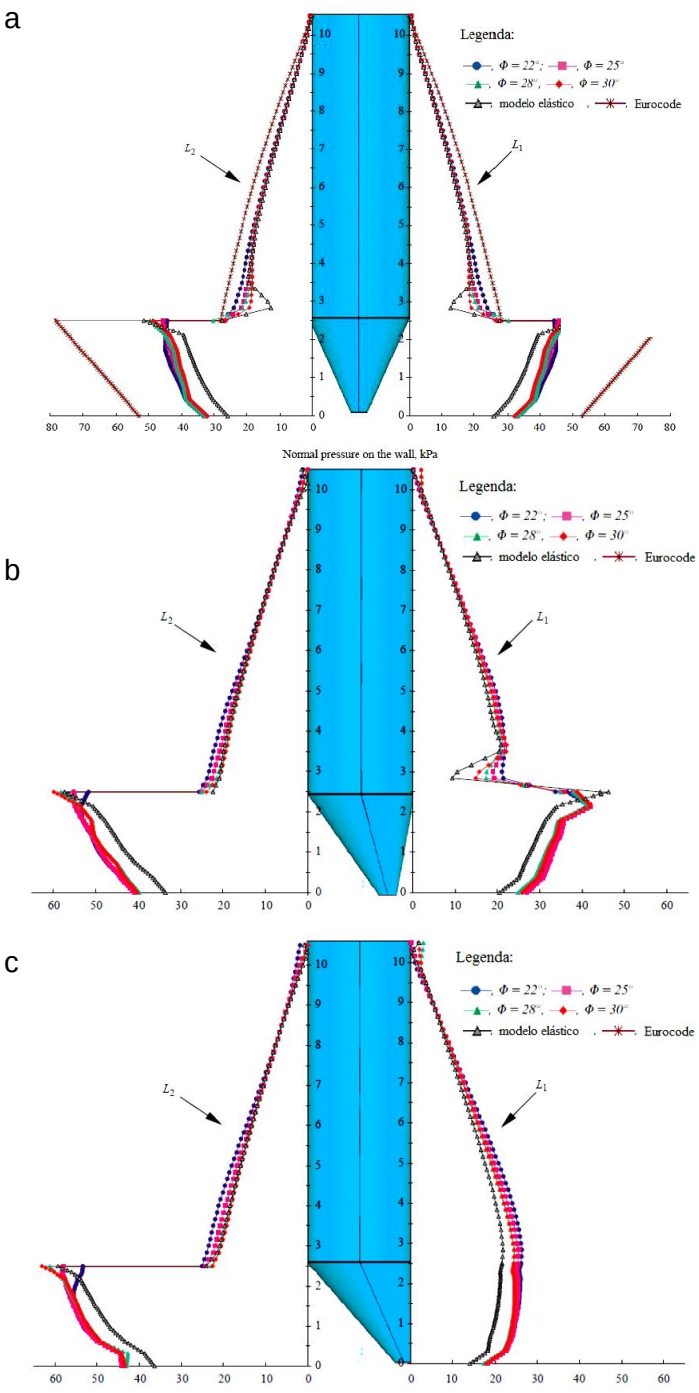


Source: Guaita, Couto and Ayuga (2003).

There is an increase in horizontal pressures at the material discharge along the entire height of the silo and, consequently, a pressure peak along the wall due to the sudden constriction in the flow transition (vertical wall and hopper).

Gallego, Ruiz and Aguado (2015) compared experimental results obtained experimentally with data calculated using the Finite Element Model (FEM) developed in ANSYS. They analyzed normal wall pressures and frictional forces.

The simulated model was made from elastoplastic material to simulate the behavior of the product bulk stored. To define the elastic behavior, two parameters were needed: the Poisson ratio, and the modulus of elasticity. To define the plastic part, three parameters were needed: the friction angle, the cohesion, and the expansion angle. A Figure 28 presents the results of normal pressures using the FEM compared to the experimental and Eurocode 1, part 4.

Figure 28 – Comparison of normal pressures on the silo wall for filling (a) and discharge (b).

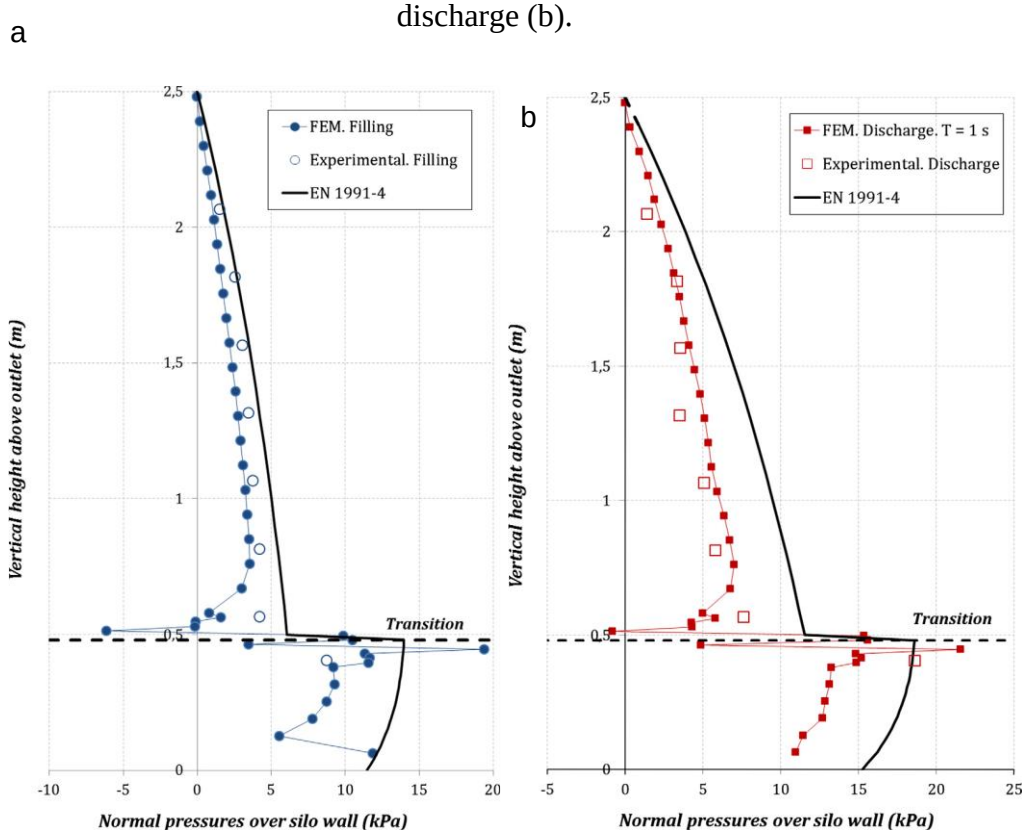


Source: Gallego, Ruiz and Aguado (2015).

The results presented showed that the numerical models predicted by the FEM are close to those obtained experimentally, both for filling and for discharge.

It was observed some studies using the FEM to obtain pressures in silos. It was found that all models were validated by experimental pressures. Therefore, the use of FEM to calculate pressures (normal and friction) in silos in the filling and discharge stages is a versatile tool and can be further explored.

# 3. GENERAL CONSIDERATIONS

The storage of agricultural products presents great national and international importance in terms of inventory control, logistics, quality and safety. Therefore, the storage of products in silos is increasing. However, there are still many gaps due to the properties of the stored products and the dynamic structure that is the silo. Therefore, the importance of the experimental study is remarkable for presenting realistic and accurate answers. However, the scale factor can make the construction and instrumentation of these experimental stations to measure pressures and evaluate flows in silos unfeasible. Consequently, the use of real scale is relevant. In addition, together with the experimental study, the association of the numerical study have a great value.

The importance of studying silos goes beyond the verification of standards, it also aims to search for answers in the relationships that cause structural failures and collapses. Some issues involving the product stored in the silo structure have not been or are still poorly studied.

This thesis is composed of two parts. The first part is a synthetic and generalized approach to the motivation and theoretical basis of the studies. The second part presents each of the six articles with theoretical and methodological depth followed by the results and conclusions.

The second part showed that the test station was validated, fully complying with the objectives and expectations proposed at the beginning of the investigation, already achieved with its execution, having also obtained novelties in conclusions about the behavior of the stored product of the pilot silo structure, as : influence of slender in consolidation; normal and friction pressure related with slender and consolidation; time of occurrence of maximum silo pressure after discharge starts; relationships between different pressure, consolidation, discharge time by flow type, influence of flow type on discharge pressures and other variables and relationships. The computational numerical simulation proved to be an efficient tool to determine the pressures in silos, showing how the specific weight and the wall friction coefficient are two variables that directly influence the pressures in silos.

**REFERENCES**

AGRICULTURA Y GANADERIA DE CASTILLA Y LEÓN. **TABLAS DE LA COSECHA DE MAÍZ 2020 EN CASTILLA Y LEÓN**. [s.l: s.n.]. Disponível em: <https://agriculturaganaderia.jcyl.es/web/jcyl/AgriculturaGanaderia/es/Plantilla100Detalle/1246464862173/Noticia/1284998741023/Recurso>.

ANSI - AMERICAN SOCIETY OF AGRICULTURAL AND BIOLOGICAL ENGINEERS. **Loads Exerted by Free-Flowing Grain on Bins. ANSI/ASAE**: S433.1 JAN2019. St Joseph: [s.n.].

AUSTRALIAN STANDARD. AS 3774. **Loads on bulk containers. AS 3774 Supplement 1 (1997)**. Sydney: [s.n.].

AYUGA, F. et al. Discharge and the Eccentricity of the Hopper Influence on the Silo Wall Pressures. **Journal of Engineering Mechanics**, v. 127, n. 10, p. 1067–1074, 2001.

AYUGA, F. et al. Experimental tests to validate numerical models in silos design. **2006 ASABE Annual International Meeting**, v. 0300, n. 06, 2006.

AYUGA, F. Some unresolved problems in the design of steel cylindrical silos. In: CHEN, J.F., TENG, J. G. (Ed.). . **Structures and Granular Solids: From Scientific Principles to Engineering Applications**. Boca Raton, USA: CRC Press-Taylor & Francis Group, 2008. p. 123–133.

BARLETTA, D.; POLETTO, M. A device for the measurement of the horizontal to vertical stress ratio in powders. **Granular Matter**, v. 15, n. 4, p. 487–497, 2013.

BARLETTA, D.; POLETTO, M. A new split cell for the measurement of the horizontal to vertical stress ratio of powders. **Powder Technology**, v. 351, p. 273–281, 2019.

BENINK, E. J. **Flow and stress analysis of cohesionless bulk materials in silos related to codes**. [s.l.] University of Twente, 1989.

BROWN, C. J.; LAHLOUH, E. H.; ROTTER, J. M. Experiments on a square planform steel silo. **Chemical Engineering Science**, v. 55, n. 20, p. 4399–4413, 2000.

BROWN, C. J.; NIELSEN, J. **Silos: Fundamentals of theory, behaviour and design**. London: [s.n.].

BUTTERFIELD, R. A theoretical study of the pressures developed in a silo containing single-size particles in a regular packing. **International Journal of Rock Mechanics and Mining Sciences and**, v. 6, n. 2, p. 227–238, 1969.

BYWALSKI, C.; KAMIŃSKI, M. A case study of the collapse of the over-chamber reinforced concrete ceiling of a meal silo. **Engineering Structures**, v. 192, n. March, p. 103–112, 2019.

CALIL, C.; PALMA, G.; CHEUNG, A. B. Failure Modes of Cylindrical Corrugated Steel Silos in Brazil. **Bulk solids handling**, v. 29, n. 6, p. 346, 2009.

CALIL, J. C. Cargas para o dimensionamento de silos. **JORNADAS SUL-AMERICANAS DE ENGENHARIA ESTRUTURAL**, v. 23, p. 1359–1379, 1985.

CALIL, J. C. **Recomendações de Fluxo e de Cargas para o Projeto de Silos Verticais**. [s.l.] Tese de Livre Docência. EESC - USP, 1990.

CALIL, J. C.; CHEUNG, A. B. **Silos: pressões, fluxo, recomendações para o projeto e exemplo de cálculo**. São Carlos: [s.n.].

CALIL, J. C.; NASCIMENTO, J. W. B. DO; ARAUJO, E. C. **Silos Metálicos Multicelulares**. [s.l.] Serviço Gráfico - EESC / USP, 1997.

CEN. **EN 1991-4:2006. Eurocode 1: Actions on Structures. Part 4: Silos and Tanks**. Brussels: [s.n.].

CHEN, J. F. et al. Correlation between the flow pattern and wall pressures in a full scale experimental silo. **Engineering Structures**, v. 29, n. 9, p. 2308–2320, 2007.

CHEN, Y. et al. Static pressure distribution characteristics of powders stored in silos. **Chemical Engineering Research and Design**, v. 154, n. 2014, p. 1–10, 2020.

CHEUNG, A. B. **MODELO ESTOCÁSTICO DE PRESSÕES DE PRODUTOS ARMAZENADOS PARA A ESTIMATIVA DA CONFIABILIDADE ESTRUTURAL DE SILOS ESBELTOS**. [s.l.] Universidade de São Paulo, 2007.

CONAB - COMPANHIA NACIONAL DE ABASTECIMENTO. **Acompanhamento da safra brasileira de grãossafra 2021/22, n. 4 quarto levantamento**. Brasilia: [s.n.]. Disponível em: <https://www.conab.gov.br/component/k2/item/download/40788_0ee9dd05157257045355d00863c854b0>.

COUTO, A. et al. Measuring pressures in a slender cylindrical silo for storing maize. Filling, static state and discharge with different material flow rates and comparison with Eurocode 1 part 4. **Computers and Electronics in Agriculture**, v. 96, p. 40–56, 2013.

COUTO, A.; RUIZ, A.; AGUADO, P. J. Design and instrumentation of a mid-size test station for measuring static and dynamic pressures in silos under different conditions - Part I: Description. **Computers and Electronics in Agriculture**, v. 85, p. 164–173, 2012.

COUTO, A.; RUIZ, A.; AGUADO, P. J. Experimental study of the pressures exerted by wheat stored in slender cylindrical silos, varying the flow rate of material during discharge. Comparison with Eurocode 1 part 4. **Powder Technology**, v. 237, p. 450–467, 2013.

DE PAULA, W. C. et al. **AVALIAÇÃO DAS PRESSÕES VERTICAIS NO FUNDO PLANO DE UM SILO ESBELTO**. XLIX Congresso Brasileiro de Engenharia Agrícola - CONBEA 2020. **Anais**...2020

DESHMUKH, O. S. et al. Ring Shear Tester as an in-vitro testing tool to study oral processing of comminuted potato chips. **Food Research International**, v. 123, n. November 2018, p. 208–216, 2019.

DEUTSH, G. P.; SCHMIDT, L. C. Pressures on Silo Walls. **Developments in Geotechnical Engineering**, v. 39, n. C, p. 125–138, 1985.

DIN. **DIN 1055-6: Basis of design and actions on structures – Part 6: design 623 loads for buildings and loads in silo bins**. Berlin, Verlaz: 2005

DOGANGUN, A. et al. Cause of damage and failures in silo structures. **Journal of Performance of Constructed Facilities**, v. 23, n. 2, p. 65–71, 2009.

DPE - DIRETORIA DE PESQUISA E COORDENAÇÃO AGROPECUÁRIA. **IBGE - Pesquisa de Estoques 2º semestre de 2019**. [s.l: s.n.].

DRUCKER, D. C.; PRAGER, W. Soil mechanics and plastic analysis or limit design. **Quart. Appl. Math**, v. 10, n. 2, p. 157–165, 1952.

FANK, M. Z. et al. Vertical pressures and compressive friction force in a large silo. **Engenharia Agricola**, v. 38, n. 4, p. 498–503, 2018.

GALLEGO, E. et al. SIMULATIONS OF GRANULAR FLOW IN SILOS WITH DIFFERENT FINITE ELEMENT PROGRAMS: ANSYS VS. SILO. **Transactions of the ASABE**, v. 53, n. 3, p. 819–829, 2010.

GALLEGO, E.; RUIZ, A.; AGUADO, P. J. Simulation of silo filling and discharge using ANSYS and comparison with experimental data. **Computers and Electronics in Agriculture**, v. 118, p. 281–289, 2015.

GANDIA, R. M. et al. Static and dynamic pressure measurements of maize grain in silos under different conditions. **Biosystems Engineering**, v. 209, p. 180–199, 2021a.

GANDIA, R. M. et al. Influence of specific weight and wall friction coefficient on normal pressures in silos using the Finite Element Method. **Revista Engenharia na Agricultura - Reveng**, v. 29, p. 192–203, 2021b.

GANDIA, R. M. et al. Evaluation of pressures in slender silos varying hopper angle and silo slenderness. **Powder Technology**, v. 394, p. 478–495, 2021c.

GANDIA, R. M. et al. Evaluation of pressures in slender silos varying hopper angle and silo slenderness. **Powder Technology**, v. 394, p. 478–495, 2021d.

GANDIA, R. M. et al. Static and dynamic pressure measurements of maize grain in silos under different conditions. **Biosystems Engineering**, v. 209, p. 180–199, 2021e.

GAYLORD, E. D.; GAYLORD, C. . **Design of steel bins for storage of bulk solids**. New Jersey: Prentice-Hall: [s.n.].

GOMES, F. C.; CALIL, J. C. Estudo Teórico experimental das ações em silos horizontais. **Cadernos de Engenharia de Estruturas**, v. 7, p. 33–62, 2005.

GONZÁLEZ-MONTELLANO, C. et al. Validation and experimental calibration of 3D discrete element models for the simulation of the discharge flow in silos. **Chemical Engineering Science**, v. 66, n. 21, p. 5116–5126, 2011.

GOODEY, R. J.; BROWN, C. J.; ROTTER, J. M. Predicted patterns of filling pressures in thin-walled square silos. **Engineering Structures**, v. 28, n. 1, p. 109–119, 2006.

GUAITA, M.; COUTO, A.; AYUGA, F. Numerical simulation of wall pressure during discharge of granular material from cylindrical silos with eccentric hoppers. **Biosystems Engineering**, v. 85, n. 1, p. 101–109, 2003.

GUTIÉRREZ, G. et al. Silo collapse under granular discharge. **Physical Review Letters**, v. 114, n. 1, p. 5–9, 2015.

HÄRTL, J. et al. The influence of a cone-in-cone insert on flow pattern and wall pressure in a full-scale silo. **Chemical Engineering Research and Design**, v. 86, n. 4, p. 370–378, 2008.

HOLST, J. M. F. G. et al. Numerical Modeling of Silo Filling. I: Continuum Analyses. **Journal of Engineering Mechanics**, v. 125, n. 1, p. 94–103, 1999.

INTERNACIONAL ORGANIZATION FOR STANDARDIZATION. **ISO 11697:2012. Bases for design of strutures - Loads due to bulk materials**. [s.l: s.n.].

JA. B LVIN. Analytical Evaluation of Pressures of Granular Materials on Silo Walls. **Powder Technology**, v. 4, n. 5, p. 280, 1971.

JANSSEN, H. A. Versuche uber getreidedruck in silozellen. **Z. Ver. Dtsch. Ing**, v. 39, n. 35, p. 1045–1049, 1895.

JENIKE, A. . **Storage and Flow of Bulk Solids Bull. 123**. USA: University of Utah, 1964.

JENIKE, A. W.; JOHANSON, J. R.; CARSON, J. W. Bin loads—part 3: mass-flow bins. **Journal of Manufacturing Science and Engineering, Transactions of the ASME**, v. 95, n. 1, p. 6–12, 1973a.

JENIKE, A. W.; JOHANSON, J. R.; CARSON, J. W. Bin Loads—Part 4: Funnel-Flow Bins. **Journal of engineering for Industry**, v. 95, p. 13–20, 1973b.

LOPES NETO, J. P.; NASCIMENTO, J. W. B. DO; FANK, M. Z. Forças verticais e de atrito em silos cilíndricos com fundo plano. **Revista Brasileira de Engenharia Agrícola e Ambiental**, v. 18, n. 6, p. 652–657, 2014.

MILANI, A. P. **Determinação das propriedades de produtos armazenados para o projeto de pressões e fluxo em silos**. [s.l.] Universidade de São Paulo, 1993.

MINISTÉRIO DA AGRICULTURA PESCA Y ALIMENTACIÓN. **Avances de superficies y producciones agrícolas. Diciembre 2020**. [s.l: s.n.].

MOYA, M. et al. MECHANICAL PROPERTIES OF GRANULAR AGRICULTURAL MATERIALS. **Transactions of the ASABE**, v. 45, n. 5, p. 1569–1577, 2002.

NASCIMENTO, J. W. B. DO; LOPES NETO, J. P.; MONTROSS, M. D. Horizontal pressures in cylindrical metal silos and comparison with different international standards. **Engenharia Agricola**, v. 4, p. 601–611, 2013.

NIELSEN, J. Pressures from flowing granular solids in silos. **Philosophical Transactions of the Royal Society A: Mathematical, Physical and Engineering**

**Sciences**, v. 356, n. 1747, p. 2667–2684, 1998.

NIELSEN, J. From silo phenomena to load models. In: CHEN, J. F.; TENG, J. G. (Eds.). . **Structures and Granular Solids: From Scientific Principles to Engineering Applications**. Boca Raton, USA: CRC Press-Taylor & Francis Group, 2008. p. 49–57.

NIELSEN, J.; ASKEGAARD, V. Scale errors in model tests on granular media with special reference to silo models. **Powder Technology**, v. 16, n. 1, p. 123–130, 1977.

PALMA, G. **PRESSÕES E FLUXO EM SILOS ESBELTOS (h/d≥1,5)**. [s.l.] Universidade de São Paulo, 2005.

PARDIKAR, K.; ZAHID, S.; WASSGREN, C. Quantitative comparison of experimental and Mohr-Coulomb finite element method simulation flow characteristics from quasi two-dimensional flat-bottomed bins. **Powder Technology**, v. 367, p. 689–702, 2020.

PIEPER, K.; SCHÜTZ, M. **Bericht Über das Forschungsvorhaben - Norm-Mess-Silo für Schüttguteigenschaften**. [s.l.] Technische Universität Braunschweig, 1980.

RAMÍREZ, A. et al. Analysis of Measurements Obtained by Plate-type Pressure Cells Having a Recess - DEM Simulation. **Bulk Solids & Powder – Science & Technology**, v. 4, n. January, 2009.

RAMÍREZ, A.; NIELSEN, J.; AYUGA, F. On the use of plate-type normal pressure cells in silos. Part 1: Calibration and evaluation. **Computers and Electronics in Agriculture**, v. 71, n. 1, p. 71–76, 2010a.

RAMÍREZ, A.; NIELSEN, J.; AYUGA, F. Pressure measurements in steel silos with eccentric hoppers. **Powder Technology**, v. 201, n. 1, p. 7–20, 2010b.

RAVENET, J. **RAVENET, J. Silo: deformaciones, falhas, explosiones, prevencion de. Barcelona, Ed. Tecnicos Associados**Barcelona, 1983.

ROTTER, J. M.; BROWN, C. J.; LAHLOUH, E. H. Patterns of wall pressure on filling a square planform steel silo. **Engineering Structures**, v. 24, n. 2, p. 135–150, 2002.

RUIZ, A.; COUTO, A.; AGUADO, P. J. Design and instrumentation of a mid-size test station for measuring static and dynamic pressures in silos under different conditions - Part II: Construction and validation. **Computers and Electronics in Agriculture**, v. 85, p. 174–187, 2012.

SADOWSKI, A. J.; MICHAEL ROTTER, J.; NIELSEN, J. A theory for pressures in cylindrical silos under concentric mixed flow. **Chemical Engineering Science**, v. 223, p. 115748, 2020.

SADOWSKI, A. J.; ROTTER, J. M. Structural Behavior of Thin-Walled Metal Silos Subject to Different Flow Channel Sizes under Eccentric Discharge Pressures. **Journal of Structural Engineering**, v. 138, n. 7, p. 922–931, 2012.

SALEHI, H. et al. Temperature and Time Consolidation Effect on the Bulk Flow Properties and Arching Tendency of a Detergent Powder. **Chemical Engineering and**

**Technology**, v. 43, n. 1, p. 150–156, 2020.

SCHULZE, D. Silos – Design Variants and Special Types. **Bulk Solids Handling**, v. 16, n. 2, 1996.

SCHURICHT, T.; FURLL, C.; EENSTAD, G. G. Full scale silo tests and numerical simulations of the „cone in cone" concept for mass flow. In: **Handbook of Powder Technology**. [s.l.] Elsevier Science BV, 2001. v. 10p. 175–180.

SCHWAB, C. V et al. WHEAT LOADS AND VERTICAL PRESSURE. v. 37, n. 5, p. 1613–1619, 1994.

SCHWEDES, J. Evolution of bulk solids technology since 1974. **Bulk solids handling**, v. 3, n. 1, 1983.

SONG, C. Y.; TENG, J. G. Buckling of circular steel silos subject to code-specified eccentric discharge pressures. **Engineering Structures**, v. 25, n. 11, p. 1397–1417, 2003.

SUN, W. et al. Multi-scale experimental study on filling and discharge of squat silos with aboveground conveying channels. **Journal of Stored Products Research**, v. 88, p. 101679, 2020.

SUN, Y.; WANG, Y. Collapse reasons analysis of a large steel silo. **Advanced Materials Research**, v. 368–373, p. 647–650, 2012.

TEIXEIRA, L. G.; GOMES, F. C. **Determinação dos ângulos de atrito interno, efetivo e do ângulo de atrito com a parede do produto café utilizando a máquina de cisalhamento TSG 70-140**. Congresso Brasileiro de Engenharia Agrícola. **Anais**...Goiânia: 2003

TENG, B. J. PLASTIC COLLAPSE AT LAP JOINTS IN PRESSURIZED CYLINDERS UNDER AXIAL LOAD. v. 120, n. 1, p. 23–45, 1994.

TENG, J. G.; LIN, X. Fabrication of small models of large cylinders with extensive welding for buckling experiments. **Thin-Walled Structures**, v. 43, n. 7, p. 1091–1114, 2005.

TENG, J. G.; ROTTER, J. M. Plastic collapse of restrained steel silo hoppers. **Journal of Constructional Steel Research**, v. 14, n. 2, p. 139–158, 1989.

TENG, J. G.; ZHAO, Y.; LAM, L. Techniques for buckling experiments on steel silo transition junctions. **Thin-Walled Structures**, v. 39, n. 8, p. 685–707, 2001.

TENG, J.; ROTTER, J. M. Collapse Behavior and Strength of Steel Silo Transition Junctions. Part I: Collapse Mechanics. **Journal of Structural Engineering**, v. 117, n. 12, p. 3587–3604, 1991.

WALKER, D. An approximate theory for pressures and arching in hoppers. **Chemical Engineering Science**, v. 22, n. 3, p. 486, 1967.

WALTERS, J. K. A theoretical analysis of stresses in axially-symmetric hoppers and

bunkers. **Chemical Engineering Science**, v. 28, n. 3, p. 779–789, 1973a.

WALTERS, J. K. A theoretical analysis of stresses in silos with vertical walls. **ChemicalEngineering Science**, v. 28, p. 13–21, 1973b.

WENZEL, F. Pressure behavior in double cylindrical silos. **Journal of Manufacturing Science and Engineering, Transactions of the ASME**, v. 95, n. 1, p. 97–100, 1973.

WÓJCIK, M. et al. Full-scale experiments on wheat flow in steel silo composed of corrugated walls and columns. **Powder Technology**, v. 311, p. 537–555, 2017.

WÓJCIK, M.; TEJCHMAN, J.; ENSTAD, G. G. Confined granular flow in silos with inserts - Full-scale experiments. **Powder Technology**, v. 222, p. 15–36, 2012.

WPMPS. **Standart Shear Testing Technique for Particulate Solids Using the Jenike Shear Cell“**. England: [s.n.].

YÁÑEZ, Á. C.; FEMÁNDEZ, M. G.; LÓPEZ, P. V. ANÁLISIS DE LA DISTRIBUCIÓN DE PRESIONES ESTÁTICAS EN SILOS CILÍNDRICOS CON TOLVA EXCÉNTRICA MEDIANTE EL M. E. F. INFLUENCIA DE LA EXCENTRICIDAD Y COMPARACIÓN CON EL EUROCÓDIGO 1. **Informes de la Construcción**, v. 52, n. 472, p. 17–27, 2001.

ZEGZULKA, J. The angle of internal friction as a measure of work loss in granular material flow. **Powder Technology**, v. 233, p. 347–353, 2013.

ZHAO, Q.; JOFRIET, J. C. Structural loads on bunker silo walls: Numerical study. **Journal of Agricultural Engineering Research**, v. 51, n. C, p. 1–13, 1992.

ZHAO, Y.; TENG, J. G. Buckling experiments on steel silo transition junctions. II: Finite element modeling. **Journal of Constructional Steel Research**, v. 60, n. 12, p. 1803–1823, 2004.

ZHONG, Z.; OOI, J. Y.; ROTTER, J. M. The sensitivity of silo flow and wall stresses to filling method. **Engineering Structures**, v. 23, n. 7, p. 756–767, 2001.

## SECOND PART

### Article 1 – Static and dynamic pressure measurements of maize grain in silos under different conditions - Biosystems Engineering journal (published version)

The article was published in the Biosystems Engineering Journal (ISSN 1537-5110). The journal has the qualis A1 and JCR 4.123.

DOI: https://doi.org/10.1016/j.biosystemseng.2021.07.001.

Available online at www.sciencedirect.com

ScienceDirect

journal homepage: www.elsevier.com/locate/issn/15375110

Research Paper

# Static and dynamic pressure measurements of maize grain in silos under different conditions

Rômulo Marçal Gandia [a,c,*], Francisco Carlos Gomes [a], Wisner Coimbra de Paula [b], Estácio Antunes de Oliveira Junior [a], Pedro José Aguado Rodriguez [c]

[a] Federal University of Lavras (UFLA), Agricultural Engineering Department, Brazil
[b] Federal University of Lavras, Engineering Department, Brazil
[c] University of León, Agricultural Engineering Department, Spain

ARTICLE INFO

*Article history:*
Received 26 March 2021
Received in revised form
24 June 2021
Accepted 4 July 2021
Published online 17 July 2021

*Keywords:*
Test silo validation
Full-scale experimental station
Concentric hopper
Friction and normal pressures
Slender silo

Silos are used worldwide to store products of high commercial value. However, many questions remain unanswered regarding storage and estimation of pressures in silos. Furthermore, there are few full-scale experimental stations in the world to facilitate the study of silo pressures, hindering progress in this area. The aim of this paper is to describe the setup, calibration, and validation of a pilot-scale test facility. The pilot silo described here contains 59 measurement cells capable of measuring loads and pressures throughout the silo. In addition, it can be used to study maximum and dynamic pressures in the filling, static, and discharge phases using a range of stored products. Validation of this test facility using maize yielded reliable and novel results, which were compared with Eurocode 1, part 4 (CEN, 2006). Pressures were obtained in the pilot silo at two different grain heights: 2.77 m and 5.30 m, and were evaluated in all three filling, static, and discharge phases. Normal and friction pressures in the silo, vertical stress at the silo–hopper transition, product weight, flow rate, and test time were recorded. The results obtained were consistent with the standard and the findings reported in other studies, demonstrating the accuracy of the pilot silo calibration and thus validating the experimental model. Some of the novel findings obtained include the moment of maximum pressure at the transition during discharge and the influence of silo slenderness on settling of the material during filling and under static conditions.



* *Corresponding author.*
E-mail addresses: romagandia@gmail.com (R.M. Gandia), fcgomes@ufla.br (F.C. Gomes), wisner.depaula@ufla.br (W.C. Paula), estacioantunes@estudante.ufla.br (E.A. Oliveira Junior), pedro.aguado@unileon.es (P.J. Aguado Rodriguez).
https://doi.org/10.1016/j.biosystemseng.2021.07.001

**Nomenclature**

*Symbols*

| | |
|---|---|
| Ø | Angle of internal friction, degrees |
| A | Plan cross-sectional area of vertical walled segment, $m^2$ |
| $d_i$ | Internal cylinder diameter, m. |
| $F_{h(1,12)u,t}$ | Force in tension load cell positioned on the upper part of the spring set - rings 1 to 12, at time t, kN |
| $F_{h(1,12)d,t}$ | Force in tension load cell positioned on the lower part of the spring set - rings 1 to 12, at time t, kN |
| $F_{w(1,12)r,t}$ | Force in tension load cell positioned on the right side of the ring support - rings 1 to 12, at time t, kN |
| $F_{w(1,12)l,t}$ | Force in tension load cell positioned on the left side of the ring support - rings 1 to 12, at time t, kN |
| $F_{vtr,t}$ | Force in tension load cell positioned on the right side of the hopper support, at time t, kN |
| $F_{vtl,t}$ | Force in tension load cell positioned on left side of the hopper support, at time t, kN |
| $F_{vbr,t}$ | Force on shear beam load cell positioned at the base of the right pillar, time t, kN |
| $F_{vbl,t}$ | Force on shear beam load cell positioned at the base of the left pillar, time t, kN |
| h | Ring height, m. |
| K | Characteristic value of lateral pressure ratio |
| $P_{ntr,t}$ | Normal pressure on the right hopper wall next to the silo–hopper transition, time t, kPa |
| $P_{ntl,t}$ | Normal pressure on left hopper wall next to the silo–hopper transition, time t, kPa |
| $P_{nir,t}$ | Normal pressure on right hopper wall between the silo–hopper transition and outlet, time t, kPa |
| $P_{nil,t}$ | Normal pressure on left hopper wall between the silo–hopper transition and outlet, time t, kPa |
| $P_{nitr,t}$ | Normal pressure on right hopper wall between the silo–hopper transition and outlet, near transition, time t, kPa |
| $P_{nitl,t}$ | Normal pressure for left hopper wall between the silo–hopper transition and the outlet, near transition, time t, kPa |
| $P_{nior,t}$ | Normal pressure on right hopper wall between the silo–hopper transition and outlet, near outlet, time t, kPa |
| $P_{niol,t}$ | Normal pressure on left hopper wall between the silo–hopper transition and outlet, near outlet, time t, kPa |
| $P_{nor,t}$ | Normal pressure on the right hopper wall next to silo outlet, time t, kPa |
| $P_{nol,t}$ | Normal pressure for the hopper wall on the left-hand side next to silo outlet, time t, kPa |
| $P_{h(1,12),t}$ | Normal pressure on cylinder wall from the tension load cells positioned on spring set - rings 1 to 12, time t, kPa |
| $P_{w(1,12),t}$ | Friction pressure for the cylinder wall from the tension load cells positioned on ring supports - rings 1 to 12, time t, kPa |
| $P_{vt,t}$ | Vertical stress of product at the silo–hopper transition from the tension load cells positioned on the hopper support, time t, kPa |
| $P_{v(1,4),t}$ | Vertical stress of product at the silo–hopper transition obtained from the pressure cells (flat bottom), time t, kPa |
| $W_{,t}$: | Weight of stored product, time t, kN |
| $W_{hto}$ | Weight of stored product between the outlet and the silo–hopper transition, zero in the case of the flat bottom, kN |
| $V_{ih}$ | Internal hopper volume, $m^3$ |
| $V_{ic}$ | Internal cylinder volume, $m^3$ |
| $r_i$ | Internal cylinder radius, m. |
| γ | Bulk unit weight |

## 1. Introduction

The study of the behaviour of materials stored in silos dates back to 1895 (Janssen, 1895). Since then, research interest in silos has increased (Butterfield, 1969; Deutsh & Schmidt, 1985; Fank, do Nascimento, Cardoso, Meira, & Willrich, 2018; González-Montellano, Ramírez, Gallego, & Ayuga, 2011; Jenike, 1964; LVIN, 1971; Sadowski, Michael Rotter, & Nielsen, 2020; Walker, 1967; Wenzel, 1973), but there remain many questions to answer and design flaws to resolve (Ayuga, 2008; Bywalski & Kamiński, 2019; Calil, Palma, & Cheung, 2009; Dogangun, Karaca, Durmus, & Sezen, 2009; Fank et al., 2018; Gallego, González-Montellano, Ramírez, & Ayuga, 2011; Nielsen & Rotter, 2018; Piskoty, Michel, & Zgraggen, 2005; Tian & Jiao, 2019).

Nowadays engineering is supported three forms of model: theoretical, experimental, and numerical. In combination, these three types of model have improved and advanced progress in all areas of engineering. As a result, recent years have witnessed a significant increase in studies using the finite element method (FEM) and discrete element method (DEM) in silos (Gallego, Ruiz, & Aguado, 2015; Holst, Ooi, Rotter, & Rong, 1999; Horabik, Parafiniuk, & Molenda, 2016; Kobyłka, Molenda, & Horabik, 2020). However, numerical studies require validation.

Although experimental studies of pressures in silos are associated with some certainties and can sometimes approximate real-life conditions, scale remains a limiting factor for experimental modelling (Nielsen & Askegaard, 1977) particularly with increasing costs restricting the number of full-scale experimental stations around the world (Brown, Lahlouh, & Rotter, 2000; Couto, Ruiz, & Aguado, 2012; Gallego et al., 2011; Härtl et al., 2008; Ruiz, Couto, & Aguado, 2012; Schuricht, Furll, & Eenstad, 2001; Schwab, Ross, White, & Colliver, 1994; Sun et al., 2020; Teng, Zhao, & Lam, 2001; Teng & Lin, 2005; Zhao & Teng, 2004; Zhong, Ooi, & Rotter, 2001). Also, recently few studies have been carried out on full-scale silos (Couto, Ruiz, & Aguado, 2013; Couto, Ruiz, Herráez, Moran, & Aguado, 2013; Ding, Dyrøy, Karlsen,

Enstad, & Jecmenica, 2011; Ramírez, Nielsen, & Ayuga, 2010b, 2010a).

The test facility described has been set up to investigate at full scale the numerous variables that directly influence the behaviour of pressures in silos (Song & Teng, 2003; Zegzulka, 2013), including use of any product with a maximum product diameter < 17 mm (Brown & Nielsen, 1998; Pieper & Schütz, 1980). The facility is designed to permit the study of three types of wall with different degrees of roughness (varying the friction coefficient between the product and the wall); twelve different height/diameter ratios; eight bottoms (1 flat bottom, 4 concentric hoppers (β: 15° to 60°) and three 100% eccentric hoppers (β: 15° to 45°).

Brazil is a continental country with favourable climatic and topographic characteristics for agricultural production with an estimated high grain production of 268.7 million tonnes in 2020 (CONAB, 2020). According to the IBGE (DPE, 2019), Brazil's storage capacity reached 177.7 million tonnes in the second half of 2019, of which silo storage accounted for 86.6 million tonnes.

Nevertheless, Brazil does not yet have a specific standard for silo storage. Therefore, the aim of this study was to describe, calibrate, and validate an experimental facility at the Federal University of Lavras designed to measure the behaviour of pressures in slender metallic cylindrical silos The validation results obtained are compared with Eurocode 1, part 4 (CEN, 2006). A secondary aim was to indicate the range of research that can be performed and future possibilities for the study of silos.

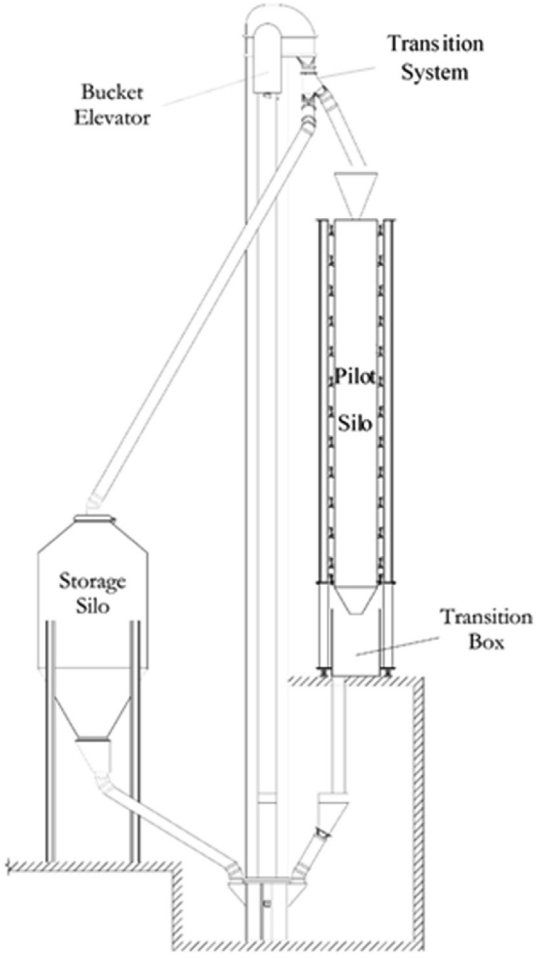


**Fig. 1 – General overview of the test facility.**

## 2. Description

The test facility is based on previously designed by Pieper & Schütz (1980) at the Technical University of Braunschweig in Germany to provide support for DIN 1055-6 (DIN, 2005).

The basis of the experimental facility consists of a slender silo, as this is the most frequently used geometry in the industry, but it could be configured to study different height/diameter ratios. The term "pilot-scale" (Brown & Nielsen, 1998) designates a scale in which the size of the structure compared to the stored product presents a given ratio between silo diameter and product diameter. Therefore, the results obtained here can be used to study real-life structures, as the behaviour of the pilot silo is quantitatively and qualitatively identical to behaviour on a 1:1 scale (full-scale) (Pieper & Schütz, 1980). The scale of the pilot silo is between 1:4 to 1:7, and considering the dimensions of all the instrumentation, the maximum diameter of the product to be stored is 17 mm (i.e., product diameter 40 times smaller than the internal diameter of the silo) (Calil & Cheung, 2007).

Here the structure and components of the test facility and the methodology for obtaining pressures, demonstrating the quality of the instrumentation is described and its validation using maize is reported.

### 2.1. *General description of the test facility*

The test facility has two silos, one to perform the tests (pilot silo) and the other to store the product used in the tests (storage silo). These are connected by a bucket elevator facilitating filling and discharge. A transition box is located between the pilot silo discharge and the elevator, which serves to enable maximum discharge flow and neutralise the influence of the bucket elevator (Fig. 1).

For the validation tests the facility was equipped with a data acquisition system and a portable computer. To measure pressures on the walls and at the bottom and base of the silo under different conditions, pressure cells and load cells were positioned throughout the height of the pilot silo (Fig. 2).

#### 2.1.1. *Pilot silo geometry*

The pilot silo geometry is cylindrical and the structure is metallic with the walls and bases (flat and hopper) made of galvanized steel with a minimum thickness of 10 mm which has rigid behaviour in relation to the stored material.

The silo cylinder is 6 m high and is segmented into 12 independent rings, each measuring 495 mm and separated by a gap of precisely 5 mm (restricting vertical influence between the rings). All the gaps between the rings are sealed with rubber seals, which are changed periodically. Each ring is mounted vertically (with a gap of 5 mm) and joined by two clamps pre-pulled by a set of three coil springs. Two tension load cells are sited on each independent ring, joining the clamps (lower and upper cell in the horizontal position). Each

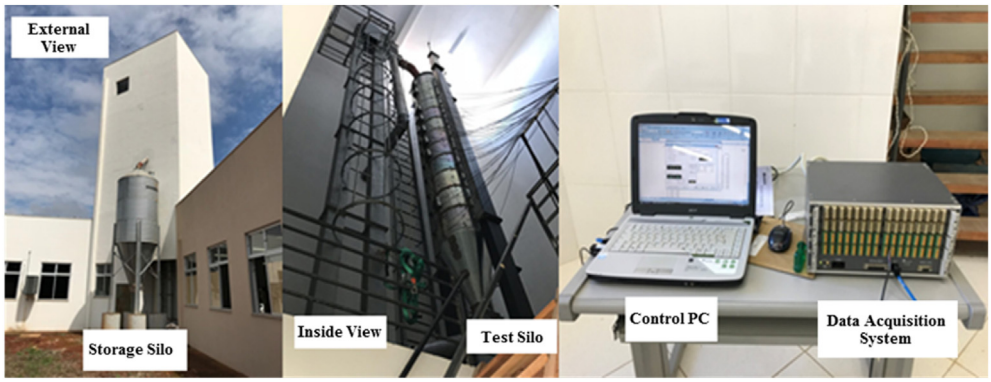


**Fig. 2 – Test silo station and instrumentation.**

ring is supported by two tension load cells attached by stainless steel pins to two pillars and positioned vertically halfway between the two ends of each ring (right and left cell in the vertical position) (Fig. 3).

The pilot silo can be fitted with either a flat or a hopper bottom and the internal diameters of the cylinder and bottoms varied between 645 and 705 mm, depending on the type of wall to be used. All the silo bottoms have the same outlet diameter, 200 mm.

Therefore, the pilot silo can be considered as a slender or intermediate slender silo depending on the depth of the material stored. When the silo is filled up to the height of three or more rings (500 mm each), it corresponds to a slender silo (H = 1.5 m and D = 0.705 m) according to the Eurocode classification (CEN, 2006), since the height/diameter ratio is greater than or equal to 2.

#### 2.1.2. *Pilot silo parts*

The pilot silo was designed for performing tests with several variables. Therefore, it is possible to change the pilot silo configuration. There are eight interchangeable silo bottoms, and all parts are connected vertically by a pair of tension load cells. In addition, each bottom has 4 to 7 openings where the pressure cells are strategically sited (Fig. 4).

The silo walls can also be changed to modify the wall friction coefficient ($\mu$), and there are three different possibilities (Fig. 5). The basic structure of the silo wall is smooth mild carbon steel, and when desired, the other walls can be superimposed onto this.

Thus, it is possible to evaluate concentric and eccentric fillings with twelve height/diameter ratios.

### 2.2. *Instrumentation*

#### 2.2.1. *Measurement cells*

In general, the pilot silo instrumentation consists of 59 measurement cells distributed throughout the pilot silo and connected to the data acquisition system controlled by a portable computer.

The measurement cells consist of two shear beam load cells with a nominal capacity of 50 kN, located at the base of each pillar (Fig. 6a); seven pressure cells with a nominal capacity of 70 kPa, positioned in the hoppers (Fig. 6b) and fifty tension load cells with a nominal capacity of 8 kN, with

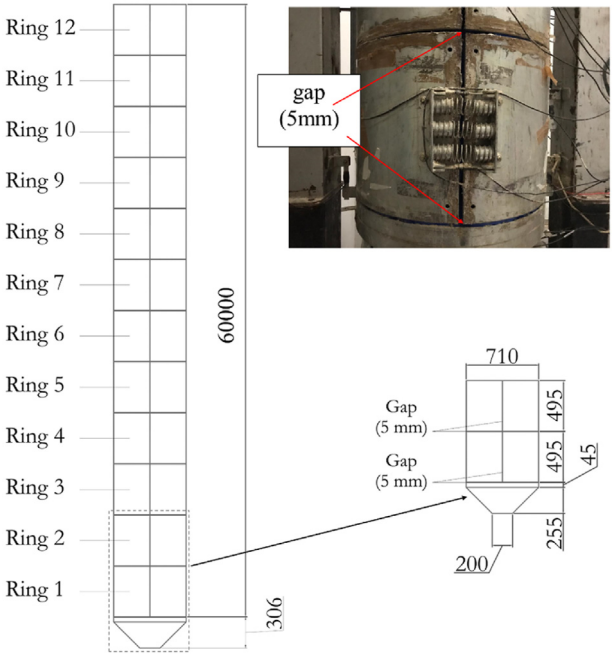


**Fig. 3 – Pilot silo geometry and detailed view of rings.**

twenty-six sited in an upright position, supporting both ends of each ring and the bottom of the silo (Fig. 6c) and twenty-four sited in the horizontal position, joining the clamps that open each ring. The load cell pairs are pre-pulled by three springs (Fig. 6c). All pressure and load cells were made of an aluminium alloy.

#### 2.2.2. *Measuring vertical forces*

Vertical forces in the pilot silo can be measured in four ways: using the tension load cell located between the cylinder ring and the support pillar; using the tension load cell located between the bottom of the silo and the supporting pillar; using the shear beam load cell located at the base of the support pillars; and, when using the flat bottom, using the pressure cell located on the flat bottom.

Vertical forces on the segmented cylinder wall (each independent ring) can be measured by pairs of tension load cells located between the cylinder wall and support pillar: This is the frictional force resulting from the vertical stress of the

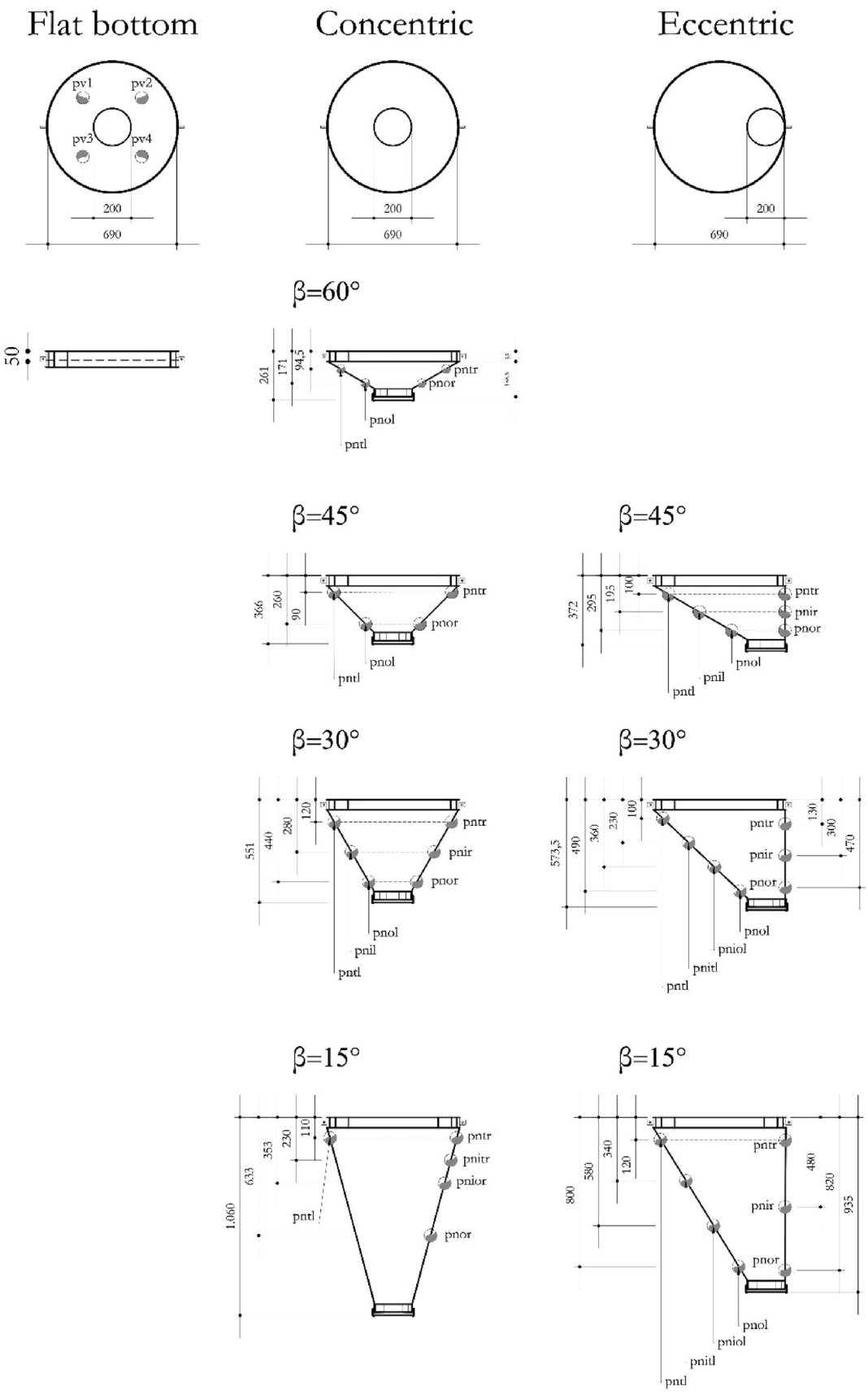


**Fig. 4 – Geometry and instrumentation of the flat bottom and hoppers.**

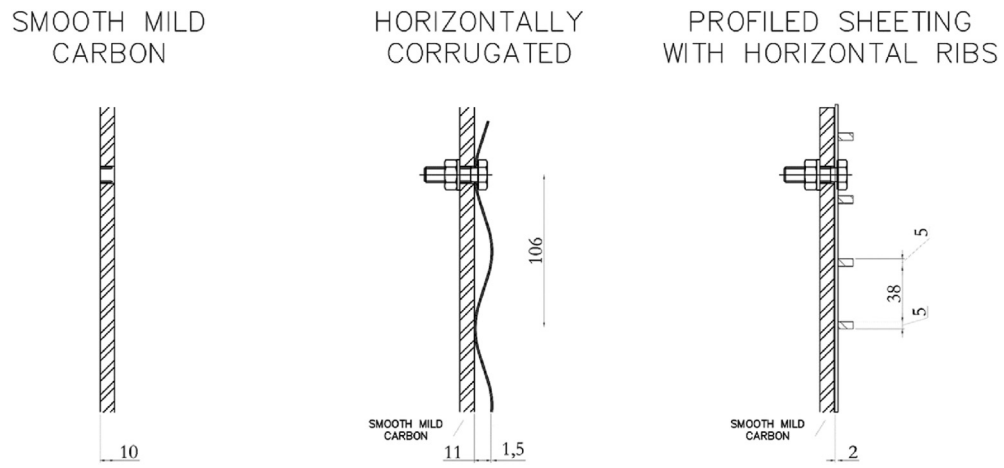


**Fig. 5 – Geometry and profile of the pilot silo walls.**


**Fig. 6 – Location of measurement cells in the pilot silo. (a) Shear beam load cell, pillar base; (b) pressure cell, bottoms; (c) tension load cell, silo rings (vertical - friction, horizontal - normal).**

cylinder wall. It is possible to obtain the frictional force distributed throughout the height of each ring thanks to segmentation of the cylinder and the gaps between each ring, which render them structurally independent.

The pair of tension load cells located between the bottom of the silo (flat bottom or hopper) and the support pillars measure vertical stress in the stored material at the transition. All tension load cells (cylinder and silo bottom) are connected to the two support pillars, making it possible to obtain the weight of the stored material from the values of the shear beam type load cells.

When using the flat bottom, the four pressure cells located on this bottom measure the vertical pressure at the bottom of the silo, which is calculated directly by the pressure cells.

#### 2.2.3. *Measuring horizontal forces*

Horizontal stresses on the cylinder wall are measured using a clamp system joined by two pre-tensioned load cells. Three springs of the same material and dimensions are located between the two cells to pre-pull the system. Each pair of cells is sited in parallel (one above and one below) and centred vertically at the union of the ring opening. The tension load cell and clamp are joined by stainless steel pins, enabling rotation of the system caused by the pressure on the ring walls that tends to disengage the semi cylinder. Thus, it is possible to obtain the horizontal force exerted by the pressure of the stored material.

#### 2.2.4. *Measuring normal pressures*

Normal pressures exerted on the hopper wall are measured directly by pressure cells located immediately below the transition until the outlet. Each hopper has other strategically located cells (Fig. 4), and eccentric hoppers have pairs of pressure cells (at the same level) sited on both sides to measure pressure distribution according to outlet eccentricity.

The distribution of the measurement cells influences the data obtained (Ramírez et al., 2010b; Ruiz et al., 2012). The pressure cells have a gap of 1 mm between the cell and the hopper structure. In addition, the internal parts of the cells are 10 mm high and since the hopper wall thickness is exactly 10 mm this ensures quality in data collection.

#### 2.2.5. *Data acquisition system*

The acquisition of signals was performed using a LYNX data acquisition system, model DS2000, with 4 acquisition cards (2 x AI2160 and 2 x AI2161), yielding a total of 64 channels. This model permits a maximum sampling frequency of 65.5 kHz. The analogue signal sent by each cell (load and pressure) (mV/V) is processed by the A/D converter in a digital reading that is transmitted over the network (Fig. 2).

Preliminary tests were conducted before selecting the sampling frequency to use in tests, which was 2 Hz. At that frequency there was no data leakage and there was relatively good data processing time. Similar sampling speeds were used by Couto et al. (2012) and Ruiz et al. (2012).

## 3. Data processing

### 3.1. Calculation

#### 3.1.1. Normal wall pressures

Normal pressures on the silo wall were calculated by applying the principle of virtual work as shown in Fig. 7. Application of this principle to moments of the ring was necessary because the pressure was measured indirectly through displacement (traction) of the tension load cell pairs.

Observation of the moments in the rings showed that: open ring, the moment ($M_0$) is positive and internal (referring to the pressures exerted by the stored material); closed ring, the moment is negative and external (referring to the initial state of the steel when the ring is closed). The three springs indicate the moment ($M_1$) when the ring is closed. As previously mentioned, the function of the three springs is to pull each ring and cancel the resistance of the negative moment generated by the steel.

By calculating the displacement caused by the unitary force z = 1, it was possible to obtain the value of the normal pressure exerted on the silo wall. Therefore,

$$z = Fh(1,\ 12)u,\ t + Fh(1,\ 12)d,\ t = \frac{\int M_0 \int M_1}{\int M_1^2} r_i.d\phi \quad (1)$$

Solving the above:

$$z = \frac{\int_{0.0721\pi}^{1.9279.\pi} ph.h_r r_i^2.(1-\cos\phi).(r_i - r_i\cos\phi + 4).r_i d\phi}{\int_{0.0721\pi}^{1.9279.\pi} (r_i - r_i\cos\phi + 4)^2.r_i d\phi}$$

$$z = ph.h_r \frac{\int_{0.0721\pi}^{1.9279.\pi} r_i^2.(1-\cos\phi).(r_i - r_i\cos\phi + 4).r_i d\phi}{\int_{0.0721\pi}^{1.9279.\pi} (r_i - r_i\cos\phi + 4)^2.r_i d\phi}$$

For $r_i = \frac{0.705}{2} = 0.353$ m

where $ph$ is the normal pressure on any cylinder ring $Ph(1, 12)$.

Solving Eq. (1), we obtained:

$$Ph(1,\ 12), t = \frac{Fh(1,\ 12)u,\ t + Fh(1,\ 12)d,\ t}{h_r r_i 0.32759} \quad (2)$$

where 0.32759 is the constant value obtained in Eq. (1) using $d_i = 0.705$ m.

Therefore, the normal pressure on each ring was related to the sum of the forces obtained in the tension load cells at each ring ($F_{h(1,12)u,t}$ and $F_{h(1,12)d,t}$), the height of the ring ($h_r = 0.495$ m), the internal radius of the ring ($r_i = 0.353$ m), and the constant value of the moments obtained by the principle of virtual works (0.32759) in Eq. (2).

#### 3.1.2. Frictional wall pressures

The friction pressure on the silo wall was measured indirectly by the pairs of tension load cells located on the vertical support (positioned 180° apart) of each ring. Because the weight of the stored material moves the silo wall (ring) down (vertically), Eq. (3) can be used to calculate the pressure exerted on the perimeter of each ring, while information on the shear stress on the wall (axial symmetrical or not) can be obtained from the pair of tension load cells at each level (1–12).

$$Pw(1,\ 12),\ t = \frac{Fw(1,\ 12)r,\ t + Fw(1,\ 12)l,\ t}{\pi.di.hr} \quad (3)$$

#### 3.1.3. Weight of stored material

The weight of the stored material at a given time ($W_{,t}$) is obtained from the sum of the forces obtained from the beam load cells positioned at the base of the right ($F_{vbr,t}$) and left ($F_{vbe,t}$) columns, using (Eq. (4)):

$$W,t = Fvbr,t + Fvbr,t \quad (4)$$

#### 3.1.4. Vertical stress in the stored product at the transition

Measurement of vertical stress at the silo–hopper transition ($P_{vt,t}$) can begin once the hopper is filled with the stored material ($W_{hto}$), using Eq (5):

$$Pvt,t = \frac{Fvtr,t + Fvtl,t - Whto}{A} \quad (5)$$

The weight of the stored product in the hopper, between the transition and the outlet, ($W_{hto}$) is obtained from Eq. (6):

$$Whto = Vih^*\gamma \quad (6)$$

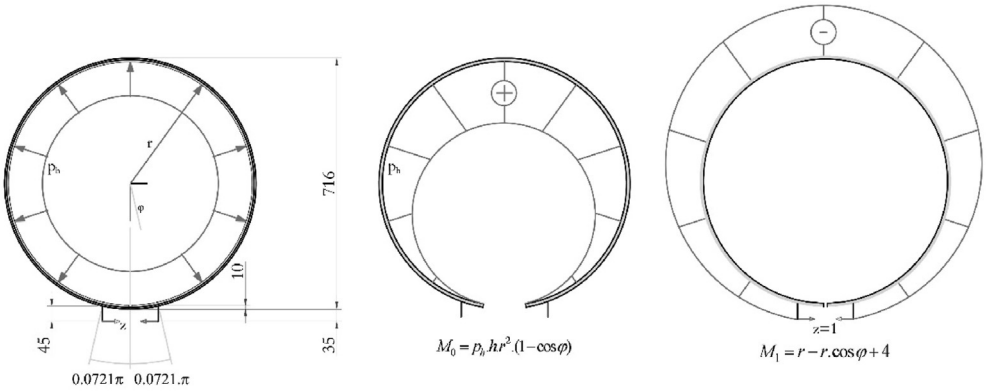


**Fig. 7 – Static scheme for application of the PVW.**

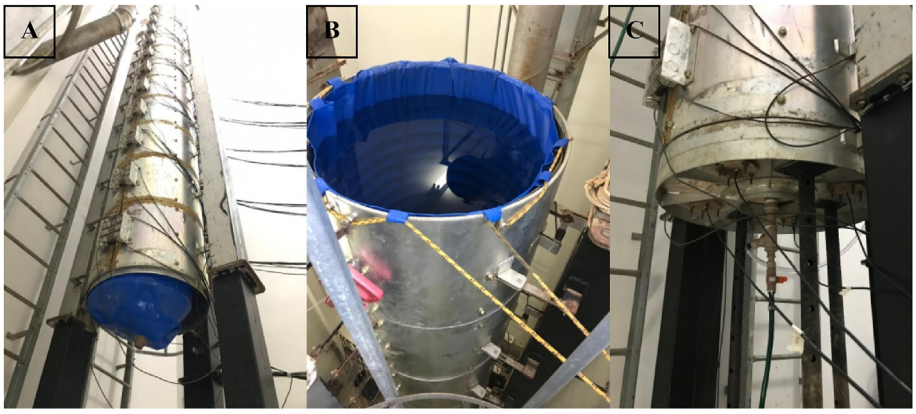


**Fig. 8 – Load test setup.**

Another way to obtain $W_{hto}$ is from direct measurements by the shear beam load cell at the base of the columns ($F_{vbr,\ t}$ and $F_{vbl,\ t}$), shown in Eq. (4). It is possible to determine when the hopper is full because the instrumentation detects the precise moment when the product has passed the silo–hopper transition from the pressure readings in the first ring ($p_{h1,\ t}$).

#### 3.1.5. *Wall friction coefficient*

The wall friction coefficient (μ) was obtained for the entire cylinder (rings 1 to 12) using:

$$\mu(1,12) = \frac{Pw(1,12)}{Ph(1,12)} \tag{7}$$

#### 3.1.6. *Lateral pressure ratio K*

The relationship between horizontal and vertical pressure on the cylinder wall (K) was obtained at any time of interest using:

$$K,t = \frac{Ph(1,12),t}{Pv(1,12),t} \tag{8}$$

#### 3.1.7. *Specific weight of stored material*

The specific weight of the stored material (γ) was obtained from the internal volume of the hopper ($V_{ih}$), the internal volume of the cylinder ($V_{ic}$) (up to the height of the stored product, obtained precisely from the pressure measurements for each cylinder ring), and the weight of the stored material at any given time ($W_{,\ t}$), using Eq. (9):

$$\gamma = \frac{W}{Vih + Vic}$$

## 4. Calibration

### 4.1. *Description of calibration*

As the pilot silo instrumentation consists of three different cell types (pressure cells, shear beam load cells, and tension load cells), different methods were used for calibration.

The pressure cells were calibrated using the pressure of water passing through a graduated tube, whilst the shear beam load cells and tension load cells were calibrated using a universal testing machine. In addition, the shear beam load cells were also calibrated using a compressive strength test and the tension load cells using a tensile strength test.

### 4.2. *Calibration verification*

#### 4.2.1. *General description of the test*

Following calibration, the entire system was checked. A load test was performed using a large, impermeable water pocket that occupied the entire volume of the silo (Fig. 8a) and was filled with water until the reaching the heights of interest (Fig. 8b). Tests were performed using the flat bottom (Fig. 8c).

Calibration of the entire system was verified by means of the load test, using water. However, the tension load cells ($F_{w\ (1.12)\ l,\ t}$ and $F_{w\ (1.12)\ r,\ t}$) used to measure frictional force on the silo wall could not be included in this test because there was no friction between the water and the silo wall. Nonetheless, it was observed that the values obtained by these cells did not fluctuate (they were close to zero at all times and in all tests), as expected.

Two types of test were conducted by varying the height of the water in the silo (2.77 m and 5.55 m), and testing before and after the tests with corn. The objective was to evaluate the dynamics of the measurement cells and determine any possible influence after the tests with corn (changing the hoppers). All tests were performed with three repetitions and produced reliable data. For brevity the only measurements at 2.77 m depth of water will be shown and discussed.

#### 4.2.2. *Calibration with water (2.77 m)*

This simple method consisted of filling the silo with water to a height of 2.77 m, waiting 10 min (static condition), and then emptying the silo completely.

The experimental values obtained for maximum pressures are plotted in Fig. 9 and compared with the theoretical pressure (hydrostatic theory). As can be seen, the experimental data showed an excellent correlation with hydrostatic pressure.

Again, for the sake of brevity, only one randomly selected repetition will be discussed. Figure 10 shows pressures over time, providing a clear illustration of measurement cell behaviour.

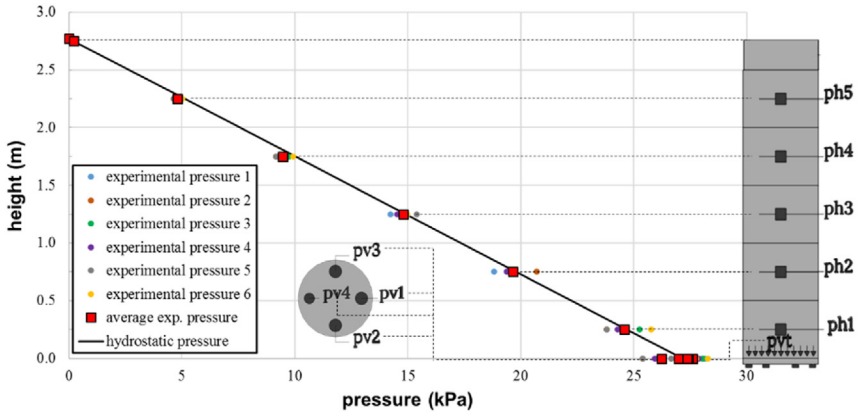


**Fig. 9 – Comparison of maximum normal pressures on the silo wall ($p_{h1}$ to $p_{h5}$) and vertical stress at the transition ($p_{v1}$ to $p_{v4}$) and hydrostatic pressure for the pilot silo, at a filling height of 2.77 m.**

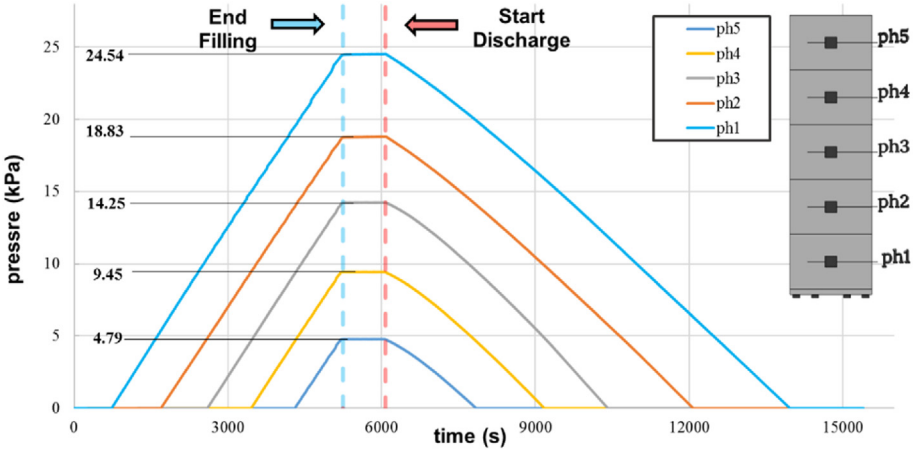


**Fig. 10 – Normal silo wall pressures ($p_{h1,t}$ to $p_{h5,t}$) at each time t, at a filling height of 2.77 m.**

Thus the behaviour of normal pressures on the silo wall presented an excellent correlation with the theory of hydrostatics. Furthermore, equidistance was observed between the pressure values obtained at the top and bottom of each ring (*ph1* to *ph5*), and linear values were obtained for the static phase, as expected.

Vertical stress at the bottom of the silo (*pvt,t*), calculated using Eq. (5), the weight of the stored material (*W,t*), and normal pressure on the silo wall in the first ring (*ph1,t*) also presented an excellent correlation with hydrostatic theory (Fig. 11).

As can be seen in Fig. 12, vertical stress at the bottom of the silo (*pvt,t*) presented only a small deviation between the value calculated by hydrostatic theory. Table 1 confirmed that this deviation did not diverge from hydrostatic theory. From the weight of the stored material (*W,t*), it is possible to obtain the flow rate (Table 1).

The pressure at the bottom of the silo, as measured by the pressure cells (*pv1,t*; *pv2,t*; *pv3,t* and *pv4,t*) (when using the flat bottom), also showed an excellent correlation with hydrostatic pressure (Fig. 12).

Therefore, the calibration and load test data confirm that the pilot silo was well instrumented and capable of producing quality results.

## 5. Validation

### 5.1. *Description of the tests*

To validate the experimental silo, tests were conducted using maize (*Zea mays*). The maize was characterised at the Federal University of Campina Grande laboratory following the method described by Jenike (Jenike, 1964), obtaining values for specific weight ($\gamma$), 8.06 kN m$^{-3}$; wall friction coefficient ($\mu$), 0.24; and humidity, 12.4%.

In order to assess the instrumentation, dynamics, and operation of all measurement cells, the tests were performed at two different material filling heights. The objective was to demonstrate the independence of the rings and obtain reliable data on normal and friction pressures on the silo wall. The heights analysed were 2.7 m and 5.3 m (height/diameter ratio of 3.8 and 7.6, respectively). The tests were performed with 8 repetitions. The product was filled at a constant flow using centralized filling and a concentric hopper with $\beta = 45°$ (Fig. 4). Here, only the highest value obtained by the pressure cell pairs ($P_{nt}$ and $P_{no}$) will be presented, and the effect of the concentricity of pressures on concentric hoppers will be examined in other tests. The tests were conducted in three phases (Fig. 13).

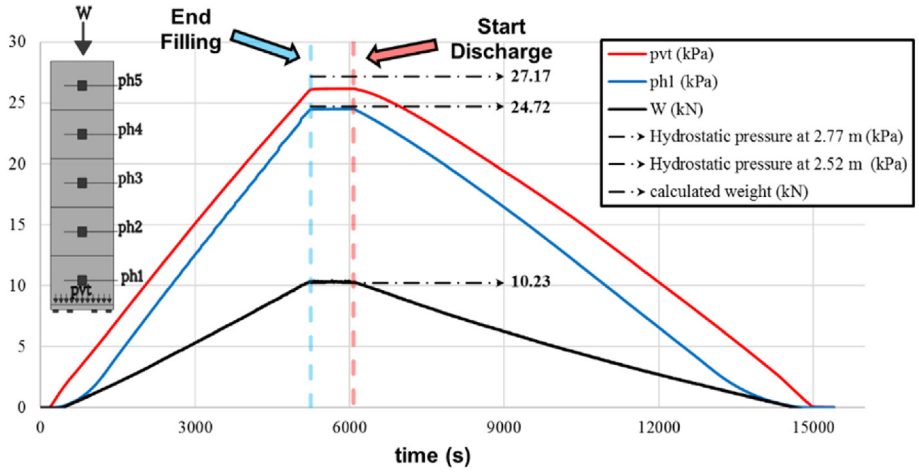


**Fig. 11 – Normal silo wall pressures ($p_{h1,t}$ to $p_{h5,t}$), vertical stress at the transition ($p_{vt,t}$), and weight of the stored material ($W_{,t}$) at time t and at a filling height of 2.77 m.**

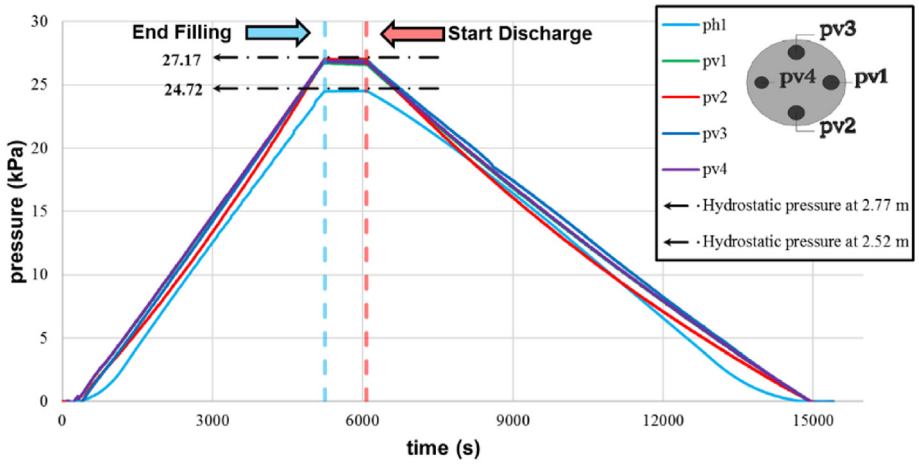


**Fig. 12 – Normal silo wall pressures ($p_{h1,t}$) and vertical stress at the transition ($p_{v1,t}$ to $p_{v4,t}$) at time t and a filling height of 2.77 m.**

**Table 1 – Mean flow for filling and discharge using 2.77 m of water.**

| | Mean value ($l\ s^{-1}$) | | Standard deviation ($l\ s^{-1}$) | |
|---|---|---|---|---|
| Test | Filling | Discharge | Filling | Discharge |
| 2.77 | 0.219 | 0.123 | 0.001 | 0.001 |

In all eight repetitions, the behaviour observed for each filling height was very similar. Therefore, only one analysis of each filling height will be presented. Despite presenting pressure values for two different filling heights, the aim of this article is not to evaluate pressure according to silo slenderness, but to show that the test station yields reliable data. Future research will focus on silo pressures according to height/diameter ratios.

The results obtained were compared with Eurocode 1, part 4 (CEN, 2006). The silo pressures calculated were taken from Annex E, Table E1: Properties of particulate solids, and included specific weight ($\gamma$), 8.0 kN.m-3; friction coefficient of the product with the silo and hopper wall ($\mu$), 0.22 (D1); lateral pressure coefficient (K), 0.53; and internal friction angle ($\emptyset_i$), 31°.

### 5.2. *Results of validation*

The results are divided into two subsections according to product filling heights: 2.77 m (H/D 3.8); and 5.30 m (H/D 7.6). Phase times are given in Table 2 to illustrate the accuracy of the repetitions of the two test configurations and the difference between them.

In order to reduce the interference related to each type of test, the flow rate in the filling and discharge stages was calculated (Table 3), verifying that all tests were performed using the same flow rates.

As can be seen, the discharge flow was at least 4 times greater than the filling flow. Table 4 shows the mean values for all data obtained and the respective deviations for the eight repetitions in each type of test (H/D ratio), at filling heights of 2.7 m and 5.3 m, respectively.

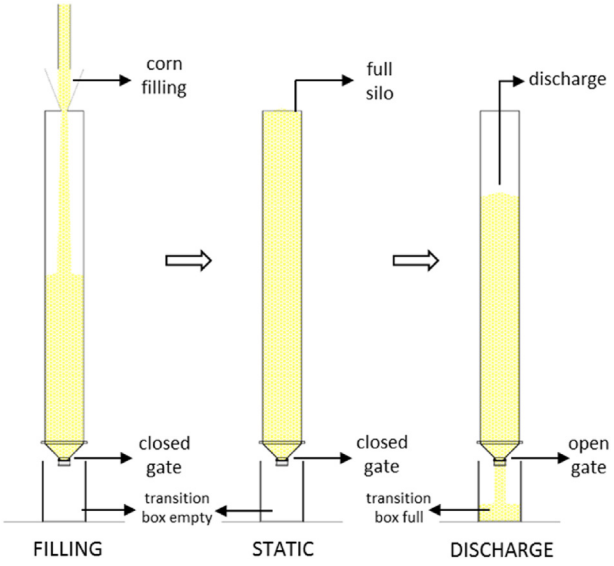


**Fig. 13 – Test configuration. Description of the assays.**

As can be seen, the tests showed little coefficient of variation. Therefore, for each type of test (H/D ratio), one of the eight repetitions was randomly selected for discussion of the results.

5.2.1. *Filling height of 2.7 m (H/D ratio 3.8)*

As can be seen in Fig. 14, maximum pressure at the silo transition ($p_{nt}$) occurred within the first seconds after the start of discharge.

It can also be seen that the variation in the weight of the stored product (W) was linear, making it possible to obtain the flow rate during filling and discharge. Figure 15 is of particular note, because although it shows three different types of measurement cell, it can be seen that the model is accurate, as the data oscillations due to settling peaks of the stored product were synchronised (Fig. 15).

The peaks seen in the three graphs (Fig. 18 A, B, and C) for frictional pressures, normal pressures, and vertical stress in the stored material at the transition occurred at the same times. The settling peaks for frictional pressures (Fig. 15 C) were negative, whereas those for normal pressures in the cylinder (Fig. 15 B) and the hopper, and vertical stress in the stored product at the silo–hopper transition (Fig. 15 A) were positive.

No explanation for this finding could be found in previous studies, but it may have been due to vertical movement of the material (alleviating friction pressure) during settling (increasing normal pressures). The material segregates and compacts, increasing the specific weight at the silo–hopper transition and consequently increasing stress.

**Table 3 – Mean flow for each test.**

| Test | Mean value (kg s$^{-1}$) | | Standard deviation (kg s$^{-1}$) | |
|---|---|---|---|---|
| | Filling | Discharge | Filling | Discharge |
| H/D 3.8 | 4.61 | 21.91 | 0.29 | 0.36 |
| H/D 7.6 | 5.00 | 20.76 | 0.43 | 1.27 |

Demonstrating the accuracy and synchronization of the instrumentation, the first graph (Fig. 15 A) shows the start of each measurement by different types of cell. Firstly, the weight of the stored material (W) was measured, immediately followed by measurement of normal pressure on the hopper wall near the outlet ($p_{no}$). Then, measurement of the vertical stress of the stored product at the silo–hopper transition ($p_{vt}$) began simultaneously with that of normal pressure on the hopper wall near the transition ($p_{nt}$). After less than 1 min, measurement started of normal pressure on the cylinder wall ($p_{h1}$), 250 mm above the transition point.

The same synchronisation is evident in Fig. 15 B for normal pressures on the cylinder. In Fig. 15 C, the start of friction pressure measurements occurred differently from the others due to the slenderness of the silo, causing the material to dissipate throughout filling and increasing friction in the upper rings before the bottom rings.

In addition, Fig. 15 B shows that near the end of filling (190 s), the pressure at $p_{h2}$ presented a value not midway between $p_{h1}$ and $p_{h3}$ but almost the same as pressure *ph3*. A similar behaviour has been reported in other studies (Couto, Ruiz, & Aguado, 2013; Couto, Ruiz, Herráez, et al., 2013).

In the static phase (Fig. 16), although the product had only been static for 10 min, frictional pressure fluctuated (at 554 s) due to settling of the product (i.e. consolidation).

Symmetry was observed in settling, whereby frictional pressures near the bottom of the silo ($p_{w1}$ and $p_{w2}$) showed an increase (positive peak) whereas those located near the top ($p_{w4}$ and $p_{w5}$) showed a decrease (negative peak), while in the middle ($p_{w3}$) there was almost no change. One possible reason for this is may be product settling due to porosity, leading to segregation. The slight vertical movement alleviated frictional pressure in the upper parts of the cylinder but increased that in the lower parts. At discharge, maximum pressures were observed immediately after opening the hopper gate (Fig. 17).

The normal pressure on the hopper wall close to outlet ($p_{no}$) also showed a significant decrease at the start of discharge (5.2–1.0 kPa), subsequently remaining stable until the end of the flow. Meanwhile, the normal pressure on the hopper wall next to the silo–hopper transition ($p_{nt}$) after discharge presented many oscillations (Wójcik, Tejchman, & Enstad, 2012).

Also in relation to $p_{nt}$, it was observed in Fig. 17 that the maximum pressure occurred 8 s after opening the hopper gate

**Table 2 – Time period for each test phase.**

| Test | Mean value (s) | | | | Standard deviation (s) | | | |
|---|---|---|---|---|---|---|---|---|
| | Filling | Static | Discharge | Total | Filling | Static | Discharge | Total |
| H/D 3.8 | 197.9 | 672.0 | 41.9 | 911.8. | 15.9 | 4.8 | 2.8 | 19.1 |
| H/D 7.6 | 355.5 | 680.4 | 84.9 | 1120.8 | 12.6 | 11.2 | 2.8 | 9.6 |

**Table 4 – Measurement variations after filling and discharge.**

| | | H/D 7.6 | | | | H/D 3.8 | | | |
|---|---|---|---|---|---|---|---|---|---|
| | | After filling | | Discharge | | After filling | | Discharge | |
| | | Value | CV (%) | Value | CV (%) | Value | CV (%) | Value | CV (%) |
| *ph10* | (kPa) | 0.60 | 11.11 | 1.64 | 8.15 | – | – | – | – |
| *ph9* | | 1.18 | 15.25 | 2.66 | 10.54 | – | – | – | – |
| *ph8* | | 2.40 | 1.05 | 5.34 | 1.45 | – | – | – | – |
| *ph7* | | 2.55 | 15.27 | 4.72 | 7.40 | – | – | – | – |
| *ph6* | | 3.54 | 5.47 | 5.96 | 1.58 | – | – | – | – |
| *ph5* | | 3.24 | 6.51 | 5.84 | 0.87 | 0.46 | 17.86 | 1.51 | 13.50 |
| *ph4* | | 3.34 | 1.74 | 6.96 | 1.45 | 1.28 | 11.06 | 3.54 | 3.33 |
| *ph3* | | 3.74 | 2.63 | 7.25 | 3.16 | 2.26 | 3.85 | 5.02 | 1.90 |
| *ph2* | | 3.00 | 5.33 | 5.69 | 3.06 | 2.27 | 10.30 | 4.89 | 2.23 |
| *ph1* | | 4.52 | 5.34 | 5.00 | 5.02 | 3.95 | 7.35 | 4.34 | 1.50 |
| *pntl* | | 6.19 | 14.70 | 6.18 | 14.13 | 1.83 | 17.10 | 17.68 | 4.17 |
| *pntr* | | 1.93 | 22.10 | 16.34 | 5.46 | 1.99 | 21.06 | 13.12 | 8.99 |
| *pnol* | | 6.39 | 14.84 | 6.11 | 16.22 | 5.61 | 0.51 | 5.40 | 5.15 |
| *pnor* | | 2.05 | 18.76 | 16.98 | 4.13 | 7.08 | 14.18 | 6.81 | 21.23 |
| *pvt* | | 12.20 | 10.98 | 11.23 | 12.45 | 9.38 | 4.98 | 8.32 | 4.00 |
| W | (kN) | 17.90 | 0.17 | 18.10 | 0.71 | 8.85 | 1.30 | 8.81 | 1.54 |
| *pw10* | (kPa) | 0.23 | 10.59 | 0.49 | 9.95 | – | – | – | – |
| *pw9* | | 0.60 | 2.59 | 0.96 | 5.93 | – | – | – | – |
| *pw8* | | 0.73 | 7.13 | 1.28 | 4.29 | – | – | – | – |
| *pw7* | | 1.08 | 5.17 | 1.41 | 1.67 | – | – | – | – |
| *pw6* | | 1.15 | 1.76 | 1.37 | 1.54 | – | – | – | – |
| *pw5* | | 1.15 | 1.74 | 1.32 | 3.51 | 0.18 | 15.44 | 0.39 | 10.13 |
| *pw4* | | 1.27 | 0.92 | 1.34 | 1.87 | 0.69 | 9.99 | 0.99 | 3.62 |
| *pw3* | | 1.50 | 4.32 | 1.56 | 4.48 | 0.95 | 1.39 | 1.32 | 0.97 |
| *pw2* | | 1.34 | 5.38 | 1.39 | 6.40 | 0.96 | 5.18 | 1.29 | 1.47 |
| *pw1* | | 1.88 | 12.42 | 1.96 | 6.78 | 1.67 | 3.11 | 1.77 | 1.24 |

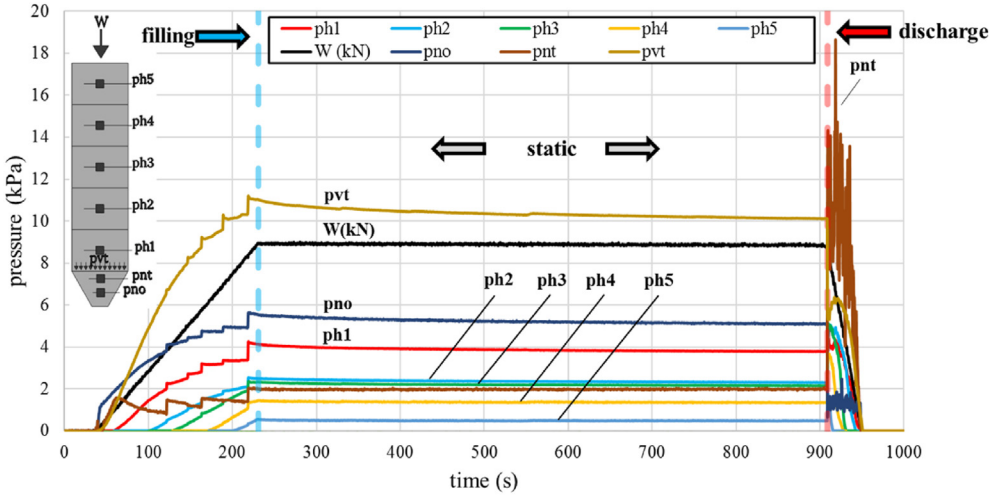


**Fig. 14 – Normal silo wall pressures ($p_{h,t}$; $p_{nt,t}$; $p_{no,t}$), vertical stress in the stored material at the transition ($p_{vt,t}$), and weight of the stored material ($W_{,t}$) at each time t, at a filling height of 2.77 m.**

(2–18.8 kPa). According to (Ruiz et al., 2012), maximum pressures in slender silos (in their study, H/D ratio = 2) occur in the first 10 s after discharge. This significant change in pressures ($p_{vt}$ and $p_{h1}$) led to an increase in the lateral pressure ratio (*K*), which rose from 0.44 to 1.10 (250%) (Fig. 18).

Thus, immediately after discharge, the lateral pressure ratio (*K*) exceeded that given by Eurocode 1, part 4. The standard only provides one value for *K* (0.54), considering solely the stored product.

Normal and friction pressures on the cylinder wall also showed maximum pressure at the time of discharge (Fig. 19).

The lowest normal overpressure occurred at the position closest to the transition ($p_{h1}$) (Fig. 19 A). The maximum normal pressures on the cylinder wall occurred at 1.25 m above the transition ($p_{h3}$), at 0.75 m ($p_{h2}$) and at 1.75 m ($p_{h4}$), respectively. The largest increase in maximum pressure ($p_{h3}$) was from 2.1 to 5.1 kPa (increase of 243%).

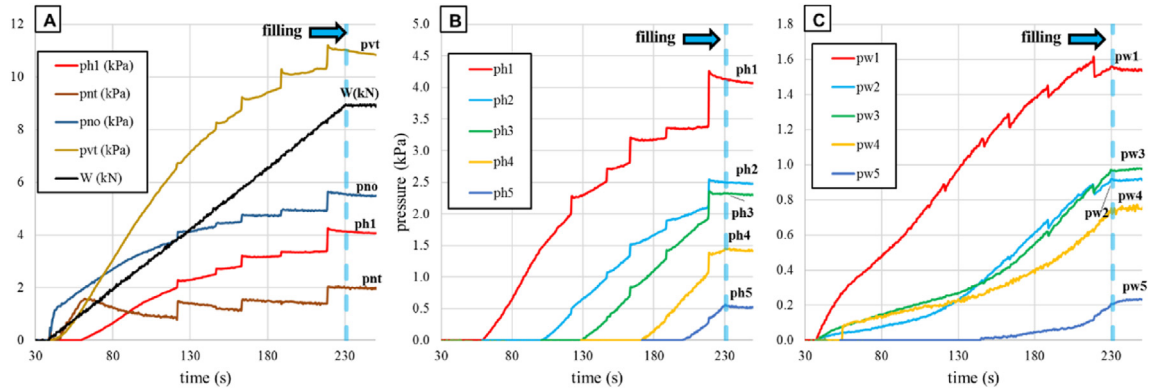


**Fig. 15 – Normal and frictional silo wall pressures ($p_{h,t}$; $p_{nt,t}$; $p_{no,t}$; $p_{w,t}$), vertical stress in the stored material at the transition ($p_{vt,t}$), and weight of the stored material ($W_t$) for each time t during filling, at a filling height of 2.77 m. (a) vertical stress in the stored material at the transition, weight of the stored material, and normal silo hopper wall pressures; (b) normal silo cylinder wall pressures; (c) frictional silo cylinder wall pressures.**

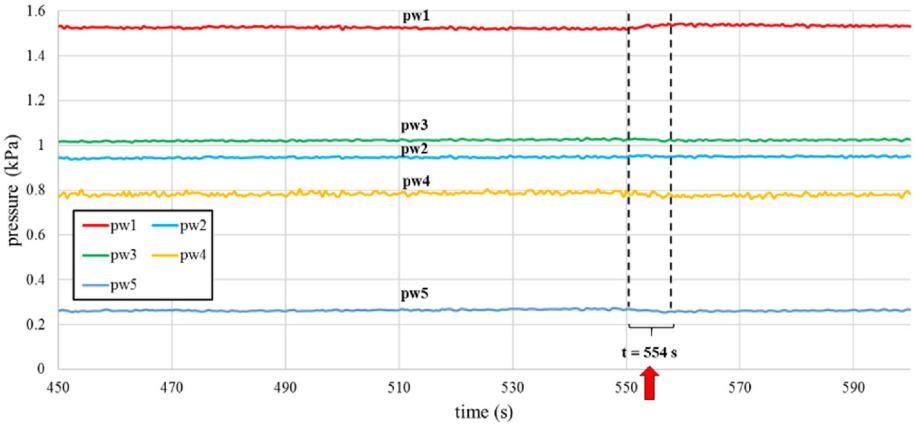


**Fig. 16 – Frictional silo wall pressures ($p_{w,t}$) for each time t during the static phase, at a filling height of 2.77 m.**

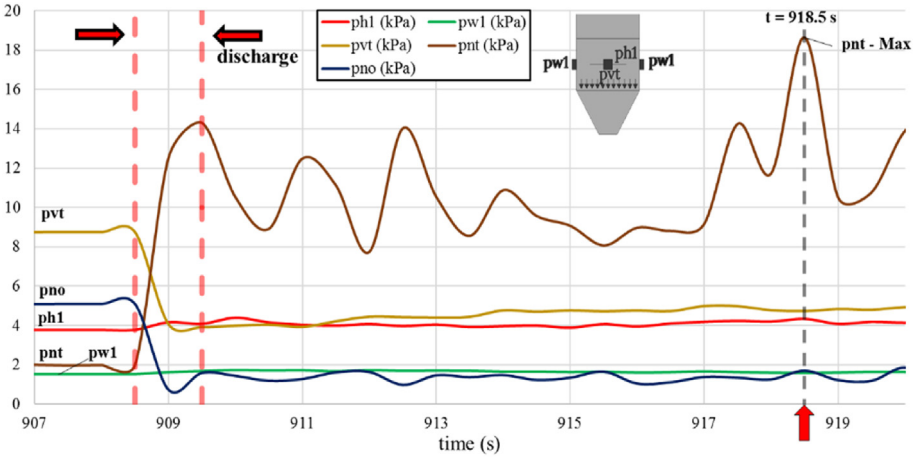


**Fig. 17 – Normal silo wall pressures ($p_{h1,t}$; $p_{nt,t}$; $p_{no,t}$), frictional silo wall pressures ($p_{w1}$), and vertical stress in the stored material at the transition ($p_{vt,t}$) for each time t during the first few seconds after the start of discharge, at a filling height of 2.77 m.**

It is interesting to note that maximum normal pressures occurred at a height of 0.75–1.25 (1/3 of the height of the silo), and that the normal and frictional pressures intersected. One possible explanation for this might be the formation of mechanical arcs or areas of static material below 0.75 m, possibly influenced by silo slenderness and hopper angle.

The values obtained for maximum normal pressures on the silo and hopper wall (Fig. 20 A) and the maximum friction pressures on the silo wall (Fig. 20B) were compared with Eurocode 1, part 4.

As can be seen in Fig. 20, the maximum normal pressures on the silo wall (Fig. 20 A) did not present the behaviour given by Eurocode 1, part 4 and were lower than that given by the standards, a behaviour similar to this has also been reported by Ruiz et al. (2012). The reason for the increase at discharge (814.33%) in maximum normal pressure on the hopper wall near the transition ($p_{nt}$) has already been well defined by other authors and in the standards (CEN, 2006; Couto, Ruiz, Herráez, et al., 2013; International Organization for Standardization, 2012; Jenike, Johanson, & Carson, 1973; Ramírez et al., 2010b; Walker, 1967; Wójcik et al., 2012).

Also differing from the behaviour given by Eurocode 1, part 4 was the maximum friction pressures on the silo wall that exhibited wave behaviour (Fig. 20 B), and the friction pressure on the silo wall near the transition ($p_{w1}$, 0.25 m) exceeded the values in the standard during the filling.

Under static conditions, the maximum friction pressures (Fig. 20 B) were noticably higher than the filling pressures and differed from maximum normal pressures, providing further support for the explanation related to settling of the stored product in static state.

### 5.2.2. *Filling height of 5.30 m (H/D ratio 7.6)*

Once again, the symmetry of normal pressures in the cylinder (*ph1*, 10) and the linearity of the weight of the stored product (*W*) (Fig. 21) provide evidence of the quality of the instrumentation.

Friction and normal pressure peaks during settling of the stored product under static conditions increased in parallel with the height (slenderness) of the stored product. This can be seen in Fig. 22, where the peaks at 654 s was greater in magnitude than those in Fig. 16 (2.77 m).

An analysis of the same moment (654 s) indicated that settling was related to normal and friction pressures on the cylinder wall, whereby normal pressures on the cylinder wall (Fig. 22 A) increased in the upper rings ($p_{h6}$ to $p_{h10}$), decreased in $p_{h5}$ (middle of the silo), and remained almost static in the lower rings ($p_{h1}$ to $p_{h4}$).

The statement made in relation to a silo slenderness of 3.8 is further reinforced here, but with values of a greater magnitude. As shown in Fig. 22 B, the behaviour of the settling peaks in relation to frictional pressures was clearly evident, showing the same symmetry as that illustrated in Fig. 16. In addition, it is possible to see the exact moment (654 s) that settling generally occurred in the cylinder.

Figure 23 shows a more frequent occurrence of settling during filling, compared to a lower filling height (Fig. 15).

The pressure at *ph2* (0.75 m) intersected with the others, whilst the pressure at *ph6* (2.75 m) showed a considerable increase. The results shown in Fig. 19 A for normal pressures were observed more clearly with greater slenderness.

The behaviour of friction pressures (Fig. 23 B) was similar to that observed at a height of 2.77 m (Fig. 15 B), whereby the friction pressure on the wall at $p_{w2}$ (0.75 m) was lower than at $p_{w3}$ (1.25 m), further supporting the notion of a possible static zone in this region (0.75 m).

Behaviour at the time of discharge (Fig. 24) was similar to that shown in Fig. 17 (2.77 m), whereby maximum pressure occurred in *pnt* whereas *pvt* and *pno* showed considerable decreases.

With a lower product height (2.7 m), the maximum pressure occurred at 10.5 s after the start of the discharge (Fig. 17), but with a greater product height (i.e. greater slenderness), the maximum pressure in $p_{nt}$ occurred after 24 s (time t = 1106.5 s) (Fig. 24).

The moment that maximum normal pressure occurs at the silo transition was influenced by silo slenderness. Thus, in contrast to the values obtained at a height of 2.77 m (Fig. 18), at this product height (Fig. 25), the lateral pressure ratio (*K*) did not present such high values.

Although the *K* value was 0.33 during filling and under static conditions, it reached 0.56 during discharge, which is higher than the value given by Eurocode 1, part 4 (0.53). The maximum normal pressure on the cylinder wall occurred 17 s after the start of the discharge (Fig. 26), differing from the result obtained at 2.77 m (10 s) (Fig. 19). Again, this supports the notion that slenderness influences the time of occurrence

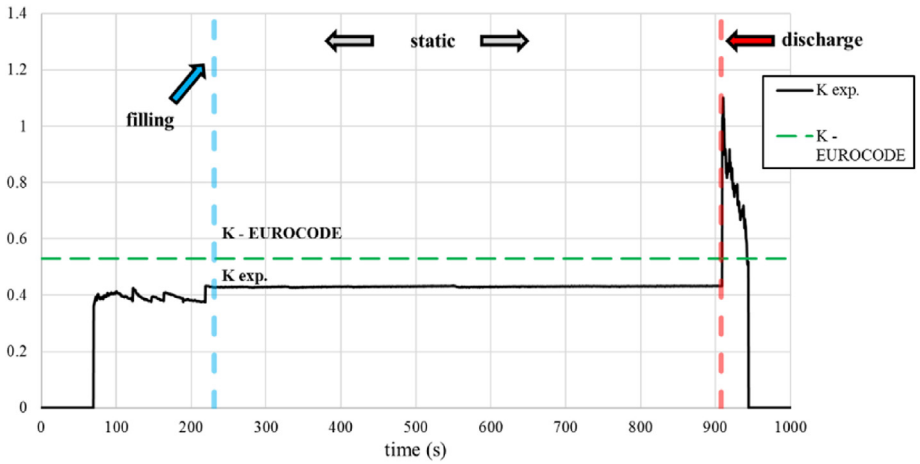


**Fig. 18 – Comparison between the values obtained for the pilot silo and those given by Eurocode 1, part 4, for lateral pressure ratio at the transition ($K_t$) at each time t, at a filling height of 2.77 m.**

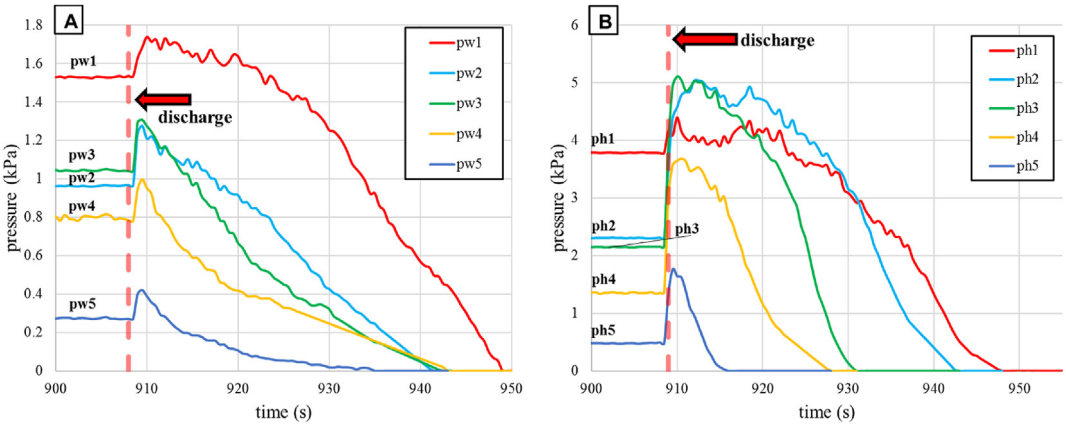


**Fig. 19 – Normal and frictional silo cylinder wall pressures ($p_{h,t}$; $p_{w,t}$) for each time t during discharge, at a filling height of 2.77 m.**

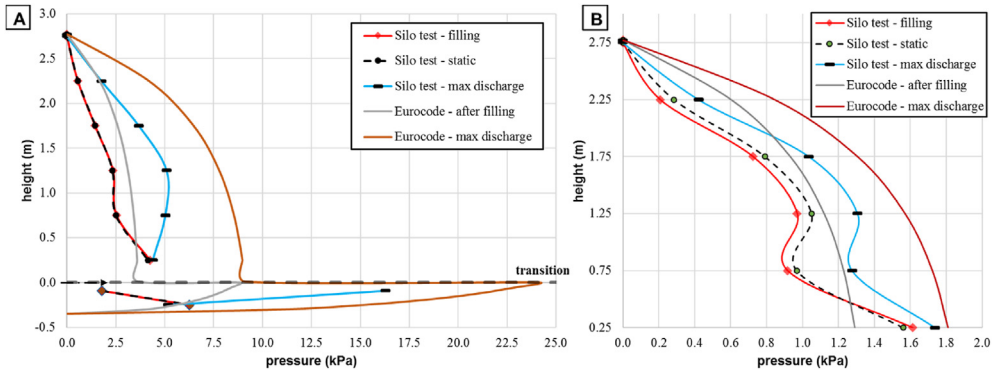


**Fig. 20 – Comparison of maximum normal and friction pressures on the silo wall given by Eurocode 1, part 4, and obtained for the pilot silo, at a filling height of 2.77 m.**

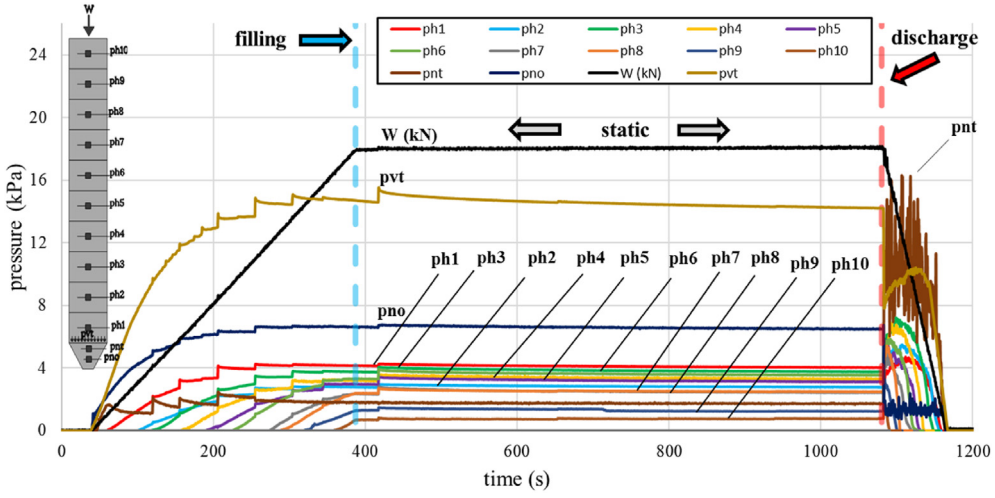


**Fig. 21 – Normal silo wall pressures ($p_{h,t}$; $p_{nt,t}$; $p_{no,t}$), vertical stress in the stored material at the transition ($p_{vt,t}$), and weight of the stored material ($W_{,t}$) at each time t, at a filling height of 5.30 m.**

of maximum normal pressure on the silo and hopper walls after the start of discharge.

In this case, maximum normal pressures occurred between the heights of 1.25 and 1.75 m (between 1/4 to 1/3 of the height of the cylinder), whereas at less slenderness it occurred at 1/3 of the height of the cylinder (Fig. 19).

The final moment of pressure on each of the cylinder rings is shown in Fig. 26, further supporting the quality of the

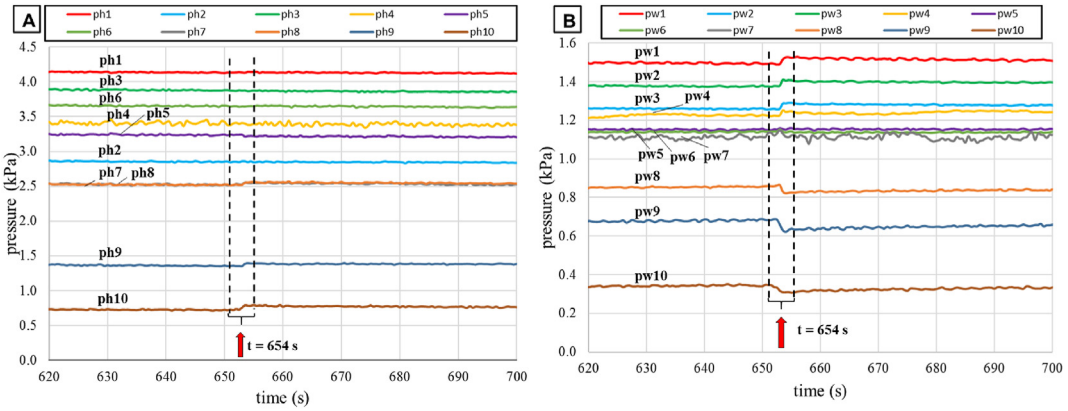


**Fig. 22 – Normal silo wall pressures ($p_{h,t}$; $p_{w,t}$) for each time t under static conditions, at a filling height of 5.30 m.**

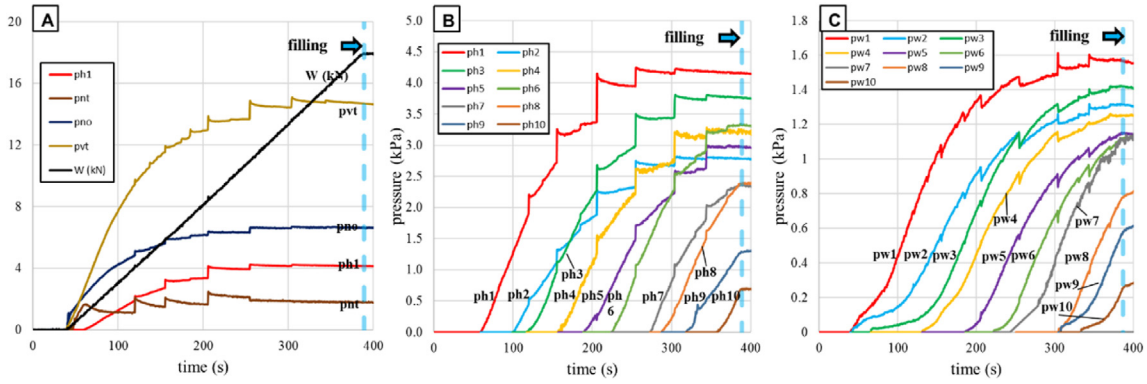


**Fig. 23 – Normal and frictional silo wall pressures ($p_{h,t}$; $p_{nt,t}$; $p_{no,t}$; $p_{w,t}$), vertical stress in the stored material at the transition ($p_{vt,t}$), and weight of the stored material ($W_{,t}$) for each time t during filling, at a filling height of 5.30 m. Thus, in relation to settling of the stored product, 5 oscillations occurred at a height of 2.77 m (Fig. 15), whereas 11 occurred at a height of 5.30 m (Fig. 23).**

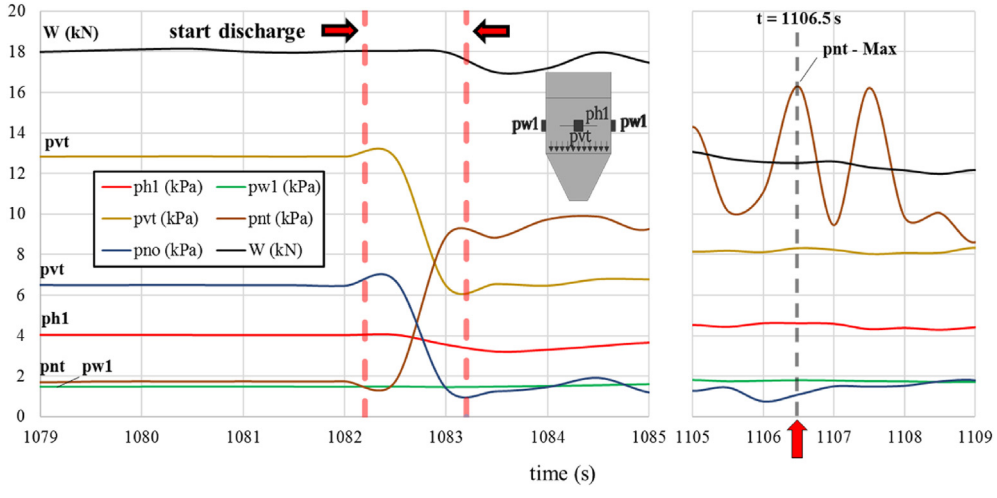


**Fig. 24 – Normal silo wall pressures ($p_{h1,t}$; $p_{nt,t}$; $p_{no,t}$), frictional silo wall pressures ($p_{w1}$), vertical stress in the stored material at the transition ($p_{vt,t}$), and weight of the stored material ($W_{,t}$) for each time t during the first few seconds after the start of discharge, at a filling height of 5.30 m.**

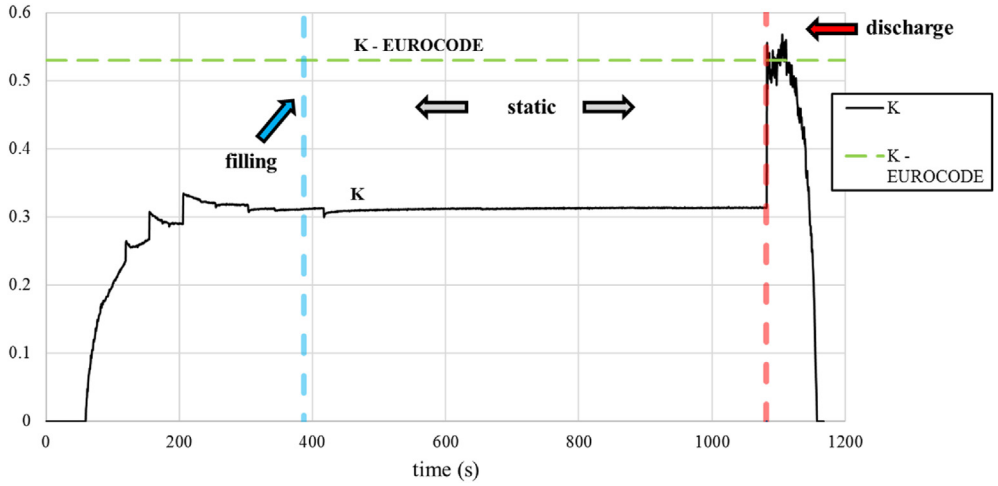


**Fig. 25 – Comparison between the values obtained for the pilot silo and those given by Eurocode 1, part 4, for lateral pressure ratio at the transition ($K_{,t}$) at each time t, at a filling height of 5.30 m.**

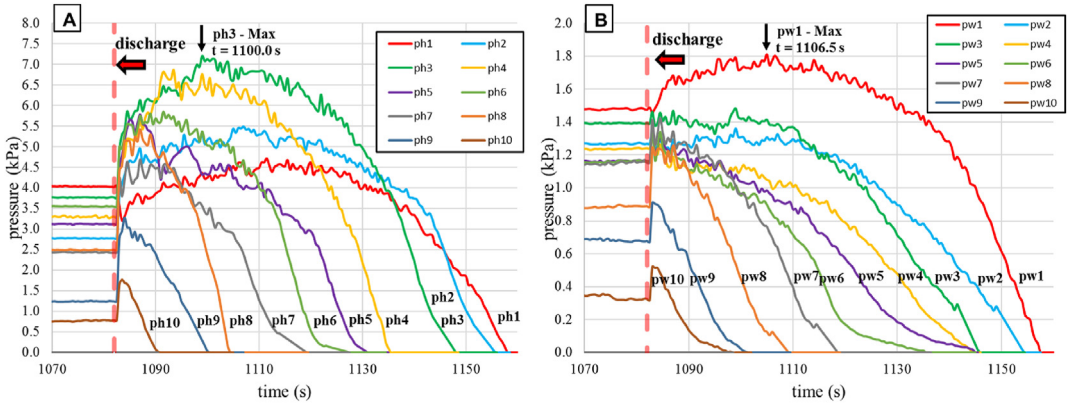


**Fig. 26 – Normal and frictional silo wall pressures ($p_{h,t}$; $p_{w,t}$) for each time t during discharge, at a filling height of 5.30 m.**

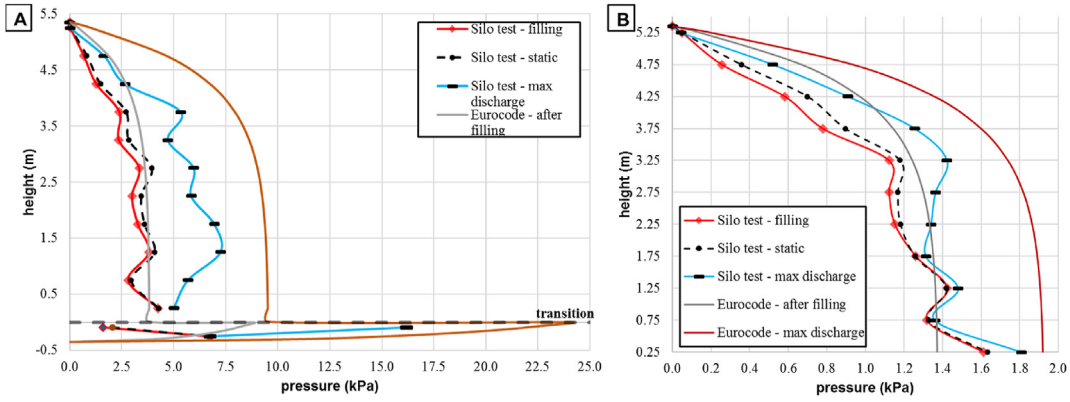


**Fig. 27 – Comparison of the maximum normal and frictional pressures on the silo wall given by Eurocode 1, part 4, and obtained for the pilot silo, at a filling height of 5.30 m.**

instrumentation. As regards friction pressures on the cylinder wall, the pressure in $p_{w2}$ was less than that in $p_{w3}$ at the time of discharge (Fig. 26 B), exhibiting the same behaviour as that observed and discussed for a height of 2.77 m (Fig. 19).

A particularly interesting point about this configuration (5.30 m) is that the maximum friction pressure on the cylinder wall in $p_{w1}$ occurred after 24.5 s, whereas at the other height (2.77 m), the maximum pressure occurred less than 5 s before the start of discharge.

Maximum normal and friction pressures differed from those given by Eurocode 1, part 4 (Fig. 27). This divergence was due to the oscillating tendency also shown in Fig. 20, and at

some points, maximum filling pressures were higher than in the standard.

A comparison with the height of 2.77 m (Fig. 20) indicated an effect of greater slenderness whereby more points of maximum pressure occurred. In this case (5.30 m), 3 maximum points of normal pressure were observed (Fig. 27 A) at 1.25 m, 2.75 m, and 3.75 m, in relation to the pressures $p_{h3}$, $p_{h6}$, and $p_{h8}$.

The difference in pressures under filling and static conditions was greater in the silo of greater slenderness (Fig. 17 A and 24 A), further supporting the notion that the greater the slenderness, the greater the settling of the stored product. By contrast, silo slenderness did not influence frictional pressures.

## 6. Conclusions

An experimental facility has be to obtain static and dynamic pressures in cylindrical silos under different conditions and its calibration, instrumentation, and validation have been described.

The facility can be used to analyse numerous boundary conditions and provide ample data for an analysis of pressures in full-scale silos. These boundary conditions will facilitate a greater understanding of numerical studies, which remain necessary since there are few experimental stations in the world. Thus, the experimental facility described can also assist in the validation of numerical models. This pilot-scale facility offers great scope for future research on silo structures thanks to the possibility of interchanging the station components. Thus, it is possible to change the walls (modifying the roughness of the material) and the silo bottom (modifying the type of flow and pressure configuration). It is also possible to vary the various agricultural or industrial materials used, analyse H/D ratios, and change the storage time of materials to analyse the consolidation and segregation of the stored product.

During validation using maize grains the following results were observed.

- During silo filling, several pressure peaks occurred during settling of the material. These oscillations occurred in normal and frictional pressures on the silo wall and the number of oscillations was influenced by silo slenderness.
- Under static conditions, pressure variations related to settling of the product were observed, which are consistent with the results reported by other authors (Ruiz et al., 2012). The quantity and magnitude of these oscillations were also influenced by silo slenderness.
- As is already known, maximum pressure occurs at discharge and in the normal position of the hopper wall near the silo transition (Couto, Ruiz, Herráez, et al., 2013; Ramírez et al., 2010b). However, the moment when this pressure occurred appeared to be influenced by silo slenderness, whereby the greater the slenderness, the greater the time of occurrence of the maximum pressure on the hopper wall near the transition.
- The moment of occurrence of the maximum friction pressure on the silo wall was also related to silo slenderness. Maximum friction pressure occurs on the silo wall near the transition, and the greater the slenderness, the later the time of occurrence of this pressure.
- Maximum pressures under filling, static, and discharge conditions showed a different pattern from that given by Eurocode 1, part 4 (CEN, 2006). The greater the slenderness of the silo, the greater the number of maximum pressure points observed, producing an oscillating tendency that differed from the curve given by Eurocode 1, part 4.

## Declaration of competing interest

The authors declare that they have no known competing financial interests or personal relationships that could have appeared to influence the work reported in this paper.

## Acknowledgments

The authors are very grateful to CAPES (Coordenação de Aperfeiçoamento de Pessoa de Nível Superior) for funding the doctoral scholarship associated with this project.

## REFERENCES

Ayuga, F. (2008). Some unresolved problems in the design of steel cylindrical silos. In J. G. Chen, & J. F. Teng (Eds.), *Structures and granular solids: From scientific principles to engineering applications* (pp. 123–133). CRC Press-Taylor & Francis Group.

Brown, C. J., Lahlouh, E. H., & Rotter, J. M. (2000). Experiments on a square planform steel silo. *Chemical Engineering Science*, 55(20), 4399–4413. https://doi.org/10.1016/S0009-2509(99)00574-6

Brown, C. J., & Nielsen, J. (1998). In E & FN Spon (Ed.), *Silos: Fundamentals of theory, behaviour and design*.

Butterfield, R. (1969). A theoretical study of the pressures developed in a silo containing single-size particles in a regular packing. *International Journal of Rock Mechanics and Mining Sciences*, 6(2), 227–238. https://doi.org/10.1016/0148-9062(69)90037-0

Bywalski, C., & Kamiński, M. (2019). A case study of the collapse of the over-chamber reinforced concrete ceiling of a meal silo. *Engineering Structures*, 192(March), 103–112. https://doi.org/10.1016/j.engstruct.2019.04.100

Calil, J. C., & Cheung, A. B. (2007). In SET/EESC-USP (Ed.), *Silos: Pressões, fluxo, recomendações para o projeto e exemplo de cálculo*.

Calil, C., Palma, G., & Cheung, A. B. (2009). Failure modes of cylindrical corrugated steel silos in Brazil. *Bulk Solids Handling*, 29(6), 346.

Cen. (2006). *EN 1991-4:2006. Eurocode 1: Actions on structures. Part 4: Silos and tanks*.

CONAB, C. N. de A. (2020). Acompanhamento da safra brasileira 2019/2020. In, *Vol. 7. Acompanhamento da Safra Brasileira de Grãos 2019/2020*. https://www.conab.gov.br/info-agro/safras.

Couto, A., Ruiz, A., & Aguado, P. J. (2012). Design and instrumentation of a mid-size test station for measuring static and dynamic pressures in silos under different conditions - Part I: Description. *Computers and Electronics in Agriculture*, 85, 164–173. https://doi.org/10.1016/j.compag.2012.04.009

Couto, A., Ruiz, A., & Aguado, P. J. (2013). Experimental study of the pressures exerted by wheat stored in slender cylindrical silos, varying the flow rate of material during discharge. Comparison with Eurocode 1 part 4. *Powder Technology, 237*, 450–467. https://doi.org/10.1016/j.powtec.2012.12.030

Couto, A., Ruiz, A., Herráez, L., Moran, J., & Aguado, P. J. (2013). Measuring pressures in a slender cylindrical silo for storing maize. Filling, static state and discharge with different material flow rates and comparison with Eurocode 1 part 4. *Computers and Electronics in Agriculture, 96*, 40–56. https://doi.org/10.1016/j.compag.2013.04.011

Deutsh, G. P., & Schmidt, L. C. (1985). Pressures on silo walls. *Developments in Geotechnical Engineering, 39*(C), 125–138. https://doi.org/10.1016/B978-0-444-42470-9.50016-7

DIN. (2005). *Din 1055-6: Basis of design and actions on structures — Part 6: Design 623 loads for buildings and loads in silo bins*.

Ding, S., Dyrøy, A., Karlsen, M., Enstad, G. G., & Jecmenica, M. (2011). Experimental investigation of load exerted on a double-cone insert and effect of the insert on pressure along walls of a large-scale axisymmetrical silo. *Particulate Science & Technology, 29*(2), 127–138. https://doi.org/10.1080/02726351.2010.520077

Dogangun, A., Karaca, Z., Durmus, A., & Sezen, H. (2009). Cause of damage and failures in silo structures. *Journal of Performance of Constructed Facilities, 23*(2), 65–71. https://doi.org/10.1061/(ASCE)0887-3828(2009)23:2(65)

Dpe, & Diretoria De Pesquisa E Coordenação Agropecuária.. (2019). Ibge - Pesquisa de Estoques 2° semestre de 2019.

Fank, M. Z., do Nascimento, J. W. B., Cardoso, D. L., Meira, A. S., & Willrich, F. L. (2018). Vertical pressures and compressive friction force in a large silo. *Engenharia Agricola, 38*(4), 498–503. https://doi.org/10.1590/1809-4430-Eng.Agric.v38n4p498-503/2018

Gallego, E., González-Montellano, C., Ramírez, A., & Ayuga, F. (2011). A simplified analytical procedure for assessing the worst patch load location on circular steel silos with corrugated walls. *Engineering Structures, 33*(6), 1940–1954. https://doi.org/10.1016/j.engstruct.2011.02.032

Gallego, E., Ruiz, A., & Aguado, P. J. (2015). Simulation of silo filling and discharge using ANSYS and comparison with experimental data. *Computers and Electronics in Agriculture, 118*, 281–289. https://doi.org/10.1016/j.compag.2015.09.014

González-Montellano, C., Ramírez, Á., Gallego, E., & Ayuga, F. (2011). Validation and experimental calibration of 3D discrete element models for the simulation of the discharge flow in silos. *Chemical Engineering Science, 66*(21), 5116–5126. https://doi.org/10.1016/j.ces.2011.07.009

Härtl, J., Ooi, J. Y., Rotter, J. M., Wojcik, M., Ding, S., & Enstad, G. G. (2008). The influence of a cone-in-cone insert on flow pattern and wall pressure in a full-scale silo. *Chemical Engineering Research and Design, 86*(4), 370–378. https://doi.org/10.1016/j.cherd.2007.07.001

Holst, J. M. F. G., Ooi, J. Y., Rotter, J. M., & Rong, G. H. (1999). Numerical modeling of silo filling. I: Continuum analyses. *Journal of Engineering Mechanics, 125*(1), 94–103. https://doi.org/10.1061/(asce)0733-9399(1999)125:1(94)

Horabik, J., Parafiniuk, P., & Molenda, M. (2016). Experiments and discrete element method simulations of distribution of static load of grain bedding at bottom of shallow model silo. *Biosystems Engineering, 149*, 60–71. https://doi.org/10.1016/j.biosystemseng.2016.06.012

International Organization for Standardization. (2012). *ISO 11697:2012. Bases for design of strutures - loads due to bulk materials*.

Janssen, H. A. (1895). Versuche uber getreidedruck in silozellen. *VDI-Z (Verein Deutscher Ingenieure-Z), 39*(35), 1045–1049.

Jenike, A. (1964). *Storage and flow of bulk solids bull* (Vol. 123). University of Utah.

Jenike, A. W., Johanson, J. R., & Carson, J. W. (1973). Bin loads—Part 4: Funnel-flow bins. *Journal of Engineering for Industry, 95*, 13–20.

Kobyłka, R., Molenda, M., & Horabik, J. (2020). DEM simulation of the pressure distribution and flow pattern in a model grain silo with an annular segment attached to the wall. *Biosystems Engineering, 193*, 75–89. https://doi.org/10.1016/j.biosystemseng.2020.02.013

Lvin, J. A. B. (1971). Analytical evaluation of pressures of granular materials on silo walls. *Powder Technology, 4*(5), 280. https://doi.org/10.1016/0032-5910(71)80050-5

Nielsen, J., & Askegaard, V. (1977). Scale errors in model tests on granular media with special reference to silo models. *Powder Technology, 16*(1), 123–130. https://doi.org/10.1016/0032-5910(77)85029-8

Nielsen, J., & Rotter, J. M. (2018). On the definition of design values for loads on silos and tanks. *Advances in Structural Engineering, 21*(16), 2499–2506. https://doi.org/10.1177/1369433217746348

Pieper, K., & Schütz, M. (1980). Bericht über das Forschungsvorhaben Norm-Mess-Silo für Schüttguteigenschaften. *Hochbaustatik, Technische Universität*.

Piskoty, G., Michel, S. A., & Zgraggen, M. (2005). Bursting of a corn silo - an interdisciplinary failure analysis. *Engineering Failure Analysis, 12*, 915–929. https://doi.org/10.1016/j.engfailanal.2005.02.002 (6 SPEC. ISS.).

Ramírez, A., Nielsen, J., & Ayuga, F. (2010a). On the use of plate-type normal pressure cells in silos. Part 1: Calibration and evaluation. *Computers and Electronics in Agriculture, 71*(1), 71–76. https://doi.org/10.1016/j.compag.2009.12.004

Ramírez, A., Nielsen, J., & Ayuga, F. (2010b). On the use of plate-type normal pressure cells in silos. Part 2: Validation for pressure measurements. *Computers and Electronics in Agriculture, 71*(1), 64–70. https://doi.org/10.1016/j.compag.2009.12.005

Ruiz, A., Couto, A., & Aguado, P. J. (2012). Design and instrumentation of a mid-size test station for measuring static and dynamic pressures in silos under different conditions - Part II: Construction and validation. *Computers and Electronics in Agriculture, 85*, 174–187. https://doi.org/10.1016/j.compag.2012.04.008

Sadowski, A. J., Michael Rotter, J., & Nielsen, J. (2020). A theory for pressures in cylindrical silos under concentric mixed flow. *Chemical Engineering Science, 223*, 115748. https://doi.org/10.1016/j.ces.2020.115748

Schuricht, T., Furll, C., & Eenstad, G. G. (2001). Full scale silo tests and numerical simulations of the „cone in cone" concept for mass flow. In, *Vol. 10. Handbook of powder technology* (pp. 175–180). Elsevier Science BV.

Schwab, C. V., Ross, I. J., White, G. M., & Colliver, D. G. (1994). *WHEAT LOADS AND VERTICAL PRESSURE. 37* pp. 1613–1619) (5).

Song, C. Y., & Teng, J. G. (2003). Buckling of circular steel silos subject to code-specified eccentric discharge pressures. *Engineering Structures, 25*(11), 1397–1417. https://doi.org/10.1016/S0141-0296(03)00105-6

Sun, W., Zhu, J., Zhang, X., Wang, C., Wang, L., & Feng, J. (2020). Multi-scale experimental study on filling and discharge of squat silos with aboveground conveying channels. *Journal of Stored Products Research, 88*, 101679. https://doi.org/10.1016/j.jspr.2020.101679

Teng, J. G., & Lin, X. (2005). Fabrication of small models of large cylinders with extensive welding for buckling experiments. *Thin-Walled Structures, 43*(7), 1091–1114. https://doi.org/10.1016/j.tws.2004.11.006

Teng, J. G., Zhao, Y., & Lam, L. (2001). Techniques for buckling experiments on steel silo transition junctions. *Thin-Walled Structures, 39*(8), 685–707. https://doi.org/10.1016/S0263-8231(01)00030-1

Tian, Z., & Jiao, D. (2019). Discrete sizing optimization of stepped cylindrical silo using PSO method and implicit dynamic FE analysis. In, *Vol. 2007. Engineering with computers*. Springer London. https://doi.org/10.1007/s00366-019-00870-6, 123456789.

Walker, D. (1967). An approximate theory for pressures and arching in hoppers. *Chemical Engineering Science, 22*(3), 486. https://doi.org/10.1016/0009-2509(67)80145-3

Wenzel, F. (1973). Pressure behavior in double cylindrical silos. *Journal of Manufacturing Science and Engineering, Transactions of the ASME, 95*(1), 97–100. https://doi.org/10.1115/1.3438170

Wójcik, M., Tejchman, J., & Enstad, G. G. (2012). Confined granular flow in silos with inserts - full-scale experiments. *Powder Technology, 222*, 15–36. https://doi.org/10.1016/j.powtec.2012.01.031

Zegzulka, J. (2013). The angle of internal friction as a measure of work loss in granular material flow. *Powder Technology, 233*, 347–353. https://doi.org/10.1016/j.powtec.2012.06.047

Zhao, Y., & Teng, J. G. (2004). Buckling experiments on steel silo transition junctions. II: Finite element modeling. *Journal of Constructional Steel Research, 60*(12), 1803–1823. https://doi.org/10.1016/j.jcsr.2004.05.001

Zhong, Z., Ooi, J. Y., & Rotter, J. M. (2001). The sensitivity of silo flow and wall stresses to filling method. *Engineering Structures, 23*(7), 756–767. https://doi.org/10.1016/S0141-0296(00)00099-7

**Article 2 – Evaluation of pressures in slender silos varying hopper angle and silo slenderness - Powder Technology journal (published version)**

The article was published in Powder Technology journal (ISSN 0032-5910). The journal has the qualis A1 and JCR 5.134.

DOI: https://doi.org/10.1016/j.powtec.2021.08.087.

Powder Technology 394 (2021) 478–495

Contents lists available at ScienceDirect

Powder Technology

journal homepage: www.elsevier.com/locate/powtec

# Evaluation of pressures in slender silos varying hopper angle and silo slenderness

Rômulo Marçal Gandia [a,c,*], Francisco Carlos Gomes [a], Wisner Coimbra De Paula [b], Pedro José Aguado Rodriguez [c]

[a] Federal University of Lavras (UFLA) (Brazil), Agricultural Engineering Department, Brazil
[b] Federal University of Lavras, Engineering Department, Brazil
[c] University of León (Spain), Department of Engineering and Egricultural Sciences, Spain

ARTICLE INFO

*Article history:*
Received 11 March 2021
Received in revised form 2 August 2021
Accepted 24 August 2021
Available online 31 August 2021

*Keywords:*
Silo pressures
Free-flowing product
Concentric hopper
Flow pattern
Slender silo

ABSTRACT

In this paper, we report the results for pressures in a full-scale silo obtained from assays performed on a test station using a free-flowing product. Six different types of silo geometry (slenderness and hopper angle) were tested by filling the silo to the height of interest and observing a static phase (10 min) followed by complete discharge. Our results show that discharge flow is not influenced by silo slenderness. The lateral pressure ratio and values obtained for vertical stress in the stored material at the transition were higher than those given in the Eurocode 1, part 4. In addition, the maximum frictional pressures in the cylinder showed peaks that exceeded the standard, as did the maximum normal pressure in the cylinder with maximum slenderness and mass flow (hopper $\beta = 15°$).



## 1. Introduction

In the international market, corn and its derivatives constitute a leading product with high consumption due to their high nutritional index and a wide prevalence in animal feed. In Brazil alone, grain production in 2020 was 268.7 million tons [1], with maize accounting for 105.2 million tons (39%) of this total. As a result of premarket trading, inventory control, logistics or cooperatives, a large part of agricultural produce is stored. In 1980, Brazil's storage capacity was 40.45 million tons of grain, but in fewer than four decades (2019), Brazil has more than quadrupled its static capacity (177.7 million tons of grain), with 86.6 million (49%) being stored in silos [2].

Tower silos have been studied since the 19th century, but due to the complexity of the laws that govern the mechanical behavior of stored materials, many aspects remain poorly understood [3–5]. This lack of knowledge hinders the development of standards for silo design.

Study of the behavior of products stored in silos has been dated since 1895 by Janssen [6], who first described the increase in pressure with depth and the compressive force that friction exerts on the wall due to the vertical load of the stored material. Since then, other theories have been developed [7] [8,9] [10] that have served to support international standards [11,12]. Jenike (1964) developed an internationally recognized device capable of determining the flow properties of stored products (Jenike Shear Tester), further refined by a group (Working Party on the Mechanics of Particulate Solids) from the European Federation of Chemical Engineering association, renamed the "Standard Shear Testing Technique for Particulate Solids Using the Jenike Shear Cell" [14]. Besides supporting international standards, this device is capable of obtaining reliable parameters for calculating pressures in silos. The pressures in silos filled with granular or powdery materials differ from hydrostatic pressure, since depending on depth, the normal pressure exerted by the stored material stops increasing and only the friction pressure on the wall continues to rise [15].

A review of several studies predicting and analyzing silo failure indicates that the main causes include design error [16,17]; pressures (normal and friction, on the wall and hopper) exerted by the stored product in the structure [3,17]; product discharge (maximum pressures in the silo, usually at the silo-hopper transition) [3,17–20]; discharge eccentricity [3,17]; and product temperature variations due to silo location and defects in the structural material [3,17,21].

Although the literature on silo failure points to several causes, research has focused on the pressures related to silo slenderness. ISO 11697 [22] limits storage in silos with a slenderness of up to 10 (height / diameter ratio = 10). Meanwhile, Eurocode 1 part 4 [12] notes that in very slender silos, different densities of the stored material may occur, leading to a mixed flow channel or asymmetric funnel and generating asymmetric pressures. Very slender silos can express the behavior of

* Corresponding author.
*E-mail addresses:* romagandia@gmail.com, romulo.gandia@estudante.ufla.br, rmarcg01@estudiantes.unileon.es (R.M. Gandia), fcgomes@ufla.br (F.C. Gomes), depaula@ufla.br (W.C.D. Paula), pedro.aguado@unileon.es (P.J. Aguado Rodriguez).

https://doi.org/10.1016/j.powtec.2021.08.087
0032-5910/

**Nomenclature**

| | |
|---|---|
| Ø | Angle of internal friction, degrees |
| A | Plan cross-sectional area of vertical walled segment, $m^2$ |
| $d_i$ | Internal cylinder diameter, m. |
| $F_{h(1,12)u,t}$ | Force in tension load cell positioned on the upper part of the spring set - rings 1 to 12, at time t, kN |
| $F_{h(1,12)d,t}$ | Force in tension load cell positioned on the lower part of the spring set - rings 1 to 12, at time t, kN |
| $F_{w(1,12)r,t}$ | Force in tension load cell positioned on the right side of the ring support - rings 1 to 12, at time t, kN |
| $F_{w(1,12)l,t}$ | Force in tension load cell positioned on the left side of the ring support - rings 1 to 12, at time t, kN |
| $F_{vtr,t}$ | Force in tension load cell positioned on the right side of the hopper support, at time t, kN |
| $F_{vtl,t}$ | Force in tension load cell positioned on left side of the hopper support, at time t, kN |
| $F_{vbr,t}$ | Force on shear beam load cell positioned at the base of the right pillar, time t, kN |
| $F_{vbl,t}$ | Force on shear beam load cell positioned at the base of the left pillar, time t, kN |
| h | Ring height, m. |
| K | Characteristic value of lateral pressure ratio |
| $P_{ntr,t}$ | Normal pressure on the right hopper wall next to the silo–hopper transition, time t, kPa |
| $P_{ntl,t}$ | Normal pressure on left hopper wall next to the silo–hopper transition, time t, kPa |
| $P_{nir,t}$ | Normal pressure on right hopper wall between the silo–hopper transition and outlet, time t, kPa |
| $P_{nil,t}$ | Normal pressure on left hopper wall between the silo–hopper transition and outlet, time t, kPa |
| $P_{nitr,t}$ | Normal pressure on right hopper wall between the silo–hopper transition and outlet, near transition, time t, kPa |
| $P_{nitl,t}$ | Normal pressure for left hopper wall between the silo–hopper transition and the outlet, near transition, time t, kPa |
| $P_{nior,t}$ | Normal pressure on right hopper wall between the silo–hopper transition and outlet, near outlet, time t, kPa |
| $P_{niol,t}$ | Normal pressure on left hopper wall between the silo–hopper transition and outlet, near outlet, time t, kPa |
| $P_{nor,t}$ | Normal pressure on the right hopper wall next to silo outlet, time t, kPa |
| $P_{nol,t}$ | Normal pressure for the hopper wall on the left-hand side next to silo outlet, time t, kPa |
| $P_{h(1,12),t}$ | Normal pressure on cylinder wall from the tension load cells positioned on spring set - rings 1 to 12, time t, kPa |
| $P_{w(1,12),t}$ | Friction pressure for the cylinder wall from the tension load cells positioned on ring supports - rings 1 to 12, time t, kPa |
| $P_{vt,t}$ | Vertical stress of product at the silo–hopper transition from the tension load cells positioned on the hopper support, time t, kPa |
| $P_{v(1,4),t}$ | Vertical stress of product at the silo–hopper transition obtained from the pressure cells (flat bottom), time t, kPa |
| $W_{,t}$ | Weight of stored product, time t, kN |
| $W_{hto}$ | Weight of stored product between the outlet and the silo–hopper transition, zero in the case of the flat bottom, kN |
| $V_{ih}$ | Internal hopper volume, $m^3$ |
| $V_{ic}$ | Internal cylinder volume, $m^3$ |
| $r_i$ | Internal cylinder radius, m. |
| γ | Bulk unit weight |

maximum normal pressures on the silo wall in the form of waves, oscillating in relation to the silo wall height [23,24].

The behavior of pressures in a silo is influenced by flow pattern, and the two parameters that directly influence this are the hopper angle and the friction angle between the material and the hopper wall. There are two possible flow patterns, mass flow and funnel flow [12], and these directly influence the magnitude and distribution of forces acting across the silo [10].

Mass flow is characterized by the movement of all the stored material at the same speed, a flow pattern that is usually achieved in silos with smooth-walled hoppers, where the flowing material generates high dynamic pressures on the walls (particularly at the silo / hopper transition). Funnel flow is characterized by a first-in last-out sequence with areas of static material, reducing silo capacity. This pattern is suitable for free-flowing materials. The pressures on the wall during discharge are slightly higher than during filling [25].

A third flow pattern, transition flow, is characterized by a distinct change in flow in a position that depends on the filling height [26]. It is possible to predict the flow pattern in bulk solids, where the hopper angle and the friction angle of the hopper wall are the two most influential parameters [12,13,22]. However, flow pressure is still poorly understood [15,24,27,28].

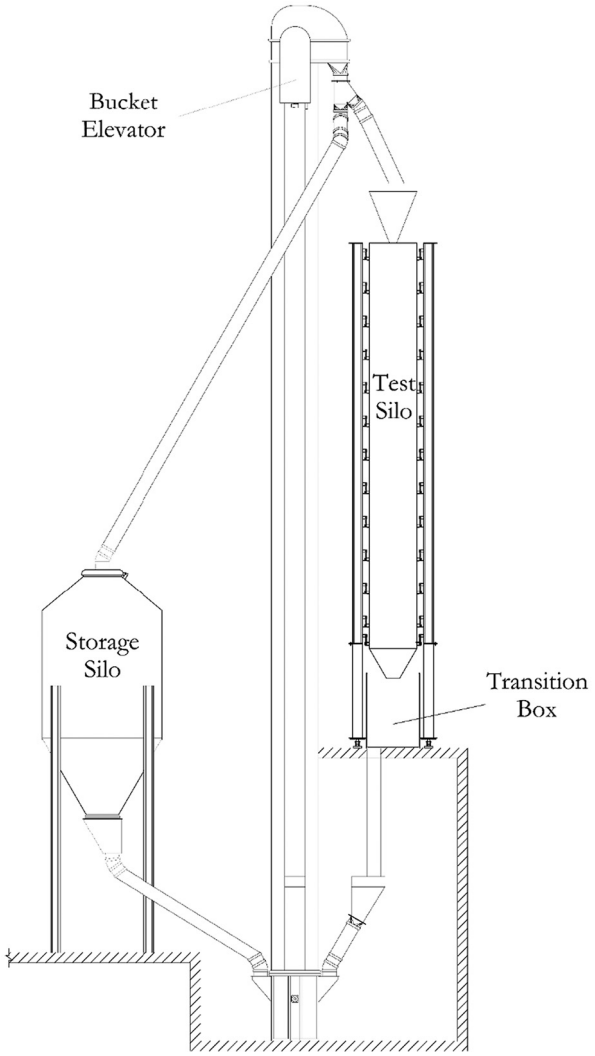


**Fig. 1.** General overview of the test silo station.

The pilot scale test station proposed by Pieper and Schütz in 1980 [29], which provided support for DIN 1055–6: *Basis of design and actions on structures – Part 6* [11], can be used to obtain numerous variables that directly influence the behavior of pressures in a silo [30,31], including: any product provided that the maximum diameter of the product is less than 1.7 cm (proportional to real scale) [29,32]; three walls of varying roughness (varying the friction coefficient between the product and the wall); twelve height / diameter ratios; eight bottoms (1 flat bottom, 4 concentric hoppers (α: 75 to 30°) and three 100% eccentric hoppers with (α: 75 to 45°) and other possible procedural variables in the tests.

Experimental models of full-scale silos provide proximity to real values, enabling confidence in the data and enhancing our understanding of pressures in silos [27]. Worldwide, the number of full-scale experimental silo stations is relatively small [33–44] due to the cost of construction, instrumentation and operations. In addition, the scale factor is extremely important to ensure reliable data [32]. However, the study of experimental pressures in silos yields advances in numerical studies as a means of validation and enables comparisons in order to construct reliable models.

Therefore, the aim of the present study was to elucidate the relationship between flow pattern and slenderness in relation to silo pressures. Six different geometric configurations were evaluated in the same silo, obtaining normal and frictional pressures on the cylinder wall and pressures on the hopper wall.

## 2. Material and methods

### 2.1. General description of the installation

The principle components consisted of two silos: one to perform the tests (pilot silo), containing the instrumentation necessary to measure the behavior of the stored material, and the other (storage silo) to store the product used in the tests, storing the material during the tests. This model is located at the Federal University of Lavras (Brazil)

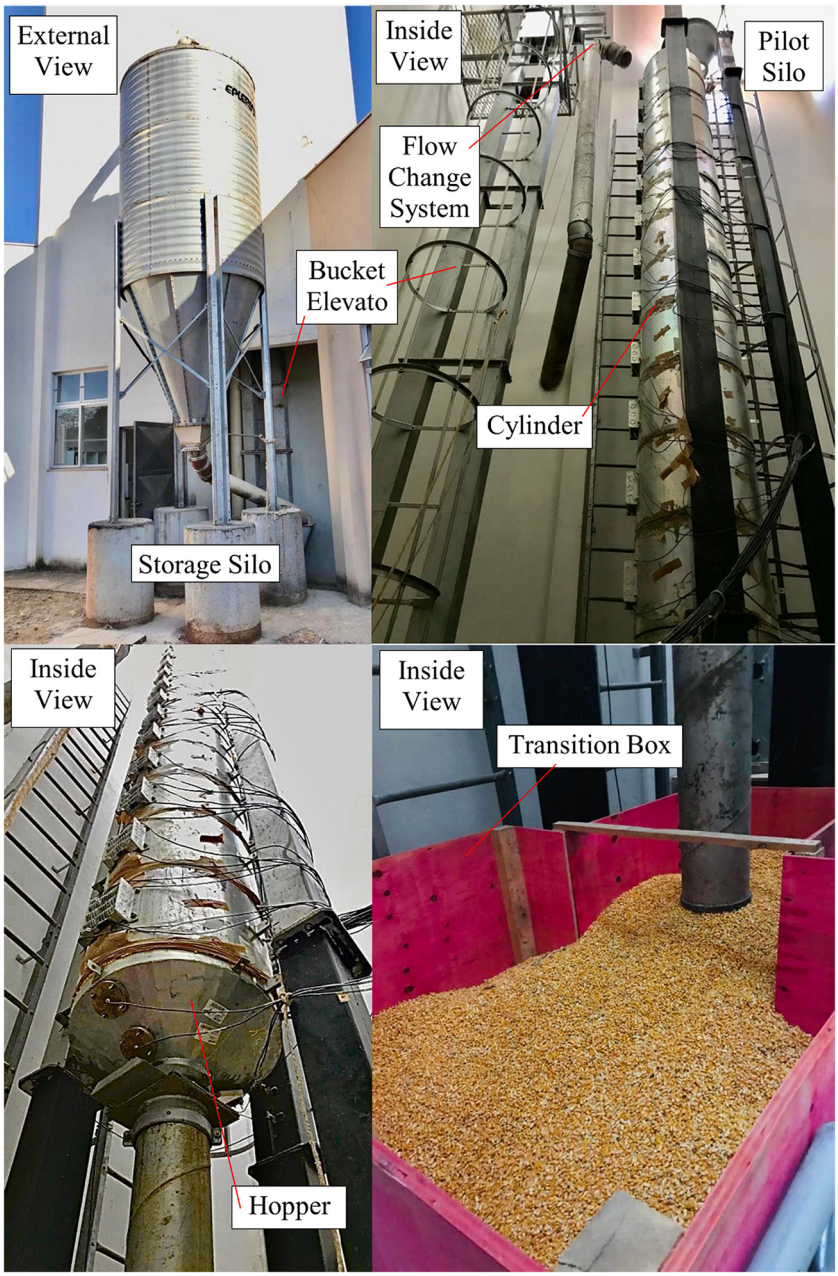


**Fig. 2.** Pilot scale test station.

and was previously validated by the researchers of the research group on pressure and flow in silos and stored product [36]. The material was transported between silos by means of a bucket elevator connected between the two silos, facilitating filling and discharge of the pilot silo. A transition box was located below the discharge from the test silo and the bucket elevator, in order to allow maximum flow discharge from the pilot silo and counteract any influence of bucket elevator transportation (Fig. 1 and Fig. 2).

*2.1.1. Geometry of the experimental silo*

The silo is cylindrical, elevated, and metallic. The silo cylinder and hopper are independent and can be dismantled. The silo cylinder is 600 cm high with a diameter of 70 cm, and is divided into 12 structurally independent semi-cylinders (rings). Each ring is 49.50 cm high with a gap of 0.50 cm, totaling the height of the silo cylinder at 6 m (Fig. 3). The use of independent rings enables measurement of vertical and horizontal force on the cylinder wall (in each ring).

The silo walls (rings) and hoppers were constructed from 10 mm-thick sheets of stainless steel. Given its dimensions and the type of material used for the walls, the silo can thus be considered a rigid, smooth-walled steel silo. The silo is supported by two vertical pillars (all instrumented) and a third pillar just to prevent rotation. According to the Eurocode classification, it corresponds to a slender silo, since the cylinder height/diameter ratio is equal to 2 (hc/dc = 2).

*2.2. Measuring vertical forces*

The entire system (pilot silo) is supported on two structural pillars with readings taken by two beam load cells (Fig. 3), enabling measurement of the weight of the stored material.

The vertical forces responsible for friction pressure on the cylinder wall and vertical stress in the stored material at the transition were measured by tension load cells located throughout the height of the pilot silo on each vertical pillar supporting each ring and the hopper (Fig. 3). Each ring has a vertical gap of 5 mm (Fig. 3) and the same gap is also present between the bottom of the silo and the first ring, rendering the system structurally independent.

Therefore, each of the two structural pillars supports 13 points (12 for rings and 1 for the silo bottom) and the instrumentation can be checked according to the sum of the 13 support points (connected to each structural pillar). The sum of the 13 points (tension load cell) corresponds to the vertical load on each structural pillar (beam load cell).

*2.3. Measuring horizontal forces*

Measurements in the hopper were performed using pressure cells (Fig. 3). Cell location and hopper geometry are shown in Fig. 4. (See Fig. 5.)

To measure normal wall pressures, a vertical generatrix was located on the cylinder wall, along which 12 pairs of readings were taken at different heights using a tension load cell, each pair yielding the normal pressure measurement for each ring. To avoid reading errors, each ring has a gap of 5 mm at the opening (Fig. 3).

The arrangement of the measuring cells influences the data obtained [23,45]. Thus, the pressure cells have a gap of 1 mm in the radius between the cell and the hopper structure. In addition, the cell is 5 mm high (the part that is internal to the silo) and the hopper wall thickness is exactly 5 mm, ensuring quality in data collection. Although a gap of 5 mm is relatively large and could influence measurements [46], pretests were carried out to determine whether the product became

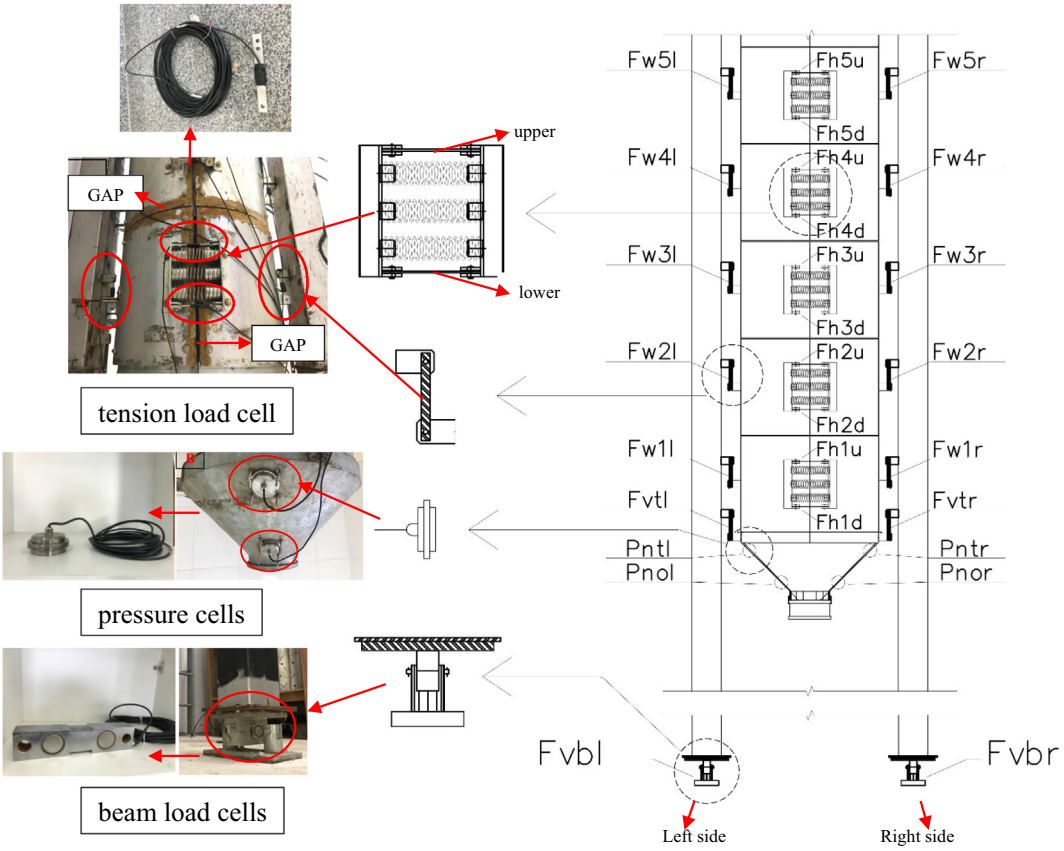


**Fig. 3.** Location of measurement cells in the pilot silo.

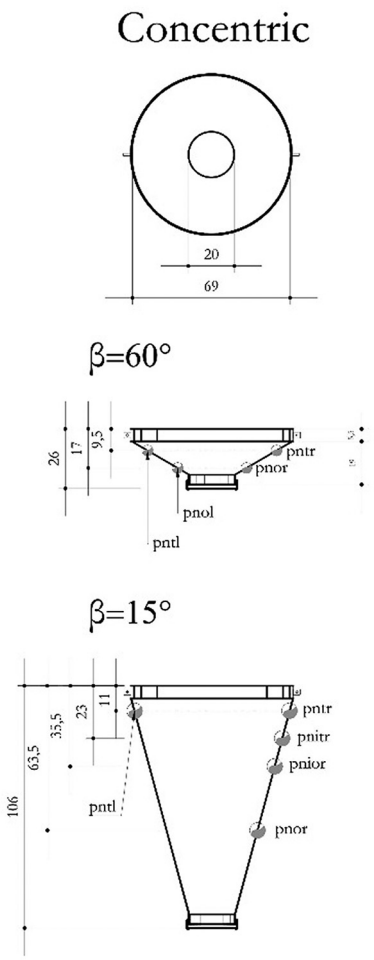


**Fig. 4.** Geometry and instrumentation of the concentric hoppers ($\beta = 15°$ and $\beta = 60°$) of the pilot silo.

stuck between the gaps. We found that the product did not get trapped when the tests were conducted without taping over the gaps and the results were similar to those obtained when taping covered the gaps.

(a) Beam load cell, pillar base. (b) Pressure cell, hoppers. (c) Tension load cell, silo rings (vertical - friction, horizontal normal).

Unit: centimeter.

### *2.4. Calculation of pressure and other components*

In this section, the station parameters are presented briefly. The most detailed explanation can be found in Gandia et al. (2021) [36].

Normal wall pressures (pH)

$$\mathbf{Ph(1,12),t} = \frac{\mathbf{Fh(1,12)u,t} + \mathbf{Fh(1,12)d,t}}{\mathbf{hr.0.32759}} \tag{1}$$

− 0.32759: constant value obtained with $d_i = 0.685$ m.

Frictional wall pressures ($P_w$)

$$\mathbf{Pw(1,12),t} = \frac{\boldsymbol{Fw(1,12)r,t} + \boldsymbol{Fw(1,12)l,t}}{\boldsymbol{\pi.di.hr}} \tag{2}$$

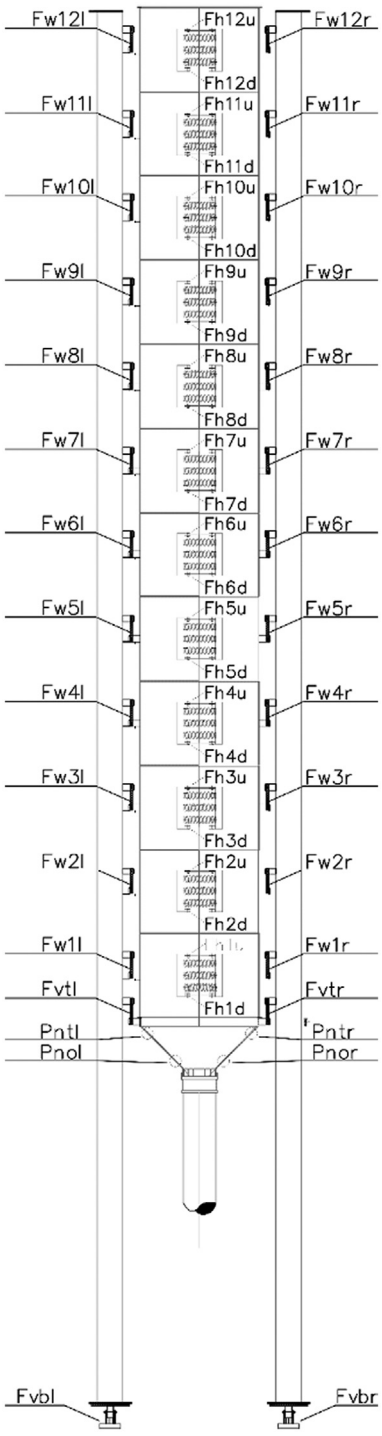


**Fig. 5.** Instrumentation and measurement points for forces and pressures on the pilot silo.

Weight of stored material (W)

$$W,t = Fvbr,t + Fvbr,t \tag{3}$$

Vertical stress in the stored solid at the transition ($P_{vt}$)

$$\mathbf{Pvt,t} = \frac{\mathbf{Fvtr,t} + \mathbf{Fvtl,t} - \mathbf{Whto}}{\mathbf{A}} \tag{4}$$

$$\mathbf{Whto} = \mathbf{Vi}\boldsymbol{h}*\boldsymbol{\gamma} \tag{5}$$

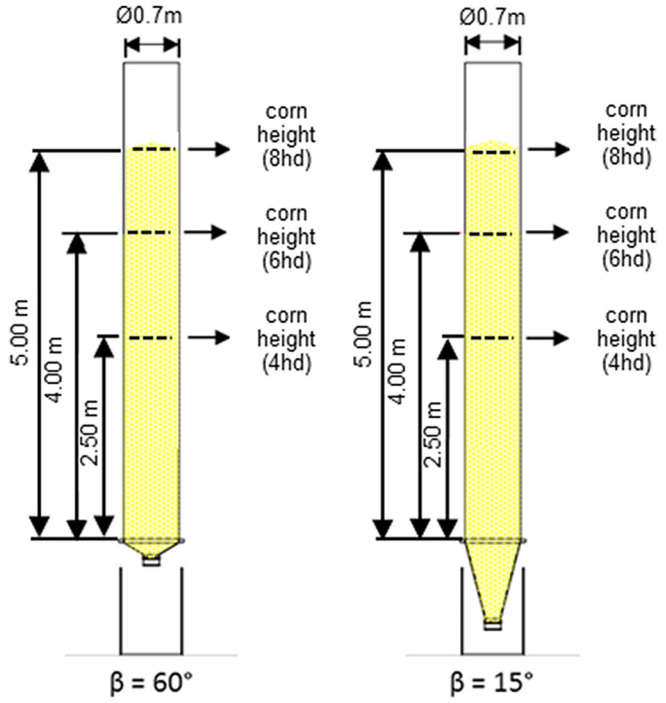


**Fig. 6.** Test configuration, varying the height of the corn filling and hopper angle.

Wall friction coefficient (μ)

$$\mu(1,12) = \frac{Pw(1,12)}{Ph(1,12)} \tag{6}$$

Lateral pressure ratio (K)

$$K,t = \frac{Ph(1,12),t}{Pv(1,12),t} \tag{7}$$

Specific weight of stored material (γ)

$$\gamma = \frac{W}{Vih + Vic} \tag{8}$$

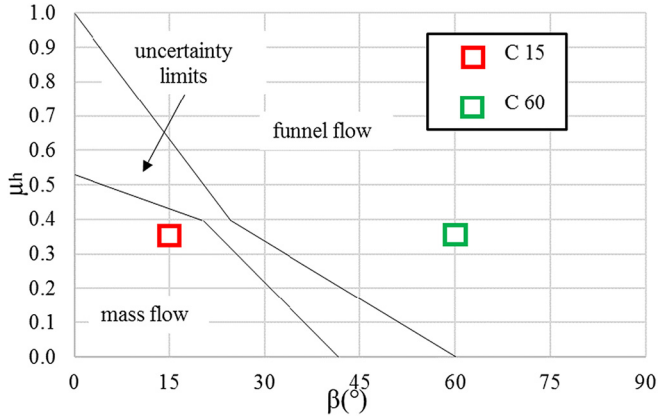


**Fig. 7.** Conditions for flow patterns according to Eurocode 1, part 4.

**Table 1**
Average flow for each test.

| Test | Average value (kg/s) | | Standard deviation (kg/s) | |
|---|---|---|---|---|
| | Filling | Discharge | Filling | Discharge |
| C60 4hd | 4.4 | 20.3 | 0.1 | 0.3 |
| C60 6hd | 4.7 | 20.2 | 0.1 | 1.0 |
| C60 8hd | 2.8 | 20.2 | 0.7 | 1.1 |
| C15 4hd | 4.5 | 31.8 | 0.1 | 0.7 |
| C15 6hd | 4.8 | 28.7 | 0.0 | 2.2 |
| C15 8hd | 4.5 | 29.8 | 0.2 | 1.8 |

**Table 2**
Average load for each test.

| Test | Average value (kN) | Standard deviation (kN) | γ (kN/m$^3$) |
|---|---|---|---|
| C60 4hd | 7.85 | 0.44 | 7.70 |
| C60 6hd | 13.24 | 0.24 | 7.62 |
| C60 8hd | 17.72 | 0.33 | 7.75 |
| C15 4hd | 9.23 | 0.20 | 7.70 |
| C15 6hd | 14.71 | 0.04 | 7.67 |
| C15 8hd | 18.65 | 0.07 | 7.80 |

### 2.5. Description of the tests

#### 2.5.1. Properties of the stored product

The product used to conduct the tests in the pilot silo was maize (*Zea mays*) with a minimum purity of 97%. The physical, mechanical, and flow properties of corn were obtained at the Federal University of Campina Grande (UFCG) following the methodology of the Jenike Shear Test [14], which conforms to Eurocode 1, part 4 [12]. The values obtained were (lower and upper limits):

- specific weight (kN/m$^3$): 7.52–7.83;
- angle of repose: 31.3° – 37.1°;
- cohesion (kPa): 0.241–1.084;

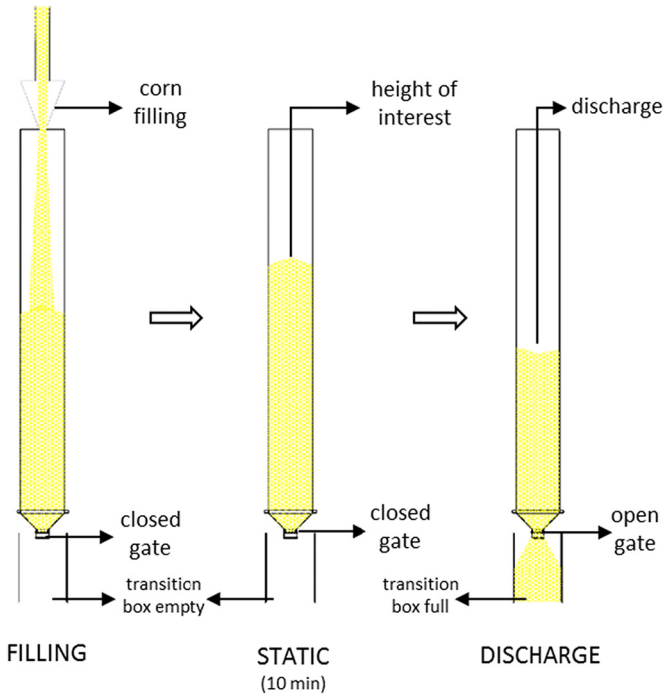


**Fig. 8.** Test configuration. Description of the assays.

**Table 3**
Time period for each test phase.

| Test | Average value (s) | | | | Standard deviation (s) | | | |
|---|---|---|---|---|---|---|---|---|
| | Filling | Static | Discharge | Total | Filling | Static | Discharge | Total |
| C60 4hd | 183.7 | 674.0 | 39.5 | 897.2 | 12.3 | 43.7 | 2.6 | 56.0 |
| C60 6hd | 287.3 | 672.8 | 67.2 | 1027.3 | 2.8 | 75.5 | 2.5 | 73.5 |
| C60 8hd | 677.3 | 668.3 | 90.0 | 984.7 | 190.4 | 59.8 | 6.5 | 49.1 |
| C15 4hd | 207.7 | 635.3 | 29.5 | 872.5 | 6.8 | 46.9 | 0.0 | 52.3 |
| C15 6hd | 311.7 | 658.3 | 52.7 | 1022.7 | 0.6 | 22.0 | 4.0 | 24.8 |
| C15 8hd | 402.3 | 724.2 | 61.0 | 1187.5 | 22.8 | 56.5 | 3.9 | 42.9 |

- steel wall friction angle: 7.37° – 9.02°;
- steel wall friction coefficient: 0.13–0.16;
- internal friction angle: 19° – 29°;
- humidity: 10.62%.

The values for specific weight obtained in these tests were very close to those obtained with the experimental silo (Table 2). The values used to obtain pressures according to the calculation method proposed in the Eurocode were those obtained in laboratory tests.

*2.5.2. Test settings*

Using the granular material described above and concentric filling, 30 tests were performed, divided into six configurations with five repetitions each. Each configuration differed as regards hopper angle and the height of the product filling (slenderness). Three filling heights were used: 2.5 m (4hd), 4.0 m (6hd), and 5.0 m (8hd) (Fig. 6); and two concentric hopper angles: $\beta = 15°$ (C15) and $\beta = 60°$ (C60). Although the height / diameter ratio was not exactly 4, 6, and 8, this term has been used to facilitate writing.

The decision to use a hopper with angles $\beta = 15°$ and $\beta = 60°$ was due to Eurocode 1, part 4. The hopper angles associated with the friction coefficient of the wall with the product ($\mu$) (in the case of this study, steel with corn) generate different flows (Fig. 7), mass flow at $\beta = 15°$ and funnel flow at $\beta = 60°$, enabling study of flow during discharge.

The silo was filled by the bucket elevator at a constant speed using the same silo gate aperture, providing approximate flow rates for the tests (Table 1), with the exception of the C60 8hd configuration in which the aperture was modified in two of the five tests due to vibration.

The silo was discharged with the gate (diameter of 0.20 m) 100% open. As can be seen in Table 1, with the same gate aperture, the discharge flow using the $\beta = 15°$ hopper was at least 30% higher than with the $\beta = 60°$ hopper, regardless of slenderness.

As each of the six configurations tested a different geometry (hopper angle and cylinder height), the product loading values were also different. Table 2 presents the values related to the load of the grain mass for each configuration and the specific weight of the corn calculated according to the volume and the load of each configuration. The

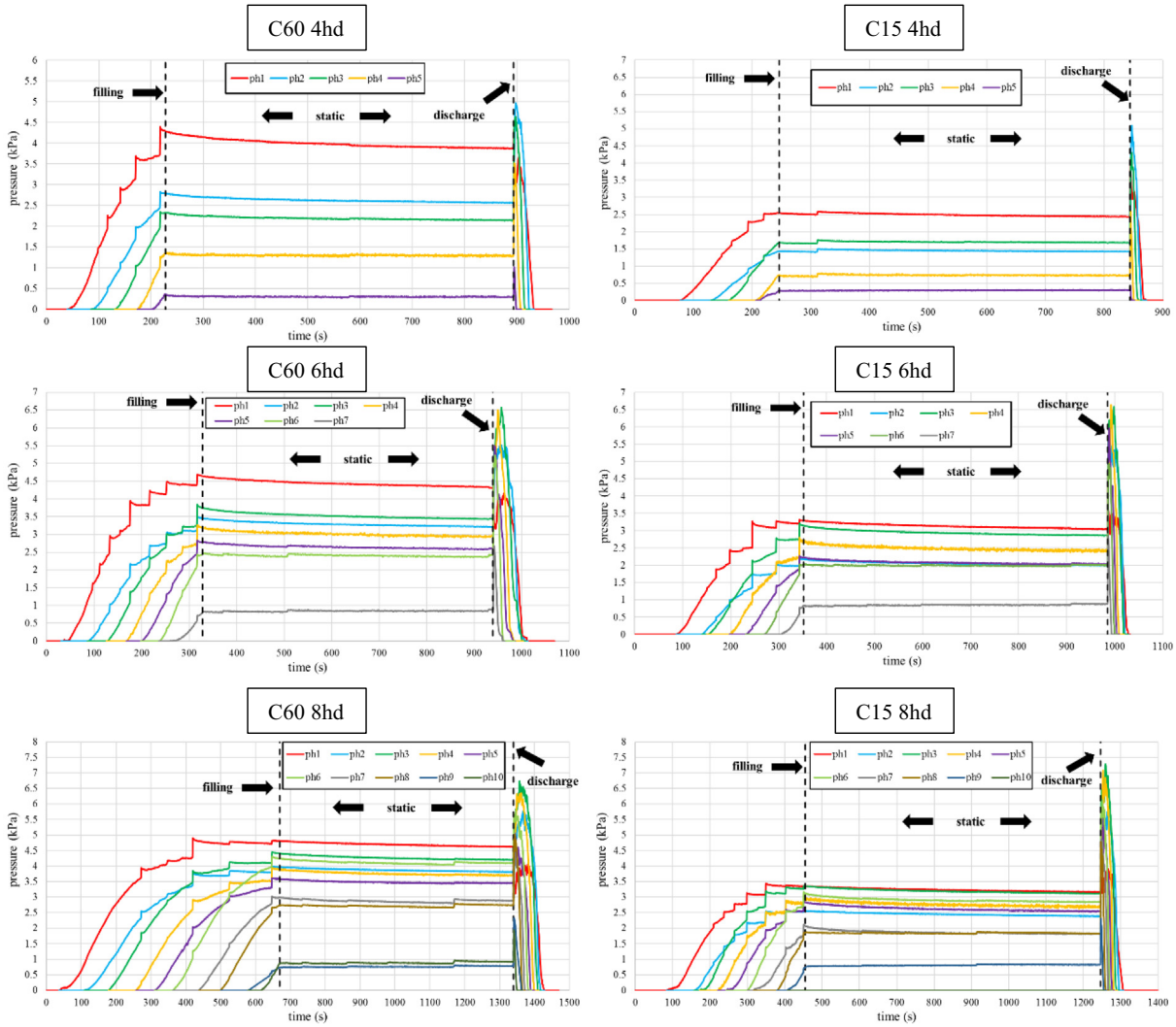


**Fig. 9.** Normal silo cylinder wall pressures (pH), at each time t. Type C15 and C60 assays, test C60 4hd, C60 6hd, C60 8hd, C15 4hd, C15 6hd, and C15 8hd.

values for the assay configurations differed; however, they were within the limits obtained in the laboratory presented previously (7.52–7.83 kN/m$^3$).

All tests were carried out as follows (Fig. 8): the silo was filled to the height of interest (verified by the tension load cell that showed the measurement for the ring above the height of interest), then a static phase was observed (for 10 min) followed by product discharge (hopper gate 100% open).

The times for each stage (filling, static, and discharge) and configuration are shown in Table 3. As can be seen, opening of the silo gate and rotation of the bucket elevator were constant, except in the case of C60 8hd (previously explained), and the values showed the expected pattern.

Filling time was longer for higher volume configurations. The pre-established 10 min static phase was approximate in all configurations. The discharge period was longer for funnel flow configurations (C60) and, as expected, was also longer as silo slenderness increased (greater volume).

### 2.5.3. Description of the analyses

In the results and discussion below, we compare and discuss the slenderness and hopper angle variables, which according to Eurocode 1 part 4 [12] shown in Fig. 7 represent two flow patterns in the discharge step.

Analysis of the results and discussion are divided into: normal pressures on the cylinder wall; friction pressures on the cylinder wall; normal hopper wall pressures, vertical stress in the stored material at the transition and weight of stored material; maximum normal pressures; maximum friction pressures; discharge overpressure in the silo cylinder; lateral pressure ratio at transition; and maximum normal pressure at the transition.

The normal and frictional pressures on the cylinder wall were evaluated at all phases of the test (filling, static, and discharge) over time. The objective was to evaluate temporal behavior in the silo cylinder as influenced by slenderness and hopper angle.

The vertical stress in the stored material at the transition and weight of stored material were evaluated in all phases of the test (filling, static, and discharge) over time. The objective was to evaluate temporal behavior in the silo-hopper transition and in the silo hopper as influenced by slenderness and hopper angle. The weight of the stored material was also evaluated.

Maximum normal and frictional pressures were evaluated in the filling and discharge phases. The objective was to evaluate the influence of slenderness and hopper angle. In addition, the results are compared with the Eurocode.

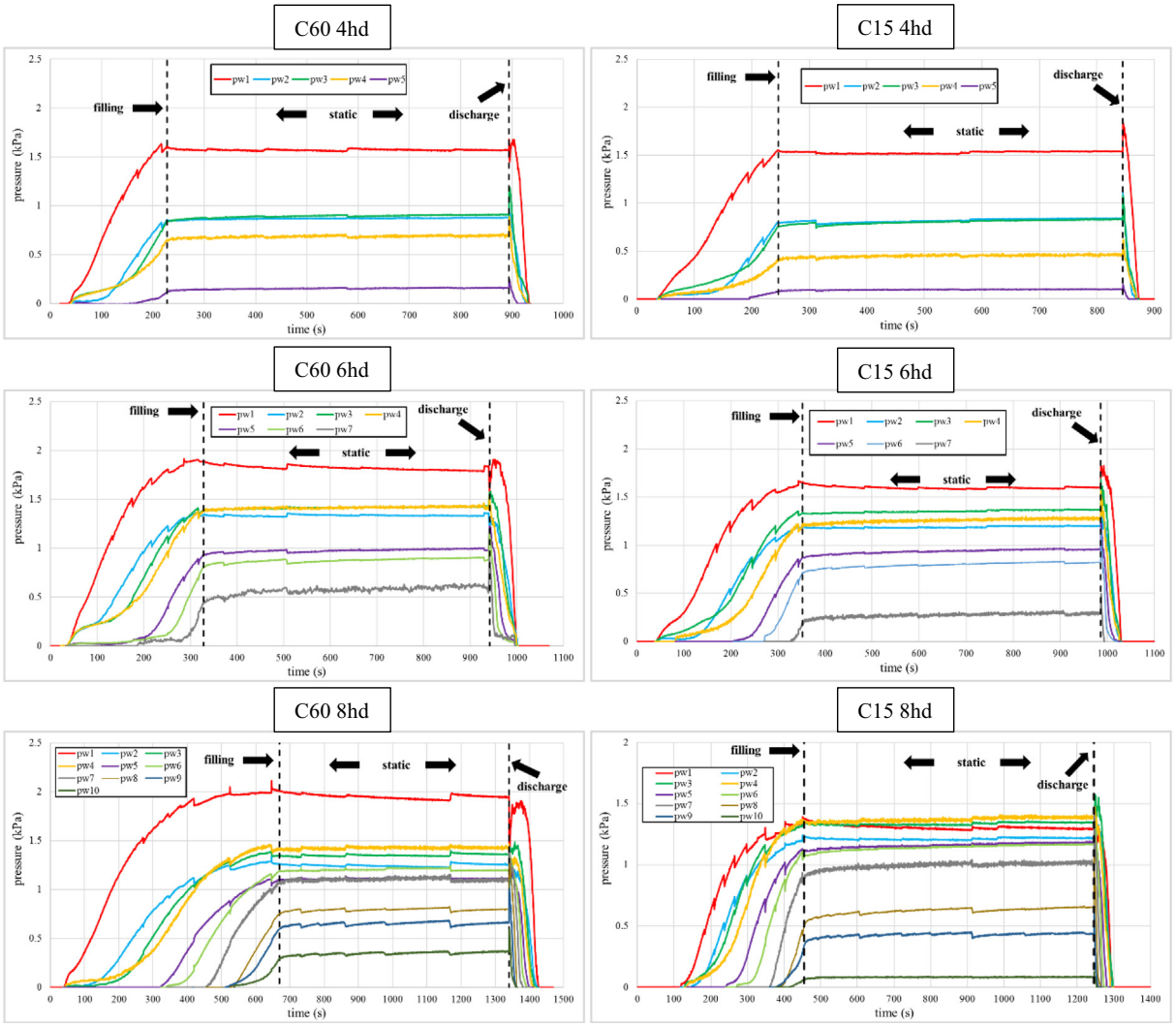


**Fig. 10.** Friction pressures on the silo cylinder wall ($p_w$), at each time t. Type C15 and C60 assays, test C60 4hd, C60 6hd, C60 8hd, C15 4hd, C15 6hd, and C15 8hd.

The discharge overpressure in the silo cylinder was obtained from the difference between maximum pressures in the static phase and maximum pressure during discharge. The objective was to understand the height and type of pressure that presents greatest overpressure during discharge, relating the flow pattern to slenderness.

The lateral pressure ratio at the transition was obtained from the horizontal and vertical pressure ratio in the silo-hopper transition [12]. The objective was to understand temporal behavior due to slenderness and hopper angle in relation to type of flow during discharge.

The maximum normal pressure at the transition was obtained at the silo-hopper transition at the start of discharge. The objective was to analyze the temporal behavior of this pressure as influenced by slenderness and flow pattern.

## 3. Results and discussion

### 3.1. Normal pressures in the cylinder wall

We found (Fig. 9) that with greater slenderness and a lower angle in β, normal pressures at the cylinder heights intersected, that is, they differed from the hydrostatic pressures, as observed in the C15 4hd test where $p_{h3}$ surpassed $p_{h2}$ shortly after 200 s, still in the filling stage. This behavior was observed in all cases, except for C60 4 hd (less slenderness and lower hopper angle).

In general, Fig. 9 shows that the normal pressures on the cylinder wall after filling were higher when using the hopper $\beta = 60°$, since the pressures increased with increasing product height (increasing in parallel with slenderness). As an example, the pressure at height 0.25 m ($p_{h1}$) increased from 3.9 kN in C60 4hd to 4.65 kN in C60 8hd, while for $\beta = 15°$ there was an increase from 2.5 kN in C15 4hd to 3.1 kN in C15 8hd.

Regarding the static phase, settling of the material was apparent after filling the silo and was more evident the greater the slenderness of the silo, with settling points occurring more frequently at the beginning [23,24].

Although the pressures in hoppers with $\beta = 60°$ were higher than at $\beta = 15°$ in the filling and static phases, we found that the maximum normal pressures during discharge reached the same magnitude at heights between 0.75 and 1.25 m ($p_{h2}$ and $p_{h3}$) for slenderness 4hd, and between 1.25 and 1.75 m for slenderness 6hd and 8hd, demonstrating that there is a difference in the height of the static channel at the time of discharge in relation to slenderness.

### 3.2. Friction pressures on the cylinder wall

During silo filling, we found (Fig. 10) that the magnitude and quantity of the settling peaks were related to a decrease in β and an increase

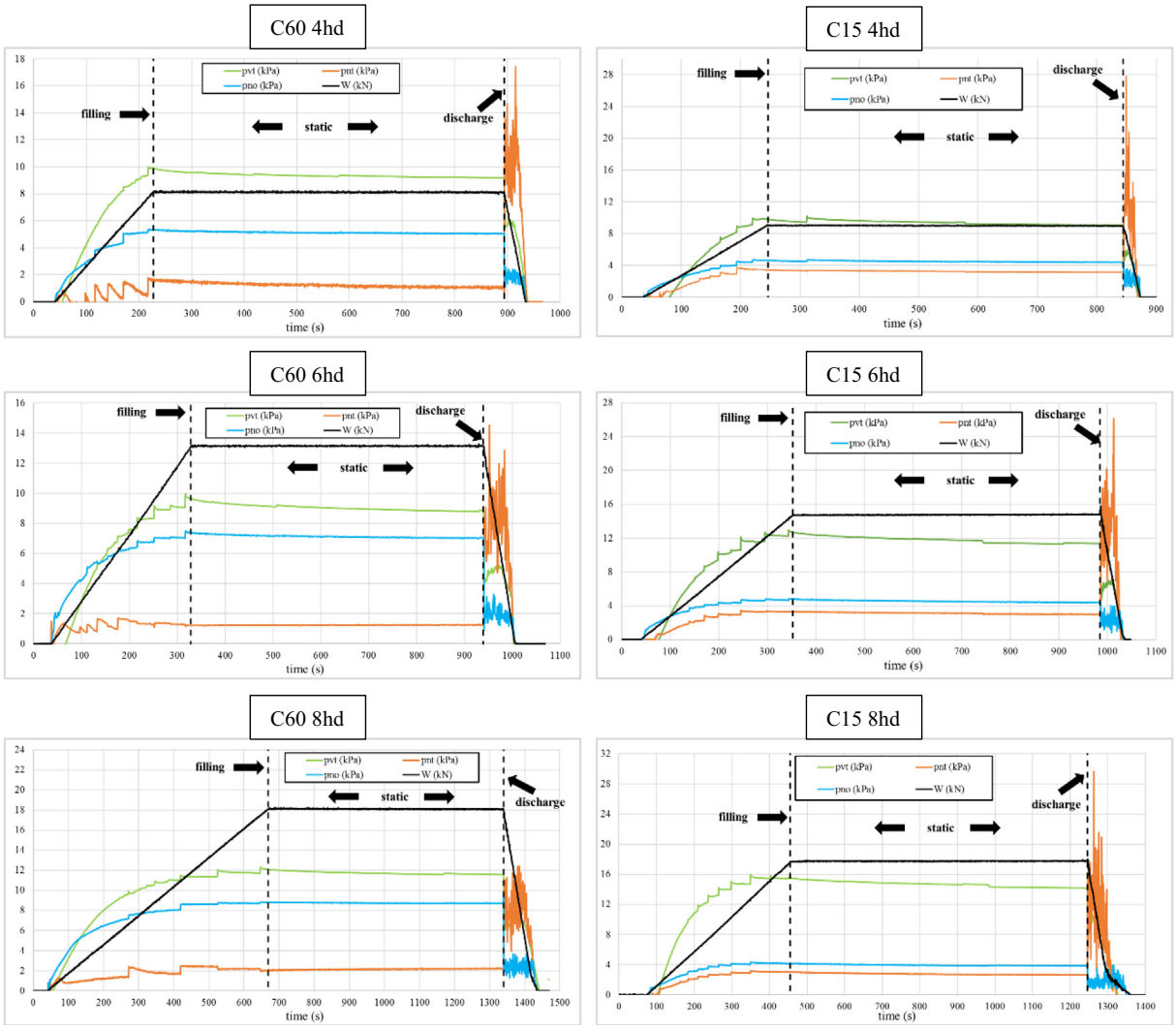


**Fig. 11.** Normal hopper wall pressures ($p_n$), vertical stress in the stored material at the transition ($p_{vt}$), and weight of stored material (W) at each time t. Type C15 and C60 assays, test C60 4hd, C60 6hd, C60 8hd, C15 4hd, C15 6hd, and C15 8hd.

in slenderness, that is, we observed fewer settling peaks and these were of lower magnitude for C60 4hd and maximum for C15 8hd.

Friction pressures on the cylinder wall at $\beta = 60°$ rose as slenderness increased, whereas at $\beta = 15°$, little difference was observed in relation to variations in slenderness.

As regards the static phase, besides the normal pressures, the settling related to displacement of the material exerting vertical force on the walls (frictional pressures on the cylinder wall) increased with greater height of the stored product. More settling occurred at the beginning, reducing the settling peaks over time [23]. Another observation concerned the symmetry of the settling peaks related to silo height, whereby frictional pressures on the wall next to the hopper increased, those located at the top decreased, and those in the central part of the silo were neutral.

Regarding discharge, flow pattern, and formation of a static channel according to hopper angle, we found that at the start of discharge with the $\beta = 60°$ hopper (funnel flow), the pressure close to transition ($p_{w1}$) showed a negative peak which intensified as slenderness increased.

### 3.3. Normal hopper wall pressures, vertical stress in the stored material at the transition and weight of stored material

Although measurements in the pilot silo hoppers could be taken 180° apart (on both sides), enabling analysis of the symmetry of pressures in the hopper, we sought to use the maximum value between the two measurements, rather than addressing the effect of symmetry of pressures in the silo even in concentric discharge or for silos under the same conditions [15]. Therefore, whenever pressures in the hopper are presented, it should be borne in mind that these refer to the greatest pressure between the two sides.

Fig. 11 shows the quality of the instrumentation according to the order in which the data were obtained. Data collection began with the weight of the stored material (W), followed by the pressure at the hopper outlet ($p_{no}$), the pressure at the transition ($p_{nt}$), and the vertical stress at the transition ($p_{vt}$). At the end of the test (discharge), the values were zeroed in reverse order to the filling, which was to be expected: $p_{vt}$, $p_{nt}$, $p_{no}$, and W.

The weight of the stored material (W) obtained during the three phases of the test showed a linear behavior, which was to be expected. However, in the final seconds of discharge in the C15 8hd test, the weight of the stored product (W) showed a curvilinear behavior, explained by the large volume of grains in this configuration, which the transition box was incapable of supporting. Nevertheless, this did not influence the results, and the transition box has been fixed.

In relation to vertical stress in the stored material transition ($p_{vt}$), we observed a higher number and greater magnitude of settling of the stored material during filling of the hopper $\beta = 15°$, explained by the greater instability, higher angle, and greater volume of the hopper, which permitted rearrangement of the material inside due to the specific weight of the product in the silo cylinder. In contrast to other studies [23,24,47], where vertical stress in the stored material transition ($p_{vt}$) in the static phase increased with time, in our study we observed a decrease in $p_{vt}$. These previous authors explained that

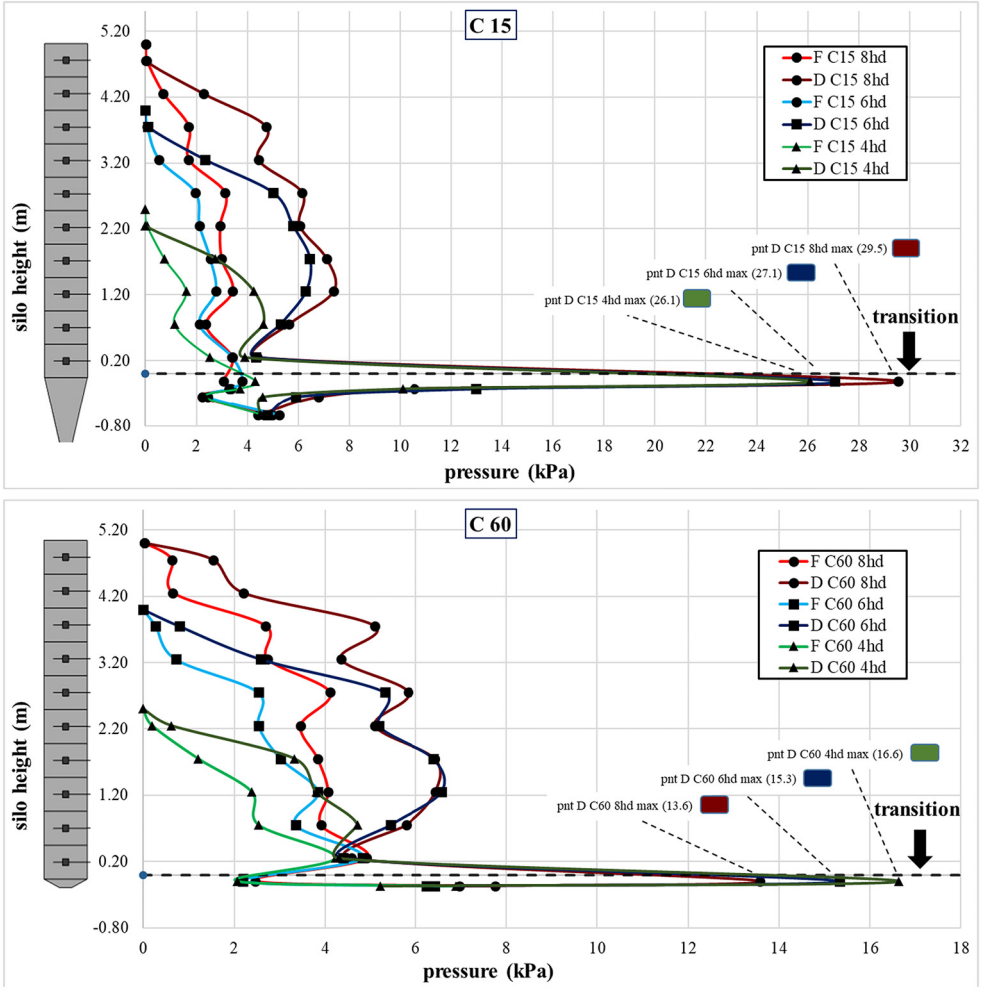


**Fig. 12.** Maximum normal pressures on the wall (pH) varying silo slenderness.

in the static phase, the cylinder walls released their load, increasing the weight resting on the hopper, and that this was due to settling of grain in the silo. Despite being a correct statement, in the present study we believe that because silo slenderness was greater than in the model proposed by these authors, the frictional pressures in the cylinder (Fig. 10) and the normal pressures in the hopper (Fig. 10) were responsible for this stress and increased over time. As expected, the vertical tension of the stored product at the transition ($p_{vt}$) showed a considerable decrease during discharge in all tests, as will be discussed in more detail below.

Figs. 9, 10, and 11 show that the settling peaks during the filling and static phases occurred at the same time and for all measurements (normal and friction pressures in the cylinder and vertical stress in the stored material transition). Therefore, the behavior of normal pressures in the hopper ($p_{nt}$ and $p_{no}$) also captured these settling. As mentioned above, the pressures in the hopper near the transition ($p_{nt}$) and the

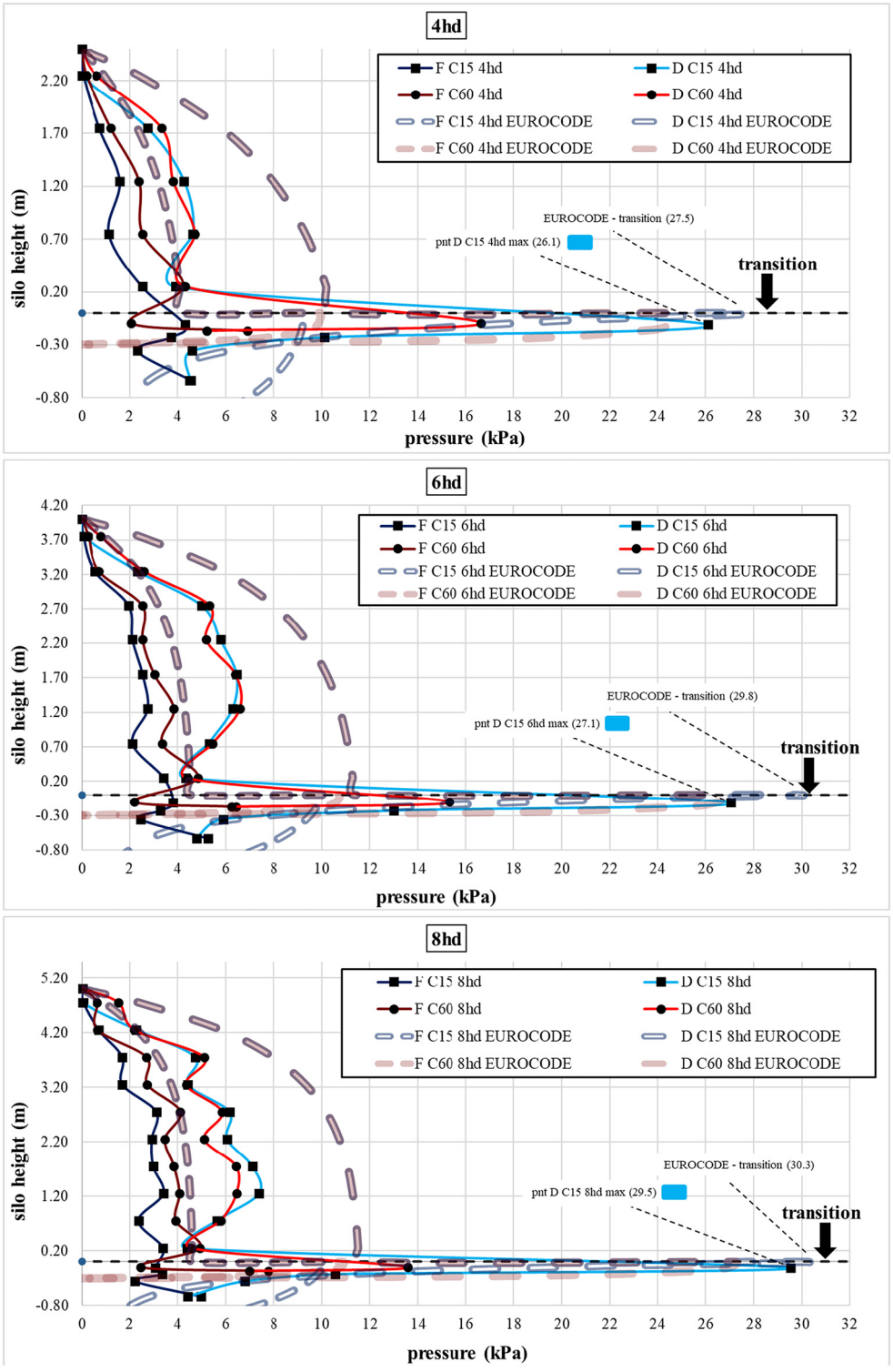


**Fig. 13.** Maximum normal pressures on the wall (pH), varying the hopper angle. Comparison with Eurocode 1, part 4.

**Table 4**
Mean values of maximum pressures at transition.

| Test | Average value pnt (kPa) | Standard deviation (kPa) |
|---|---|---|
| C60 4hd | 16.22 | 0.43 |
| C60 6hd | 15.63 | 1.53 |
| C60 8hd | 13.57 | 1.22 |
| C15 4hd | 26.08 | 2.05 |
| C15 6hd | 27.78 | 1.60 |
| C15 8hd | 31.13 | 1.31 |

outlet increased slightly in the static phase due to the increased friction pressure in the entire cylinder (Fig. 10) and the increase in normal pressures in the upper half of the cylinder (Fig. 9). This behavior is explained by the settling, segregation, and slight vertical movement of the stored product.

As expected, normal hopper wall ($p_{nt}$ and $p_{no}$) pressures varied considerably at the beginning of discharge. This is because of the influence of the low-pressure zone at the junction between the vertical wall and the hopper. During discharge, this produces a dead zone (material remains static), and therefore $p_{nt}$ values are lower. Maximum values occurred at the hopper wall transition ($p_{nt}$), at the level of the silo-hopper transition, as reported by many authors and in standards [12,22] and confirmed in international tests on real silos [23,42,48].

### 3.4. Maximum normal pressures (ph max)

For ease of comparison, Fig. 12 shows the maximum pressures due to hopper angle compared with slenderness in each case. As expected, maximum pressures at the transition were of greater magnitudes

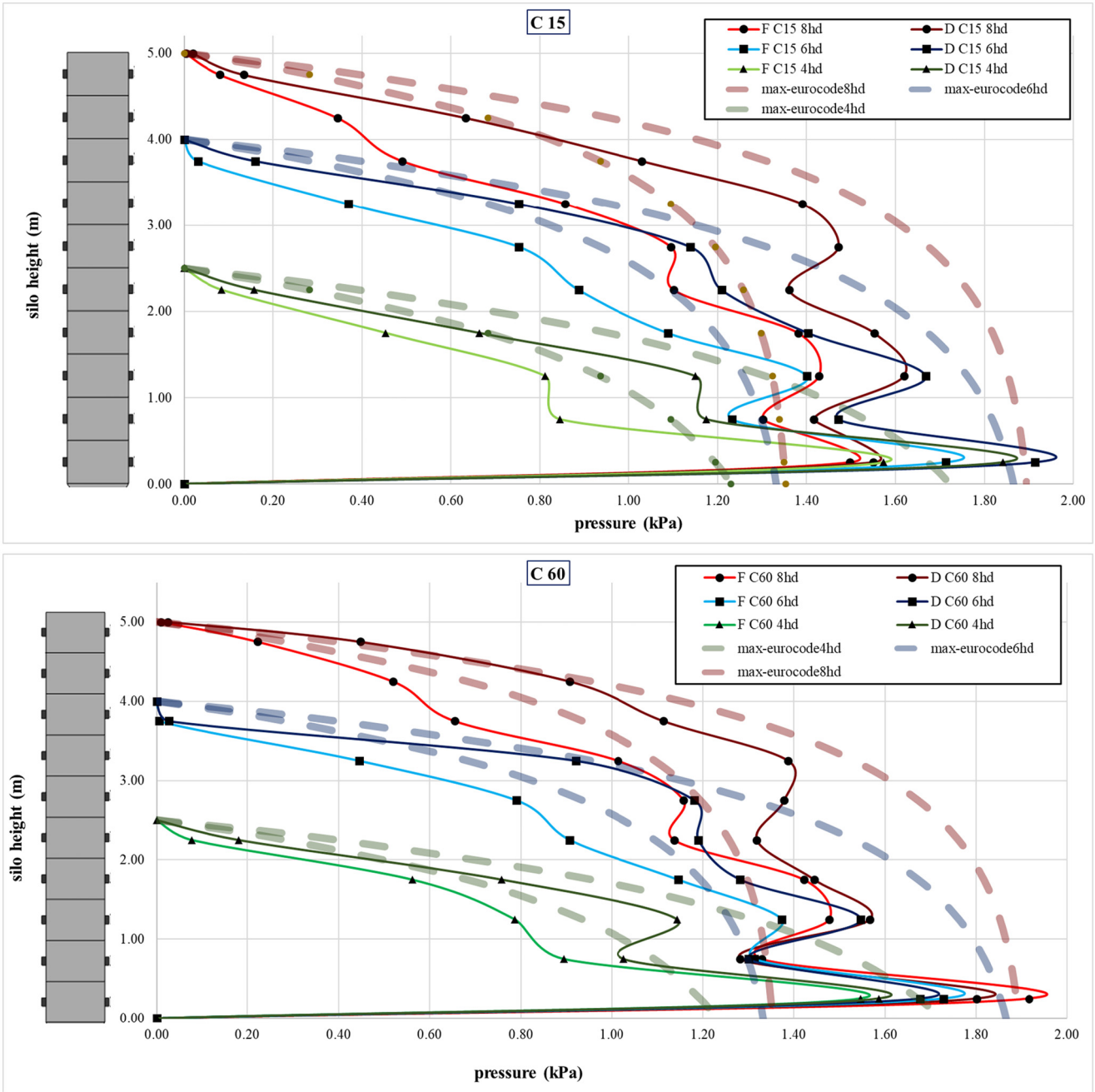


**Fig. 14.** Maximum friction pressures on the wall ($p_w$). Comparison with Eurocode 1, part 4.

when using a hopper characterized as mass flow (Fig. 7), $\beta = 15°$ (C15), according to [12].

F: Filling. D: Discharge.

The maximum normal pressures on the cylinder wall using the $\beta = 15°$ hopper (C15) showed no maximum pressure distribution pattern during filling or discharge. However, some interesting observations were recorded. For example, maximum pressure for 8hd occurred at the same time during filling and discharge, at 1/4 of the height of the silo (1.25 m, $p_{h3}$). For all height / diameter ratios (4hd, 6hd, and 8hd), maximum normal pressure on the cylinder wall during filling occurred at the same height, close to the transition at 0.25 m ($p_{h1}$). In contrast, the maximum pressure during discharge occurred at different heights (4hd: 0.75 m, 6hd: 1.75 m, and 8hd: 1.25 m, in positions $p_{h2}$, $p_{h4}$ and $p_{h3}$).

For hopper $\beta = 60°$ (C60) at all heights of the material (4hd, 6hd, and 8hd), the maximum normal pressure on the cylinder wall during filling occurred at a fixed height, close to the transition at 0.25 m ($p_{h1}$). During discharge, however, it occurred at different heights but in the same proportion, at 1/3 of the maximum height of the silo in relation to the transition (4hd: 0.75 m, 6hd: 1.25 m, and 8hd: 1.75 m, in positions $p_{h2}$, $p_{h3}$, and $p_{h4}$).

It is already known that maximum pressures during discharge occur at the hopper silo transition [8,9,12,22], and the same phenomenon was observed in this study, regardless of slenderness or hopper angle (changing the flow pattern); however, it is also known that the magnitude of the pressure varies according to the flow pattern [10,25,49]. It is interesting to note that for mass flow (C15), the maximum pressures at the transition ($p_{nt}$) increased in parallel with an increase in slenderness, whereas the opposite occurred for funnel flow (C60), where pressures decreased in parallel with an increase in slenderness, a finding that will be discussed in further detail below.

The maximum pressures were also compared with those calculated by Eurocode 1, part 4, as shown in Fig. 13, which also depicts the pressure curves for slenderness and in relation to hopper angle.

During discharge, none of the six configurations exceeded the values calculated by the standard. As shown in Fig. 13, with the C15 8hd configuration, the normal pressure value at the silo hopper transition was close to that given in the standard. However, the average of the five repetitions of the C15 8hd configuration, shown in Table 4, exceeded the value calculated by Eurocode 1, part 4 (30.3 kPa).

During filling, we observed that at all heights when using hopper $\beta = 60°$ (C60), the normal pressure on the silo wall at height 0.25 m ($p_{h1}$) exceeded the curve calculated by the standard. With the C60 8hd configuration, a second point at height 2.75 m ($p_{h6}$) also exceeded the value obtained by the standard. Therefore, our results

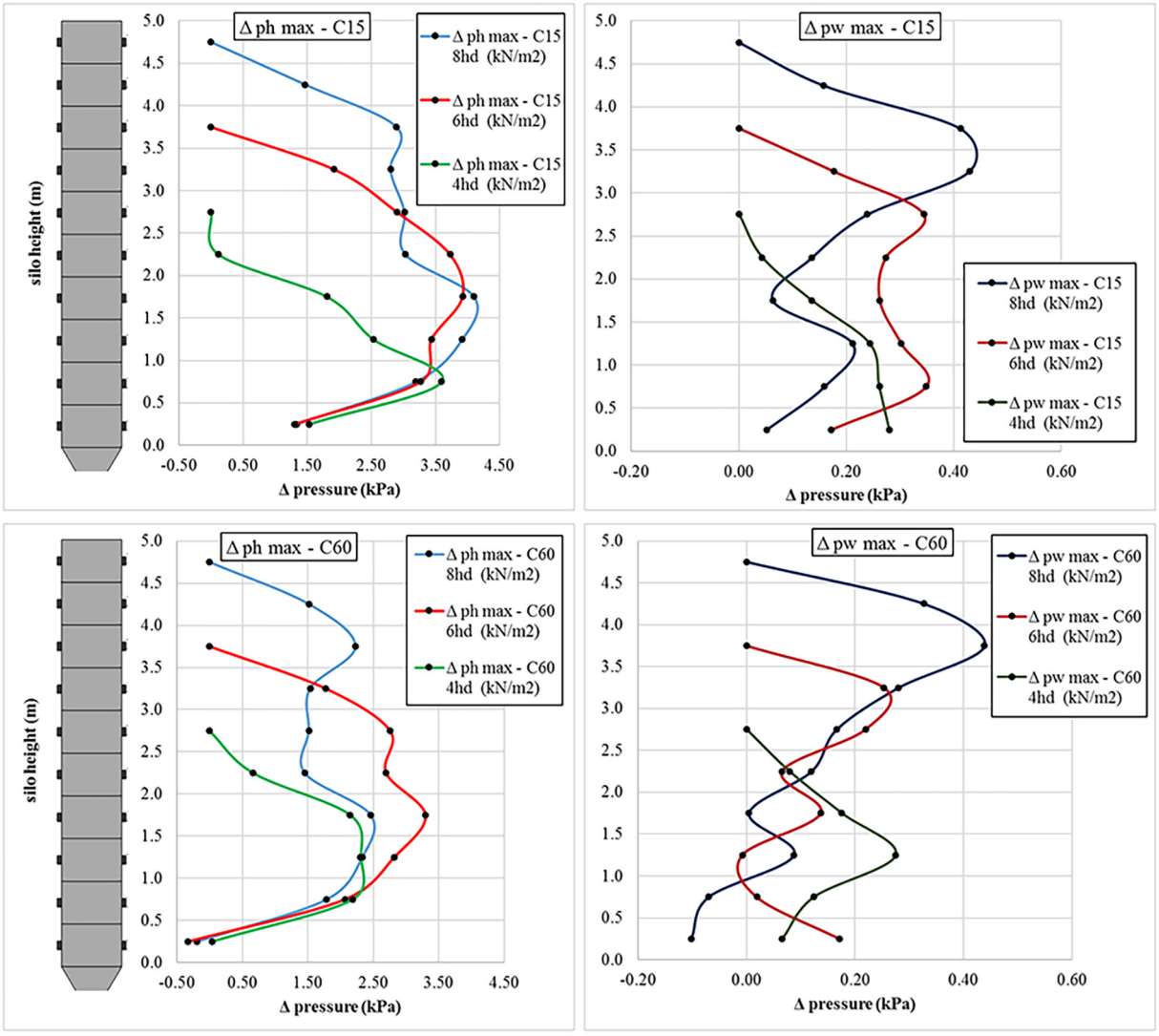


**Fig. 15.** Discharge overpressure in the silo cylinder according to silo height ($\Delta p_h$ max and $\Delta p_w$ max).

support the notion that maximum pressures in slender silos tend to behave in waveforms, regardless of hopper configuration [23].

### 3.5. Maximum friction pressures ($p_w$ max)

Fig. 14 gives the maximum frictional pressures in the cylinder compared with those given in Eurocode 1, part 4, showing the six configurations divided between the two hopper geometries ($\beta = 15°$ and $\beta = 60°$).

The maximum experimental frictional pressures in the pilot silo exceeded those obtained by Eurocode 1, part 4 at several points. Brazil does not have a specific standard for silo storage, and several failures have occurred related to buckling due to the vertical force exerted on the wall of the silo.

With the $\beta = 15°$ (C15) hopper, we found that the maximum friction pressure occurred close to the transition at 0.25 m ($p_{w1}$) for the diameter ratio 6 hd, exceeding the standard during filling and discharge alike. With hopper $\beta = 60°$ (C60), maximum friction pressure occurred at the highest diameter/height ratio (8 hd) during filling at height 0.25 m ($p_{w1}$), also exceeding that calculated by Eurocode 1, part 4.

### 3.6. Discharge overpressure in the silo cylinder - $\Delta p_h$ max and $\Delta p_w$ max

The aim of this analysis was to determine the silo heights at which the greatest pressure increases occurred during discharge, rather than maximum pressures during discharge (Fig. 15).

A comparison of normal overpressures revealed that the pattern was more strongly influenced by slenderness than by hopper angle. Thus, for 4hd, the greatest overpressures were located at the bottom of the silo (near the transition), for 6 hd they occurred toward the central part of

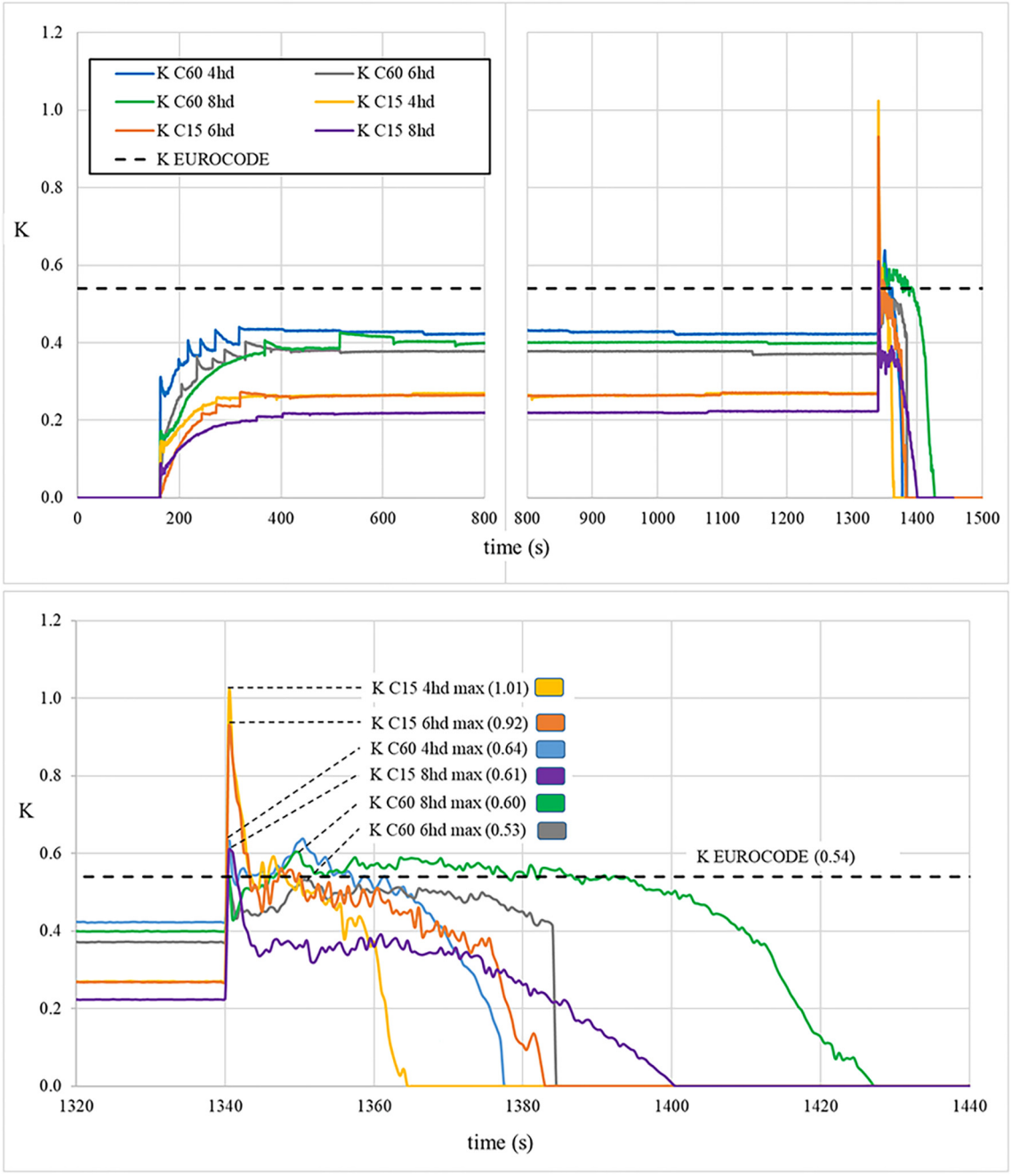


**Fig. 16.** Temporal behavior of the coefficient of lateral pressures (K).

the silo, and for 8hd there was a wave pattern, with the highest overpressures at the extremities (near the transition and in the upper part) and the lowest in the central part of the cylinder.

A more detailed analysis of normal overpressures in relation to hopper angle showed that for 4hd, C60 presented 3 maximum points ($p_{h2}$, $p_{h3}$, and $p_{h4}$) while C15 only had one maximum point ($p_{h2}$), indicating that material in the static zone during discharge is most influenced by shallower hoppers and funnel flow (C60). However, in slender silos (in this case, 6hd and 8hd), the behavior of the overpressures in the two types of flow was similar. One of the possible reasons for this behavior [12,23,27] is that in very slender silos, flow channels form even in very highly angled hoppers and the pressures show an undulating behavior (pressures change between high and low).

Friction overpressures showed a different behavior to normal overpressures. For slenderness 8hd, we found that normal and friction overpressures presented the same pattern, which can be explained by the same reason given above, the presence of flow channels in very slender silos. For slenderness 4hd with mass flow ($\beta = 15°$), the overpressures occurred in a triangular manner, reaching a maximum near the transition and decreasing until the top of the silo, whereas with funnel flow ($\beta = 60°$), the maximums occurred in the central part of the cylinder, possibly due to flow channel formation and stationary material. For slenderness 6hd, both showed a wave pattern, but this differed between the two hopper angles.

### 3.7. Coefficient of lateral pressures (K)

The lateral pressure ratio (K) is obtained by (CEN - European Committee for Standardization, 2006), calculated solely according to the type of stored material, regardless of slenderness or hopper geometry. Fig. 16 gives the values obtained during the tests performed on all configurations, from which it is possible to evaluate the behavior of K in each of them.

As can be seen in Fig. 16, the values obtained in the pilot silo for all configurations were lower than that given in Eurocode 1, part 4, except during discharge. This has also been reported by other authors, who have reported a considerable increase in K during the first seconds of discharge that exceeded Eurocode 1, part 4 [23,24,47].

C60 6hd was the only configuration that obtained a lower K value during discharge than that in Eurocode 1, part 4, while C15 4hd obtained the highest increase (87%), followed by C15 6hd (70%). This indicates that mass flow is associated with higher values of K (the three

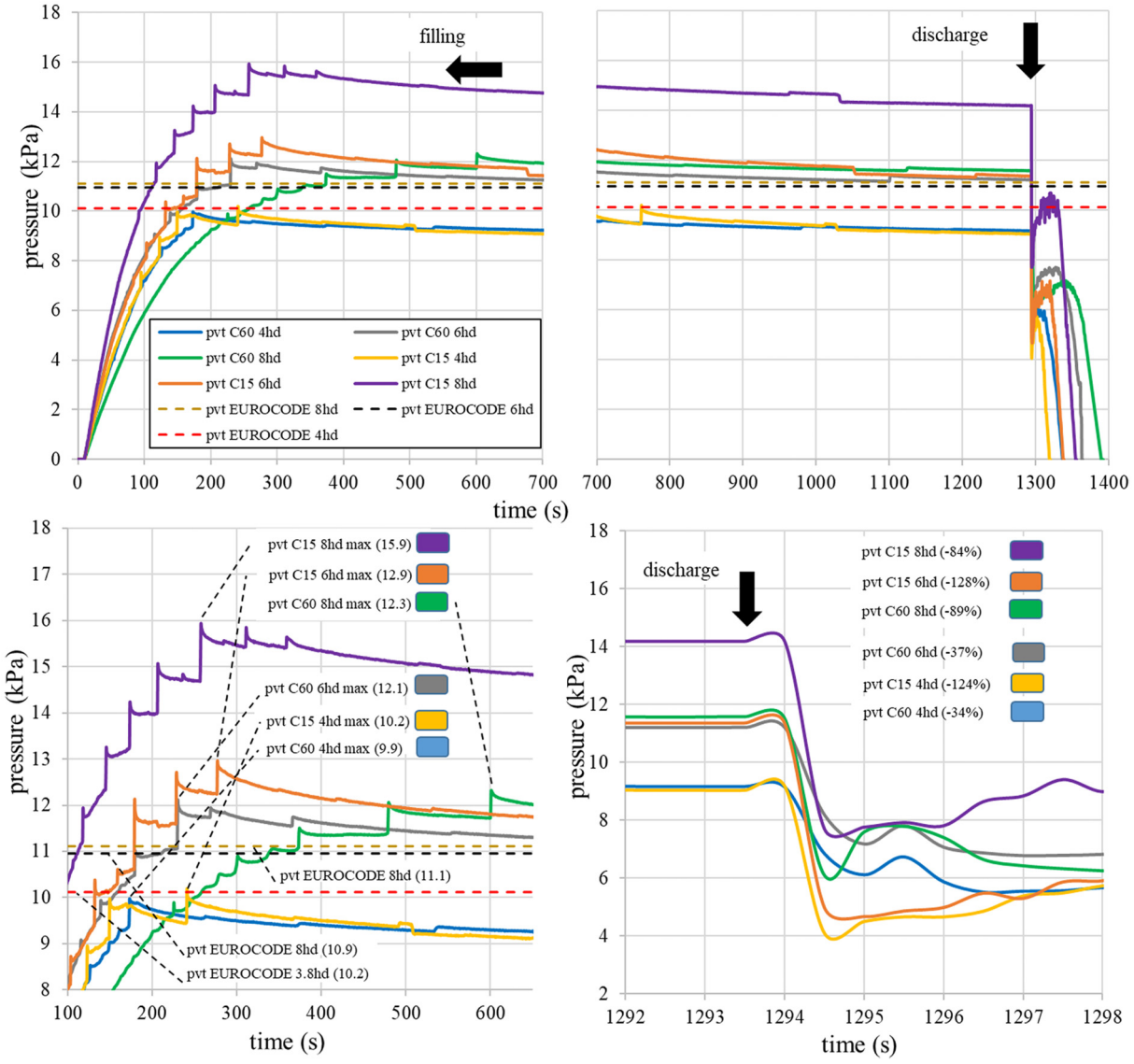


**Fig. 17.** Temporal behavior of vertical stress in the stored material at the transition ($p_{vt}$).

configurations exceeded the values of the standard). Despite not showing such a significant increase over the values stipulated by the standard (12% for C15 8hd), the values obtained when using hopper angle $\beta = 15°$ remained higher for more than half of the total discharge time.

### 3.8. Vertical stress in the stored material at the transition ($p_{vt}$)

Vertical stress in the stored material at the transition ($p_{vt}$) is obtained by (CEN - European Committee for Standardization, 2006), and is influenced solely by the size of the silo cylinder. However, as shown in Fig. 17, the $p_{vt}$ value was influenced not only by silo cylinder geometry, but also by hopper angle and/or flow pattern.

As mentioned earlier in reference to Fig. 11, vertical stress in the stored material at the transition ($p_{vt}$) decreased as a function of time in the static phase. However, with very slender silos, above 4hd, vertical stress in the stored material at the transition ($p_{vt}$) considerably exceeded that given in Eurocode 1, part 4.

Another interesting observation was that vertical stress in the stored material at the transition ($p_{vt}$) occurred moments after filling the silo, and this value was related to the first peak of settling after the silo had been filled. As noted, the magnitude of this value was influenced by silo slenderness and hopper geometry. This indicates that the lower the hopper angle (in relation to β) and the greater the silo slenderness, the greater the stress in the stored material at the transition ($p_{vt}$).

Another interesting pattern was observed in very slender silos, (in this case, 8hd) at the beginning of discharge, whereby hopper angle did not influence the sharp drop in $p_{vt}$ (84% and 89%, for C15 and C60 respectively). This can again be explained by the possible formation of flow channels due to silo slenderness.

An analysis of slenderness 4hd and 6hd in relation to hopper angle revealed an inversion of this pattern. For funnel flow (C60), a less marked drop in $p_{vt}$ was observed (34% and 37% for 4hd and 6hd, respectively), while for mass flow (C15), a very considerable drop in stress was observed (124% and 128% for 4hd and 6hd, respectively). This can be explained by a change of the state of the stresses, providing the packaging of the particles during discharge, increasing or decreasing in different areas according to the previous static state [24,47]. Therefore, the change in this state is less pronounced with funnel flow than with mass flow.

### 3.9. Maximum normal pressure at transition ($p_{nt}$)

As expected, in all cases this value presented a marked increase when discharge began; however, normal pressures on the silo wall during discharge were erratic, alternating between high and low values after the start of discharge for mass flow [50]. Fig. 18 shows that in mass flow ($\beta = 15°$), the pressures during discharge oscillated considerably. Such oscillations also occurred with funnel flow ($\beta = 60°$), but were of lesser magnitude and more standardized.

The behavior of maximum pressure at the transition ($p_{nt}$) evidenced a pattern that was influenced by slenderness and hopper angle. We found that in general, funnel flow (C60) presented lower maximum pressure values than mass flow (C15), which was to be expected [10,12,22,25,26].

The moment of occurrence of maximum pressure after the beginning of discharge was different for the two flow patterns. For mass flow, it occurred in the first half of the total discharge time, whereas for funnel flow it was the opposite, occurring in the second half of the total discharge time. This pattern was not influenced by slenderness.

It is possible that the moment of maximum pressure is influenced by slenderness because in general, the slenderer the silo, the longer it took for maximum pressure to occur. However, this conclusion remains tentative because in the C15 6hd test, the moment of maximum pressure did not comply within this pattern.

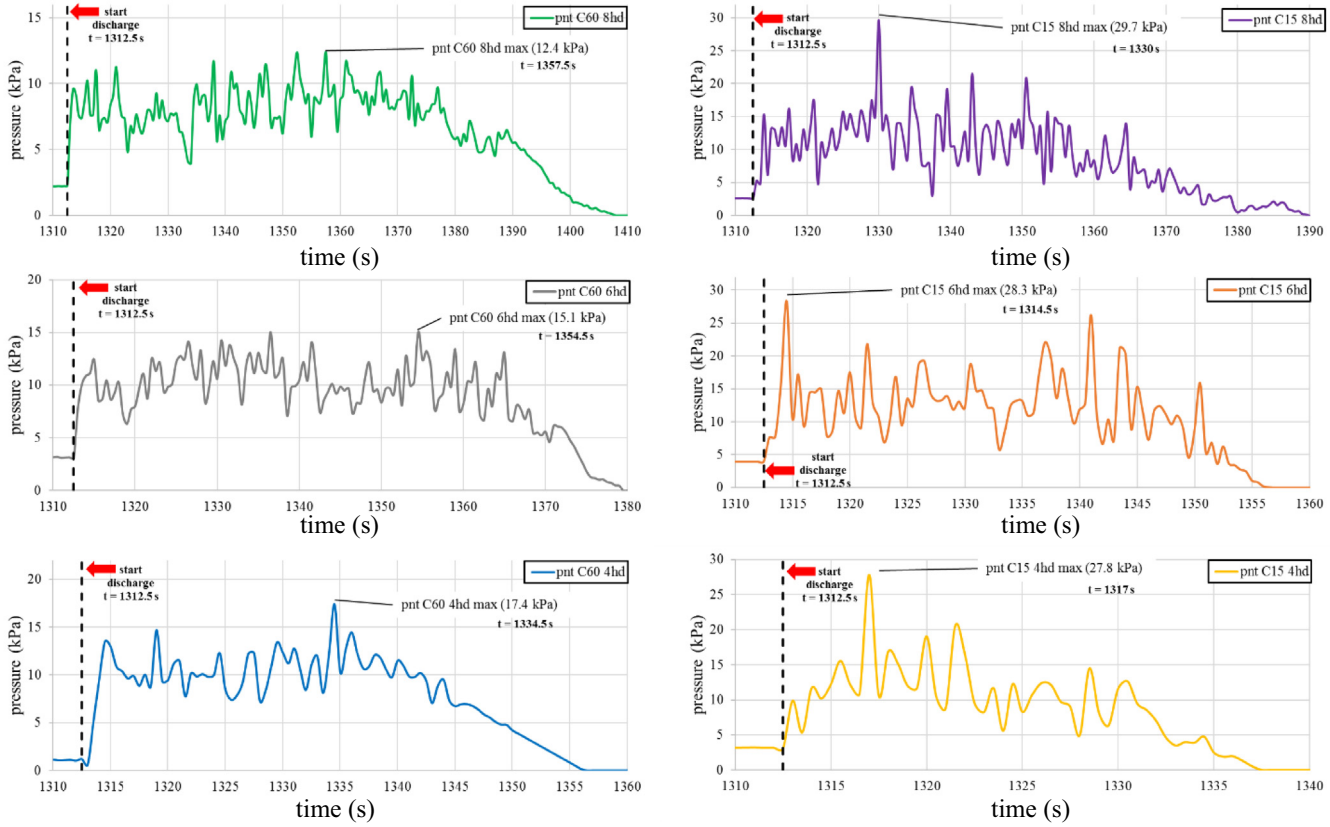


**Fig. 18.** Temporal behavior of maximum normal pressures in the hopper after discharge (pnt).

Another interesting observation regarding the two flow patterns, irrespective of silo slenderness, was the behavior of the pressure at the transition ($p_{nt}$). For funnel flow, the pressure presented a more standardized (linear) oscillation frequency, whereas in mass flow it presented sporadic peaks (Chen et al., 2007), confirming erratic behavior in mass flow [50].

This indicates that for mass flow, the greater the silo slenderness, the greater the maximum pressure at the transition. The opposite was true for funnel flow, whereby the greater the silo slenderness, the lower the maximum pressure. Nevertheless, when analyzing repetitions of the tests (Table 4), we only found a significant difference between the 4hd and 8hd configurations, for both flow patterns.

## 4. Conclusions

Just a few papers show the effect of the slenderness of silos. No work has been found that relates silo slenderness and flow pattern to pressures. Our research aimed to understand and presents relationships in a quantitative way relating the flow pattern and slenderness with silo pressures. Some gaps, such as basic information regarding discharge flow and overpressures during discharge are not easily discussed and found in scientific works and standards. Friction and normal pressures due to settling of the stored product during the static phase was verified in only a few works. In our pilot-scale experimental station, all these gaps were discussed relating the silo slenderness and the flow pattern.

We found that discharge flow was influenced by flow pattern, being 49% higher for mass flow. Nevertheless, discharge flow was not influenced by silo slenderness.

The hoppers with $\beta = 60°$ produced greater normal pressures on the cylinder wall (at least 40%) during the filling and static phases. However, at discharge, the maximum pressures tended to coincide. Thus, overpressure during discharge using $\beta = 15°$ was greater (twice bigger). In addition, the settling peaks and the magnitude of the pressure during settling rose as silo slenderness increased.

As regards maximum normal pressures on the cylinder wall during discharge compared to Eurocode, only the configuration with a height diameter ratio = 8 and mass flow pattern (C15 8hd) exceeded (in 3%) that calculated by the standard.

For very slender silos ($h / d \leq 4$), maximum pressure on the silo wall during filling occurred close to the transition ($p_{h1}$ = 0.25 m above transition, 1/10 of silo height), regardless of silo slenderness or hopper angle. During discharge, mass flow silos did not follow a pattern in the location of the maximum pressure on the wall. However, for funnel flow silos, the maximum pressure on the wall occurred at 1/3 of the silo height, regardless of slenderness.

The maximum frictional pressures on the cylinder wall it is inversely proportional between the hopper angles and the silo's slenderness: maximum pressures for $\beta = 15°$ and height diameter ratio = 4 and maximum pressures for $\beta = 60°$ and height diameter ratio = 8, in other words, for $\beta = 15°$ the pressures decrease (14%) by increasing the height diameter ratio and for $\beta = 60°$ the pressures increase (13%) by increasing the height diameter ratio.

Usually, the frictional pressures for hoppers with $\beta = 60°$ are slightly larger (2 to 6%) for filling than at discharge. We found that at some points of heights on the cylinder wall (mainly for C15 8hd and C60 6hd configurations), the pressures exceeded the Eurocode 1, part 4.

Frictional pressures in the cylinder during the static phase presented settling peaks that were symmetrical to the height of the silo. In other words, from half the height of the silo downwards, the peaks were positive; from half the height upwards they were negative, and in the central region, they were neutral. These friction peaks showed higher values in parallel with an increase in the height-to-diameter ratio.

In relation to the lateral pressure ratio (K), slenderness was inversely proportional to the magnitude of K; thus, slender silos obtained a smaller K immediately after discharge. Mass flow (in all h / d ratios) showed the highest K values at the transition, exceeding (up to 87%) those given in Eurocode 1, part 4.

Vertical stress in the stored material at the transition ($p_{vt}$) was influenced by silo slenderness but also by hopper angle, although Eurocode 1, part 4 does not consider hopper geometry when calculating this value. We found that the greater the silo slenderness and the lower the hopper angle (in relation to $\beta$), the greater the magnitude of $p_{vt}$. Furthermore, we also found that the maximums occurred immediately after filling the silo, at the first peak of settling of the material, regardless of silo slenderness or hopper angle.

As silo slenderness increased, maximum pressures at the transition increased in silos with mass flow (up to 19.4%) and decreased in silos with funnel flow (up to 19.5%). Transition overpressures ($p_{nt}$) are inversely quantitatively proportional to slender and hopper angle.

The moment of occurrence of maximum pressures at the silo-hopper transition differed according to flow pattern. For mass flow, it occurred in the first half of the total discharge time (2.0 to 17.5 s, depending on the slenderness), while for funnel flow it occurred in the second half (22.0 to 45.0 s, depending on the slenderness).

## CRediT author statement

**Gandia Rômulo M**: Conceptualization, Methodology, Validation, Formal analysis, Investigation, Data curation, Writing- Original draft, Writing - Review & Editing, Visualization. **Gomes Francisco C**: Resources, Supervision, Project administration, Funding acquisition. **De Paula Wisner C**: Writing - Review & Editing. **Aguado Pedro J R**: Supervision, Project administration, Funding acquisition.

## Declaration of Competing Interest

The authors declare that they have no competing financial interests or personal relationships that influenced the research reported in this paper.

## Acknowledgments

The authors are very grateful to Capes (Coordenação de Aperfeiçoamento de Pessoa de Nível Superior) for funding the doctoral scholarship related to this project.

## References

[1] C.N. de A. CONAB, Acompanhamento da safra brasileira 2019/2020, 2020 https://www.conab.gov.br/info-agro/safras.
[2] DPE - DIRETORIA DE PESQUISA E COORDENAÇÃO AGROPECUÁRIA, IBGE - Pesquisa de Estoques 2º semestre de 2019, 2019.
[3] A. Dogangun, Z. Karaca, A. Durmus, H. Sezen, Cause of damage and failures in silo structures, J. Perform. Constr. Facil. 23 (2009) 65–71, https://doi.org/10.1061/(ASCE)0887-3828(2009)23:2(65).
[4] F. Ayuga, Some unresolved problems in the design of steel cylindrical silos., in: J.G. Chen, J.F., Teng (Ed.), Struct. Granul. Solids From Sci. Princ. to Eng. Appl., CRC Press-Taylor & Francis Group, Boca Raton, USA, 2008: pp. 123–133.
[5] J. Nielsen, From silo phenomena to load models, in: J.F. Chen, J.G. Teng (Eds.), Struct. Granul. Solids from Sci. Princ. To Eng. Appl, CRC Press-Taylor & Francis Group, Boca Raton, USA 2008, pp. 49–57, https://doi.org/10.1201/9780203884447.
[6] H.A. Janssen, Versuche uber getreidedruck in silozellen, Z. Ver. Dtsch. Ing. 39 (1895) 1045–1049.
[7] D. Walker, An approximate theory for pressures and arching in hoppers, Chem. Eng. Sci. 22 (1967) 486, https://doi.org/10.1016/0009-2509(67)80145-3.
[8] J.K. Walters, A theoretical analysis of stresses in axially-symmetric hoppers and bunkers, Chem. Eng. Sci. 28 (1973) 779–789, https://doi.org/10.1016/0009-2509(77)80012-2.
[9] J.K. Walters, A theoretical analysis of stresses in silos with vertical walls, Chem. Sci. 28 (1973) 13–21.
[10] A.W. Jenike, J.R. Johanson, J.W. Carson, Bin loads—part 3: mass-flow bins, J. Manuf. Sci. Eng. Trans. ASME. 95 (1973) 6–12, https://doi.org/10.1115/1.3438163.
[11] DIN, DIN 1055-–6, Basis of design and actions on structures – Part 6: design 623 loads for buildings and loads in silo bins, Berlin, Verlaz, 2005.
[12] CEN, EN 1991-–4:2006, Eurocode 1: Actions on Structures. Part 4: Silos and Tanks, Brussels, 2006.
[13] A. Jenike, Storage and Flow of Bulk Solids Bull, 123, University of Utah, 1964.

[14] WPMPS, Standart Shear Testing Technique for Particulate Solids Using the Jenike Shear Cell, England 1989.
[15] J. Nielsen, Pressures from flowing granular solids in silos, Philos. Trans. R. Soc. A Math. Phys. Eng. Sci. 356 (1998) 2667–2684, https://doi.org/10.1098/rsta.1998.0292.
[16] C. Bywalski, M. Kamiński, A case study of the collapse of the over-chamber reinforced concrete ceiling of a meal silo, Eng. Struct. 192 (2019) 103–112, https://doi.org/10.1016/j.engstruct.2019.04.100.
[17] Y. Sun, Y. Wang, Collapse reasons analysis of a large steel silo, Adv. Mater. Res. 368–373 (2012) 647–650, https://doi.org/10.4028/www.scientific.net/AMR.368-373.647.
[18] G. Gutiérrez, C. Colonnello, P. Boltenhagen, J.R. Darias, R. Peralta-Fabi, F. Brau, E. Clément, Silo collapse under granular discharge, Phys. Rev. Lett. 114 (2015) 5–9, https://doi.org/10.1103/PhysRevLett.114.018001.
[19] B.J. Teng, Plastic collapse at lap joints in pressurized cylinders under axial load, 120, 1994 23–45.
[20] J.G. Teng, J.M. Rotter, Plastic collapse of restrained steel silo hoppers, J. Constr. Steel Res. 14 (1989) 139–158, https://doi.org/10.1016/0143-974X(89)90020-5.
[21] J.M. Morán, A. Juan, R. Robles, P.J. Aguado, Effects of environmental temperature changes on steel silos, Biosyst. Eng. 94 (2006) 229–238, https://doi.org/10.1016/j.biosystemseng.2006.02.017.
[22] Internacional Organization for Standardization, ISO 11697, Bases for design of strutures - Loads due to bulk materials, 2012.
[23] A. Ruiz, A. Couto, P.J. Aguado, Design and instrumentation of a mid-size test station for measuring static and dynamic pressures in silos under different conditions - part II: construction and validation, Comput. Electron. Agric. 85 (2012) 174–187, https://doi.org/10.1016/j.compag.2012.04.008.
[24] A. Couto, A. Ruiz, P.J. Aguado, Experimental study of the pressures exerted by wheat stored in slender cylindrical silos, varying the flow rate of material during discharge. Comparison with Eurocode 1 part 4, Powder Technol. 237 (2013) 450–467, https://doi.org/10.1016/j.powtec.2012.12.030.
[25] M. Wójcik, J. Tejchman, G.G. Enstad, Confined granular flow in silos with inserts - full-scale experiments, Powder Technol. 222 (2012) 15–36, https://doi.org/10.1016/j.powtec.2012.01.031.
[26] E.J. Benink, Flow and Stress Analysis of Cohesionless Bulk Materials in Silos Related to Codes, University of Twente, 1989.
[27] J.F. Chen, J.M. Rotter, J.Y. Ooi, Z. Zhong, Correlation between the flow pattern and wall pressures in a full scale experimental silo, Eng. Struct. 29 (2007) 2308–2320, https://doi.org/10.1016/j.engstruct.2006.11.011.
[28] A.J. Sadowski, J.M. Rotter, Structural behavior of thin-walled metal silos subject to different Flow Channel sizes under eccentric discharge pressures, J. Struct. Eng. 138 (2012) 922–931, https://doi.org/10.1061/(asce)st.1943-541x.0000530.
[29] K. Pieper, M. Schütz, Bericht über das Forschungsvorhaben Norm-Mess-Silo für Schüttguteigenschaften, Technische Universität, Hochbaustatik, 1980.
[30] J. Zegzulka, The angle of internal friction as a measure of work loss in granular material flow, Powder Technol. 233 (2013) 347–353, https://doi.org/10.1016/j.powtec.2012.06.047.
[31] C.Y. Song, J.G. Teng, Buckling of circular steel silos subject to code-specified eccentric discharge pressures, Eng. Struct. 25 (2003) 1397–1417, https://doi.org/10.1016/S0141-0296(03)00105-6.
[32] C.J. Brown, J, Nielsen, Silos, Fundamentals of theory, behaviour and design, London, 1998.
[33] C.V. Schwab, I.J. Ross, G.M. White, D.G. Colliver, Wheat loads and vertical pressure, 37, 1994 1613–1619.
[34] C.J. Brown, E.H. Lahlouh, J.M. Rotter, Experiments on a square planform steel silo, Chem. Eng. Sci. 55 (2000) 4399–4413, https://doi.org/10.1016/S0009-2509(99)00574-6.
[35] W. Sun, J. Zhu, X. Zhang, C. Wang, L. Wang, J. Feng, Multi-scale experimental study on filling and discharge of squat silos with aboveground conveying channels, J. Stored Prod. Res. 88 (2020) 101679, https://doi.org/10.1016/j.jspr.2020.101679.
[36] R.M. Gandia, F.C. Gomes, W.C. de Paula, E.A.O. Junior, P.J.A. Rodriguez, Static and dynamic pressure measurements of maize grain in silos under different conditions, Biosyst. Eng. 209 (2021) 180–199, https://doi.org/10.1016/j.biosystemseng.2021.07.001.
[37] T. Schuricht, C. Furll, G.G. Eenstad, Full Scale silo Tests and Numerical Simulations of the Cone in Cone Concept for Mass Flow, in: Handb, Powder Technol, Elsevier Science BV, 2001 175–180.
[38] J.G. Teng, Y. Zhao, L. Lam, Techniques for buckling experiments on steel silo transition junctions, Thin-Walled Struct. 39 (2001) 685–707, https://doi.org/10.1016/S0263-8231(01)00030-1.
[39] Z. Zhong, J.Y. Ooi, J.M. Rotter, The sensitivity of silo flow and wall stresses to filling method, Eng. Struct. 23 (2001) 756–767, https://doi.org/10.1016/S0141-0296(00)00099-7.
[40] Y. Zhao, J.G. Teng, Buckling experiments on steel silo transition junctions. II: Finite element modeling, J. Constr. Steel Res. 60 (2004) 1803–1823, https://doi.org/10.1016/j.jcsr.2004.05.001.
[41] J.G. Teng, X. Lin, Fabrication of small models of large cylinders with extensive welding for buckling experiments, Thin-Walled Struct. 43 (2005) 1091–1114, https://doi.org/10.1016/j.tws.2004.11.006.
[42] J. Härtl, J.Y. Ooi, J.M. Rotter, M. Wojcik, S. Ding, G.G. Enstad, The influence of a cone-in-cone insert on flow pattern and wall pressure in a full-scale silo, Chem. Eng. Res. Des. 86 (2008) 370–378, https://doi.org/10.1016/j.cherd.2007.07.001.
[43] A. Ramírez, J. Nielsen, F. Ayuga, On the use of plate-type normal pressure cells in silos. Part 1: calibration and evaluation, Comput. Electron. Agric. 71 (2010) 71–76, https://doi.org/10.1016/j.compag.2009.12.004.
[44] A. Couto, A. Ruiz, P.J. Aguado, Design and instrumentation of a mid-size test station for measuring static and dynamic pressures in silos under different conditions - part I: description, Comput. Electron. Agric. 85 (2012) 164–173, https://doi.org/10.1016/j.compag.2012.04.009.
[45] A. Ramírez, J. Nielsen, F. Ayuga, On the use of plate-type normal pressure cells in silos. Part 2: validation for pressure measurements, Comput. Electron. Agric. 71 (2010) 64–70, https://doi.org/10.1016/j.compag.2009.12.005.
[46] A. Ramírez, P. Ansourian, J. Nielsen, K. Rasmussen, F. Ayuga, Analysis of Measurements Obtained by Plate-type Pressure Cells Having a Recess - DEM Simulation, Bulk Solids Powder – Sci. Technol. 4 (2009).
[47] A. Couto, A. Ruiz, L. Herráez, J. Moran, P.J. Aguado, Measuring pressures in a slender cylindrical silo for storing maize. Filling, static state and discharge with different material flow rates and comparison with Eurocode 1 part 4, Comput. Electron. Agric. 96 (2013) 40–56, https://doi.org/10.1016/j.compag.2013.04.011.
[48] A. Ramírez, J. Nielsen, F. Ayuga, Pressure measurements in steel silos with eccentric hoppers, Powder Technol. 201 (2010) 7–20, https://doi.org/10.1016/j.powtec.2010.02.027.
[49] A.W. Jenike, J.R. Johanson, J.W. Carson, Bin loads—part 4: funnel-flow bins, J. Eng. Ind. 95 (1973) 13–20.
[50] A.J. Sadowski, J.M. Rotter, Buckling of very slender metal silos under eccentric discharge, Eng. Struct. 33 (2011) 1187–1194, https://doi.org/10.1016/j.engstruct.2010.12.040.

**Article 3 – Effect of the hopper angle of a silo on the vertical stress at the cylinder-to-hopper transition - Agronomy journal (published version)**

The article was selected at the 11th Iberian Agroengineering Congress as a special issue for the journal Agronomy (ISSN 2073-4395) with a JCR of 3.417.

The article was published in the Agronomy journal (ISSN 2073-4395).

The journal has JCR 3.417.

DOI: https://doi.org/10.3390/agronomy12040830.

agronomy

MDPI

*Article*

# Effect of the Hopper Angle of a Silo on the Vertical Stress at the Cylinder-to-Hopper Transition

**Rômulo Marçal Gandia [1,2,*], Wisner Coimbra de Paula [3], Estácio Antunes de Oliveira Junior [1], Gerardo Hernández Rodrigo [2], Ángel Ruiz Padín [2], Alberto Tascón Vegas [4], Francisco Carlos Gomes [1] and Pedro José Aguado Rodríguez [2]**

1 Department of Agricultural Engineering, School of Engineering, Federal University of Lavras, Campus Lavras, Lavras 37200-900, Brazil; estacioantunes@gmail.com (E.A.d.O.J.); fcgomes@ufla.br (F.C.G.)
2 Department of Engineering and Agricultural Sciences, University of León, Av. Portugal 41, 24071 León, Spain; gherr@unileon.es (G.H.R.); aruip@unileon.es (Á.R.P.); pedro.aguado@unileon.es (P.J.A.R.)
3 Department of Engineering, School of Engineering, Federal University of Lavras, Campus Lavras, Lavras 37200-900, Brazil; wisner.depaula@ufla.br
4 Department of Agriculture and Food, Faculty of Science and Technology, University of La Rioja, C/Madre de Dios 53, 26006 Logroño, Spain; alberto.tascon@unirioja.es
* Correspondence: romagandia@gmail.com; Tel.: +55-35-998-337-777

**Abstract:** Silos are used worldwide to store granular and powdered materials. Agricultural, food and feed products are commonly stored in silos. However, many questions remain unanswered about how to estimate the pressures applied by the bulk material, which are needed to design and calculate the structure of the silo. The complexity of the laws that govern the mechanical behavior of the stored material along with the low number of experimental stations in the world hinder progress in this field. The aim of this study was to elucidate the relationship of the hopper angle, flow pattern and vertical stress at the cylinder-to-hopper transition in slender silos. Therefore, a set of experiments was conducted on a test station to measure the vertical stress produced by maize at the cylinder-to-hopper transition. Five different hopper angles were used. The experiments comprised the filling, the static phase and the discharge. The results obtained show that the hopper angle influences the vertical stress at the cylinder-to-hopper transition. Some bottom configurations (flat bottom and bottom with an angle of 30°) led to vertical stresses that exceeded the value calculated according to Eurocode 1. It is clear that further experimental studies are still necessary to understand the underlying physical phenomena and the relations between pressures, silo geometry and flow pattern of the stored material.

**Keywords:** experimental silo; pressures; slender silo; maize; flow pattern; silo design



**Citation:** Gandia, R.M.; de Paula, W.C.; de Oliveira Junior, E.A.; Rodrigo, G.H.; Padín, Á.R.; Vegas, A.T.; Gomes, F.C.; Rodríguez, P.J.A. Effect of the Hopper Angle of a Silo on the Vertical Stress at the Cylinder-to-Hopper Transition. *Agronomy* **2022**, *12*, 830. https://doi.org/10.3390/agronomy12040830

Academic Editors: Adriana Correa, María Dolores Gómez-López and Jesús Montero Martínez

Received: 20 February 2022
Accepted: 27 March 2022
Published: 29 March 2022



## 1. Introduction

Maize and its derivatives are important human food sources, and also have a wide prevalence in animal feed due to their high nutritional index. As an example, Brazil had a maize production of 87 million tons in 2021 [1], and Spain 4.1 million tons in 2020 [2]. This huge amount of maize requires handling and storage in industrial facilities. Silos are normally used for storing maize and other agricultural, food and feed products.

Tower silos have been studied since the 19th century, but many aspects concerning the mechanical behavior of stored products remain poorly understood due to the complexity of the laws that govern the underlying physical phenomena [3–8]. Although a review of this literature indicates that structural failures in silos can be attributed to various different causes, the pressures exerted by the stored material are usually a key factor.

The friction angle between the stored product and the hopper wall along with the hopper angle directly influence the flow pattern and, consequently, the behavior of pressures. There are two main flow patterns, mass flow and funnel flow. Mass flow is characterized

by the movement of all the stored material at the same speed, and it follows a first-in, first-out pattern; the material generates high dynamic pressures on the walls, particularly at the cylinder-to-hopper transition. On the contrary, funnel flow is associated with the presence of stagnant zones and a first-in, last-out sequence. A third flow pattern, transition flow, is characterized by a distinct change in the type of flow that takes place in a position that depends on the filling height [9]. As mentioned above, the hopper angle and the wall friction coefficient are the two most influential parameters [10–12]. However, the relations between flow, pressure and the vertical stresses at the cylinder-to-hopper transition are still poorly understood [7,13–17].

Ding et al. [18] studied the critical hopper angle for achieving a mass flow and also analyzed the effects of double-cone inserts on the flow of particulate solids. The effects of the material type, particle size and moisture content on the static pressure distribution were analyzed in a lab-scale test silo with conical hopper by Chen et al. [19]. Several authors have studied the influence of the hopper angle on the mass flow rate by using lab size cylindrical silos [20–22]. Villagrán Olivares et al. performed experiments for different hopper angles in a 2D lab container and proposed a theoretical description to predict the behavior of the flow and the transition zone angle from mass flow to funnel flow [23]. These recent studies indicate that the effect of the hopper angle on pressures and flow patterns is consistently a topic of interest and that further research into these phenomena is still required.

Despite the high cost of construction and instrumentation, experimental stations are considered the best approach to understand what happens inside real silos. Experiments in test silos provide pressure values and reliable information to understand the behavior of the bulk material and the flow patterns [7]. In addition, experimental models are used for validations of numerical models [16,24–26].

A pilot-scale test station, which is based on the design proposed by Pieper and Schütz in 1980 [27], is located in the Federal University of Lavras. This experimental station has been previously applied to the study of static and dynamic pressures (friction and normal) after previous calibration and verification of all instrumentation [17,28,29]; these experiments demonstrated that pressures are influenced by the slenderness and angle of the hopper. Furthermore, the DIN 1055-6: Design Basis and Actions on Structures—Part 6 [30] is partly based on studies conducted at the pilot-scale test station used by Pieper and Schütz.

Therefore, the present paper offers new experimental information from this pilot scale test station. The aim was to study the influence of hopper angle and flow pattern on the vertical stress at the cylinder-to-hopper transition, analyzing the maximum pressures during filling, static phase and discharge of maize.

## 2. Materials and Methods

The experimental station was located at the Federal University of Lavras (Brazil) (Figure 1) and was previously validated by the members of the research group on pressures and flow in silos and stored products [29].

The station consisted of a fully instrumented pilot silo, a storage silo to store the bulk material during the tests and a bucket elevator to transport the material between the silos (Figure 1). All the measuring cells of the pilot silo were connected to the data acquisition system controlled by a portable computer.

The pilot test silo was cylindrical and metallic. The cylinder was 6 m high and 0.7 m in internal diameter. The cylinder was segmented into 12 structurally independent rings, allowing the forces in each division to be obtained; all rings were connected vertically by a pair of tension load cells. The pair that supported the bottom of the silo was responsible for providing the vertical force at the silo–hopper transition (Figure 2). The pairs that supported each cylinder ring were responsible for providing the frictional wall forces (Figure 2). The silo hoppers can vary depending on the opening angle β (Figure 2).

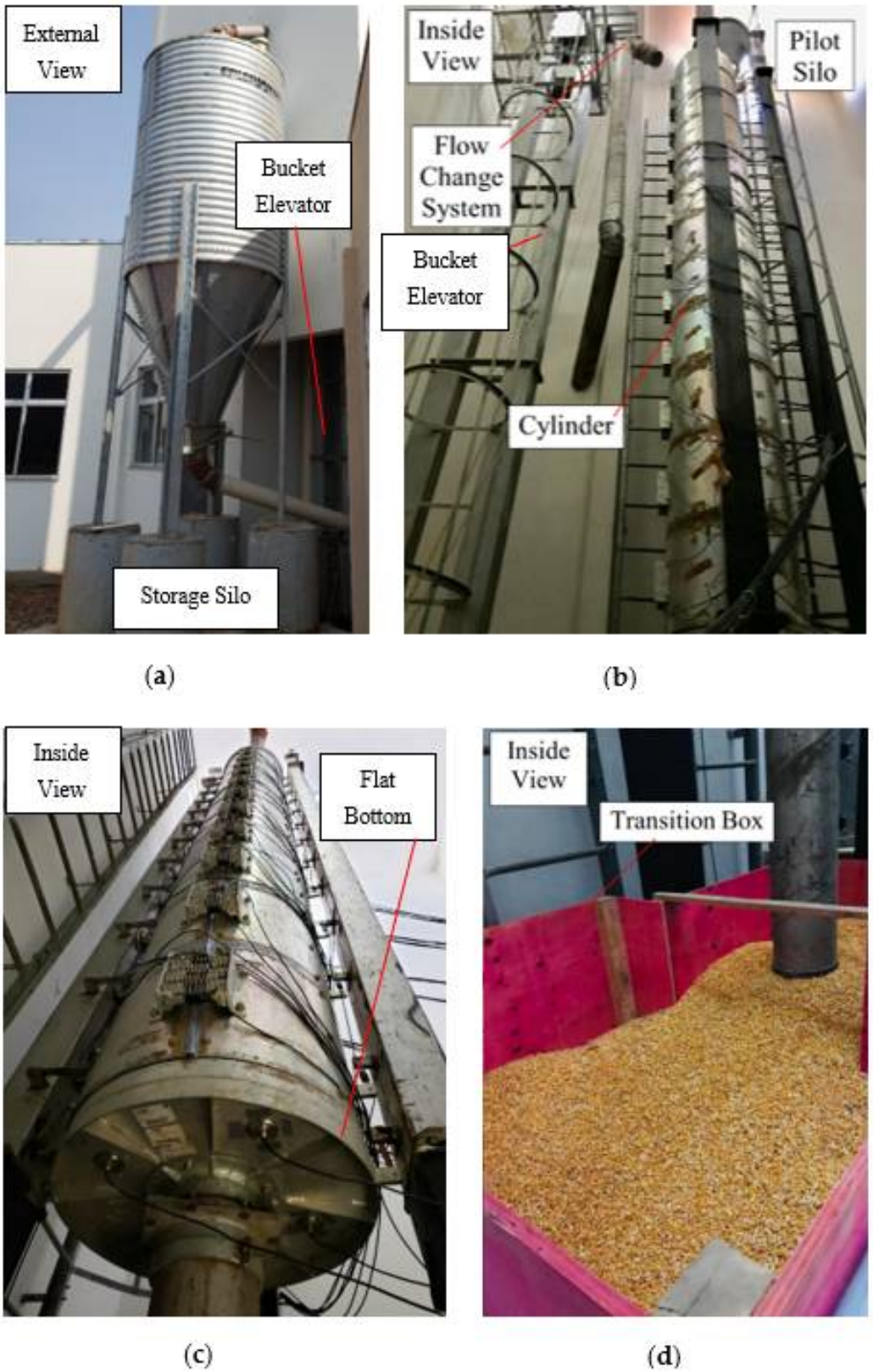


**Figure 1.** Pilot-scale test station. (**a**) External view, storage silo; (**b**) inside view, pilot silo and bucket elevator; (**c**) inside view, pilot silo; (**d**) inside view, transition box.

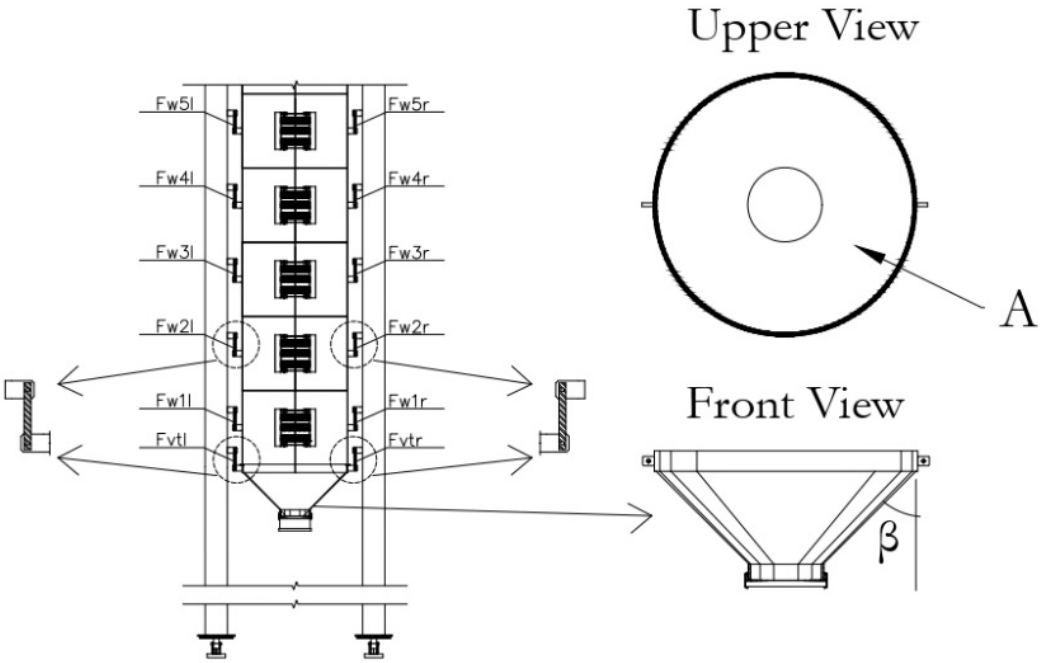


**Figure 2.** Measurement cells for vertical stress at the silo–hopper transition (Pvt,t) and frictional wall pressures (Pw,t).

The measurement of vertical stresses at the silo–hopper transition (Pvt,t) begin once the hopper is filled with the stored material, using Equation (1):

$$\mathrm{Pvt,t} = \frac{\mathrm{Fvtr,t} + \mathrm{Fvtl,t} - \mathrm{Whto}}{\mathrm{A}} \quad (1)$$

According to Eurocode 1, part 4 [11], the definitions of the different terms of the equation are:

- Pvt,t: Value of the vertical stress of the stored product at the silo–hopper transition obtained from the tension load cells positioned on the hopper support, at time t, kPa;
- Fvtr,t: Value of the force obtained in the tension load cell positioned on the right-hand side of the hopper support, at time t, kN;
- Fvtl,t: Value of the force obtained in the tension load cell positioned on the left-hand side of the hopper support, at time t, kN;
- Whto: Weight of stored material between the outlet and the silo–hopper transition, zero in the case of the flat bottom, kN;
- A: Plan cross-sectional area of vertical walled segment, $m^2$.

The frictional wall stresses (Pw,t) can be determined indirectly by the pair of tension load cells located on the vertical support (positioned 180° apart) of each ring, using Equation (2):

$$\mathrm{Pw(1,5),t} = \frac{\mathrm{Fw(1,5)r,t} + \mathrm{Fw(1,5)l,t}}{\pi.\mathrm{di.hr}} \quad (2)$$

According toEurocode 1, part 4 [11], the definitions of the different terms of the equation are:

- Pw(1,5),t: Frictional wall stresses for the cylinder wall from the tension load cells positioned on ring supports—rings 1 to 5, time t, kPa;
- Fw(1,5)r,t: Force in tension load cell positioned on the right side of the ring support, rings 1 to 5, at time t, kN;

- Fw(1,5)l,t: Force in tension load cell positioned on the left side of the ring support, rings 1 to 5, at time t, kN;
- di: Internal cylinder diameter, m;
- hr: Ring height, m.

The frictional wall stresses for the cylinder wall Pw(1,5) could be determined in the five rings at heights 0.25, 0.75, 1.25, 1.75 and 2.25 m above the silo hopper transition (Figure 2). In this study, only the frictional wall stresses for the cylinder wall at the height 0.25 m above the transition was used, i.e., in the first ring as shown in Figure 2. Therefore, the frictional wall stresses for the cylinder wall at a height of 0.25 is called Pw1.

Vertical stresses in the stored material at the transition (Pvt,t) and frictional wall stresses (Pw,t) were calculated for the filling, static phase and discharge for each of the bottom configurations, and the maximum values were selected. In addition, experimental values were compared with Eurocode 1, part 4 [11]. Figure 3 illustrates the locations of vertical stresses in the stored solid at the transition (base of the vertical walled segment) (Pvft) and the wall frictional traction after filling (Pwf) according to Eurocode 1. The parameter Pvt,t, which is used throughout this paper, has the same meaning as the parameter Pvtf in Eurocode 1. It is noteworthy that Eurocode 1 does not include the hopper angle (β) in the calculation method for Pvft (see Equations (3) and (4) for slender silos); Eurocode 1 determines the vertical stress in the stored solid at the transition after filling (Pvtf) by multiplying the vertical stress in the stored solid (Pvf) at the depth corresponding to the transition by a bottom load magnifier ($C_b$) to account for the possibility of larger loads being transferred to the hopper or bottom from the vertical walled segment.

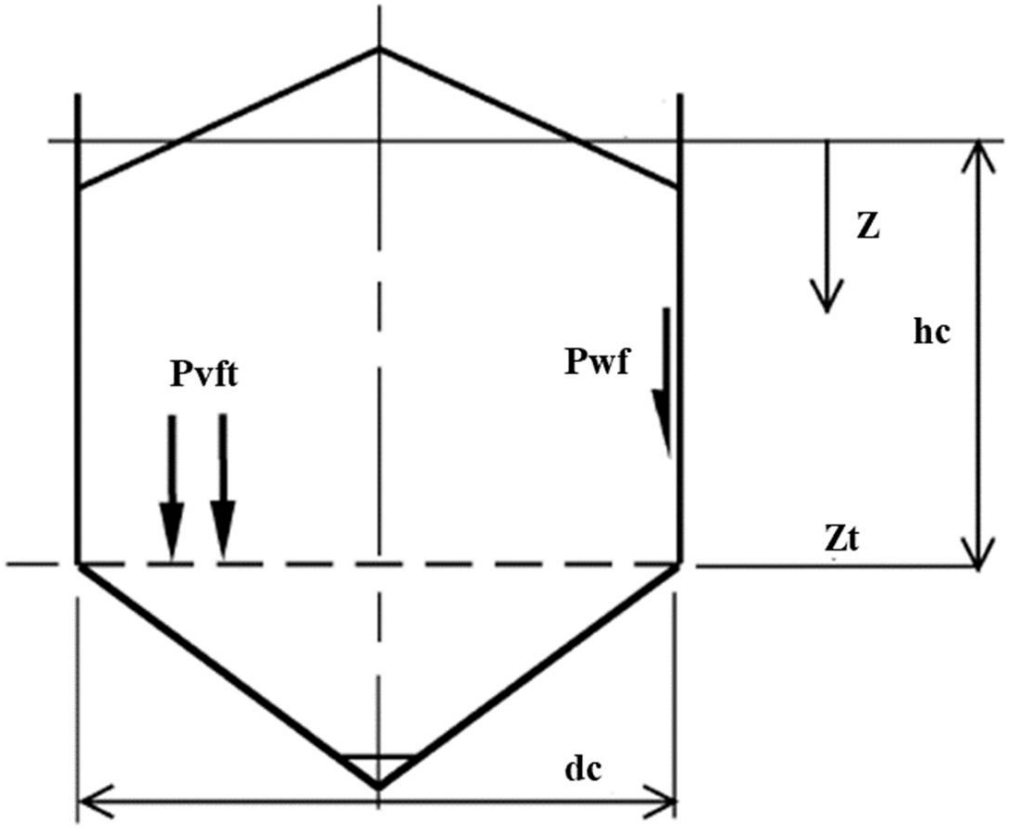


**Figure 3.** Some symmetrical filling pressures in the vertical-walled segment according to Eurocode 1, part 4.

$$Pvft = Cb\ Pvf \quad (3)$$

$$Pvf = \frac{Pho}{K} Yj(z) \quad (4)$$

The definitions for these parameters according to Eurocode 1, part 4, are:
Pvft: vertical stress in the solid after filling at transition;
Pvf: vertical stress in the solid after filling;
$P_{ho}$: asymptotic horizontal pressure at great depth for the disaggregated solid stored;
Yj: function of Janssen pressure variation with depth;
K: characteristic value of the lateral pressure coefficient;
Cb: coefficient of increase in loads on the bottom.

In this study, Equation (1) was applied to calculate the vertical stresses at the cylinder-to-hopper transition (Pvt,t) as a function of time, i.e., during the filling, static phase and discharge, and the values obtained were compared with the value calculated according to Eurocode 1 following Equations (3) and (4).

The product used in these experimental tests was maize with a minimum purity of 97%. The physical, mechanical and flow properties of maize were obtained following the methodology of the Jenike Shear Test [31], which conforms to Eurocode 1 [11], and are shown in Table 1.

**Table 1.** Physical, mechanical and flow properties of maize.

| Properties | Lower Limit | Upper Limit |
|---|---|---|
| specific weight (kN/m$^3$) | 7.52 | 7.83 |
| angle of repose | 31.3° | 37.1° |
| cohesion (kPa) | 0.241 | 1.084 |
| steel wall friction angle | 7.37° | 9.02° |
| steel wall friction coefficient | 0.13 | 0.16 |
| internal friction angle | 19° | 29° |
| humidity | 10.62% | |

Using the granular material described above, a series of experimental tests was performed with 5 different configurations of the silo hopper and 6 repetitions for each test. Thus, 30 tests were performed in total. The tests were conducted with concentric filling and discharge. The hopper inclinations used in the five different configurations were: β = 15° (β15°); β = 30° (β30°); β = 45° (β45°); β = 60° (β60°) and β = 90°, named flat bottom (FlatB).

The reason of using this hopper inclinations was to encompass the different types of flow included in Eurocode 1 [11]. Eurocode 1 states that the inclination of the hopper in conjunction with the friction coefficient of the wall with the product ($\mu$ = 0.24) lead to different types of flow patterns (Figure 4): mass flow for β = 15°; transition flow for β = 30°; and funnel flow for β = 45°, β = 60° and flat bottom. Additionally, following Eurocode 1, the 5 different bottoms can be classified in three groups depending on the geometry of the silo: steep hopper (β15°, β30° and β45°), shallow hopper (β60°) and flat bottom (FlatB).

All tests were conducted according to the sequence illustrated in Figure 5: filling the silo to the height of interest (verified by the tension load cell that shows the measurement in the semi-cylinder above the height of interest), static condition (for 10 min), and product discharge. The silo was discharged with the gate (diameter of 0.20 m) 100% opened.

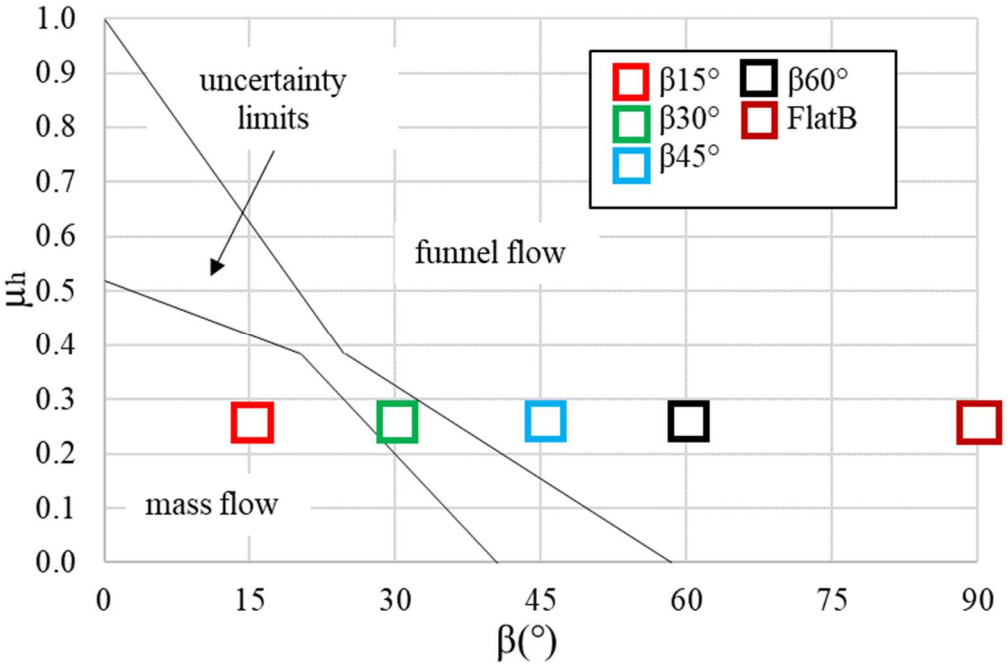


**Figure 4.** Conditions for flow patterns according to Eurocode 1, part 4 [11].

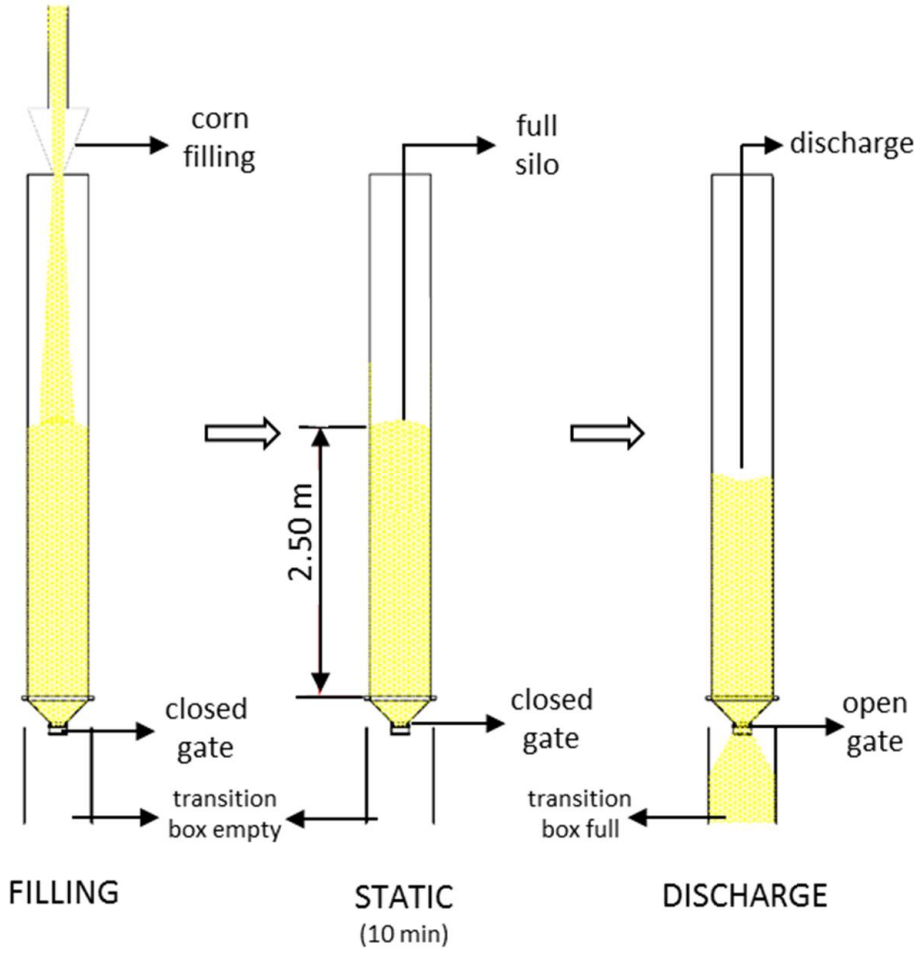


**Figure 5.** Test configuration. Description of the assays.

## 3. Results

The experiments carried out generated a large volume of data. Therefore, to avoid exposing unnecessary data, the values of average and standard deviation in each measurement cell referring to filling and discharge are shown in Table 2. As can be seen, the six repetitions for each test showed a low coefficient of variation. Therefore, for each type of test, one of the six repetitions was chosen randomly to discuss the results.

**Table 2.** Maximum values of Pvt after filling and discharge in each test configuration.

| After Filling Pressure (kPa) | | | | | | | | | | |
|---|---|---|---|---|---|---|---|---|---|---|
| Cell | FlatB | | β60° | | β45° | | β30° | | β15° | |
| | $\overline{X}$ | σ | $\overline{X}$ | σ | $\overline{X}$ | σ | $\overline{X}$ | σ | $\overline{X}$ | σ |
| Pvt | 10.77 | 0.43 | 9.87 | 1.94 | 9.38 | 0.47 | 11.53 | 0.76 | 9.91 | 0.79 |
| Discharge pressure (kPa) | | | | | | | | | | |
| Cell | FlatB | | β60° | | β45° | | β30° | | β15° | |
| | $\overline{X}$ | σ | $\overline{X}$ | σ | $\overline{X}$ | σ | $\overline{X}$ | σ | $\overline{X}$ | σ |
| Pvt | 10.56 | 0.48 | 7.43 | 0.70 | 8.32 | 0.33 | 10.88 | 0.71 | 8.21 | 1.34 |

$\overline{X}$: mean value; σ: standard deviation.

Table 2 shows that a connection between the type of flow (mass, transition or funnel flow) and the Pvt values exists. During filling, for funnel flow (FlatB, β60° and β45°) the mean values were higher when the beta angle increased, and the transition flow (β30°) presented the highest average value. During discharge, there was no significant difference in comparison to filling for the flat hopper tests, while the shallow hopper (β60°) had the greatest pressure decrease (25%). Again, the transition flow (β30°) presented the highest average value for the discharge phase.

As the weight of the material in the hopper is part of the Equation (1), it is important to note that this weight varies with the volume of the hopper, which depends on the angle β. Table 3 shows the values of the loads for each of the test configurations.

**Table 3.** Average load for each test.

| Test | $\overline{X}$ (kN) | σ (kN) |
|---|---|---|
| FlatB | 7.49 | 0.53 |
| β60° | 7.86 | 0.45 |
| β45° | 8.46 | 0.15 |
| β30° | 8.38 | 0.81 |
| β15° | 9.26 | 0.19 |

$\overline{X}$: mean; σ: standard deviation.

It is noteworthy that the β30° test had a mean value different from that expected and a standard deviation higher than the others. The reason is that two of the six repetitions for the β30° test showed flaws in the filling, resulting in heights of the stored product below that of interest. It should be emphasized that these two repetitions were used for calculating the mean and the standard deviation in Table 3, but they were removed during the random choice of one single repetition for the later analysis of the individual tests presented below.

Figure 6 shows the vertical stresses at the transition (Pvt) obtained in the test station for different concentric hopper inclinations during the filling, the static storage phase and the discharge. These measurements were also compared with the value calculated following Eurocode 1 [11]. Figures 7 and 8 show the results of the end of the filling and the beginning of the discharge in detail, respectively.

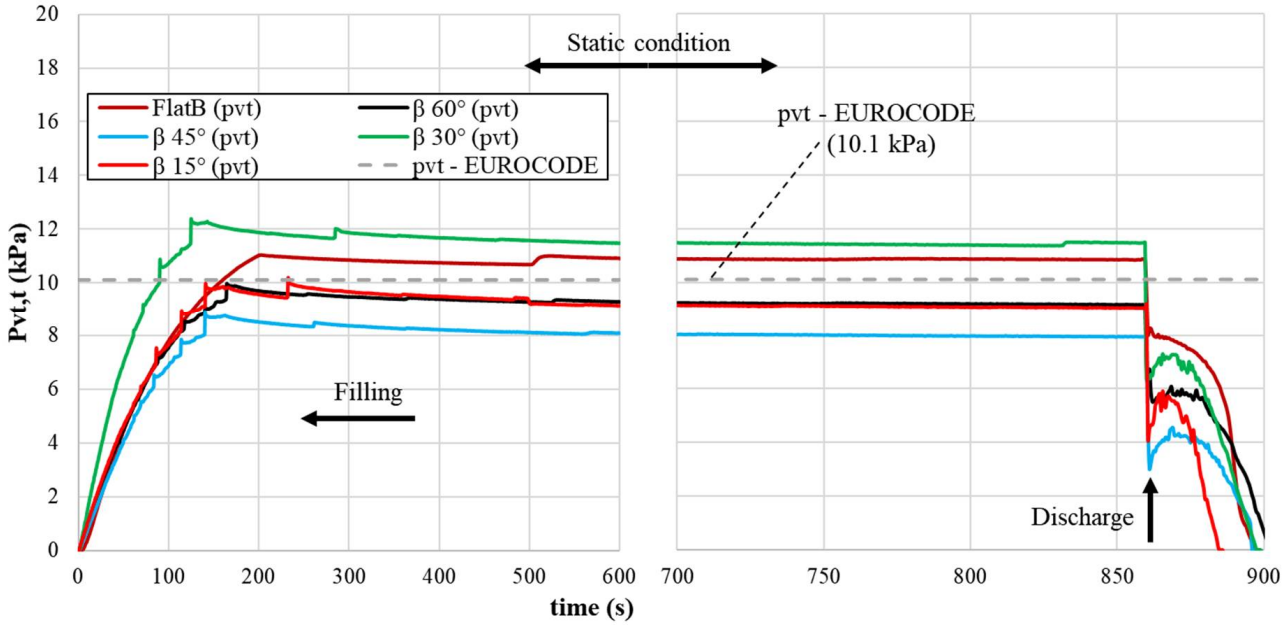


**Figure 6.** Vertical stress in the stored material at the transition (Pvt,t) versus time. Complete test from 0 to 900 s.

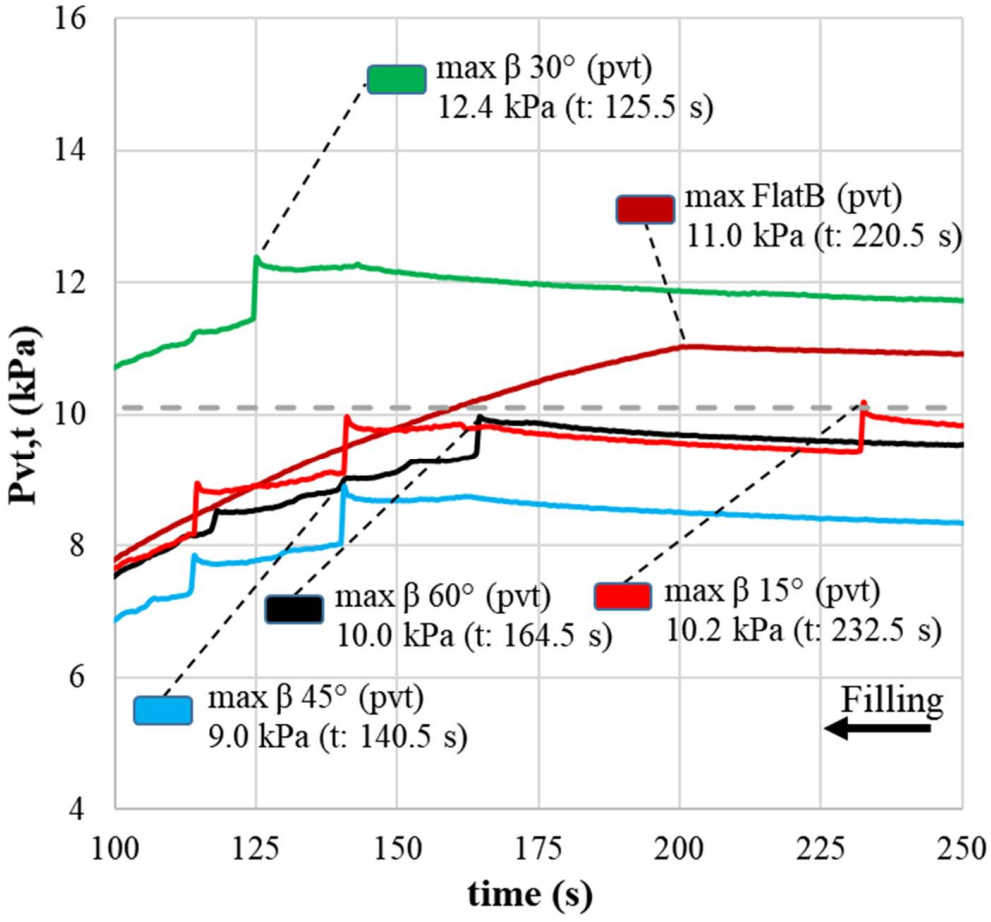


**Figure 7.** Last stage of the filling operation. Vertical stress in the stored material at the transition (Pvt,t) versus time.

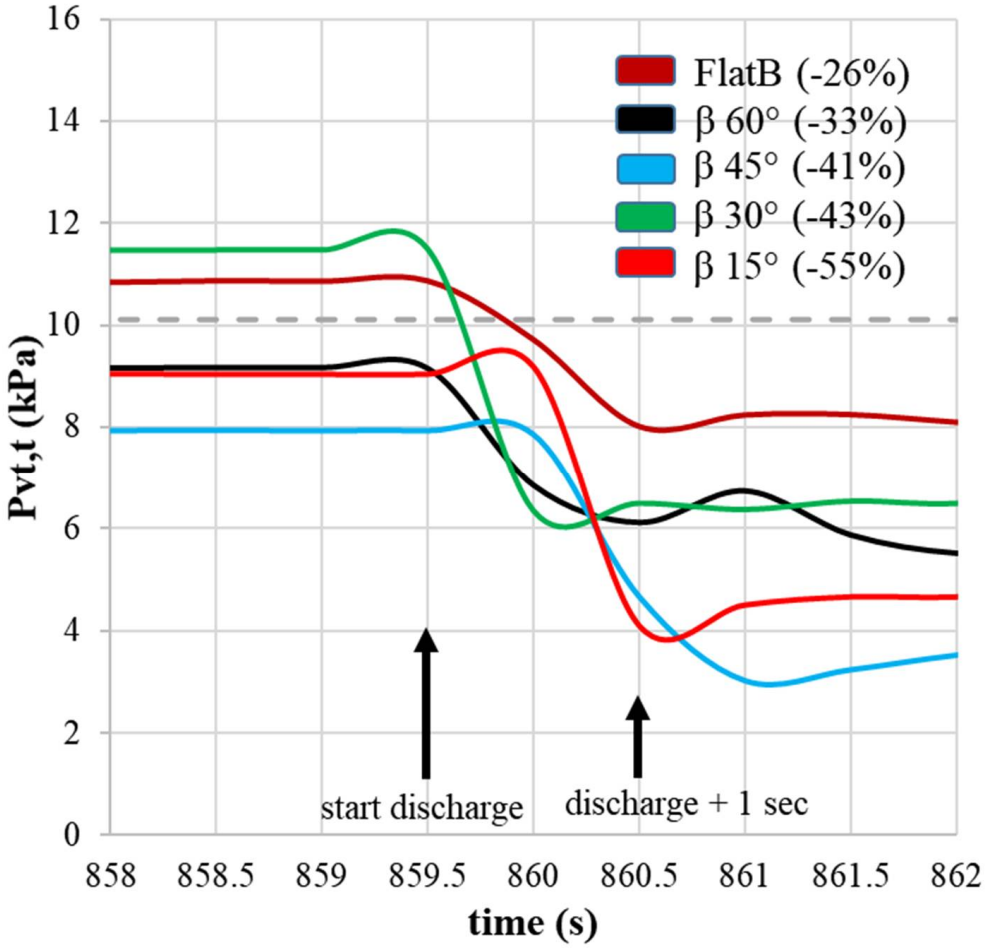


**Figure 8.** First stage of the discharge. Vertical stress in the stored material at the transition (Pvt,t) versus time.

The vertical stress in the stored material at the transition (Pvt) obtained using Eurocode 1 was influenced only by the size of the silo cylinder, not by the hopper geometry. However, it can be observed that the experimental results were influenced by the geometry of the bottom.

The maximum values of Pvt during filling, as well as the values during discharge (from 859.5 from 860.5 s) are shown in Table 4.

**Table 4.** Average of the maximum vertical stress at the silo–hopper transition for each test.

| Test | Pvt (kPa) | | | |
|---|---|---|---|---|
| | Max (Filling) | 859.5 s | 860.5 s | Δ Pvt (859.5–860.5 s) |
| FlatB | 11.04 | 10.87 | 8.02 | 2.85 |
| β 60° | 9.97 | 9.15 | 6.12 | 3.04 |
| β 45° | 8.90 | 7.93 | 4.67 | 3.27 |
| β 30° | 12.38 | 11.49 | 6.49 | 5.00 |
| β 15° | 10.18 | 9.04 | 4.10 | 4.94 |

Frictional pressures measured at a height of 0.25 m above the transition (Pw1) are shown in Figure 9. The results of and the trends in these pressures showed a relationship with Pvt.

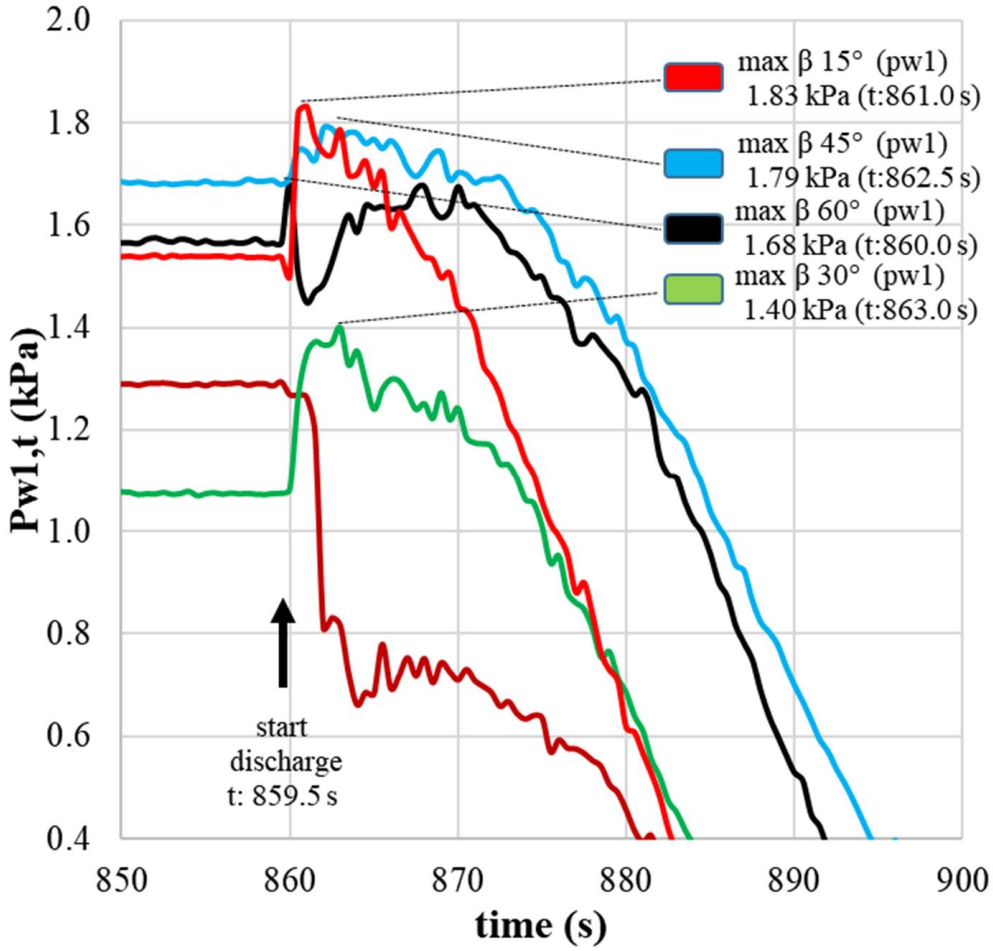


**Figure 9.** Friction stresses in the cylinder (Pw1,t) 0.25 m above the transition at discharge.

For the flat bottom and β60° tests, there was a sharp drop in pressure a few seconds after the commencement of the discharge. For the β45°, β30° and β15° tests, the pressure peak occurred at the beginning of the discharge.

It is interesting to note a certain relationship between the Pvt accommodation peaks during filling (Figure 6) and the frictional overpressures at a height of 0.25 m (Pw1). Pvt accommodation peaks were higher for steep hoppers (β15°, β30° and β45°), were lower for the shallow hopper (β60°), and were not present for flat hoppers (FlatB). Pw1, analogously, presented high peaks for steep hoppers (β15°, β30° and β45°), a moderate drop for the shallow hopper (β60°), and a deep pressure drop for the flat hopper (FlatB).

It was also observed (Figure 9) that the lowest friction pressure on the cylinder wall (Pw1) before the discharge corresponded to the steep hopper and funnel flow configuration (β30°). However, the time of occurrence of the maximum pressure was the longest (t = 863 s).

In Figure 9, it can also be seen that in mass flow (β = 15°) the silo is discharged faster, because there are no dead zones. The curves are not fully comparable, since varying the angle of the hopper changes its volume.

## 4. Discussion

Table 2 shows that for β = 15°, that is, for mass flow, the values are lower both in filling and in discharge; this reveals the influence that flow type has on the Pvt values. This fact is especially interesting since it is known [11] that in mass flow, horizontal overpressures can occur near the transition, which shows that there is a change between the ratio of horizontal and vertical pressures.

It is remarkable that the highest values for Pvt during filling and the static phase were measured for β = 30°. It is believed that this behavior was due to the distribution of pressures in the silo, i.e., the friction pressure at 0.25 m above the transition in the β30° test was the smaller (Figure 9). If the friction was lower, less weight was supported by the walls; therefore, more weight was being transferred to the vertical stresses.

Frictional pressures (Pw) were inversely linked with Pvt. It is observed in Figure 8, at the moment of discharge, that the magnitude of frictional pressures (Pw1) at 0.25 m above the transition was inversely proportional to Pvt. The maximum friction pressure in FlatB occurred during filling (Figure 9). The steep hoppers (β15°; β30° and β45°) presented a friction overpressure at the beginning of the discharge due to the vertical movement of the product stored in the region at 0.25 m above the transition (Pw1); this volume movement caused the grain mass to rub against the wall, creating resistance against the z-axis. On the contrary, in the case of mass flow (β15°), the discharge was faster as there were no dead zones.

It was also observed (Figure 7) that the maximum Pvt in all configurations always occurred at the end of filling, at the last settling peak of the material before entering in the static phase.

In the case of the discharge pressures, the negative peaks (difference between the pressure during the static phase and the lowest pressure that was measured in the initial moment of the discharge phase, specifically from 859.5 s to 860.5 s) were proportional to the β angle. A lower β angle corresponded to a higher negative peak ΔPvt (Table 4). This can be explained by the change in stress state during discharge, i.e., the packaging of the particles during the discharge increased or decreased in certain areas in relation to the previous static state [14,32]. The flow pattern could also partly explain the behavior of the discharge pressures; for example, in the β15° test there was mass flow and a fast discharge with a peak at the start followed by a considerable drop in the pressures.

The β30° and FlatB configurations had the highest Pvt values, respectively, and exceeded the values proposed by the Eurocode (Figure 6). However, Pvt values for β15° did not exceed the Eurocode ones despite having a higher inclination than the β30° case. This could be explained by the mass flow pattern corresponding to β15° (see Figure 4), which differs from the rest of cases.

Figure 6 shows that the pressures decrease when the hopper angle decreases from β = 0° to β = 45°, but for β = 30° and 15 the trend changes; this is due to the fact that in these last two cases the type of flow rate is mass (β = 15°) and close to the transition zone (β = 30°). In these cases, there is no or very little channel flow, which causes a change in the stress state, as mentioned when discussing Table 2.

It is important to remark that the five hopper configurations applied in this study defined five different volumes, so the volume and the weight of the product stored in the silo also changed. Thus, results are not fully comparable.

## 5. Conclusions

The relationships between flow pattern, hopper angle, and vertical stress at the cylinder-to-hopper transition have been studied by means of experimental tests in an experimental station located at the Federal University of Lavras (Brazil). Maize was used in all tests.

The maximum values of the vertical stress in the stored material at the transition (Pvt) occurred due to the settlement of the material at the end of the silo filling for all bottom configurations. During the discharge phase, the negative pressure peaks depended on the hopper angle (β); the larger the β angle, the smaller the difference between pressures. There was an inverse relationship between friction pressures and Pvt values near the transition (0.25 m above).

The transition flow (β = 30°) presented the lowest friction pressure in the cylinder (Pw1) 0.25 m above the transition and the highest vertical stress in the stored material at the transition (Pvt).

Some bottom configurations (β 30° and FlatB) exceeded vertical stresses at the transition calculated according to Eurocode 1, part 4. At the moment, this standard does not consider the hopper angle when calculating the vertical stresses. However, the collection of experimental data obtained in this study suggests that the calculation method in the Eurocode should be revised.

**Author Contributions:** Conceptualization, R.M.G. Methodology, R.M.G. Validation, R.M.G. Formal analysis, R.M.G. Investigation, R.M.G. and E.A.d.O.J. Resources, Á.R.P. Data curation, P.J.A.R. Writing—original draft preparation, R.M.G. Writing—review and editing, W.C.d.P., A.T.V. and P.J.A.R. Visualization, W.C.d.P., G.H.R. and A.T.V. Supervision, F.C.G. and P.J.A.R. Project administration, F.C.G. Funding acquisition, F.C.G. All authors have read and agreed to the published version of the manuscript.

**Funding:** This research received no external funding.

**Data Availability Statement:** Not applicable.

**Acknowledgments:** The authors are very grateful to the Stored Product Flow Properties Laboratory of Federal University of Lavras and to the Department of Engineering and Agricultural Sciences of the University of León.

**Conflicts of Interest:** The authors declare no conflict of interest.

## References

1. CONAB—Companhia Nacional de Abastecimento. Acompanhamento da Safra Brasileira de Grãos, Brasilia, 2022. Available online: https://www.conab.gov.br/component/k2/item/download/40788_0ee9dd05157257045355d00863c854b0 (accessed on 2 January 2022).
2. Ministério da Agricultura Pesca y Alimentación. Avances de Superficies y Producciones Agrícolas. Diciembre 2020. Available online: https://www.mapa.gob.es/es/estadistica/temas/estadisticas-agrarias/cuaderno_diciembre2020_tcm30-558173.pdf (accessed on 2 January 2022).
3. Ayuga, F. Some unresolved problems in the design of steel cylindrical silos. In *Structures and Granular Solids from Scientific Principles to Engineering Applicationsl*; Chen, J.G., Teng, J.F., Eds.; CRC Press-Taylor & Francis Group: Boca Raton, FL, USA, 2008; pp. 123–133.
4. Dogangun, A.; Karaca, Z.; Durmus, A.; Sezen, H. Cause of damage and failures in silo structures. *J. Perform. Constr. Facil.* **2009**, *23*, 65–71. [CrossRef]
5. Nielsen, J. From silo phenomena to load models. In *Structures and Granular Solids from Scientific Principles to Engineering Applications*; Chen, J.F., Teng, J.G., Eds.; CRC Press-Taylor & Francis Group: Boca Raton, FL, USA, 2008; pp. 49–57. [CrossRef]
6. Teng, J.G. Collapse strength of complex metal shell intersections by the effective area method. *J. Press. Vessel Technol. Trans. ASME* **1998**, *120*, 217–222. [CrossRef]
7. Chen, J.F.; Rotter, J.M.; Ooi, J.Y.; Zhong, Z. Correlation between the flow pattern and wall pressures in a full scale experimental silo. *Eng. Struct.* **2007**, *29*, 2308–2320. [CrossRef]
8. Morán, J.M.; Juan, A.; Robles, R.; Aguado, P.J. Effects of Environmental Temperature Changes on Steel Silos. *Biosyst. Eng.* **2006**, *94*, 229–238. [CrossRef]
9. Benink, E.J. *Flow and Stress Analysis of Cohesionless Bulk Materials in Silos Related to Codes*; University of Twente: Enschede, The Netherlands, 1989.
10. Jenike, A. *Storage and Flow of Bulk Solids Bull. 123*; University of Utah: Salt Lake, UK, USA, 1964.
11. *CEN, EN 1991-4:2006*; Eurocode 1: Actions on Structures. Part 4: Silos and Tanks. AENOR: Brussels, Belgium, 2006.
12. *ISO 11697:2012*; Bases for Design of Strutures—Loads Due to Bulk Materials. Internacional Organization for Standardization: Geneva, Switzerland, 2012.
13. Nielsen, J. Pressures from flowing granular solids in silos. *Philos. Trans. R. Soc. A Math. Phys. Eng. Sci.* **1998**, *356*, 2667–2684. [CrossRef]
14. Couto, A.; Ruiz, A.; Aguado, P.J. Experimental study of the pressures exerted by wheat stored in slender cylindrical silos, varying the flow rate of material during discharge. Comparison with Eurocode 1 part 4. *Powder Technol.* **2013**, *237*, 450–467. [CrossRef]
15. Sadowski, A.J.; Rotter, J.M. Structural Behavior of Thin-Walled Metal Silos Subject to Different Flow Channel Sizes under Eccentric Discharge Pressures. *J. Struct. Eng.* **2012**, *138*, 922–931. [CrossRef]
16. Gandia, R.M.; Gomes, F.C.; de Paula, W.C.; Aguado, P.J.R. Influence of specific weight and wall friction coefficient on normal pressures in silos using the Finite Element Method. *Rev. Eng. Na Agric. Reveng.* **2021**, *29*, 192–203. [CrossRef]
17. Gandia, R.M.; Gomes, F.C.; de Paula, W.C.; Rodriguez, P.J.A. Evaluation of pressures in slender silos varying hopper angle and silo slenderness. *Powder Technol.* **2021**, *394*, 478–495. [CrossRef]

18. Ding, S.; Li, H.; Ooi, J.Y.; Rotter, J.M. Prediction of flow patterns during silo discharges using a finite element approach and its preliminary experimental verification. *Particuology* **2015**, *18*, 42–49. [CrossRef]
19. Chen, Y.; Liang, C.; Wang, X.; Guo, X.; Chen, X.; Liu, D. Static pressure distribution characteristics of powders stored in silos. *Chem. Eng. Res. Des.* **2020**, *154*, 1–10. [CrossRef]
20. Méndez, D.; Hidalgo, R.C.; Maza, D. The role of the hopper angle in silos: Experimental and CFD analysis. *Granul. Matter.* **2021**, *23*, 1–13. [CrossRef]
21. Darias, J.R.; Gella, D.; Fernández, M.E.; Zuriguel, I.; Maza, D. The hopper angle role on the velocity and solid-fraction profiles at the outlet of silos. *Powder Technol.* **2020**, *366*, 488–496. [CrossRef]
22. Mehdizad, M.; Fullard, L.; Galvosas, P.; Holland, D. Quantitative measurements of flow dynamics in 3D hoppers using MRI. *Powder Technol.* **2021**, *392*, 69–80. [CrossRef]
23. Olivares, M.C.V.; Benito, J.G.; Uñac, R.O.; Vidales, A.M. Towards a one parameter equation for a silo discharging model with inclined outlets. *Powder Technol.* **2018**, *336*, 265–272. [CrossRef]
24. Ayuga, F.; Aguado, P.; Gallego, E.; Ramirez, A. Experimental tests to validate numerical models in silos design. *ASABE Annu. Int. Meet.* **2006**, *1–15*. [CrossRef]
25. Gallego, E.; Rombach, G.A.; Neumann, F.; Ayuga, F. Simulations of Granular Flow in Silos with Different Finite Element Programs: Ansys vs. silo. *Trans. ASABE* **2010**, *53*, 819–829. [CrossRef]
26. Gallego, E.; Ruiz, A.; Aguado, P.J. Simulation of silo filling and discharge using ANSYS and comparison with experimental data. *Comput. Electron. Agric.* **2015**, *118*, 281–289. [CrossRef]
27. Pieper, K.; Schütz, M. *Bericht Über das Forschungsvorhaben—Norm-Mess-Silo Für Schüttguteigenschaften*; Technische Universität Braunschweig: Braunschweig, Germany, 1980.
28. Gandia, R.M.; Júnior, E.A.D.O.; Gomes, F.C.; de Paula, W.C.; Dornelas, K.C. Experimental Pressures Exerted by Maize in Slender Cylindrical Silo: Comparison with Iso 11697. *Eng. Agric.* **2021**, *41*, 576–590. [CrossRef]
29. Gandia, R.M.; Gomes, F.C.; de Paula, W.C.; Junior, E.A.d.; Rodriguez, P.J.A. Static and dynamic pressure measurements of maize grain in silos under different conditions. *Biosyst. Eng.* **2021**, *209*, 180–199. [CrossRef]
30. DIN. *DIN 1055-6: Basis of Design and Actions on Structures—Part 6: Design 623 Loads for Buildings and Loads in Silo Bins*; Verlaz: Berlin, Germany, 2005.
31. WPMPS. *Standart Shear Testing Technique for Particulate Solids Using the Jenike Shear Cell*; IChemE: Warwickshire, UK, 1989.
32. Couto, A.; Ruiz, A.; Herráez, L.; Moran, J.; Aguado, P.J. Measuring pressures in a slender cylindrical silo for storing maize. Filling, static state and discharge with different material flow rates and comparison with Eurocode 1 part 4. *Comput. Electron. Agric.* **2013**, *96*, 40–56. [CrossRef]

**Article 4 – Experimental pressures exerted by maize in slender cylindrical silo: comparison with ISO 11697 - Engenharia Agrícola journal (published version)**

The article was published in *Engenharia Agrícola* journal (ISSN 0100-6916). The journal has the qualis B1 and JCR 0.716.

DOI: https://doi.org/10.1590/1809-4430-Eng.Agric.v41n6p576-590/2021.

Engenharia Agrícola

ISSN: 1809-4430 (on-line)

www.engenhariaagricola.org.br

Doi: http://dx.doi.org/10.1590/1809-4430-Eng.Agric.v41n6p576-590/2021

# EXPERIMENTAL PRESSURES EXERTED BY MAIZE IN SLENDER CYLINDRICAL SILO: COMPARISON WITH ISO 11697

**Rômulo M. Gandia[1*], Estácio A. de Oliveira Júnior[1], Francisco C. Gomes[1], Wisner C. de Paula[1], Karoline C. Dornelas[2]**

[1*]Corresponding author. Federal University of Lavras/ Lavras - MG, Brazil.
E-mail: romagandia@gmail.com | ORCID: https://orcid.org/0000-0002-7786-1525

**KEYWORDS**

funnel flow, normal pressures, frictional pressures, test silo.

**ABSTRACT**

Pilot-scale test stations make it possible to obtain reliable and comparable results applicable to full–scale systems by conforming to specified proportional limits. Therefore, in this study, normal and frictional pressures were evaluated in a pilot-scale test station composed of a slender cylinder silo using maize, a free-flowing product, as the stored product. Temporal effects were analyzed and verified during filling, static, and discharge conditions. The maximum normal and frictional pressures were also evaluated. The results were compared with ISO 11697: 1995. During filling, accommodation peaks occurred only in the α: 30° hopper. In general, normal pressures were higher for the flat bottom whereas higher frictional pressures occurred for the 30° hopper. The maximum experimental pressures (normal and frictional) were lower than those provided by ISO 11697. Therefore, it is concluded that the coefficients used in the ISO standard are sufficient to promote safety in silo projects.

## INTRODUCTION

Brazil's economic growth has been influenced by agribusiness, spurred by increasing productivity in the sector in recent years. From January to October 2020, the contribution of agribusiness to the gross internal product or produto interno bruto (PIB) was 16.81%, equivalent to 274 billion reais, or approximately 49 billion USD (CEPEA, 2021). For the year 2021, agriculture production is estimated to reach 256.8 million tons, where maize represents 100.6 million tons in the first and second harvests (IBGE, 2020). Brazil, being a continental country with a favorable climate for production throughout the year, increases its agricultural export sector annually. With such production, the use of silos for the storage of products is essential, and an estimated static capacity of 171.542 billion tons is currently available (CONAB, 2020).

However, despite these significant numbers, Brazil does not have its own standard for silo design. Currently, the Brazilian standard is being discussed (CE-203:020.001 – *Comissão de Estudo de Máquinas e Equipamentos para Sistemas de Armazenagem e Beneficiamento de Grãos Vegetais*). The importance of a specific standard is necessary not only for structure design, but to maintain records of the properties of the products stored in the country and the properties of the building materials of the silo, in addition to cultural factors of operation regarding storage and climatic conditions.

The study of the behavior of products stored in silos was first proposed and conducted by Janssen (Janssen, 1895). Since then, various theories have been developed (Jenike & Johanson 1973a, 1973b; Walker, 1967; Walters 1973a, 1973b) that support current international standards (ANSI, 2019; CEN, 2006; DIN, 2005; ISO, 2012).

Most standards classify a product's discharge flow graphically. ISO 11697 uses pressure graphs based on the hopper angle and on the friction angle between the grain and the silo wall. The flow can be classified into mass flow, funnel flow, or intermediate flow (mixed). Mass flow is the most desirable and, whenever feasible, a silo is designed to achieve mass flow. The advantage of mass flow is that it promotes a uniform discharge, where all particles are in motion, thus preventing the formation of static zones. In funnel flow, a channel is formed above the discharge gate, generating static side zones where the product remains

[1] Federal University of Lavras/ Lavras - MG, Brazil.
[2] Federal University of Mato Grosso/ *Campus* Sinop/ Sinop - MT, Brazil.

Area Editor: Edilson Costa
Received in: 3-11-2021
Accepted in: 9-17-2021

stationary (Calil & Cheung 2007; Jenike et al., 1973b, 1973a; Wójcik et al., 2012).

Flow determination is fundamental in the analysis of the forces acting on the silo, which are evaluated during the filling and discharge phases. ISO 11697 provides equations for horizontal, vertical, and frictional pressure during the filling phase in the silo cylinder and hopper. In the case of discharge, effects are described through an overpressure coefficient "C," which is established according to the slenderness (diameter) of the silo.

From several studies on silo failures and collapses (Bywalski & Kamiński, 2019; Gutiérrez et al., 2015; Dogangun et al., 2009; Teng, 1994; Teng & Rotter, 1989, 1991), it was found that the main causes were attributable to design error, pressure (normal and frictional, on the wall and in the hopper) created by the product stored in the structure, excess moisture in the stored product (causing unexpected overpressure), product discharge (producing maximum pressures in the silo, usually in the silo-hopper transition area), discharge eccentricity, temperature variation in the product attributed to the location of the silo, and imperfections in the structural material.

A full-scale experimental model of a silo can be used to obtain or approximate real values, making it possible to understand the effects of pressure in silos. Worldwide, the number of full-scale experimental silo stations is relatively small (Sun et al., 2020; Couto et al., 2012; Härtl et al., 2008; Ramírez et al., 2010a) because of the costs associated with construction, instrumentation, and operations. In addition, the scale factor of the plant with respect to an actual silo is extremely important for reliable data (Brown & Nielsen 1998). Furthermore, the study of experimental pressures in silos allows advances in numerical studies as a means of validation and comparison to ensure the reliability of the models.

The pilot-scale test station proposed by Pieper and Schütz in 1980 (Pieper & Schütz, 1980), which helped to develop DIN 1055-6: Basis of design and actions on structures–Part 6 (DIN, 2005), allows the evaluation of numerous variables that directly influence the behavior of the pressures in a silo related to any stored product, provided that the maximum diameter of the product is less than 1.7 cm (to be accurately proportional to the real scale) (Brown & Nielsen, 1998; Pieper & Schütz, 1980). The station can be used to analyze three walls having different roughness (thus varying the friction coefficient between the product and the wall), twelve height/diameter ratios, eight bottoms (one flat bottom, four concentric hoppers (α: 75º to 30º) and three 100% eccentric hoppers (α: 75° to 45º)) and other possible procedural variables pertaining to silo storage.

Through catalogs of the main silo manufacturers in Brazil (GSI, PAGÉ, and Kepler Weber), the models of silos sold for the storage of maize and soybeans have flat bottoms or hoppers with beta of 45° and 60° and maximum H/D ratio = 3. Flat-bottom silos are widely used because they optimize storage volume, are easier to handle, and are less expensive (Calil & Cheung, 2007). When using a flat bottom, it is necessary to use manual labor or mechanical systems to remove the remaining product at the bottom of the silo after discharge, a requirement that may not be necessary when using an inclination in the discharge base (a hopper).

Owing to the economic importance of maize, the uncertainties (Dogangun et al., 2009) in silo pressures and the high number of slender silos and funnel flow silos used in Brazil, this study aims to provide information to support a Brazilian standard. In addition, the objective of this study was to experimentally evaluate the pressures using maize, a free-flow product, in a slender silo considering hopper and flat bottom configurations, and to compare the values obtained to those of ISO 11697.

## MATERIAL AND METHODS

### General description of the installation

Tests were conducted at the test station located in the Federal University of Lavras (UFLA) in the Laboratório de propriedades físicas e de fluxo de produtos armazenados. The station was previously validated by our research team regarding pressure and flow in silos associated with stored products (Gandia et al., 2021). The station (Figure 1) consists of a storage silo where the product to be tested is stored, a bucket elevator that transports the material, and an instrumented pilot silo for pressure analysis.

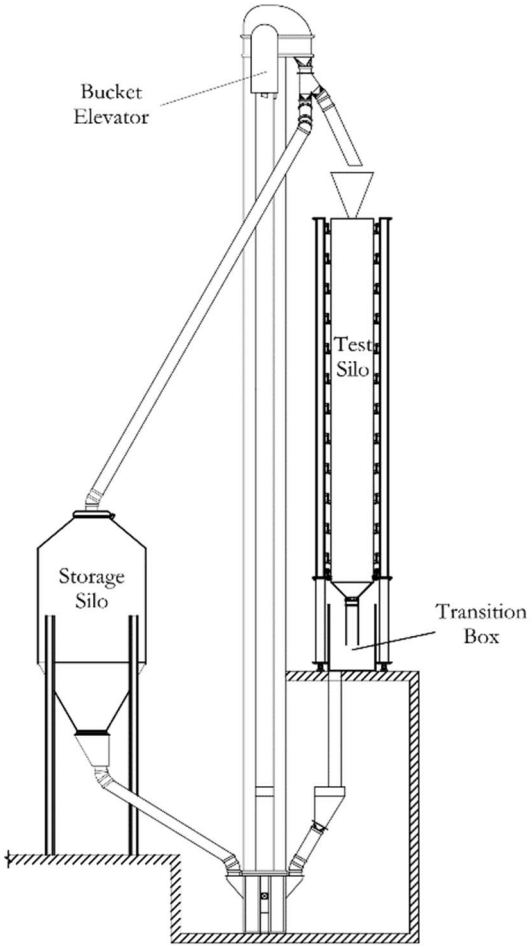


FIGURE 1. Pilot silo test station.

**Geometry of pilot silo**

The pilot silo has a total height of 6 m and is subdivided into 12 independent and suspended rings (495 mm height and 688 mm internal diameter each). The silo wall consists of smooth galvanized steel with a thickness of 10 mm, designed to ensure that the stresses created during the tests are transferred to the wall without deformation of the same.

Each ring has a vertical cut with a spacing of 5 mm in the gap between rings, which guarantees structural interdependence. The instrumentation of each ring consists of two pairs of traction load cells. The first pair is located in the center and is perpendicular to the vertical opening of the ring, determining the horizontal pressure on the wall, which in its normal state is pre-tensioned with three helical springs, making the setup more sensitive to any stress effects (Figure 2). The second pair is located next to the outer wall of the ring and is fixed using clamps articulated to the pillars of the silo and measures any vertical acting force (Figure 2).

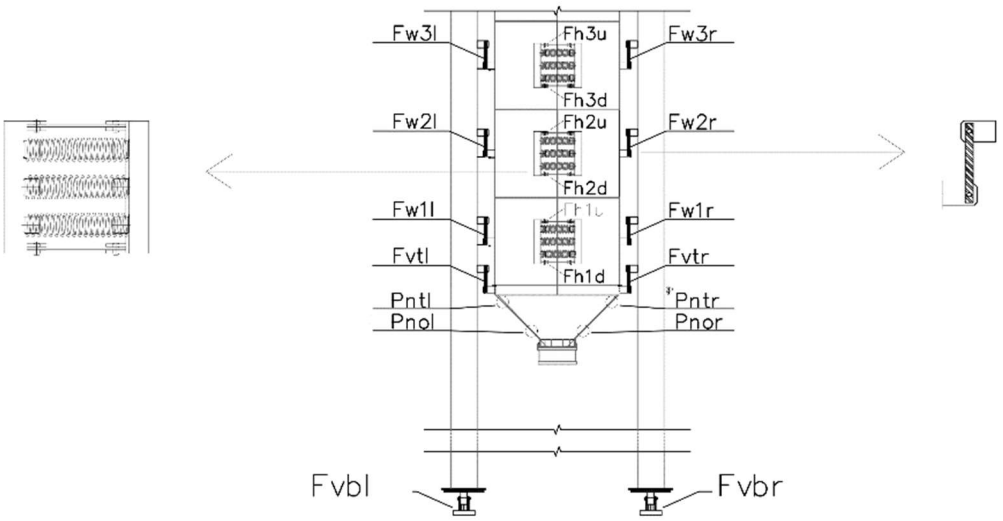


FIGURE 2. Locations of measurement cells.

The rings are suspended and supported by three pillars, one of which only has the function of stabilizing the rings and preventing rotation. The other two have a beam load cell with a capacity of 50 kN at their base, which allow the weight of the stored product to be determined from the sum of the load on the two pillars (Figure 3).

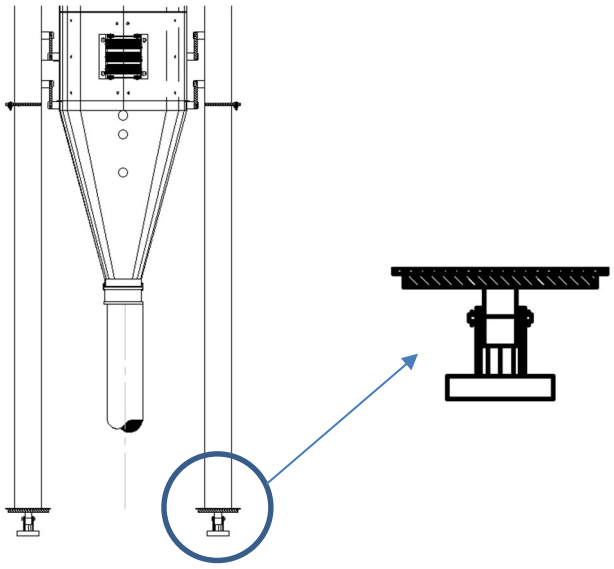

FIGURE 3. Support pillars and locations of beam load cells.

The station allows four hopper configurations with a concentric discharge (α: 30°, 45°, 60°, and 75°), three eccentric hoppers (α: 45°, 60°, and 75°), and a flat bottom with concentric discharge. The α: 30° hopper and the flat bottom used in this study were instrumented using four pressure cells distributed and attached to their walls, as shown in Figure 4.

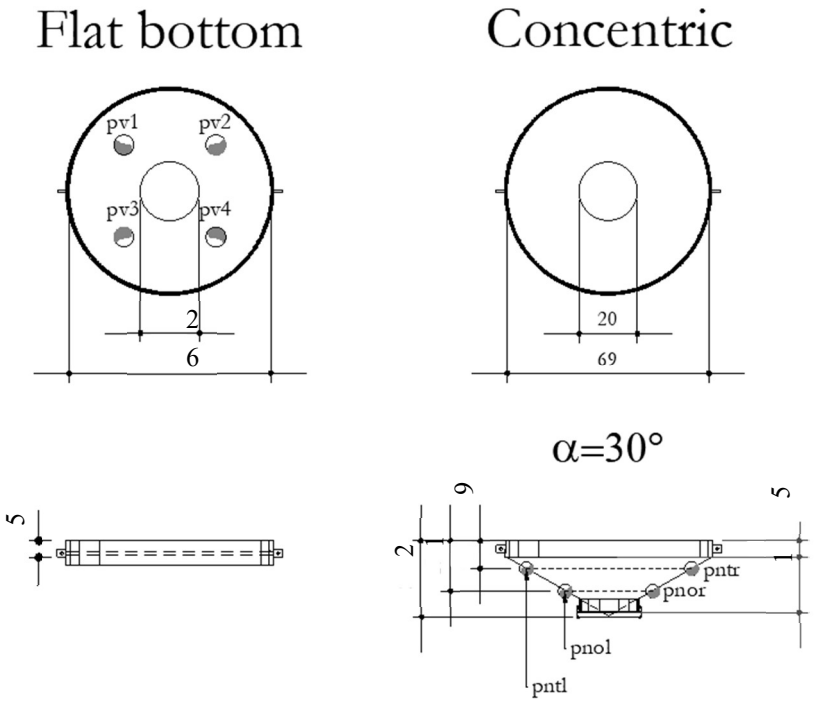


FIGURE 4. Hopper geometry and positioning of pressure cells.

During the experiments, the hopper was connected to the support pillars. Each support pillar has a set of one clamp and one traction load cell, which have articulated connections at both ends and are connected through a stainless-steel pin. The same system was used in the vertical support of each ring (Figure 2).

The acquisition of electrical signals (in mV/V) was performed by a module (LYNX model DS2000) with a capacity of 64 channels and a maximum frequency of 65.5 kHz. The calibration and treatment of the data were performed using the Aqdados software package (version 7.5).

**Description of tests**

The physical characteristics of the maize were determined at the Centro de Tecnologia e Recursos Naturais da Universidade Federal de Campina Grande (UFCG), using Jenike's shear device (Jenike Shear Cell) (Building, 1989).

Pressure analysis was performed during filling, static, and discharge phases. The filling height of the product was 1.50 m, and the height/diameter ratio was 2.18. The acquisition system was configured to collect data at a frequency of 2 Hz. The test variables were as follows: α: 30° hopper and flat bottom, both with concentric discharge. Three repetitions were performed to evaluate each variable, totaling six complete tests.

The maize was transferred to the pilot silo through a bucket elevator that provided constant flow and centralized filling until the grain mass reached a height of approximately 1.5 m. After filling, the maize was allowed to settle for 10 min (static condition) to stabilize the system and accommodate the stored product.

Figure 5 shows the three phases (filling, static, and discharge) At the discharge, the hopper gate was completely open, promoting free discharge, where the highest pressure was expected in this stage. After opening the discharge gate, the maize fell into the transition box so as not to exceed the bucket elevator carrying capacity. Finally, the product was transferred from the transition box to the storage silo using the bucket elevator, completing the test.

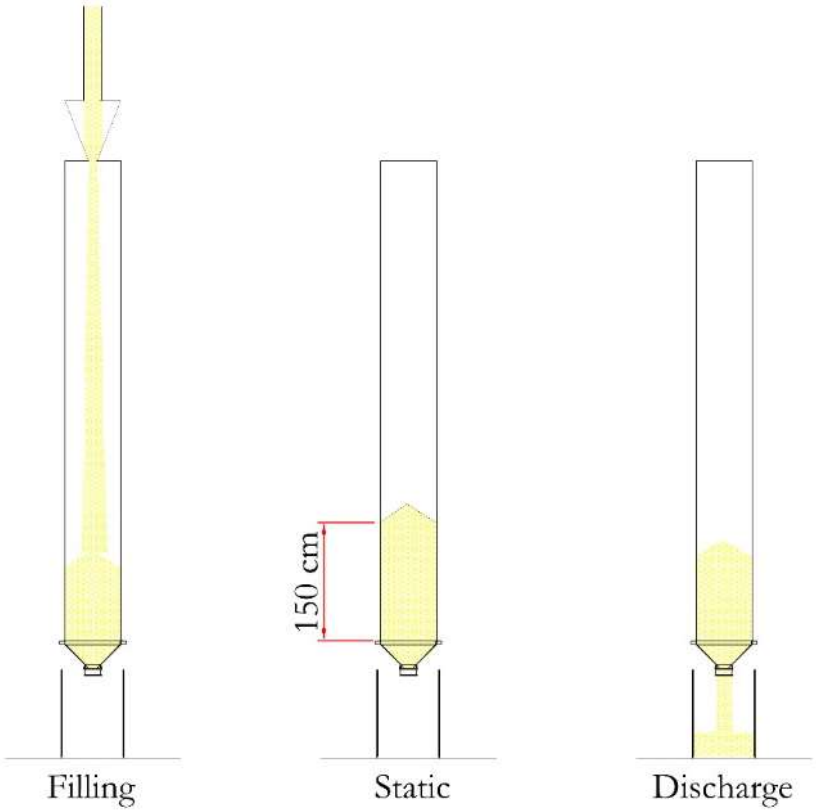


FIGURE 5. Testing stage: Filling, static, and discharge conditions.

According to ISO 11697 (ISO, 2012), flow characterization (available from ISO "Figure 2 - Limit between mass flow and funnel flow for circular hoppers"), the friction coefficient for maize is 7.38 – 9.23 and funnel flow discharge characteristics for the 30º hopper and flat bottom were evaluated based on this friction coefficient.

**RESULTS AND DISCUSSION**

To evaluate the uniformity of the repetitions of the tests and the difference between the two configurations, Table 1 presents the average loading values (weight of the stored product) during the filling and discharge phases in the pilot silo.

TABLE 1. Product weight.

| | Average value (kN) | | Standard deviation (%) | |
|---|---|---|---|---|
| | Filling | Discharge | Filling | Discharge |
| Concentric (α = 30°) | 5.4 | 5.5 | 7.3 | 7.4 |
| Flat Bottom | 5.1 | 5.0 | 3.4 | 3.9 |

From this information, it is possible to verify that the repetitions between each configuration presented low variability (statistically equal). It is also possible to state that the two configurations differ because of the greater volume of the 30° hopper.

Table 2 shows the average of the times in each phase of the tests and the standard deviation calculated for the test repetitions.

TABLE 2. Trial time.

| | Average value (s) | | | Standard deviation (%) | | |
|---|---|---|---|---|---|---|
| Test | Filling | Static | Discharge | Filling | Static | Discharge |
| Concentric (α = 30°) | 189.0 | 646.2 | 47.2 | 8.9 | 2.3 | 27.5 |
| Flat Bottom | 189.3 | 631.5 | 34.8 | 3.0 | 1.6 | 30.4 |

There was considerable deviation in the discharge phase, which was caused by turbulence and complexity in the flow. To verify that the same test conditions were present, the discharge flow between the two configurations was compared (Table 3).

TABLE 3. Average flow rate for each test.

| | Average value (Kg/s) | | Standard deviation (%) | |
|---|---|---|---|---|
| Test | Filling | Discharge | Filling | Discharge |
| Concentric (α = 30°) | 2.9 | 12.8 | 1.9 | 38.3 |
| Flat Bottom | 2.8 | 15.7 | 5.6 | 36.6 |

The filling flow rate, in addition to having a relatively low deviation between repetitions, was statistically equal between the two configurations. As expected, the discharge rate deviation was higher. The deviation between repetitions is relatively greater than for filling because of the funnel flow pattern (ISO, 2012), exhibiting random behavior during the discharge phase (Calil & Cheung, 2007; Jenike et al., 1973b).

This study generated a large volume of data. Therefore, to avoid presenting unnecessary data, Tables 4 and 5 present the average values from each measurement cell obtained from the pilot silo instrumentation for the 30° concentric hopper and flat bottom configurations, respectively, in the three phases.

TABLE 4. Mean pressure values in the hopper configuration (α = 30°).

| | Load (kPa) | | | Standard deviation (%) | | |
|---|---|---|---|---|---|---|
| Sensor | Filling | Static | Discharge | Filling | Static | Discharge |
| ph3 | 0.78 | 0.91 | 1.55 | 19.97 | 15.25 | 11.12 |
| ph2 | 1.70 | 1.92 | 2.81 | 15.41 | 11.50 | 6.82 |
| ph1 | 2.95 | 3.32 | 3.43 | 3.32 | 9.49 | 3.19 |
| pntr | 1.17 | 1.27 | 11.16 | 17.15 | 25.80 | 15.56 |
| pntl | 1.71 | 1.21 | 10.88 | 19.11 | 29.72 | 14.82 |
| pnor | 5.87 | 6.42 | 5.23 | 12.49 | 9.21 | 10.83 |
| pnol | 4.55 | 4.96 | 4.88 | 15.09 | 17.92 | 16.70 |
| pvt | 10.20 | 10.67 | 10.07 | 3.85 | 3.00 | 2.29 |
| pw3 | 0.21 | 0.30 | 0.40 | 7.35 | 4.76 | 9.40 |
| pw2 | 0.47 | 0.55 | 0.65 | 18.01 | 7.85 | 3.99 |
| pw1 | 1.06 | 1.08 | 1.13 | 13.34 | 11.44 | 10.55 |

TABLE 5. Mean pressure values in the flat bottom configuration.

| | Load (kPa) | | | Standard deviation (%) | | |
|---|---|---|---|---|---|---|
| Sensor | Filling | Static | Discharge | Filling | Static | Discharge |
| ph3 | 0.91 | 0.90 | 1.55 | 44.37 | 45.80 | 39.04 |
| ph2 | 2.50 | 2.51 | 2.81 | 6.89 | 6.65 | 6.51 |
| ph1 | 3.82 | 3.82 | 4.34 | 4.67 | 4.86 | 2.87 |
| pv1 | 7.84 | 7.93 | 8.11 | 10.72 | 10.07 | 7.54 |
| pv2 | 7.30 | 7.44 | 8.43 | 6.90 | 6.08 | 3.19 |
| pv3 | 8.93 | 9.04 | 9.41 | 9.51 | 9.28 | 8.40 |
| pv4 | 5.68 | 5.79 | 6.71 | 1.72 | 2.50 | 8.04 |
| pvt | 10.34 | 10.33 | 9.59 | 2.74 | 2.81 | 4.88 |
| pw3 | 0.18 | 0.22 | 0.36 | 11.93 | 11.51 | 22.22 |
| pw2 | 0.45 | 0.50 | 0.61 | 2.17 | 1.53 | 12.78 |
| pw1 | 0.95 | 0.95 | 0.86 | 3.37 | 3.18 | 9.30 |

One of the three repetitions of each configuration is shown (chosen randomly). The results show the pressures in three regions of the silo: cylinder (normal pressure and friction), transition (tension caused by the product being stored during the transition phase), and flat or 30° hopper bottom (normal pressure). The analysis of the results is discussed based on three phases: filling, static, and discharge.

**Concentric ($\alpha$ = 30°)**

The temporal analysis of the behavior of the normal pressures in the silo with a 30° hopper during the three phases is shown in Figure 6.

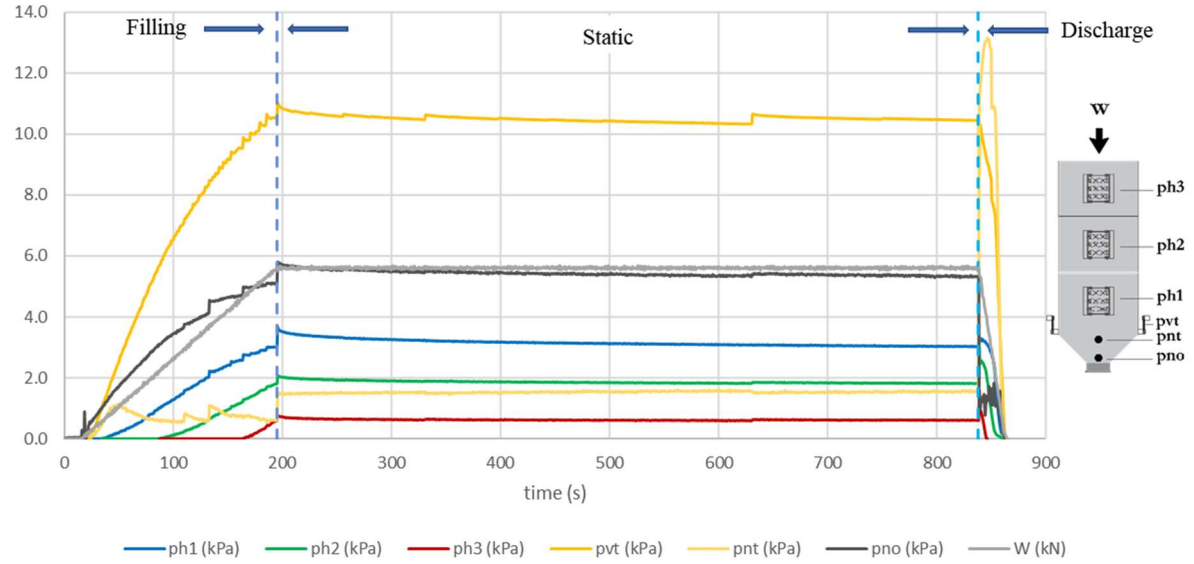


FIGURE 6. Normal pressures on the silo wall (ph, i; pnt; pno), vertical stress in the stored material at the transition (pvt) and the weight of the stored material (W) using 30° hopper.

There is an increase in pressure near the hopper outlet (pno) in the first seconds of filling, which is explained by the height as the product falls to the bottom of the silo (6 m). The weight of the stored product (W) does not vary, so it exhibits a linear behavior with respect to pressure throughout the test, allowing us to obtain the flow rate during the filling and discharge steps (Table 3).

The maximum pressure occurred in the silo-hopper transition (pnt) shortly after the beginning of the discharge of the product (ISO, 2012), and is a well-known behavior (Härtl et al. 2008; Ramírez et al., 2010b). Additionally, frictional pressures were obtained in the cylinder, as shown in Figure 8.

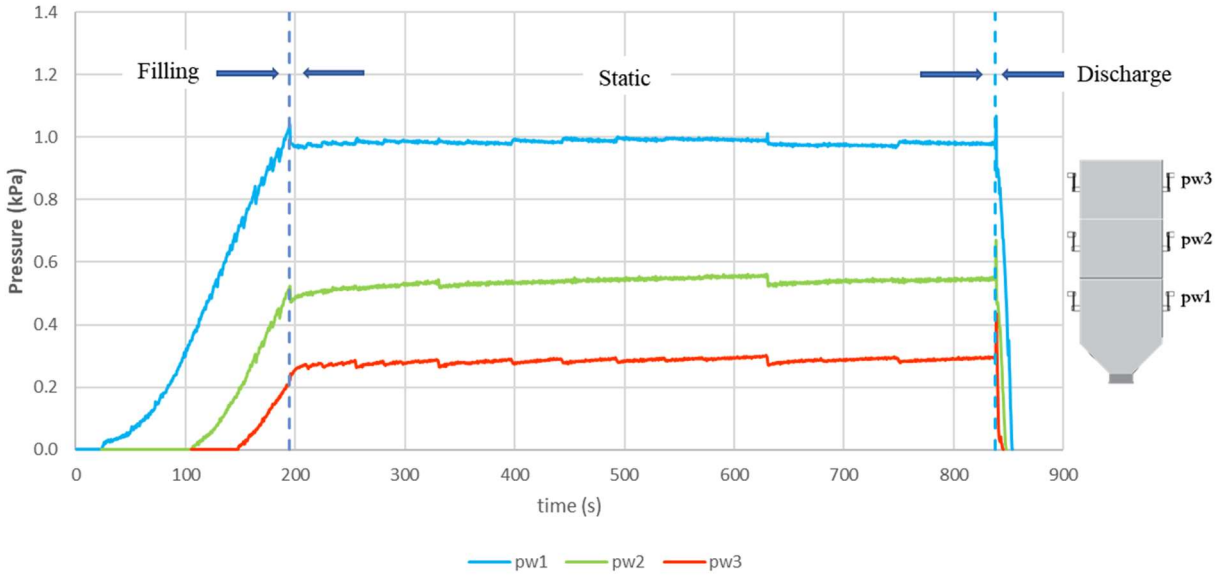


FIGURE 7. Friction pressures on the silo wall (pw, i) using 30° hopper.

Figure 7 verifies the quality of the instrumentation. During filling, the beginning of the measurements in each of the rings is observed, with temporal intervals that confirm the precision of the instrumentation. In addition, during the static phase, the peaks related to the accommodation (settling) of the material can be observed, which are synchronous in all measurement cells, regardless of whether they are pressure or load cells.

Another observation related to the static phase is related to the vertical stress caused by the stored material at the transition (pvt) and to the friction pressure in the cylinder (pwi). It is observed that while frictional pressures show decreasing accommodation peaks, the vertical stress in the stored material at the transition (pvt) shows increasing accommodation peaks. In other words, while the stored product accommodates and tends to move slightly vertically, decreasing the frictional force in the cylinder, a simultaneous increase in vertical stress in the stored material at the transition (pvt) occurs owing to the increase in the vertical pressure caused by the movement of the stored product.

**Flat bottom**

The temporal analysis behavior of normal pressures in the flat bottom silo during the three phases is shown in Figure 8.

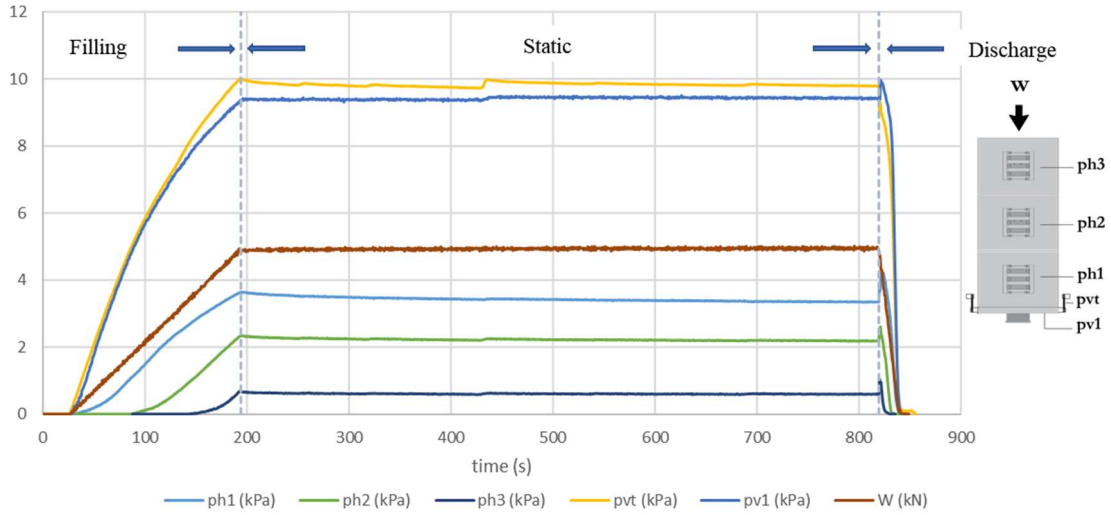


FIGURE 8. Normal pressures on the silo wall (ph, i; pnt; pno), vertical stress in the stored material at the transition (pvt) and the weight of the stored material (W) using flat bottom.

The filling phase for a flat bottom differs from the 30° hopper, as no accommodation peaks are observed during filling. The reason is that with the 30 ° hopper, the material is destabilized at the bottom of the silo because of the inclination of the hopper, promoting the accommodation of the material during filling, unlike the flat bottom, in which the material stabilizes during filling, and there is no such accommodation.

As predicted, the normal pressure at the bottom (pv1) is very similar to the vertical stress in the stored material at the transition (pvt). In general, the normal pressures in the cylinder in the filling and static phases are higher for a low-inclination hopper (in this case a flat bottom). Therefore, it is observed that for the flat bottom, the pressures are greater than those of the α = 30° hopper; however, in the discharge, the opposite occurs, and greater pressure peaks are observed for greater inclinations (CEN, 2006; ISO, 2012; Jenike, 1964; Jenike et al., 1973a; Wójcik et al., 2012). The frictional pressures for the flat bottom silo are shown in Figure 9.

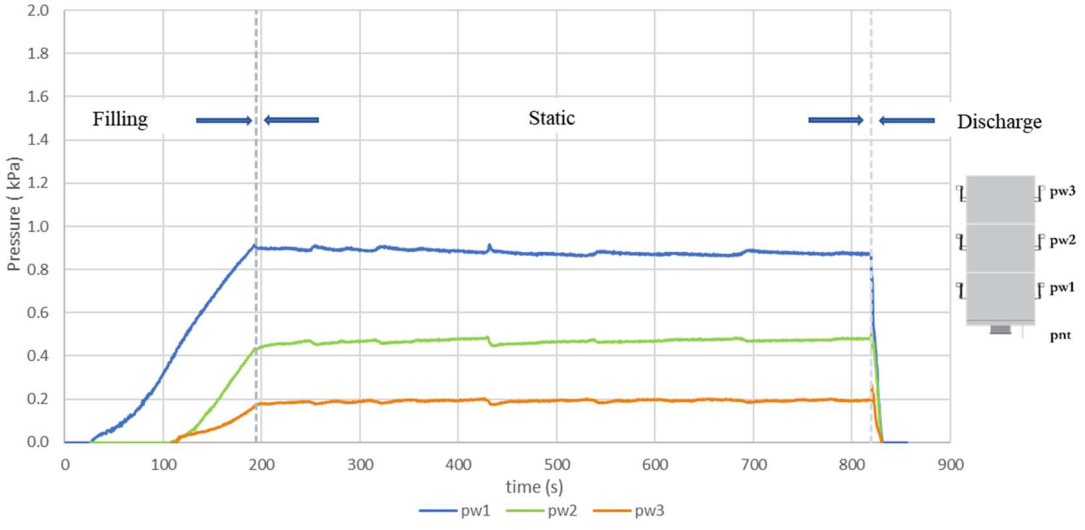


FIGURE 9. Friction pressures on the silo wall (pw, i) using flat bottom.

Once again, it was possible to observe the quality of the instrumentation based on the time intervals during filling in the rings and also by the synchrony among the accommodation peaks during the static phase. The friction pressure in ring 3 (pw3) was observed to begin at the same time as ring 2 (pw2). A possible reason for this unexpected result is the dissipation of the product in the discharge resulting from the slenderness of the pilot silo, promoting the beginning of a vertical force at the height of ring 3 before the grain mass actually reaches this level.

As previously mentioned, the friction pressure (pwi) and the vertical stress in the stored material at the transition (pvt) exhibit the same behavior during the static phase as occurred for the 30° hopper.

**Filling**

During filling, the pressures exhibited different time patterns. In Figures 10 and 11, the normal pressures up to a height of 1.50 m and the vertical stress in the stored material at the transition (pvt) are shown for the 30° hopper and the flat bottom, respectively.

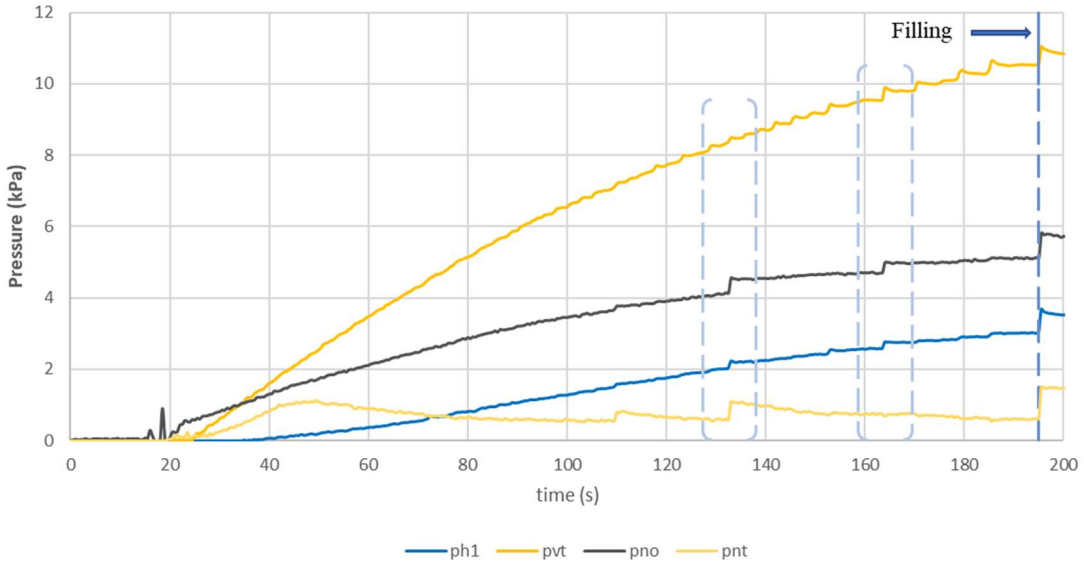


FIGURE 10. Filling pressures, 30° hopper.

The fluctuations in the accommodation of the material during filling due to the inclination of the hopper can be observed in Figure 10. The greater the height of the product in the silo (the greater the weight of the grain mass), the greater the magnitude of the accommodation peaks at 126.5 and 171 s and also when filling is completed. The behavior of pressures on the flat bottom exhibits some differences (Figure 11).

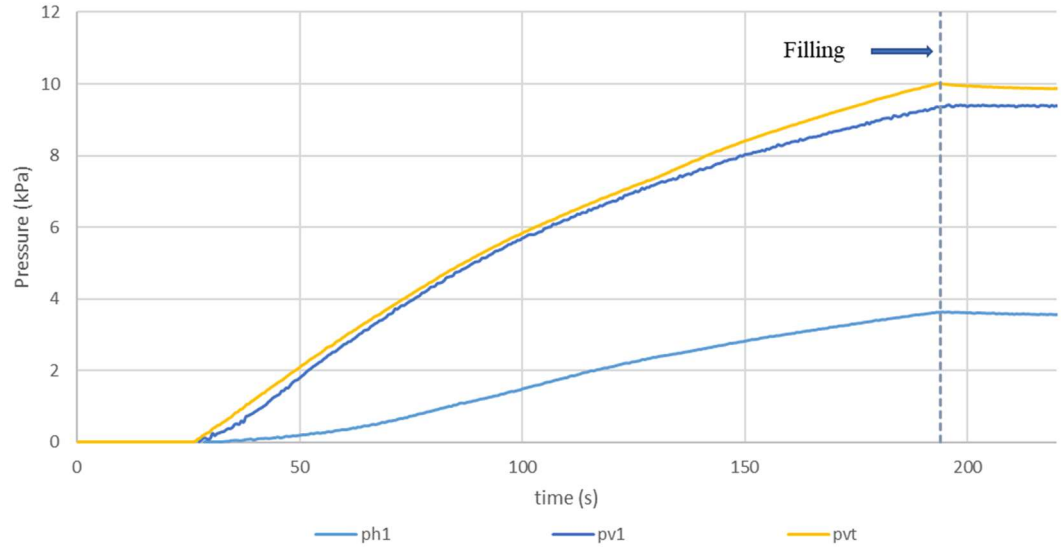


FIGURE 11. Filling pressures, flat bottom.

As explained above, because of the stabilization provided by the flat bottom (90° angle), the pressures do not fluctuate significantly.

**Static**

Observations regarding the nonlinearities of the material pressures during the static condition, that is, after accommodation, were discussed for the first time in 2012 (Couto et al., 2013b; Ruiz et al., 2012). Figures 12 and 13 show an enhanced visualization of the static condition regarding the normal and frictional pressures in the silo for the α = 30° hopper and the flat bottom, respectively.

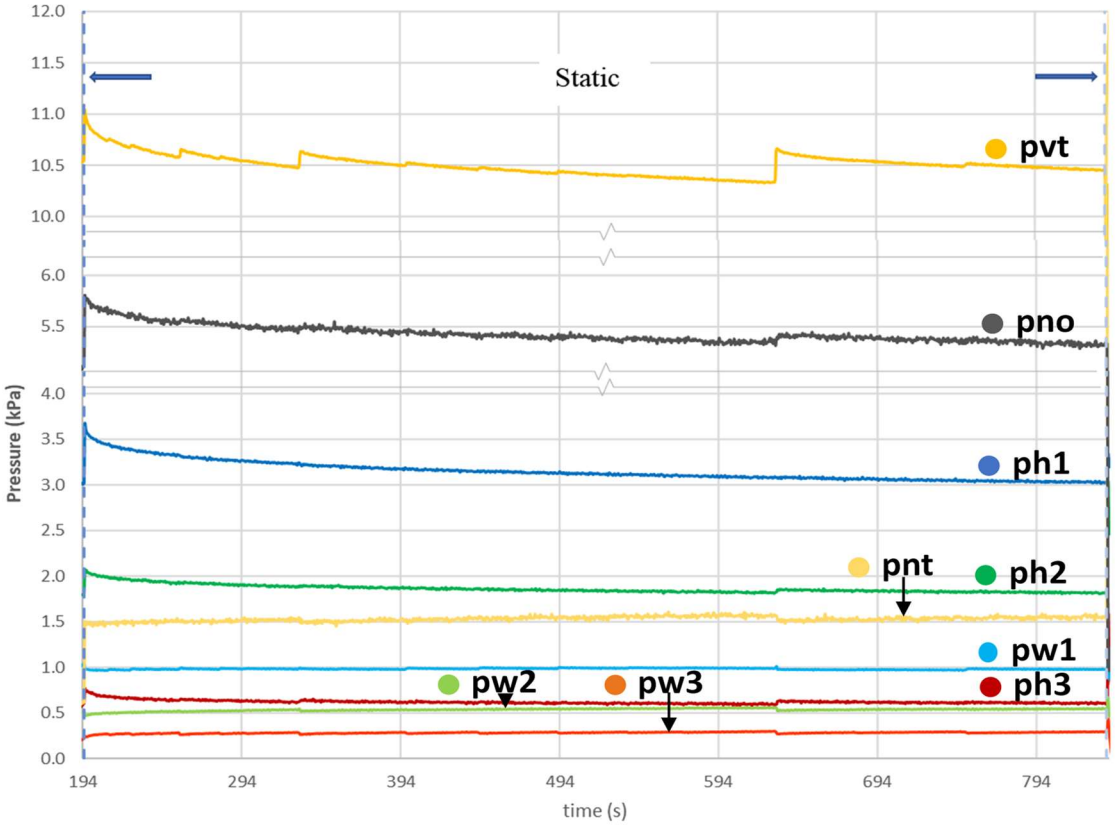


FIGURE 12. Pressures in static condition, 30° hopper.

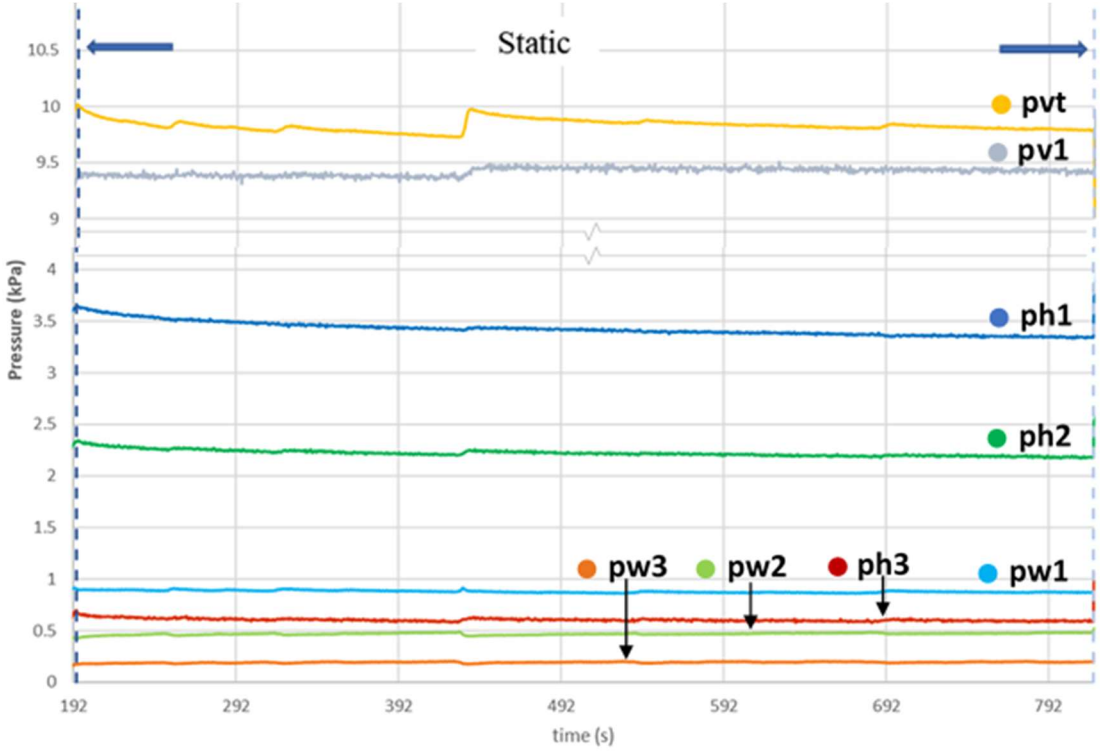


FIGURE 13. Pressures in static condition, flat bottom.

As shown in Figures 12 and 13, after filling the silo, the frequency of the accommodation peaks decreases over time. This is influenced by the segregation of the material, the variation in the specific weight of the material along the height of the silo and the angle of friction between the product and the silo wall, and the angle of friction of the stored product.

From the figures, the magnitude of the peaks is greater for the 30° hopper than for the flat bottom, reinforcing the statements regarding the destabilization of the stored product due to the inclination of the hopper.

It is also noted that while normal pressures (ph, i; pnt; pno) oscillated upward, frictional pressures behaved in an opposite manner. The material tends to compact by moving vertically (releasing frictional stress), which increases the normal stresses on the cylinder and hopper.

**Discharge**

As expected, maximum stresses occur during material discharge (Couto et al., 2013a; Jenike et al., 1973b; Sadowski et al., 2020; Sadowski et al., 2011). It is known that for funnel flow as defined in this paper (ISO, 2012), maximum pressures occur despite the discharge flow being less than the mass flow (Jenike et al., 1973b, 1973a; Wójcik et al., 2012). The pressures in the silo cylinder are shown in Figure 14. Discharge effects occur between 838 s and 864 s from the start of the test.

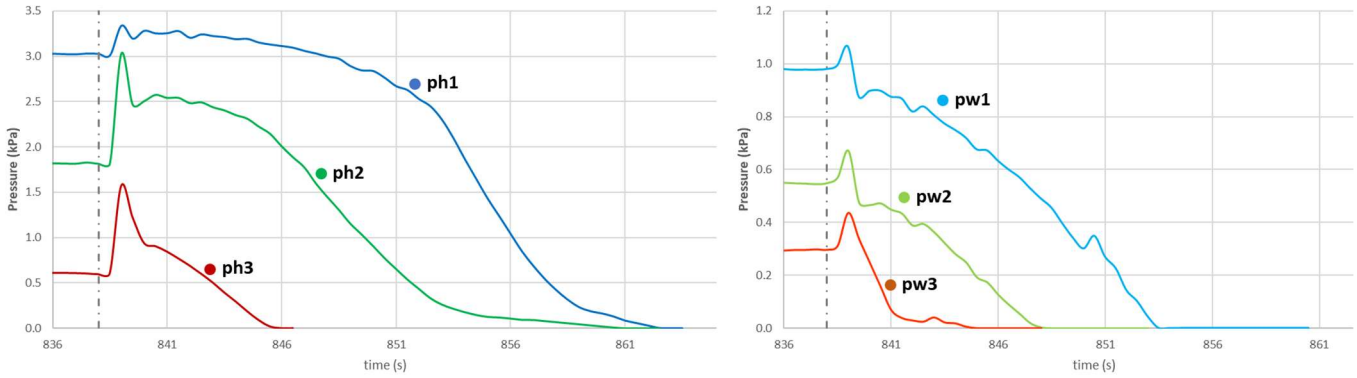


FIGURE 14. Discharge cylinder pressures (normal and frictional), 30° hopper.

An increase in both friction and normal pressures was observed over the entire cylinder. The flow channel is assumed to form in the middle of the first ring (ph1 and pw1), and as soon as discharge started, the volume of the hopper product was displaced, resulting in a small pressure peak proportional to the displaced volume. The second ring (ph2 and pw2) exhibited the highest pressure peak, indicating the absence of a static zone and a greater volume flow of stored product than through the third ring, inducing greater pressure. The third ring (ph3 and pw3), with less volume of stored product and the absence of a flow channel experienced an overpressure lower than that of the second ring.

The magnitude of the normal overpressure in the silo-hopper transition has been well defined (CEN, 2006; Couto et al. 2013a; Couto et al., 2013b; ISO, 2012; Jenike et al., 1973a), and as expected, the transition area (Figure 15) exhibited the greatest pressure (pnt) under the discharge phase. Mass flow produces higher pressures than incident flow (funnel) (Jenike et al., 1973b; Wójcik et al., 2012), however, the transition area remains as the maximum pressure point in the silo because the state of the stored material changes from static to dynamic.

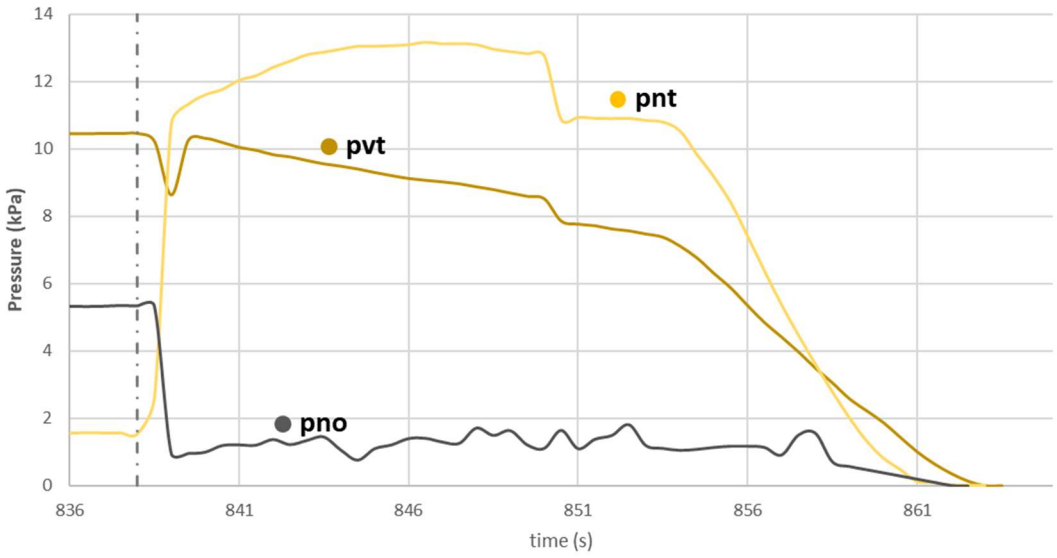


FIGURE 15. Discharge pressures (normal and vertical) in the 30° hopper.

The momentary pressure drops observed in pvt occurs because of the relief caused by the beginning of the flow and the movement of the stored product, which is related to the height of the stored product and the inclination of the hopper. This pressure is resumed instantly because from the moment the volume of the stored product is moved below the transition plane, this space is quickly filled and the pressure is transmitted again to the transition plane.

Discharge effects for the flat bottom occurred between 819 s and 843 s from the beginning of the test (Figures 16 and 17).

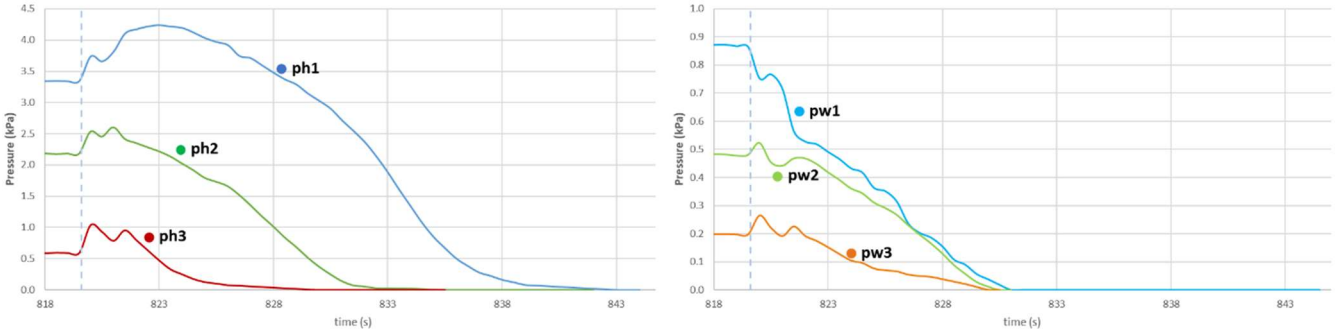


FIGURE 16. Discharge pressures (normal and frictional) in flat bottom cylinder.

As shown in Figure 16, just after discharge begins, the magnitude of the overpressure is inversely proportional to the height of the silo; in other words, ph1 < ph2 < ph3. However, the normal pressure in the first ring (ph1) continues to increase. A possible reason is the collapse of the flow channel formed in the cylinder, causing the pressure to increase over time until the volume stabilizes, after which the pressure decreases.

The frictional temporal pressure in the first ring (pw1) behaves differently from the other rings. A decrease in pressure is observed at the beginning of the flow, reinforcing that the stored product stagnated in that region (a flow channel was present), resulting in less flow, and therefore less vertical force was exerted in the region of the first ring.

The vertical pressure at the bottom of the silo (pv1) and the vertical stress in the stored material at the transition (pvt) exhibit the same behavior because of their proximity within the silo (Figure 17).

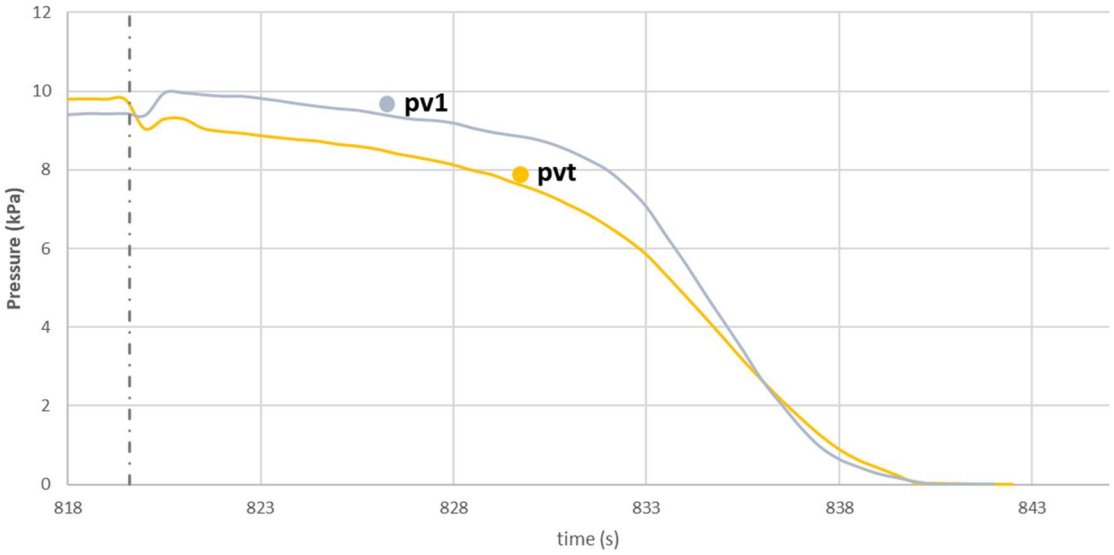


FIGURE 17. Discharge vertical pressures, flat bottom.

The behavior of the pressures in Figure 17 implies the formation of a flow funnel (static zone), because there was no significant increase in pressure in the discharge, which characterizes flow through a funnel (Jenike et al., 1973b).

**Maximum pressure**

The maximum normal and frictional experimental pressures for both test configurations (α: 30° hopper and flat bottom) were plotted and compared with ISO 11697: 1995 (Figures 18 and 19, respectively).

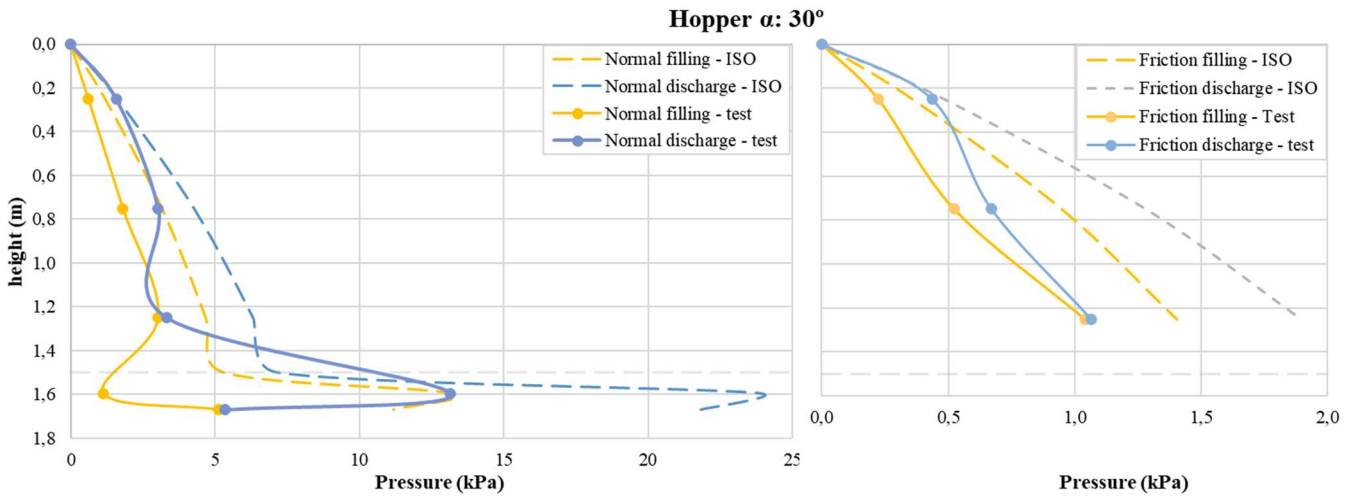


FIGURE 18. Maximum experimental and ISO pressures, α: 30° hopper.

The experimental pressures were lower than those published by ISO (ISO, 2012). In order to obtain pressures fitted to the standard, a 35% "C" overpressure coefficient is used to account for the slenderness of the cylinder, in addition to the "ps" coefficient representing an increase of 2 * ph0 (where ph0 is the horizontal filling pressure in the parallel section) over an inclined distance of 0.2 * diameter of the silo below the transition.

In the results obtained, it was noted that the experimental pressure is 53% lower than that calculated by the standard in the first ring (ph1) above the transition, and 55% in the transition region (pnt), demonstrating that the ISO standard aims to provide significant safety factors regarding silo projects.

For a flat bottom silo, the ISO recommends use of the "C" overpressure coefficient related to slenderness, which is 35%. In addition to this coefficient, an empirical safety factor of 35% must also be applied with respect to the vertical pressure during the filling and discharge phases.

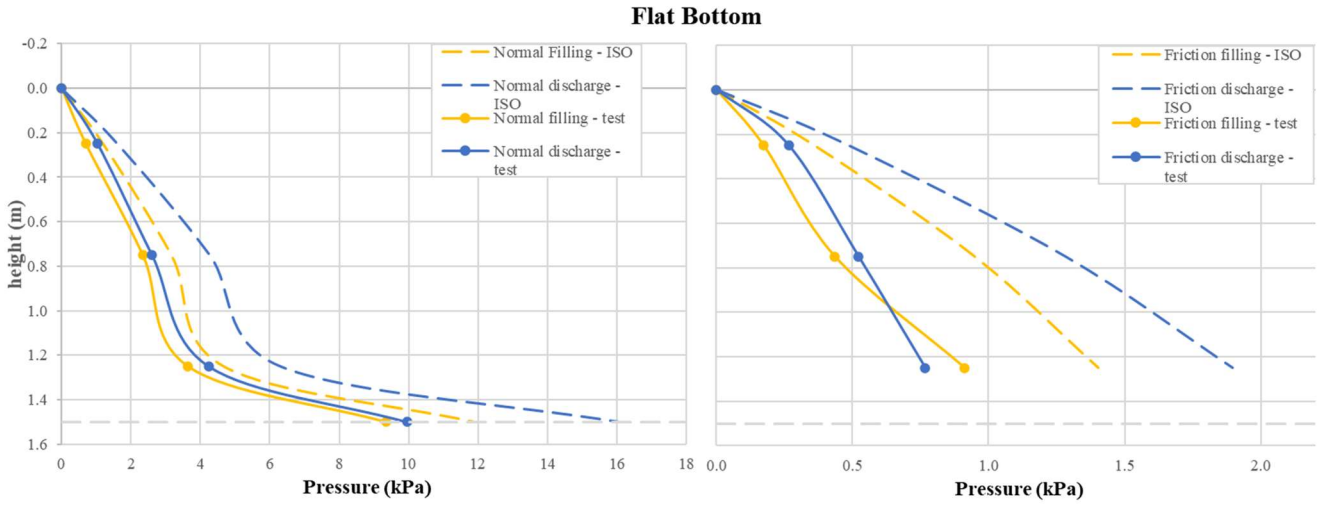


FIGURE 19. Maximum experimental and ISO pressures, flat bottom.

The experimental pressures at the transition region of the silo were lower than those obtained by the standard, which was higher by 22% in the filling and 38% in the discharge, demonstrating that the safety factors are sufficient to guarantee safe silo operations based on the results obtained in this study.

A different situation than expected occurred with respect to the frictional pressures, where the maximum pressures occurred during filling and rather than discharge, which was attributed to the height of the effective transition having passed ring 1. However, the pressure in either phase remained well below the ISO standard.

## CONCLUSIONS

During filling, pressures in the α: 30° hopper exhibited accommodation peaks because of the instability caused by the hopper inclination, which differed from the flat bottom results (no oscillations) in this stage. The pressures were not constant in the static condition, exhibiting greater variability in the friction pressures, both in the flat bottom and 30° hopper configurations.

In general, the normal cylinder pressures were higher for the flat bottom, which was expected, whereas the frictional pressures in the cylinder were higher for the 30° hopper.

At discharge, as expected, maximum pressures (normal and frictional) occurred in the cylinder in the α: 30° hopper configuration. However, in the flat bottom configuration, the friction pressure was higher during the filling stage than during the discharge phase.

The maximum normal pressures in the α: 30° hopper cylinder were approximately half those proposed by ISO 11697. For the flat bottom, the vertical experimental pressures at the transition were 38% less than those of ISO 11697, indicating a wide safety margin for silo projects. In both configurations, the frictional pressure on the cylinder was lower than the ISO standard in all phases.

## REFERENCES


ANSI - American Society of Agricultural and Biological Engineers (2019) Loads exerted by Free-Flowing Grain on Bins. ANSI/ASAE.

Brown CJ, Lahlouh EH, Rotter JM (2000) Experiments on a square planform steel silo. Chemical Engineering Science 55(20): 4399–4413. DOI: http://dx.doi.org/10.1016/S0009-2509(99)00574-6

Brown CJ, Nielsen J (1998) Silos: Fundamentals of theory, behaviour and design, London, E & FN Spon.

Building GED (1989) Standart shear testing technique for particulate solids using the Jenike Shear Cell. Rugby, The Instituition of Chemical Engineers.

Bywalski C, Kamiński M (2019) A case study of the collapse of the over-chamber reinforced concrete ceiling of a meal silo. Engineering Structures 192: 103–112. DOI: http://dx.doi.org/10.1016/j.engstruct.2019.04.100

CEN - European Committee for Standardization (2006) EN 1991-4:2006. Eurocode 1: Actions on Structures. Part 4: Silos and Tanks. CEN.

CONAB, CNA (2020) Acompanhamento da safra brasileira 2019/2020. In: Acompanhamento da Safra Brasileira de Grãos 2019/2020. CONAB. Available: https://www.conab.gov.br/info-agro/safras

Couto A, Ruiz A, Aguado PJ (2012) Design and instrumentation of a mid-size test station for measuring static and dynamic pressures in silos under different conditions - Part I: Description. Computers and Electronics in Agriculture 85: 164–173. DOI: http://dx.doi.org/10.1016/j.compag.2012.04.009

Couto A, Ruiz A, Aguado PJ (2013a) Experimental study of the pressures exerted by wheat stored in slender cylindrical silos, varying the flow rate of material during discharge. Comparison with Eurocode 1 part 4. Powder Technology 237: 450–467. DOI: http://dx.doi.org/10.1016/j.powtec.2012.12.030

Couto A, Ruiz A, Herráez L, Moran J, Aguado PJ (2013b) Measuring pressures in a slender cylindrical silo for storing maize. Filling, static state and discharge with different material flow rates and comparison with Eurocode 1 part 4. Computers and Electronics in Agriculture 96: 40–56. DOI: http://dx.doi.org/10.1016/j.compag.2013.04.011

DEUTSCHE NORM (2005) DIN 1055-6: Basis of design and actions on structures – Part 6: design 623 loads for buildings and loads in silo bins. Berlin, Verlaz.

Dogangun A, Karaca Z, Durmus A, Sezen H (2009) Cause of damage and failures in silo structures. Journal of Performance of Constructed Facilities 23(2): 65–71. DOI: http://dx.doi.org/10.1061/(ASCE)0887-3828(2009)23:2(65)

ESALQ, CEPEA, CNA (2021) PIB do agronegócio avança novamente em outubro.

Gandia RM, Gomes FC, Paula WC, Junior EA, Aguado PJ (2021) Static and dynamic pressure measurements of maize grain in silos under different conditions, Biosystems Engineering 209: 180–199. DOI: https://doi.org/10.1016/j.biosystemseng.2021.07.001.

Gutiérrez G, Colonnello C, Boltenhagen P, Darias JR, Peralta-Fabi R, Brau F & Clément E (2015) Silo collapse under granular discharge. Physical Review Letters, 114(1), 5–9. DOI: http://dx.doi.org/10.1103/PhysRevLett.114.018001

Härtl J, Ooi JY, Rotter JM, Wojcik M, Ding S, Enstad GG (2008) The influence of a cone-in-cone insert on flow pattern and wall pressure in a full-scale silo. Chemical Engineering Research and Design 86(4): 370–378. DOI: http://dx.doi.org/10.1016/j.cherd.2007.07.001

IBGE (2020) Levantamento sistemático da produção agrícola - Estatística da produção agrícola. IBGE.

ISO - Internacional Organization for Standardization (2012) ISO 11697:2012. Bases for design of strutures - Loads due to bulk materials. ISO.

Janssen HA (1895) Versuche uber getreidedruck in silozellen. Z. Ver. Deutsch Ingineering 39(35): 1045–1049.

Jenike A (1964) Storage and flow of Bulk solids bull. 123. University of Utah.

Jenike AW, Johanson JR, Carson JW (1973a) Bin loads—part 3: mass-flow bins. Journal of Manufacturing Science and Engineering, Transactions of the ASME 95(1): 6–12. DOI: http://dx.doi.org/10.1115/1.3438163

Jenike AW, Johanson JR, Carson JW (1973b) Bin Loads—Part 4: Funnel-Flow Bins. Journal of Engineering for Industry 95: 13–20.

Junior CC, Cheung AB (2007) Silos: pressões, fluxo, recomendações para o projeto e exemplo de cálculo. São Carlos, SET/EESC, USP Ed.

Pieper K, Schütz M (1980) Bericht über das Forschungsvorhaben Norm-Mess-Silo für Schüttguteigenschaften. Hochbaustatik, Technische Universität.

Ramírez A, Nielsen J, Ayuga F (2010a) On the use of plate-type normal pressure cells in silos. Part 1: Calibration and evaluation. Computers and Electronics in Agriculture 71(1): 71–76. DOI: http://dx.doi.org/10.1016/j.compag.2009.12.004

Ramírez A, Nielsen J, Ayuga F (2010b) On the use of plate-type normal pressure cells in silos. Part 2: Validation for pressure measurements. Computers and Electronics in Agriculture 71(1): 64–70. DOI: http://dx.doi.org/10.1016/j.compag.2009.12.005

Ruiz A, Couto A, Aguado PJ (2012) Design and instrumentation of a mid-size test station for measuring static and dynamic pressures in silos under different conditions - Part II: Construction and validation. Computers and Electronics in Agriculture 85: 174–187. DOI: http://dx.doi.org/10.1016/j.compag.2012.04.008

Sadowski AJ, Michael Rotter J, Nielsen J (2020) A theory for pressures in cylindrical silos under concentric mixed flow. Chemical Engineering Science 223: 115748. DOI: http://dx.doi.org/10.1016/j.ces.2020.115748

Sadowski AJ, Rotter JM (2011) Buckling of very slender metal silos under eccentric discharge. Engineering Structures 33(4): 1187–1194. DOI: http://dx.doi.org/10.1016/j.engstruct.2010.12.040

Sun W, Zhu J, Zhang X, Wang C, Wang L, Feng J (2020) Multi-scale experimental study on filling and discharge of squat silos with aboveground conveying channels. Journal of Stored Products Research 88: 101679. DOI: http://dx.doi.org/10.1016/j.jspr.2020.101679

Teng BJ (1994) Plastic Collapse at lap joints in pressurized cylinders under axial load. Journal of Structural Engineering 120(1): 23-45.

Teng JG, Rotter JM (1989) Plastic collapse of restrained steel silo hoppers. Journal of Constructional Steel Research 14(2): 139–158. DOI: http://dx.doi.org/10.1016/0143-974X(89)90020-5

Teng J, Rotter JM (1991) Collapse Behavior and Strength of Steel Silo Transition Junctions. Part I: Collapse Mechanics. Journal of Structural Engineering 117(12): 3587–3604. DOI: http://dx.doi.org/10.1061/(asce)0733-9445(1991)117:12(3587)

Walker D (1967) An approximate theory for pressures and arching in hoppers. Chemical Engineering Science 22(3): 486. DOI: http://dx.doi.org/10.1016/0009-2509(67)80145-3

Walters JK(1973a) A theoretical analysis of stresses in axially-symmetric hoppers and bunkers. Chemical Engineering Science 28(3): 779–789. DOI: http://dx.doi.org/10.1016/0009-2509(77)80012-2

Walters JK (1973b) A theoretical analysis of stresses in silos with vertical walls. ChemicalEngineering Science 28: 13–21.

Wójcik M, Tejchman J, Enstad GG (2012) Confined granular flow in silos with inserts - Full-scale experiments. Powder Technology 222: 15–36. DOI: http://dx.doi.org/10.1016/j.powtec.2012.01.031

**Article 5 – Influence of specific weight and wall friction coefficient on normal pressures in silos using the Finite Element Method - Engenharia na Agricultura journal (published version)**

The article was invited at the XLIX *Congresso Brasileiro de Engenharia Agrícola* - CONBEA 2020 to publish in the *Engenharia na Agricultura* Journal (ISSN 2175-6813) with Qualis B3, following the conventional editorial flow of peer review.

The article was published in the *Engenharia na Agricultura* Journal (ISSN 2175-6813). The journal has the B3 qualis.

DOI: https://doi.org/10.13083/reveng.v29i1.12336.

ISSN 2175-6813

Revista Engenharia na Agricultura

Viçosa, MG, DEA/UFV - DOI: 10.13083/reveng.v29i1.12336 V.29, p.192-203, 2021

# INFLUENCE OF SPECIFIC WEIGHT AND WALL FRICTION COEFFICIENT ON NORMAL PRESSURES IN SILOS USING THE FINITE ELEMENT METHOD

Rômulo Marçal Gandia*[1], Francisco Carlos Gomes[1], Wisner Coimbra de Paula[2] & Pedro José Aguado Rodriguez[3]

1 - Federal University of Lavras, Department of Agricultural Engineering, Lavras, Minas Gerais, Brazil

2 - Federal University of Lavras, Department of Engineering, Lavras, Minas Gerais, Brazil

3 - University of León, School of Agricultural and Forestry Engineering, Léon, Castilla y León, Spain

**Keywords**:
Jenike shear test
Maximum normal pressures
Numerical model
Properties of stored products
Simulation

**ABSTRACT**

The objective of this work was to develop models using the Finite Element Method (FEM) to assess the maximum normal pressures in the static condition in silos using different wall friction coefficient and specific weight of the stored product compared to the pressures obtained by the Eurocode 1, part 4. The geometries of the silos models were developed based on the dimensions of the experimental station at the Universidad de Leon (Spain). The material properties were obtained by Jenike shear cell tests and were used to generate the models by the MEF. 3D models were generated varying the friction coefficient (0.2, 0.4, and 0.6) and the specific weight (6; 7.5 and 9 KN $m^{-3}$). It was verified that the models by FEM follow the theory of pressures in silos: normal pressures increase due to the increase in specific weight and decrease due to the increase in the friction coefficient. Moreover, the maximum normal pressure occurs at the hopper silo transition. The experimental pressures (FEM models) compared with Eurocode 1, part 4 allowed to validate the models developed, presenting trends of similar values to those found by the MEF. The experimental models demonstrated that the influence of the wall friction coefficient and specific weight significantly interferes with the pressures in slender silos.

**Palavras-chave:**
Simulação
Propriedades dos produtos armazenados
Máquina de cisalhamento de Jenike
Modelo numérico
Pressões normais máximas

**INFLUÊNCIA DO PESO ESPECÍFICO E DO COEFICIENTE DE ATRITO DA PAREDE NAS PRESSÕES NORMAIS EM SILOS USANDO O MÉTODO DOS ELEMENTOS FINITOS**

**RESUMO**

O objetivo deste trabalho foi desenvolver modelos utilizando o Método dos Elementos Finitos (MEF) para avaliar as pressões máximas normais na condição estática em silos variando o peso específico e o coeficiente de atrito do produto armazenado e posterior comparação com a Eurocode 1, parte 4. Foram desenvolvidas as geometrias dos modelos dos silos baseadas nas dimensões da estação experimental da Universidad de Leon (Espanha). As propriedades dos materiais foram obtidas por ensaios da célula de cisalhamento de Jenike e foram utilizadas para geração dos modelos pelo MEF para posterior comparação com as pressões calculadas pela Eurocode. Foram gerados modelos 3D variando o coeficiente de atrito (0,2; 0,4 e 0,6) e o peso específico (6; 7,5 e 9 KN $m^{-3}$). Foi verificado que os modelos correspondem ao que é esperado diante das teorias: as pressões normais aumentam em decorrência do aumento do peso específico e diminuem pelo aumento do coeficiente de atrito. Foi constatado que a pressão normal máxima ocorre na transição silo tremonha. A das pressões comparação com a Eurocode 1, parte 4 viabilizou a validação dos modelos desenvolvidos, apresentando valores próximos e inferiores ao encontrado pelo MEF. Os modelos gerados pelo MEF demonstraram que a influência do coeficiente de atrito e peso específico interfere significantemente nas pressões em silos esbeltos. Além disso, verificou a viabilidade dos modelos para obtenção das pressões normais pelo MEF, pois apresentaram comportamento semelhante a modelo experimentais e pela Eurocode.



SECTION EDITOR IN CHARGE
Fernanda Campos Sousa

Received 12 Apr, 2021 • Accepted 28 Jun, 2021 • Published 31 Aug, 2021
Email (corresponding author)*: romagandia@gmail.com

## INTRODUCTION

In 2020, the estimated grain production in Brazil was 268.7 million tons (CONAB, 2020). In less than 39 years (2019), Brazil has more than quadrupled its static capacity (177.7 million tons of grain). Out of this total, 86.6 million tons of grain (49%) were stored in silos (DPE, 2019).

Since 1895, Janssen (JANSSEN, 1895) has been studying the flow and pressure of products stored in silos. Ever since then, other theories have been developed (WALKER, 1967) (WALTERS, 1973a, 1973b) (JENIKE *et al*., 1973) supporting international standards (CEN, 2006; DIN, 2005). It is necessary to understand the different theories that support the standards to comprehend the actions (flow and pressures) in silos. However, many factors are still not conclusive due to the randomness of the physical properties of the stored products (differently from liquids) (CALIL; CHEUNG, 2007).

The specific weight of the main agricultural products in Brazil (corn, soybeans, rice, wheat, and beans) (CONAB, 2020) and products derived from the feed and flour industry vary widely. For example, flour can have bulk unit weight from 6.5 to 7 KN $m^{-3}$, while corn and soybean from 7 to 8 KN $m^{-3}$ and wheat from 7.5 to 9 KN $m^{-3}$ (CEN, 2006). The wall friction coefficient and the specific mass of the main agricultural products grown in Brazil varies considerably and is directly influenced by the roughness of the wall of the silo. The wall friction coefficient of this stored products are: flour (0.24 to 0.48); corn (0.22 to 0.53); soybean 0.24 to 0.48 and wheat 0.24 to 0.57 (CEN, 2006).

The main reason for the several failures and collapses in silos are the design errors and overpressures (BYWALSKI; KAMIŃSKI, 2019; GUTIÉRREZ *et al.*, 2015; DOGANGUN *et al*., 2009; SUN *et al*., 2006; WANG, 2012; TENG *et al*., 2001; TENG, 1994; TENG; ROTTER, 1989, 1991).

The reason for the small number of silo full-scale experimental stations in the world is the high cost of installation, handling and, instrumentation (BROWN *et al*., 2000; COUTO *et al*., 2012; GANDIA *et al*., 2021; HÄRTL *et al*., 2008; NETO; NASCIMENTO; SILVA, 2014; RAMÍREZ *et al*., 2010; SCHURICHT *et al*., 2001; SCHWAB *et al*., 1994; SUN *et al*., 2020; TENG; LIN, 2005; TENG *et al*., 2001; ZHAO; TENG, 2004; ZHONG *et al*., 2001). In addition, the scale factor is crucial for reliable data (scale errors) (BROWN; NIELSEN, 1998). Therefore, even though the experimental study is vital in most science, the search for other alternatives with relatively more minor costs and less time for analysis for scientific advancement is inevitable.

Due to the advancement of engineering combined with computational development, modeling is supported by a tripod: theoretical model, experimental model, and numerical model. These three models (working together) optimize and advance studies in most areas of engineering. For example, the finite element method (FEM) is a numerical procedure to determine approximate solutions of value problems on the contour of differential equations. The FEM subdivides the problem domain into smaller parts, denominated finite elements. Therefore, in recent years, studies using the FEM in silos have significantly increased (JOFRIET, 1992; HOLST *et al*., 1999; AYUGA *et al*., 2006; GALLEGO *et al*., 2010; GALLEGO; RUIZ; AGUADO, 2015; PARDIKAR *et al*., 2020; WASSGREN, 2020; ZHAO, 2004), mainly for the quality of the answers and for the relative time and cost-saving in comparison to the experimental models in real scale.

Therefore, the objective of this paper is to simulate through the Finite Element Method, the interference of the specific mass and the wall friction coefficient using representative values of the leading Brazilian agricultural products to obtain the normal static pressures in slender silos compared to the Eurocode 1, part 4 (CEN, 2006).

## MATERIAL AND METHODS

The numerical simulation was performed using elements and the software Ansys 2020R2 student version. The model was developed by simulating the static condition (after filling the silo). The dimensions of the silo, hopper inclination were based on the silo of the experimental station designed to evaluate the pressure in silos at the University of León (Spain) designed and built by the research group of the Department of Agricultural Engineering and Sciences (COUTO; RUIZ; AGUADO, 2012; RUIZ; COUTO; AGUADO, 2012).

The silo was 2.00 meters high and had one

meter in diameter with a concentric hopper angle of 34.3 and 0.48 meters in height. The silo is made of polished steel metal. According to Eurocode 1, part 4 (CEN, 2006), this silo is classified as slender (height/diameter ratio = 2) and can be seen in Figure 1.

**Figure 1.** Silo geometry (COUTO *et al*., 2012)

For the numerical simulation, three different wall friction coefficients and the product (u) were used: 0.2; 0.4, and 0.6 (values that include the limits of wall friction coefficient of most of the leading national agricultural products (corn, soybeans, rice, wheat, and beans) (CEN, 2006) and also products characterized as feed and flour. In addition, as variables, the specific weight of the stored product (γ) (6; 7.5 and 9 KN $m^{-3}$) was also analyzed. Those are values that include the upper and lower specific weight of most agricultural products, such as corn, wheat, soybeans, rice, beans, and flour products from the animal feed industry.

The parameters of the stored product and the steel sheet of the silo were obtained in the literature (Table 1).

The proposed model was performed using elastoplastic material (DRUCKER; PRAGER, 1952) to simulate the pressure of the stored product (solid) inside the silo. The standard isotropic and linear model was used to represent the elastic behavior of the silo, while Drucker and Prager's perfect plasticity criterion (DRUCKER; PRAGER, 1952) was used to define the plastic part.

The model was created in 3D geometry, aiming at further studies to understand the volume of the

**Table 1.** Stored product and steel parameters

| Material parameter | Value | Reference |
|---|---|---|
| **stored material** | | |
| Specific weight, $\gamma$ (KN $m^{-3}$) | 6; 7.5; 9 | - |
| Modulus of elasticity, $E$ (kPa) | 5000 | GALLEGO *et al*., 2015) |
| Poisson's ratio, ν | 0.3 | GALLEGO *et al*., 2015) |
| Wall friction coefficient, $\mu$ | 0.2; 0.4; 0.6 | - |
| Cohesion, $c$ (kPa) | 0.71 | (MOYA *et al*., 2002) |
| Angle of dilatancy of bulk material, $\psi i$ | 2.5 | (MOYA *et al.*, 2006) |
| Effective angle of internal friction of bulk material, $\phi i$ | 25 | (MOYA *et al.,* 2006) |
| **steel sheet** | | |
| Modulus of elasticity, $E$ (kPa) | 210000000 | (GALLEGO *et al*., 2015) |
| Poisson's ratio, ν | 0.3 | (GALLEGO *et al*., 2015) (MOYA *et al.*, 2006) |
| Thickness (m) | 0.02 | - |

model. The modeling was done initially using a small number of elements (mesh simplification). After the model was defined and generated, the mesh was refined, mainly in the areas of most significant interest (silo-hopper transition) (Figure 2). The size of the elements was 0.15 m for the solid and 0.075 m for the silo, totaling 14688 elements. The generated mesh was composed of prismatic elements with 8 and 4 knots, as shown in Figure 2. This type of mesh is stable and, when possible, allows analysis with better results. For the stored product (solid), an element with eight nodes (Solid 45, Lagrangian type) was used, which is an element that supports large deformations (GALLEGO *et al.*, 2015). The silo (shell) wall was modeled using the 8-node shell element (Shell 63), ideal for analyzing non-linear applications. For the contact (friction) between the stored product (solid) and the silo wall (shell), 4-node elements were used (Conta 173 and Target 170) (GALLEGO *et al*., 2010). The model was vertically (z-axis) constrained in the contour of the silo-hopper transition. The gravitational force was inserted towards the z-axis.

The models were subsequently compared with Eurocode 1, part 4(CEN, 2006). The normal static pressure curves were calculated using the same parameters proposed in the development of the model using FEM: silo dimensions (height: 2 meters; internal diameter: 1 meter; β: 34.3 °); work variables (wall friction coefficient: 0.2; 0.4 and 0.6); specific weight: 6; 7.5 and 9 KN $m^{-3}$); other values extracted from Table E.1 - Properties of Disaggregated Solids used for the product (CEN, 2006).

## RESULTS AND DISCUSSION

Information on Z displacement (m), Z stress ( KN $m^{-2}$), and main stress ( KN $m^{-2}$) of the mass of the product inside the silo was extracted according to the variation of the wall friction coefficient (Figure 3) and a specific weight (Figure 4).

The main tension increased as the wall friction coefficient (Figure 3a) decreased. The maximum values (SMN) are negative because they are in the opposite direction to the Z-axis, which corroborates the statements (CEN, 2006; JENIKE *et al*., 1973). It is observed that the lowest stresses (red) occur at the top of the silo and the highest (blue) near the silo-hopper transition.

The maximum stresses in Z showed the opposite behavior, increasing according to the increase of the wall friction coefficient, mainly in the silo-hopper transition. The reason is that with the increase in

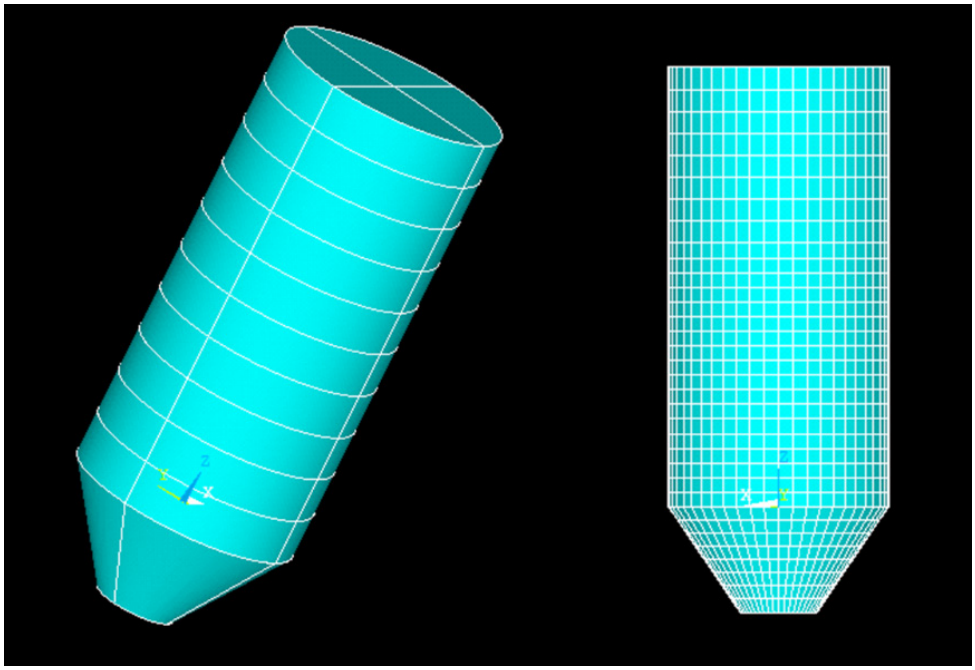

**Figure 2.** Geometry and mesh of the developed model

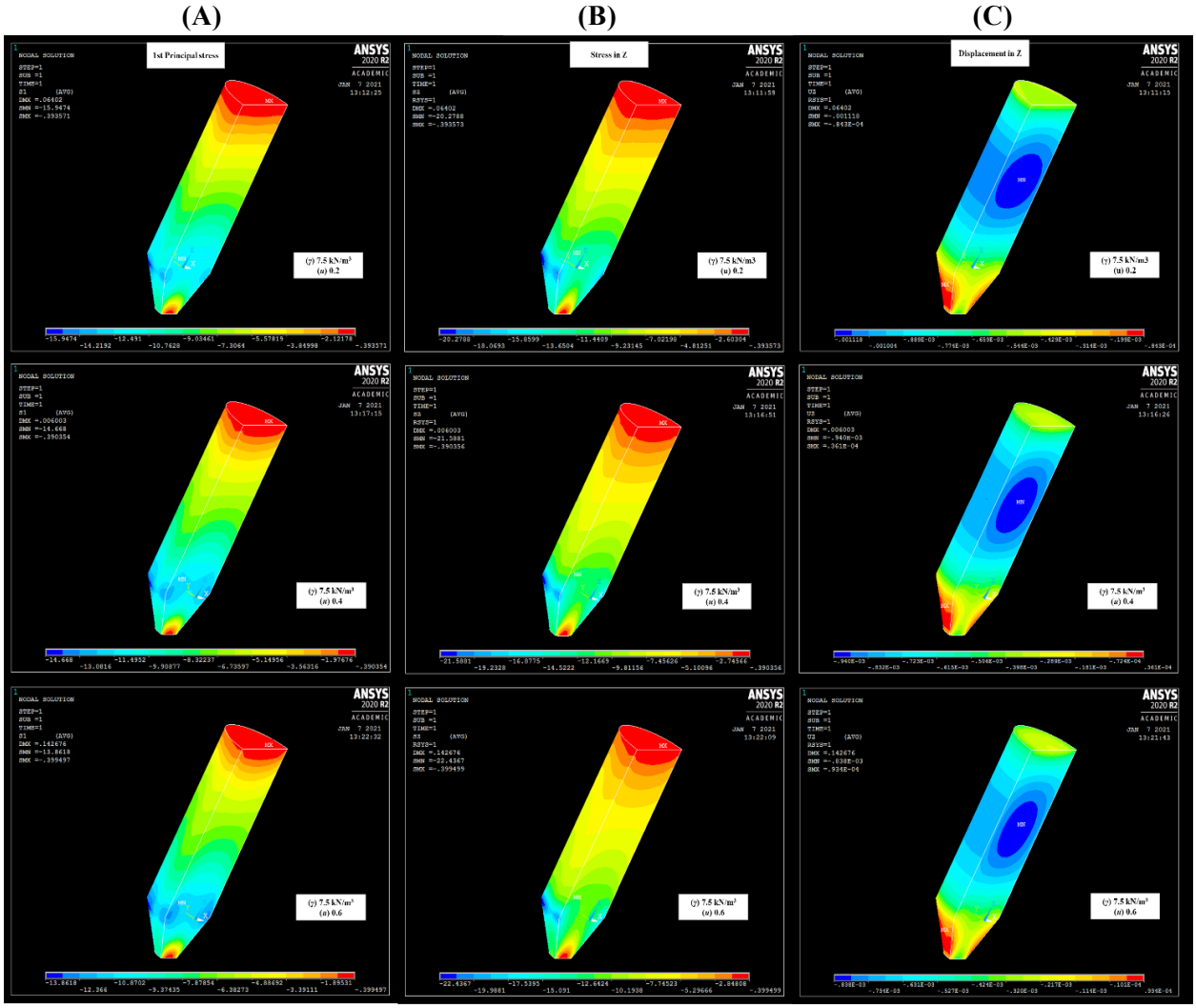


**Figure 3.** Main stress (a), stress in Z (b), and displacement in Z (c) by increasing the wall friction coefficient

the wall friction coefficient, the friction pressure increases, resulting in a reduction in the normal pressure in the silo's wall and the occurrence of a slight increase in the vertical tension in the silo-hopper transition.

A decrease was found in the displacement of the grain mass (Figure 3c) caused by the vertical displacement (z) due to the increase in the wall friction coefficient, which was visually observed through the smaller area of the ellipse (blue) approximately in the middle of the silo and numerically confirmed by the displacement value (SMN) plotted in each simulation: 1.118; 0.940 and 0.838 mm respectively for the wall friction coefficient 0.2; 0.4 and 0.6.

The main tension increased according to the increase in the specific weight of the stored product (CEN, 2006; JENIKE *et al*., 1973) (Figure 4a). The lowest stresses (red) occur at the top of the silo and the highest (blue) near the silo-hopper transition. However, for the specific weight of 9 KN $m^{-3}$, the minimum main stress occurs at the outlet gate because the increase in the specific weight of the material and the pressure of the material column above the hopper provides a mechanical arc above the outlet opening.

The maximum stresses in Z have the same dynamic, increasing according to the increase in the specific weight of the stored product, mainly in the silo-hopper transition. Thus, the maximum and minimum principal stresses occur at the hopper silo transition and the top of the silo. Except for the specific weight of 9 KN $m^{-3}$, where the minimum occurs at the outlet gate due to the formation of the mechanical arc provided by the increase in weight of the product, the hopper's inclination, and the wall friction coefficient of the hopper.

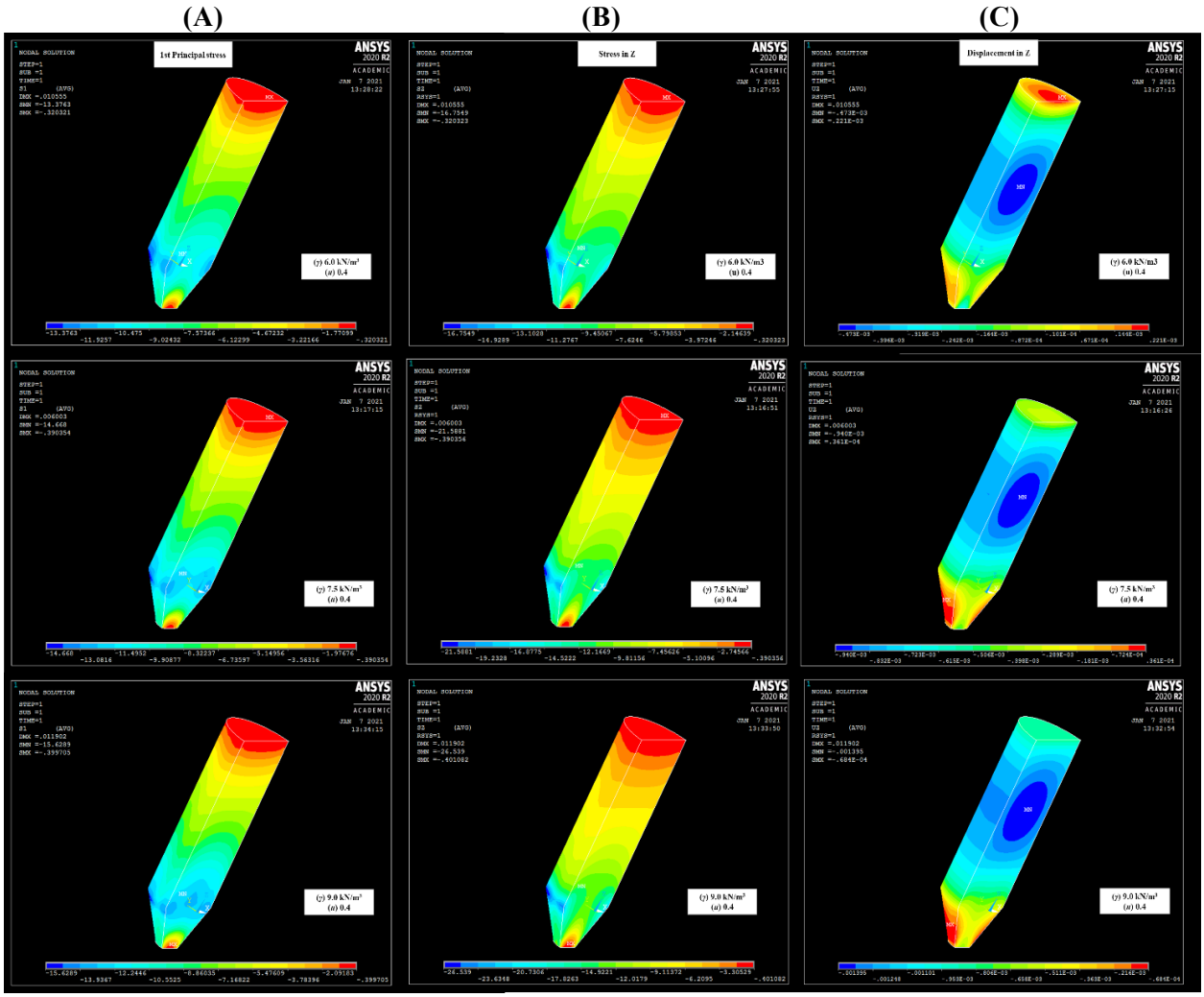


**Figure 4.** Main stress (a), stress in Z (b), and displacement in Z (c) by increasing the specific weight of the stored product

The displacement in the z (vertical) direction increased according to the specific weight of the stored material. The greater the weight of the product, the greater the displacement of the grain mass, as compression occurs according to the upper layers of the product, forcing the more significant displacement in the lower positions of the silo.

For a better comparison among the developed simulations, the normal static pressure curves were measured throughout the silo. The curves comparing the three models varying the wall friction coefficients (Figure 5) and the specific weight of the stored product (Figure 6) are shown below.

The natural behavior among the three curves varying the wall friction coefficient (u) is expected in view of the theories and experiments (CEN, 2006; INTERNACIONAL ORGANIZATION FOR STANDARDIZATION, 2012; JENIKE *et al*., 1973; WALKER, 1967). The reason is that normal pressures have maximum values close to the hopper transition. Also, as expected in the face of theories (JENIKE; JOHANSON; CARSON, 1973; WALKER, 1967) and standards (CEN, 2006; INTERNACIONAL ORGANIZATION FOR STANDARDIZATION, 2012), the higher the wall friction coefficient, the lower the normal pressures will be due to the increased friction pressure. Therefore, the model with a wall friction coefficient (u) 0.2 was the one with the highest normal pressures and 0.6 showed the lowest normal pressure values.

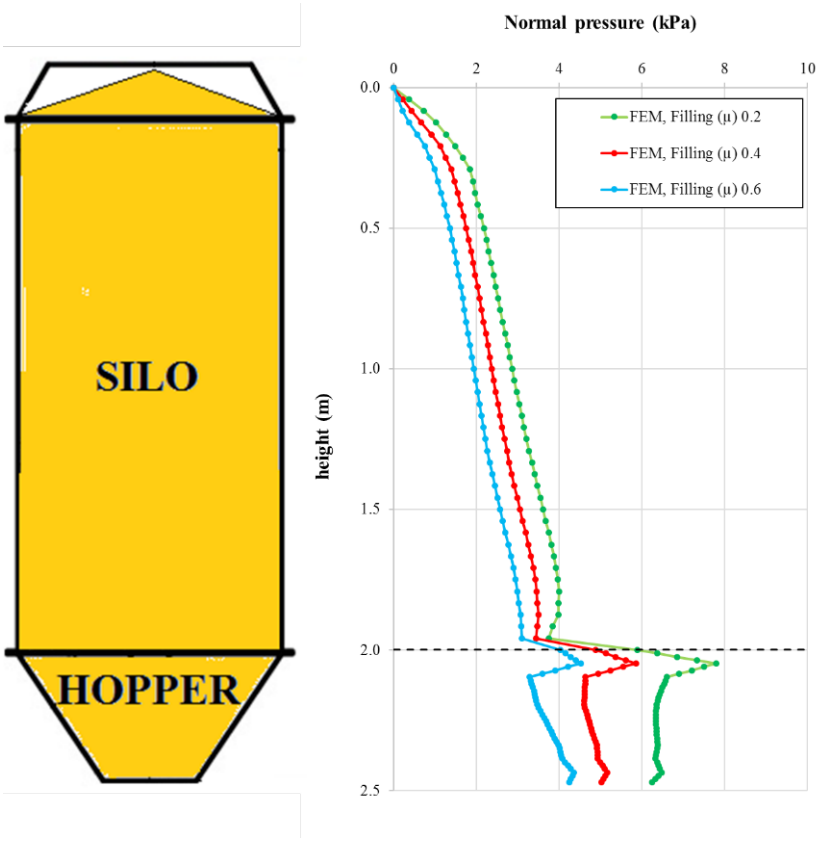


**Figure 5.** Normal static pressures varying with the wall friction coefficient

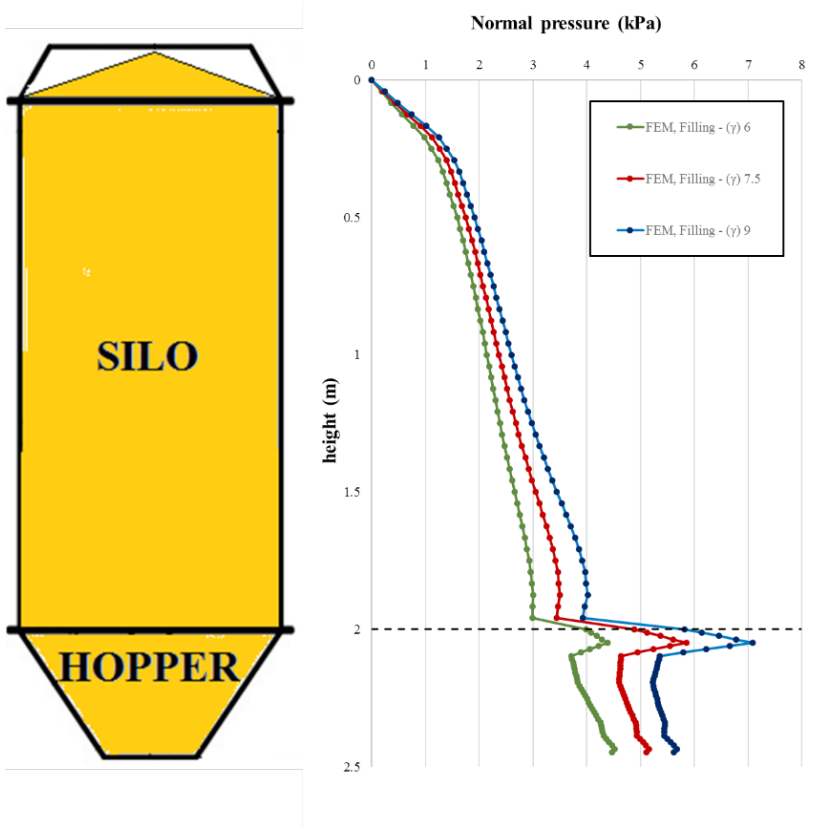


**Figure 6.** Normal static pressures varying with the specific weight of the stored product

The standard behavior among the three curves varying the specific weight of the stored product (γ) was expected given the theories and codes (CEN, 2006; INTERNACIONAL ORGANIZATION FOR STANDARDIZATION, 2012; JENIKE *et al*., 1973; WALKER, 1967). Thus, normal pressures have maximum values close to the hopper transition. Also, as expected given theories and standards, the greater the specific weight of the stored product, the greater the normal pressures on the wall and hopper. Therefore, it is observed that the model with specific weight (γ) 9 KN $m^{-3}$ was the one with the highest pressure values and 6 KN $m^{-3}$ showed the lowest values.

Aiming to validate the models and analyze Eurocode 1, part 4 (CEN, 2006), all the developed models were compared to the standard. The curves comparing the three models varying the wall friction coefficients and the pressures obtained by Eurocode 1, part 4 are shown below (Figure 7). The curves comparing the three models varying the specific weight of the stored product and the pressures obtained by Eurocode 1, part 4 are shown below (Figure 8).

The analysis of errors relating to the pressures obtained through the simulation using FEM and those calculated with Eurocode 1, part 4 was shown in Table 2.

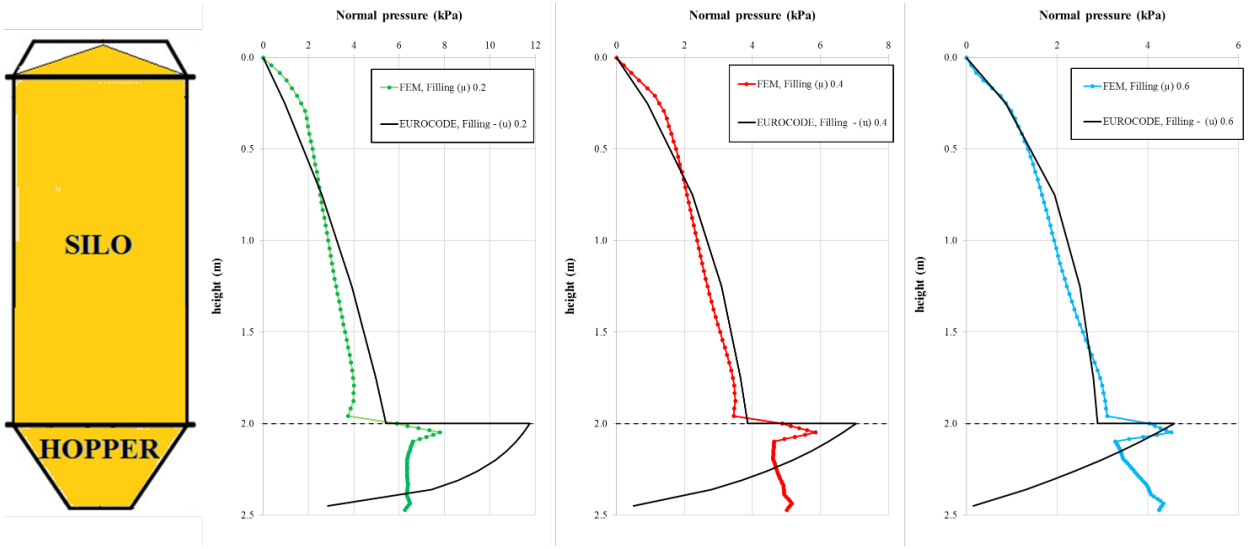


**Figure 7.** Normal static pressures varying the wall friction coefficient and compared with Eurocode 1, part 4

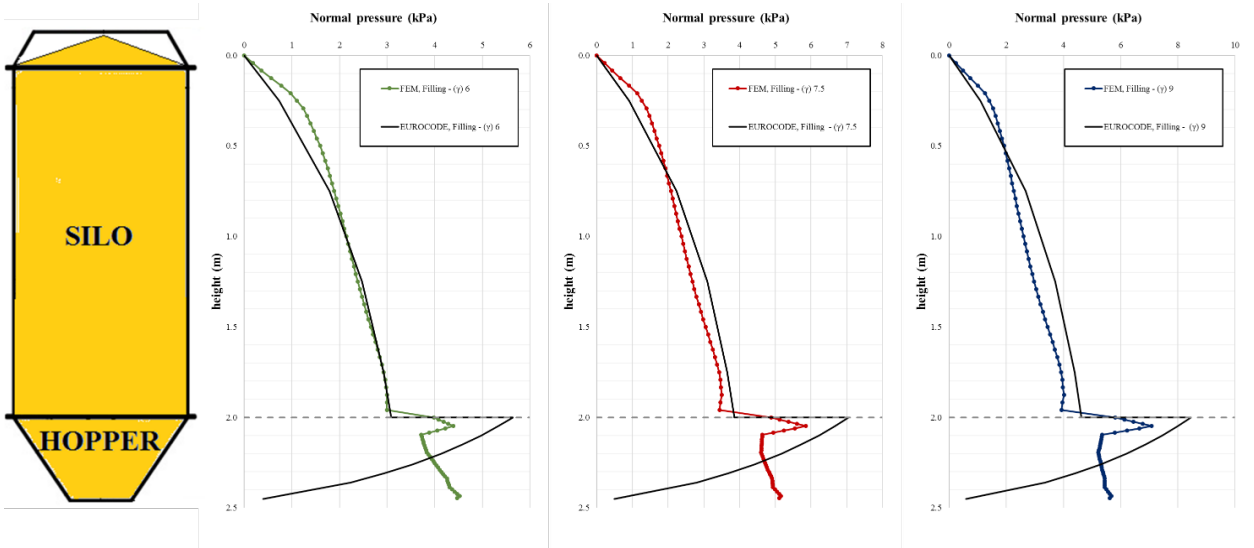


**Figure 8.** Normal static pressures varying the specific weight of the stored product and compared with Eurocode 1, part 4

**Table 2.** Error analysis – FEM / Eurocode1, part 4

| Silo height (m) | Error (%) | | | | | |
|---|---|---|---|---|---|---|
| | specific weight (γ) - KN m$^{-3}$ | | | wall friction coefficient (μ) | | |
| | 6.0 | 7.5 | 9.0 | 0.2 | 0.4 | 0.6 |
| 0.00 | 0.00 | 0.00 | 0.00 | 0.00 | 0.00 | 0.00 |
| 0.25 | 34.17 | 27.79 | 21.83 | 42.42 | 27.79 | 0.80 |
| 0.75 | 5.36 | -7.85 | -18.51 | -2.87 | -7.85 | -16.69 |
| 1.25 | -3.85 | -15.57 | -24.83 | -21.73 | -15.57 | -13.10 |
| 1.75 | 0.13 | -6.79 | -11.86 | -25.44 | -6.79 | 5.00 |
| 2.00 | 22.51 | 21.01 | 20.46 | 7.91 | 21.01 | 28.34 |
| 2.05 | -28.50 | -20.46 | -19.28 | -50.66 | -20.46 | -1.57 |
| 2.10 | -43.25 | -43.59 | -49.04 | -69.07 | -34.14 | -16.40 |
| 2.15 | -31.98 | -34.58 | -40.83 | -66.08 | -23.96 | -0.23 |
| 2.20 | -18.46 | -23.83 | -31.21 | -61.27 | -11.90 | 15.76 |
| 2.26 | -2.59 | -9.11 | -16.70 | -49.00 | 6.95 | 36.04 |
| 2.31 | 15.47 | 8.98 | 1.96 | -34.98 | 24.28 | 52.11 |
| 2.36 | 31.40 | 25.38 | 19.09 | -16.85 | 43.20 | 67.52 |
| 2.45 | 49.98 | 45.29 | 40.31 | 55.53 | 90.33 | 96.46 |

In comparison with Eurocode 1, part 4, it is possible to observe that the initial normal static pressures obtained by the FEM at the top of the silo (height 0 to 0.75 m) were higher than the standard ones. Furthermore, in relation to the increase in the wall friction coefficient and consequently a decrease in normal pressures, it is observed that the greater tendency of the pressures calculated using FEM to exceed the pressures obtained from the standard, also in the case of the wall friction coefficient u = 0.6.

Although the pressures in the static phase were generally lower than the discharge, it is possible to assume that the standard should increase the pressures when the wall friction coefficient is greater than 0.5. In addition, concerning the decrease in the specific weight of the stored product and consequently the decrease in normal pressures, it is observed a greater tendency of the pressures calculated through the MEF to exceed the pressures obtained from Eurocode 1, part 4, even exceeding in the case of the specific weight of the product (γ) 6.0 KN m$^{-3}$. Therefore, despite being pressures in the static phase, generally lower than the discharge, it is possible to assume that the standard should increase the pressures for products with lower specific weights. It can be seen that Eurocode safely increases the normal static pressures for silo projects in extreme conditions (products with higher specific weights and lower wall friction coefficient), however, under conditions of low normal pressures the trend of pressures by FEM exceeds those of Eurocode 1, part 4.

According to Gallego (GALLEGO *et al*., 2015) in evaluating wheat efforts experimentally, numerically, and by comparing with Eurocode 1, part 4 (CEN, 2006), pressures with magnitudes close to that of this work are found for similar properties of the stored material. Ruiz and collaborators (COUTO *et al*., 2012), also using wheat, found that the maximum vertical pressure obtained experimentally in loading is close to the model proposed in the present work. The experimental study using corn (COUTO *et al*., 2013) also showed a tendency for pressure values in the silo during loading close to those presented in this work.

The variation of the wall friction coefficient considerably influences the study and silo projects, changing the coefficient by only 0.4; an increase is found in the maximum normal static pressure of 58%. The same importance can be considered for the specific weight of the stored product, with an increase of 62% due to the increase in weight by 3 KN m$^{-3}$. The specific weight of the stored product has an increase of 62% due to the increase in weight by 3 KN m$^{-3}$.

For all the generated models, the location was

exactly 4.8 cm below the transition (both for the variation of the wall friction coefficient and the specific weight of the stored product).

## CONCLUSIONS

- The use of FEM for the calculation of pressures in silos is recommended. The two variables (specific weight and wall friction coefficient) influence the static pressures in the silo, which were observed in the pressures obtained by Eurocode and also in the results of the simulated models.
- Products with similar particular characteristics are considered. In this experiment, the highest normal static pressures will occur in the products with the highest specific weight and the lowest wall friction coefficient.
- Compared with Eurocode 1, part 4 (CEN, 2006), it could be seen that all models generated by the MEF show consistent errors, presenting normal static pressures below the standard. However, two issues were observed: although the normal pressures at the top of the silo are the lowest, the model created by the MEF presented a divergence from the standard; the second issue is related to the higher coefficient used in the standards for products that tend to have higher pressures and lower coefficients for products that tend to generate lower pressures, in other words, for products stored with lower specific weight and higher wall friction coefficient, the standard presents lower safety coefficients that could be observed in the comparisons with MEF.
- The variation of the wall friction coefficient and specific weight considerably influences the study and silo projects.
- The location of the maximum normal static pressure in the silo is located in the silo-hopper transition zone.

## ACKNOWLEDGMENTS

The authors would like to thank CAPES for financing the study and the partnership between the Federal University of Lavras and the University of León. They are also grateful for the partnership with the University of León (Spain).

## AUTHORSHIP CONTRIBUTION STATEMENT

**GANDIA, R.M.**: Formal Analysis, Investigation, Methodology, Validation, Writing – original draft; Writing – review & editing; **GOMES, F.C.**: Conceptualization, Funding acquisition, Resources, Visualization; **DE PAULA, W.C.**: Investigation, Software, Supervision, Visualization, Writing – review & editing; **RODRIGUEZ, P.J.A.**: Data curation, Project administration, Supervision, Validation, Writing – review & editing.

## DECLARATION OF INTERESTS

The authors declare that they have no knowledge of a conflict of interest that could have appeared to influence the work reported in this paper.

## REFERENCES

AYUGA, F.; AGUADO, P.; GALLEGO, E.; RAMIREZ, A. Experimental tests to validate numerical models in silos design. **2006 ASABE Annual International Meeting**, v. 0300, n. 06, 2006.

BROWN, C. J.; LAHLOUH, E. H.; ROTTER, J. M. Experiments on a square planform steel silo. **Chemical Engineering Science**, v. 55, n. 20, p. 4399-4413, 2000.

BROWN, C. J.; NIELSEN, J. **Silos: Fundamentals of theory, behaviour and design**. London: [s.n.].

BYWALSKI, C.; KAMIŃSKI, M. A case study of the collapse of the over-chamber reinforced concrete ceiling of a meal silo. **Engineering Structures**, v. 192, p. 103-112, 2019.

CALIL, J. C.; CHEUNG, A. B. **Silos: pressões, fluxo, recomendações para o projeto e exemplo de cálculo**. São Carlos: [s.n.].

CEN. **EN 1991-4:2006. Eurocode 1: Actions on Structures. Part 4: Silos and Tanks**. Brussels: [s.n.].

CONAB - Companhia Nacional de Abastecimento. **Acompanhamento da safra brasileira 2019/2020Acompanhamento da Safra Brasileira de Grãos 2019/2020**. [s.l: s.n.]. Available in: <https://www.conab.gov.br/info-agro/safras>.

COUTO, A.; RUIZ, A.; AGUADO, P.J. Measuring pressures in a slender cylindrical silo for storing maize. Filling, static state and discharge with different material flow rates and comparison with Eurocode 1 part 4. **Computers and Electronics in Agriculture**, v. 96, p. 40-56, 2013.

COUTO, A.; RUIZ, A.; AGUADO, P. J. Design and instrumentation of a mid-size test station for measuring static and dynamic pressures in silos under different conditions - Part I: Description. **Computers and Electronics in Agriculture**, v. 85, p. 164-173, 2012.

DIN. **DIN 1055-6: Basis of design and actions on structures – Part 6: design 623 loads for buildings and loads in silo bins**. Berlin, Verlaz: 2005.

DOGANGUN, A.; KARACA, Z.; DURMUS, A.; SEZEN, H. Cause of damage and failures in silo structures. **Journal of Performance of Constructed Facilities**, v. 23, n. 2, p. 65-71, 2009.

DPE - DIRETORIA DE PESQUISA E COORDENAÇÃO AGROPECUÁRIA. **IBGE - Pesquisa de Estoques 2º semestre de 2019**. [s.l: s.n.].

DRUCKER, D. C.; PRAGER, W. Soil mechanics and plastic analysis or limit design. **Quart. Appl. Math**, v. 10, n. 2, p. 157-165, 1952.

GALLEGO, E.; ROMBACH, G.A.; NEUMANN, F.; AYUGA, F. SIMULATIONS OF GRANULAR FLOW IN SILOS WITH DIFFERENT FINITE ELEMENT PROGRAMS: ANSYS VS. SILO. **Transactions of the ASABE**, v. 53, n. 3, p. 819-829, 2010.

GALLEGO, E.; RUIZ, A.; AGUADO, P. J. Simulation of silo filling and discharge using ANSYS and comparison with experimental data. **Computers and Electronics in Agriculture**, v. 118, p. 281-289, 2015.

GANDIA, R.M.; GOMES, F.C.; PAULA, W.C. DE, JUNIOR; E.A. DE O.; RODRIGUEZ, P.J.A. Static and dynamic pressure measurements of maize grain in silos under different conditions. **Biosystems Engineering**, v. 209, p. 180-199, 2021.

GUTIÉRREZ, G.; COLONNELLO, C.; BOLTENHAGEN, P.; DARIAS, J.R.; PERALTA-FABI, R.; BRAU, F.; CLÉMENT, E. Silo collapse under granular discharge. **Physical Review Letters**, v. 114, n. 1, p. 5-9, 2015.

HÄRTL, J.; OOI, J.Y.; ROTTER, J.M.; WOJCIK, M.; DING, S.; ENSTAD, G.G. The influence of a cone-in-cone insert on flow pattern and wall pressure in a full-scale silo. **Chemical Engineering Research and Design**, v. 86, n. 4, p. 370–378, 2008.

HOLST, J.M.F.G.; OOI, J.Y.; ROTTER, J.M.; RONG, G.H. Numerical Modeling of Silo Filling. I: Continuum Analyses. **Journal of Engineering Mechanics**, v. 125, n. 1, p. 94-103, 1999.

INTERNACIONAL ORGANIZATION FOR STANDARDIZATION. **ISO 11697:2012. Bases for design of strutures - Loads due to bulk materials**. [s.l: s.n.].

JANSSEN, H. A. Versuche uber getreidedruck in silozellen. **Z. Ver. Dtsch. Ing**, v. 39, n. 35, p. 1045-1049, 1895.

JENIKE, A. W.; JOHANSON, J. R.; CARSON, J. W. Bin loads—part 3: mass-flow bins. **Journal of Manufacturing Science and Engineering, Transactions of the ASME**, v. 95, n. 1, p. 6-12, 1973.

MOYA, M.; AYUGA, F.; GUAITA, M.; AGUADO, P. MECHANICAL PROPERTIES OF GRANULAR AGRICULTURAL MATERIALS. **Transactions of the ASABE**, v. 45, n. 5, p. 1569-1577, 2002.

MOYA, M.; GUAITA, M.; AGUADO, P.; AYUGA, F. MECHANICAL PROPERTIES OF GRANULAR AGRICULTURAL MATERIALS, PART 2. **Transactions of the ASABE**, v. 49, n. 1998, p. 479-490, 2006.

NETO, J. P. L.; NASCIMENTO, J. W. B. DO; SILVA, R. C. FORÇAS DE ATRITO EM SILOS VERTICAIS DE PAREDES LISAS EM DIFERENTES RELAÇÕES ALTURA/ DIÂMETRO. **Eng. Agríc., Jaboticabal**, v. 34, n. 1, p. 8-16, 2014.

PARDIKAR, K.; ZAHID, S.; WASSGREN, C. Quantitative comparison of experimental and Mohr-Coulomb finite element method simulation flow characteristics from quasi two-dimensional flat-bottomed bins. **Powder Technology**, v. 367, p. 689-702, 2020.

RAMÍREZ, A.; NIELSEN, J.; AYUGA, F. On the use of plate-type normal pressure cells in silos. Part 1: Calibration and evaluation. **Computers and Electronics in Agriculture**, v. 71, n. 1, p. 71-76, 2010.

RUIZ, A.; COUTO, A.; AGUADO, P. J. Design and instrumentation of a mid-size test station for measuring static and dynamic pressures in silos under different conditions - Part II: Construction and validation. **Computers and Electronics in Agriculture**, v. 85, p. 174-187, 2012.

SCHURICHT, T.; FURLL, C.; EENSTAD, G. G. Full scale silo tests and numerical simulations of the „cone in cone" concept for mass flow. In: **Handbook of Powder Technology**. [s.l.] Elsevier Science BV, 2001. v. 10p. 175-180.

SCHWAB, C. V.; ROSS, I.J.; WHITE, G.M.; COLLIVER, D.G. WHEAT LOADS AND VERTICAL PRESSURE. v. 37, n. 5, p. 1613-1619, 1994.

SUN, W.; ZHU, J.; ZHANG, X.; WANG, C.; WANG, L.; FENG, J. Multi-scale experimental study on filling and discharge of squat silos with aboveground conveying channels. **Journal of Stored Products Research**, v. 88, e101679, 2020.

SUN, Y.; WANG, Y. Collapse reasons analysis of a large steel silo. **Advanced Materials Research**, v. 368–373, p. 647-650, 2012.

TENG, B. J. Plastic collapse at lap joints in pressurized cylinders under axial load. **Journal of Structural Engineering.** v. 120, n. 1, p. 23-45, 1994.

TENG, J. G.; LIN, X. Fabrication of small models of large cylinders with extensive welding for buckling experiments. **Thin-Walled Structures**, v. 43, n. 7, p. 1091-1114, 2005.

TENG, J. G.; ROTTER, J. M. Plastic collapse of restrained steel silo hoppers. **Journal of Constructional Steel Research**, v. 14, n. 2, p. 139-158, 1989.

TENG, J. G.; ZHAO, Y.; LAM, L. Techniques for buckling experiments on steel silo transition junctions. **Thin-Walled Structures**, v. 39, n. 8, p. 685-707, 2001.

TENG, J.; ROTTER, J. M. Collapse Behavior and Strength of Steel Silo Transition Junctions. Part I: Collapse Mechanics. **Journal of Structural Engineering**, v. 117, n. 12, p. 3587-3604, 1991.

WALKER, D. An approximate theory for pressures and arching in hoppers. **Chemical Engineering Science**, v. 22, n. 3, p. 486, 1967.

WALTERS, J. K. A theoretical analysis of stresses in axially-symmetric hoppers and bunkers. **Chemical Engineering Science**, v. 28, n. 3, p. 779-789, 1973a.

WALTERS, J. K. A theoretical analysis of stresses in silos with vertical walls. **ChemicalEngineering Science**, v. 28, p. 13-21, 1973b.

ZHAO, Q.; JOFRIET, J. C. Structural loads on bunker silo walls: Numerical study. **Journal of Agricultural Engineering Research**, v. 51, n. C, p. 1-13, 1992.

ZHAO, Y.; TENG, J. G. Buckling experiments on steel silo transition junctions. II: Finite element modeling. **Journal of Constructional Steel Research**, v. 60, n. 12, p. 1803-1823, 2004.

ZHONG, Z.; OOI, J. Y.; ROTTER, J. M. The sensitivity of silo flow and wall stresses to filling method. **Engineering Structures**, v. 23, n. 7, p. 756-767, 2001.

**Article 6 – The influence of flow pattern and hopper angle on static and dynamic pressures in slender silos - Powder Technology journal (preliminary version)**

The article was submitted to the Powder Technology journal (ISSN 0032-5910). The journal has the qualis A1 and JCR 5.134.

# The influence of flow pattern and hopper angle on static and dynamic pressures in slender silos

**Rômulo Marçal Gandia[1,2*], Francisco Carlos Gomes[1], Pedro José Aguado Rodriguez[2]**

[1]Federal University of Lavras (Brazil), Agricultural Engineering Department
[2]University of León (Spain), Department of Engineering and Agricultural Sciences

## ABSTRACT

Our experimental station for pilot-scale silo pressure measurements was the basis for data collection in this article. Results were reported for pressures and flows analysis using a free-flowing product at our experimental station. Five different hopper angles were tested by filling the silo, and observing a static phase followed by complete discharge. Our results show that: Hopper angle influences the normal pressures in the silo wall; Silos with transition flow have no pattern results; Pressures are proportional to the increase and decrease of β°during filling and discharge; Mechanical arches vary according to the hopper angles completely modifying the behavior of static and dynamic pressures. Some parameters exceeded those calculated by the standard: friction pressure and lateral pressure ratio. Many aspects remain poorly understood and still need to be studied experimentally for a better understanding of the patterns and theories regarding pressures, stored material, hopper angle and flow in silos.

**KEYWORDS:** experimental station for silo pressures, slender silo, friction and normal pressures, free-flowing product, flow pattern.

## Nomenclature

### Symbols

Symbols

Ø: Angle of internal friction, degrees

A: Plan cross-sectional area of vertical walled segment, $m^2$

$d_i$: Internal cylinder diameter, m.

$F_{h(1,12)u,t}$: Force in tension load cell positioned on the upper part of the spring set - rings 1 to 12, at time t, kN

$F_{h(1,12)d,t}$: Force in tension load cell positioned on the lower part of the spring set - rings 1 to 12, at time t, kN

$F_{w(1,12)r,t}$: Force in tension load cell positioned on the right side of the ring support - rings 1 to 12, at time t, kN

$F_{w(1,12)l,t}$: Force in tension load cell positioned on the left side of the ring support - rings 1 to 12, at time t, kN

$F_{vtr,t}$: Force in tension load cell positioned on the right side of the hopper support, at time t, kN

$F_{vtl,t}$: Force in tension load cell positioned on left side of the hopper support, at time t, kN

$F_{vbr,t}$: Force on shear beam load cell positioned at the base of the right pillar, time t, kN

$F_{vbl,t}$: Force on shear beam load cell positioned at the base of the left pillar, time t, kN

h: Ring height, m.

K: Characteristic value of lateral pressure ratio

$P_{ntr,t}$: Normal pressure on the right hopper wall next to the silo–hopper transition, time t, kPa

$P_{ntl,t}$: Normal pressure on left hopper wall next to the silo–hopper transition, time t, kPa

$P_{nir,t}$: Normal pressure on right hopper wall between the silo–hopper transition and outlet, time t, kPa

$P_{nil,t}$: Normal pressure on left hopper wall between the silo–hopper transition and outlet, time t, kPa

$P_{nitr,t}$: Normal pressure on right hopper wall between the silo–hopper transition and outlet, near transition, time t, kPa

$P_{nitl,t}$: Normal pressure for left hopper wall between the silo–hopper transition and the outlet, near transition, time t, kPa

$P_{nior,t}$: Normal pressure on right hopper wall between the silo–hopper transition and outlet, near outlet, time t, kPa

$P_{niol,t}$: Normal pressure on left hopper wall between the silo–hopper transition and outlet, near outlet, time t, kPa

$P_{nor,t}$: Normal pressure on the right hopper wall next to silo outlet, time t, kPa

$P_{nol,t}$: Normal pressure for the hopper wall on the left-hand side next to silo outlet, time t, kPa

$P_{h(1,12),t}$: Normal pressure on cylinder wall from the tension load cells positioned on spring set - rings 1 to 12, time t, kPa

$P_{w(1,12),t}$: Friction pressure for the cylinder wall from the tension load cells positioned on ring supports - rings 1 to 12, time t, kPa

$P_{vt,t}$: Vertical stress of product at the silo–hopper transition from the tension load cells positioned on the hopper support, time t, kPa

$P_{v(1,4),t}$: Vertical stress of product at the silo–hopper transition obtained from the pressure cells (flat bottom), time t, kPa

$W_{,t}$: Weight of stored product, time t, kN

$W_{hto}$: Weight of stored product between the outlet and the silo–hopper transition, zero in the case of the flat bottom, kN

$V_{ih}$: Internal hopper volume, $m^3$

$V_{ic}$: Internal cylinder volume, $m^3$

$r_i$: Internal cylinder radius, m.

$\gamma$: Bulk unit weight

## 1. Introduction

The study of the behavior of products stored in silos is dated from 1895 by Janssen [1]. Since then, other theories have been developed [2] [3,4] [5] supporting international standards [6,7]. Jenike [8] developed a device, internationally known, capable of determining the flow properties of stored products (Jenike Shear Tester), later improved by a group (Working Party on the Mechanics of Particulate Solids) of the European Federal of Chemical Engineers, renamed to "*Standart Shear Testing Technique for Particulate Solids Using the Jenike Shear Cell*" [9]. This device, in addition to supporting international standards, is capable of obtaining reliable parameters for calculating projects in silos.

The main reason that the study in silos is broad and complex is due to the behavior of the stored products. The laws that govern the mechanical behavior is presents complexities, therefore, many aspects remain poorly understood [10–12]. Consequently, to study actions, pressures and flows in silos, it is necessary to understand the structure, the product inside the structure and the interaction between them.

Brazil is a continental country with a favorable climate and relief for agricultural production. Therefore, the agricultural sector in Brazil is growing. The estimated grain production for the 2021/2022 harvest is 284.4 million tons [13]. Of this total, 87 million tons (25%) correspond to maize. Motivated by the future market, storage control, logistics or cooperatives, most agricultural products are stored. In 1980, the Brazilian storage capacity was 40.45 million tons of grain. In less than 4 decades (2019), Brazil more than quadrupled its static capacity (177.7 million tons of grain), with 86.6 million (49%) being in silos [14]. In addition, maize is also a leading product in the international market, for example, in Spain, with a production of 4.1 million tons [15], with León being the Spanish province with the highest production, 0.9 million [16].

In addition to the complexity of the mechanical behavior of maize and its derivatives, both have the highest load magnifying factor coefficient due to geometric unevenness ($C_{op}$ = 1,0 e 0,9 for animal feed mix and maize respectively), Table E.1 – Particulate solids properties, Eurocode 1, part 4 [7]. This coefficient is directly related to obtaining the pressures in the silos [7]. Experimental studies aid in the responses to these irregular stored products, quantifying pressure values throughout the silo.

The complexity of studying pressures in silos is due to the behavior being different from hydrostatic pressures, in other words, the stored product in silos presents friction pressures on the wall that increase according to the storage height [17].

The causes of silo failures and collapses are driven by several reasons. A review of some studies showed that the design error [18,19] and pressures stand out. The pressure (normal and friction) occurs in the silo wall and in the hopper. These pressures are static [10,19] (during filling and storage period) and dynamic (at the time of discharge) [10,19–22] and are exerted by the stored product in the structure.

The pressures in the silo are related by flow pattern that is directly influenced by the stored material and the hopper geometry. There are two possible flow patterns, mass flow [5] and funnel flow [23], and also has a flow transition zone: transition flow, that is characterized by a distinct change in flow in a position that depends on the filling height [24]. These flow patterns directly influence the magnitude and distribution of forces acting across the silo. The hopper angle and the wall friction coefficient are the two most influential parameters [7,8,25,26]. [7,8,25]However, flow pressure is still poorly understood [17,27–29].

Faced with the several causes that lead to failures in the silo structure include the pressures (normal and friction, on the wall and hopper) exerted by the stored product in the structure [10,19] and the product discharge (maximum pressures in the silo, usually at the silo-

hopper transition) [10,19–22]. Reinforcing the need for studies involving pressures, especially at discharge. The study of friction pressures in relation to silo height has been little studied.

A pilot-scale test station proposed by Pieper and Schütz in 1980 [30] supported DIN 1055-6: *Basis of design and actions on structures – Part 6* [6] allows obtaining numerous variables that directly influence the behavior of pressures in the silo [31,32], of which: use of any product as long as the maximum diameter of the product is less than 1.7 centimeters (to be allowed values proportional to the real scale) [30,33]; three walls with different roughness (varying the coefficient of friction between the product and the wall); twelve height/diameter ratios; 8 bottoms (1 flat bottom, 4 concentric hoppers (α: 75 to 30o) and 3 100% eccentric hoppers with (α: 75 to 45o) and other possible test procedure variables. The test station was developed and studied at the University from Sao Paulo [34] later, in partnership, it was calibrated and studies are currently being developed at the Federal University of Lavras [35].

The experimental model of real-scale silos provides proximity to real values, enabling confidence in the data and enabling the understanding of pressures in the silos. In the world, the number of real-scale experimental silo stations for investigating pressures is relatively small. [35–46] due to the cost of construction, instrumentation and operations. In addition, the scale factor is extremely important for reliable data. [33]. Furthermore, the study of experimental pressures in silo allows the advancement of numerical studies as a form of validation and comparisons in order to make the models reliable.

Therefore, the aim of the present study was to elucidate the relationship involving the hopper angle, flow pattern and the pressures in slender cylindrical silos, obtaining normal and frictional pressures on the wall and pressures on the hopper wall during filling, static phase and discharge of the stored product.

## 2. Material and methods

### 2.1. General description of the installation

The silo test station corresponds to the pilot scale [33], that is, if the appropriate proportions between the stored product and the internal diameter of the silo are used, the values of the loads and pressures correspond to the real scale. The station consists of a pilot silo (fully instrumented), a storage silo (store the product stored during the tests) and a bucket elevator (transport between the silos). All the measuring cells of the pilot silo are connected in the acquisition system data controlled by a portable computer (Figure 1).

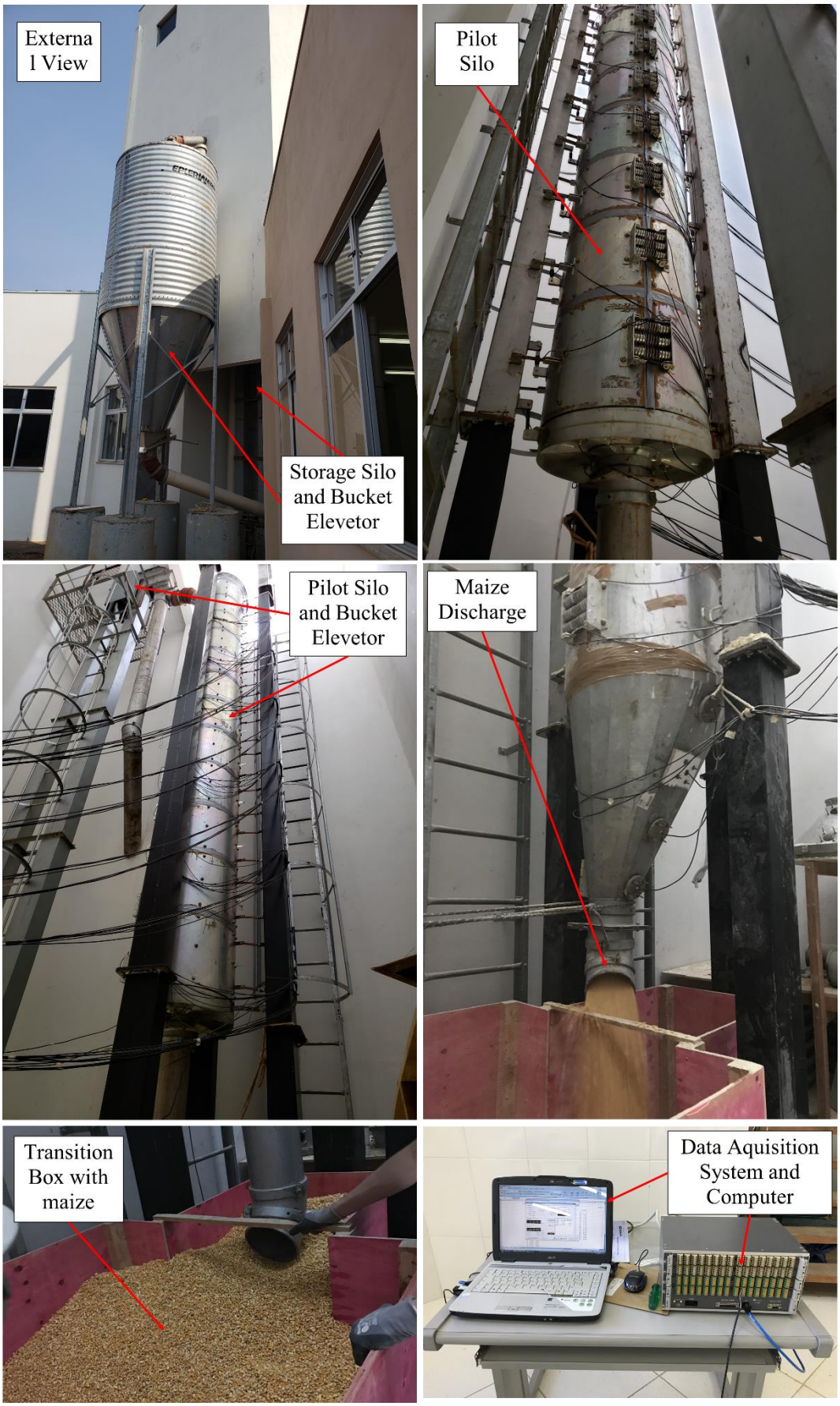


**Figure 1.** Pilot silo station and instrumentation.

### 2.1.2. Geometry of the experimental pilot silo

The pilot test silo is cylindrical and metallic. The cylinder is 6 meters high and 0.7 meters in internal diameter. The cylinder is segmented into 12 structurally independent rings, allowing to obtain the forces in each division. The pilot silo is classified as slender [6,7,25]. As only 5 rings were used in this work, the Figure 2 shows the location of the measurement cells up to the height of 2.50 m (5 rings).

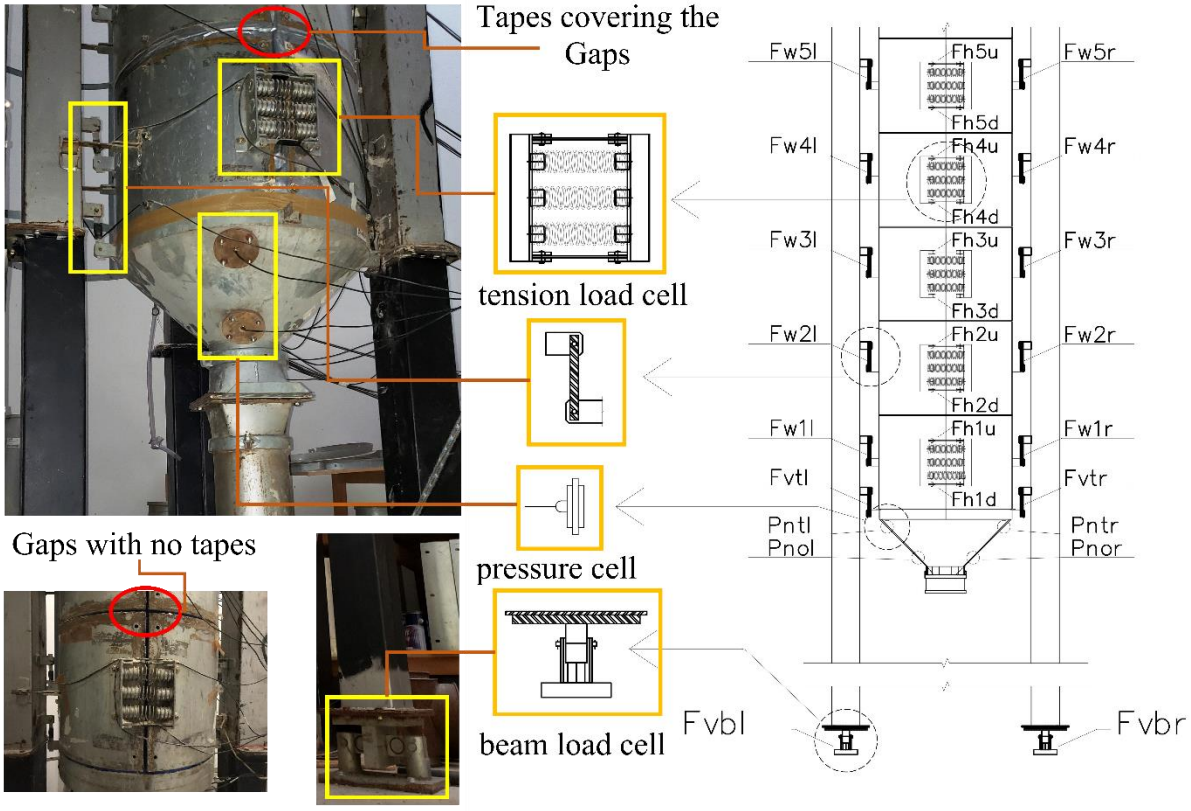


**Figure 2. Instrumentation and measurement cells for loads and pressures of the pilot silo.**

### 2.2. Measuring vertical forces

The pilot silo is supported by two support pillars supporting pillars with shear beam load cells at its bases (Figure 2), enabling the measurement of the weight of the stored material.

The vertical forces responsible for measuring the friction pressure of the cylinder wall and vertical stress in the stored material at the transition were measured by tension load cell located on each support pillar along the height of the pilot silo vertically supporting each ring and the bottom (Figure 2).

## 2.3. Measuring horizontal forces and normal pressures

Measurements in the hopper were conducted using pressure cells (Figure 2). To measure normal wall pressures, a vertical generatrix was located on the cylinder wall, along which 12 pairs of readings were taken at different heights using a tension load cell, each pair were responsible for providing normal pressure at each ring (Figure 2).

The arrangement of the measuring cells influences the data obtained [47,48]. The pressure cells have a gap of 2.5 mm in the radius between the cell and the hopper structure. In addition, the cell is 10 mm high (part that is internal to the silo), the wall thickness of the hoppers is exactly 10 mm, ensuring quality in data collection. Each ring was spaced 5 mm apart (vertical distance) and had a gap of 5 mm in the opening (horizontal distance).

## 2.4. Calculation of parameters

In this section, the station parameters are presented briefly. The most detailed explanation of the parameters is in Gandia et al. (2021) [49].

Normal wall pressures (Ph)

$$\mathbf{Ph(1,5),t} = \frac{\mathbf{Fh(1,5)u,t + Fh(1,5)d,t}}{\mathbf{hr.0.32759}}, \text{ equation (1)}$$

– 0.32759: constant value obtained with $d_i$ = 0.685 m.

Frictional wall pressures (Pw)

$$\mathbf{Pw(1,5),t} = \frac{\boldsymbol{Fw(1,5)r,t + Fw(1,5)l,t}}{\boldsymbol{\pi.di.hr}}, \text{ equation (2)}$$

Weight of stored material (W)

$$W,t = Fvbr,t + Fvbr,t \quad \text{equation (3):}$$

Vertical stress in the stored solid at the transition ($P_{vt}$)

$$\mathbf{Pvt,t} = \frac{\mathbf{Fvtr,t + Fvtl,t - Whto}}{\mathbf{A}} \text{ equation (4):}$$

$$\mathbf{Whto} = \mathbf{Vi}\boldsymbol{h} * \boldsymbol{\gamma} \text{ equation (5):}$$

Wall friction coefficient (μ)

$$\mu(1,5) = \frac{Pw(1,12)}{Ph(1,12)}$$ equation (6):

Lateral pressure ratio (K)

$$K,t = \frac{Ph(1,5),t}{Pv(1,5),t}$$ equation (7):

Specific weight of stored material (γ)

$$\gamma = \frac{W}{Vih+Vic}$$ equation (8)

## 2.5. Description of the tests

### 2.5.1. Properties of the stored product

The product used to conduct the tests in the pilot silo was maize with a minimum purity of 97%. The physical, mechanical and flow properties of maize were obtained following the methodology of Jenike Shear Test [9] which conforms to Eurocode 1, part 4 [7]. The values obtained were (lower and upper limits):

- specific weight (kN/m$^3$): 7.52 – 7.83
- angle of repose, 31.3° - 37.1;
- cohesion (kPa): 0.241 – 1.084;
- steel wall friction angle: 7.37° – 9.02°;
- steel wall friction coefficient: 0.13 - 0.16;
- internal friction angle: 19° - 29°;
- humidity, 10.62%.

### 2.5.2. Test settings

Using the granular material described above, 30 tests were performed. The tests were conducted with concentric filling. The 30 tests were divided into five configurations (Figure 3) with six repetitions each. The configurations have different hopper inclinations, where: β =

15 ° (β15°); β = 30 ° (β30°); β = 45 ° (β45°); β = 60 ° (β60°) and β = 90 °, named a flat bottom (FlatB).

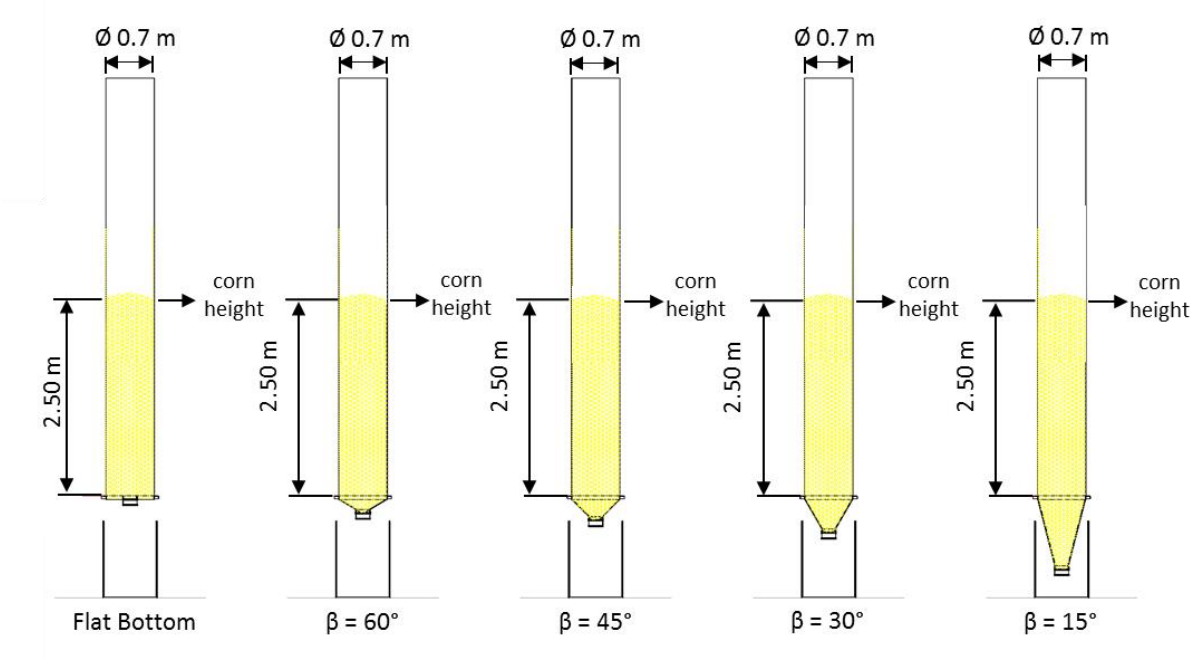


**Figure 3.** Test configuration, varying the hopper angle.

The reason of using this hopper inclinations was due to Eurocode 1, part 4. The inclinations of the hoppers associated with the friction coefficient of the wall with the product (μ) (in the case of this work smooth steel wall with maize) provide different flows (Figure 4). Mass flow for β = 15 °; transition flow for β = 30 ° and funnel flow for β = 45 and 60° and flat bottom. Therefore, it possible to study the flow during discharge.

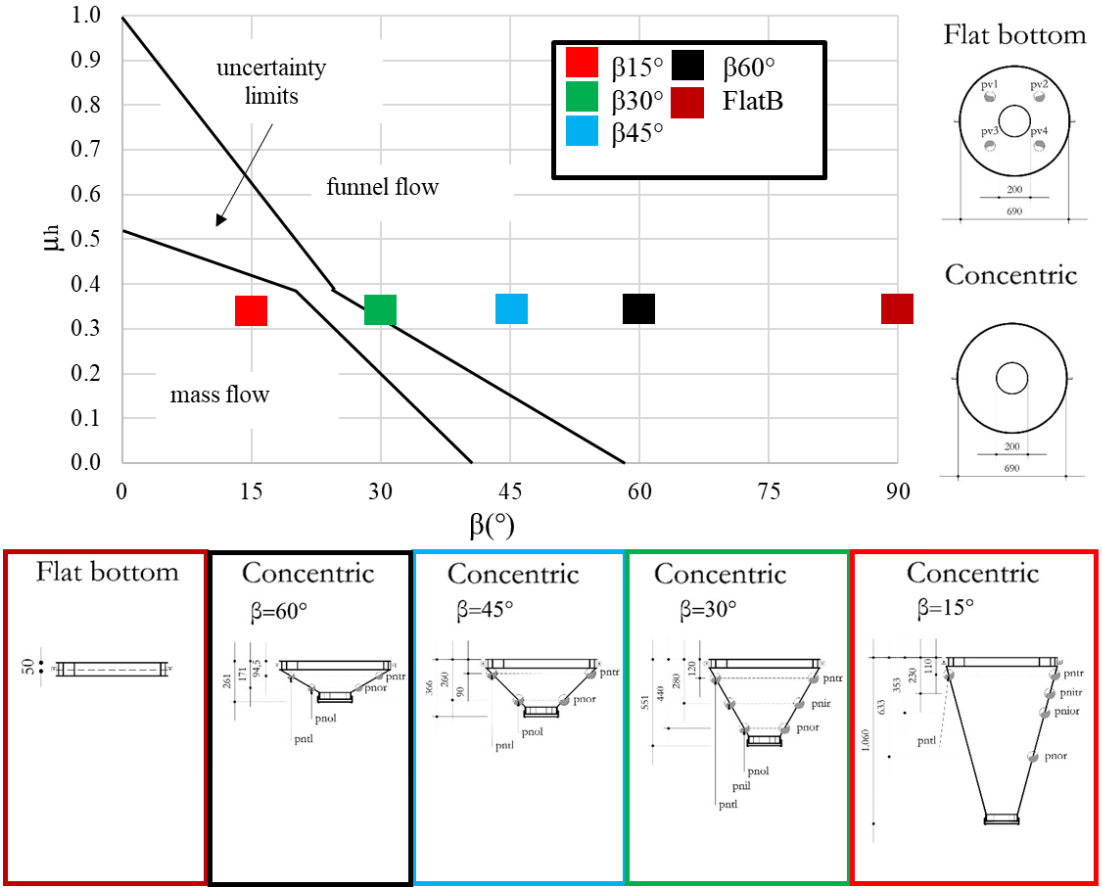


**Figure 4.** Hopper angles and conditions for flow patterns according to Eurocode 1, part 4.

Also, according to Eurocode, it was possible to distinguish the 5 different bottoms in three other groups regarding the type of silo: steep hopper, shallow hopper and flat bottom. Therefore, the bottoms were classified and calculated as follows:

- Flat bottom (FlatB) is a flat bottom because $\alpha < 5$ °;
- $\beta = 60$ ° is a shallow hopper because $\tan\beta > \frac{1-K}{2\mu_h}$;
- $\beta = 15$ °; $\beta = 30$ ° and $\beta = 45$ ° are a steep hopper because $\tan\beta < \frac{1-K}{2\mu_h}$.

The pilot silo was filled at a constant speed, providing approximate flow rates for the tests (Table 1).

**Table 1**. Average flow for each test.

| | $\bar{X}$ (kg/s) | | σ (kg/s) | |
|---|---|---|---|---|
| Test | Filling | Discharge | Filling | Discharge |
| FlatB | 4.1 | 20.2 | 0.1 | 0.5 |
| β60° | 4.4 | 20.0 | 0.1 | 0.2 |

| | | | | |
|---|---|---|---|---|
| β45° | 4.6 | 22.3 | 0.3 | 0.2 |
| β30° | 5.0 | 24.2 | 0.5 | 0.9 |
| β15° | 4.5 | 31.4 | 0.1 | 0.2 |

$\bar{X}$: mean; σ: standard deviation

The silo was discharge with the gate (diameter of 0.20 m) 100% open. In addition, still in relation to Table 1, it can be seen that the discharge flow rate it is directly influenced by the hopper inclination (and type of flow), greater for hoppers with smaller β. In addition, in this model of the pilot silo it was observed that the discharge flow is at least 5 times greater than that of the filling.

As each of the five configurations had different volume (because the volume of each hopper), the product loading values were also different. Table 2 presents the values related to the load of the storage product of each configuration.

**Table 2**. Average load for each test.

| Test | $\bar{X}$ (kN) | σ (kN) |
|---|---|---|
| FlatB | 7.49 | 0.53 |
| β60° | 7.86 | 0.45 |
| β45° | 8.46 | 0.15 |
| β30° | 8.38 | 0.81 |
| β15° | 9.26 | 0.19 |

$\bar{X}$: mean; σ: standard deviation

It is noteworthy that the β30° (β = 30°) test had a mean value different from that expected and a standard deviation higher than the others. The reason is that of the 6 repetitions, two showed flaws in the filling, resulting in heights of the stored product below that of interest. It should be emphasized that the two repetitions were used for calculations of means and standard deviations, however in the analysis of the individual test (presented later) they were removed during the random choice.

All tests were conducted in three steps: filling the silo to the height of interest (verified by the tension load cell that shows the measurement in the semi-cylinder above the height of interest), static condition (for 10 min); product discharge (hopper gate 100% opened).

### 2.5.3 Description of the analyzes

The topics presented in results and discussions compared and discussed the different concentric hopper inclinations evaluating the load and pressures, which according to Eurocode 1 part 4 [7] in Figure 4 represents three flow patterns at discharge.

The analysis of the results and discussions were divided into: Temporal behavior of the test configurations; Normal pressures in the cylinder 0.25 m above the transition ($p_{h1}$); Normal pressures in the cylinder 0.75 m above the transition ($p_{h2}$); Friction pressures in the cylinder 0.25 m above the transition ($p_{w1}$); Vertical stress in the stored material at the transition ($p_{vt}$); Coefficient of lateral pressures (K); Normal pressure at transition ($p_{nt}$); Maximum normal pressures ($p_h$ max); Maximum friction pressures ($p_w$ max).

Temporal behavior of the test configurations presents the temporal behavior of all instrumentation during the complete test, aiming to reinforce the quality of data collection and instrumentation. In addition, it discusses the differences, in general, between the different inclinations of the bottoms

Normal pressures in the cylinder 0.25 m above the transition ($p_{h1}$), Normal pressures in the cylinder 0.75 m above the transition ($p_{h2}$) and Friction pressures in the cylinder 0.25 m above the transition ($p_{w1}$) present the most detailed behavior of pressures (normal and friction) in these locations. Aiming to evaluate mainly the moment and the magnitude of the maximum pressures and the influence by the inclination of the bottom associated with a flow channel and static material. In addition to comparing with Eurocode.

Coefficient of lateral pressures (K) presents the temporal behavior of the coefficient of lateral pressures, emphasizing the moment of discharge and comparing with the coefficient (K) calculated by Eurocode.

Normal pressure at transition ($p_{nt}$) details the pressure behavior slightly below the silo-bottom transition, comparing the test configurations and verifying the magnitude and moment of pressure occurrence.

Maximum normal pressures ($p_h$ max) and Maximum friction pressures ($p_w$ max) the curve of maximum pressures (friction and normal) is plotted for each configuration and compares with those calculated by Eurocode.

## 3. Results and discussion

This paper generated a large volume of data. Therefore, to avoid exposing unnecessary data, are presented the values of average and standard deviation in each measurement cell referring to filling and discharge (Table 4).

**Table 4**. Maximum mean values of pressures after filling and discharge in each test configuration.

| After filling pressure (kPa) | | | | | | | | | | |
|---|---|---|---|---|---|---|---|---|---|---|
| Cell | FlatB | | β60° | | β45° | | β30° | | β15° | |
| | $\bar{X}$ | σ | $\bar{X}$ | σ | $\bar{X}$ | σ | $\bar{X}$ | σ | $\bar{X}$ | σ |
| $p_{h5}$ | 0.44 | 0.35 | 0.19 | 0.17 | 0.18 | 0.03 | 0.12 | 0.06 | 0.08 | 0.06 |
| $p_{h4}$ | 1.96 | 0.51 | 1.21 | 0.15 | 0.69 | 0.07 | 0.75 | 0.24 | 0.74 | 0.02 |
| $p_{h3}$ | 3.16 | 0.70 | 2.39 | 0.05 | 0.95 | 0.01 | 1.53 | 0.57 | 1.59 | 0.21 |
| $p_{h2}$ | 3.76 | 0.21 | 2.54 | 0.25 | 0.96 | 0.05 | 1.28 | 0.07 | 1.14 | 0.25 |
| $p_{h1}$ | 4.81 | 0.09 | 4.22 | 0.15 | 1.67 | 0.05 | 2.83 | 0.07 | 2.53 | 0.07 |
| $p_{nt}$ | - | - | 2.06 | 0.12 | 1.99 | 0.42 | 1.71 | 0.10 | 4.30 | 0.46 |
| $p_{ni}$ | - | - | - | - | - | - | 2.99 | 0.17 | - | - |
| $p_v$ | 8.70 | 0.29 | - | - | - | - | - | - | - | - |
| $p_{nit}$ | - | - | - | - | - | - | - | - | 3.72 | 0.51 |
| $p_{nio}$ | - | - | - | - | - | - | - | - | 2.33 | 0.80 |
| $p_{no}$ | - | - | 6.89 | 0.30 | 7.08 | 1.00 | 5.63 | 0.33 | 4.56 | 0.29 |
| $p_{vt}$ | 10.77 | 0.43 | 9.87 | 1.94 | 9.38 | 0.47 | 11.53 | 0.76 | 9.91 | 0.79 |
| $p_{w5}$ | 0.13 | 0.06 | 0.08 | 0.06 | 0.18 | 0.03 | 0.06 | 0.02 | 0.08 | 0.01 |
| $p_{w4}$ | 0.43 | 0.11 | 0.56 | 0.16 | 0.69 | 0.07 | 0.30 | 0.22 | 0.45 | 0.05 |
| $p_{w3}$ | 0.71 | 0.10 | 0.79 | 0.09 | 0.95 | 0.01 | 0.68 | 0.08 | 0.81 | 0.08 |
| $p_{w2}$ | 0.94 | 0.10 | 0.89 | 0.10 | 0.96 | 0.05 | 0.69 | 0.14 | 0.84 | 0.05 |
| $p_{w1}$ | 1.41 | 0.05 | 1.55 | 0.36 | 1.67 | 0.05 | 1.07 | 0.13 | 1.57 | 0.10 |
| Discharge pressure (kPa) | | | | | | | | | | |
| Cell | FlatB | | β60° | | β45° | | β30° | | β15° | |
| | $\bar{X}$ | σ | $\bar{X}$ | σ | $\bar{X}$ | σ | $\bar{X}$ | σ | $\bar{X}$ | σ |

| | | | | | | | | | | |
|---|---|---|---|---|---|---|---|---|---|---|
| $p_{h5}$ | 0.64 | 0.71 | 0.61 | 0.51 | 0.39 | 0.04 | 0.15 | 0.13 | 0.00 | 0.10 |
| $p_{h4}$ | 3.21 | 0.59 | 3.33 | 0.28 | 0.99 | 0.04 | 2.53 | 0.73 | 2.74 | 0.13 |
| $p_{h3}$ | 4.04 | 0.54 | 3.81 | 0.31 | 1.32 | 0.01 | 4.33 | 0.62 | 4.26 | 0.27 |
| $p_{h2}$ | 3.68 | 0.14 | 4.71 | 0.22 | 1.29 | 0.02 | 4.41 | 0.11 | 4.63 | 0.40 |
| $p_{h1}$ | 4.78 | 0.12 | 4.30 | 0.12 | 1.77 | 0.02 | 4.95 | 0.11 | 3.90 | 0.21 |
| $p_{nt}$ | - | - | 13.20 | 1.10 | 13.12 | 1.18 | 15.89 | 1.68 | 26.08 | 2.05 |
| $p_{ni}$ | - | - | - | - | - | - | 4.33 | 0.45 | - | - |
| $p_{v}$ | 9.97 | 0.45 | - | - | - | - | - | - | - | - |
| $p_{nit}$ | - | - | - | - | - | - | - | - | 10.11 | 1.97 |
| $p_{nio}$ | - | - | - | - | - | - | - | - | 4.59 | 0.19 |
| $p_{no}$ | - | - | 6.57 | 0.21 | 6.81 | 1.45 | 5.06 | 0.15 | 4.50 | 0.21 |
| $p_{vt}$ | 10.56 | 0.48 | 7.43 | 0.70 | 8.32 | 0.33 | 10.88 | 0.71 | 8.21 | 1.34 |
| $p_{w5}$ | 0.27 | 0.13 | 0.18 | 0.13 | 0.39 | 0.04 | 0.12 | 0.05 | 0.16 | 0.01 |
| $p_{w4}$ | 0.77 | 0.18 | 0.76 | 0.23 | 0.99 | 0.04 | 0.44 | 0.36 | 0.66 | 0.05 |
| $p_{w3}$ | 1.14 | 0.11 | 1.14 | 0.06 | 1.32 | 0.01 | 0.98 | 0.16 | 1.15 | 0.09 |
| $p_{w2}$ | 1.08 | 0.08 | 1.03 | 0.11 | 1.29 | 0.02 | 1.15 | 0.07 | 1.18 | 0.08 |
| $p_{w1}$ | 1.35 | 0.05 | 1.59 | 0.41 | 1.77 | 0.02 | 1.36 | 0.21 | 1.84 | 0.16 |

$\bar{X}$: mean value; σ: standard deviation

As noted, the tests showed little coefficient of variation. Therefore, for each type of test, one of the six repetitions were chosen randomly to discuss the results.

**Temporal behavior of the test configurations**

It can be seen that the model is accurate (Figure 5) showing the behavior of the measurement cells in the 15 pressure curves. The images refer to the five test configurations and the three divisions of the measurement cells. It is observed the equidistance of the normal pressures ($p_{h\,(1.5),\,t}$) and the linearity of the weight of the stored product (W).

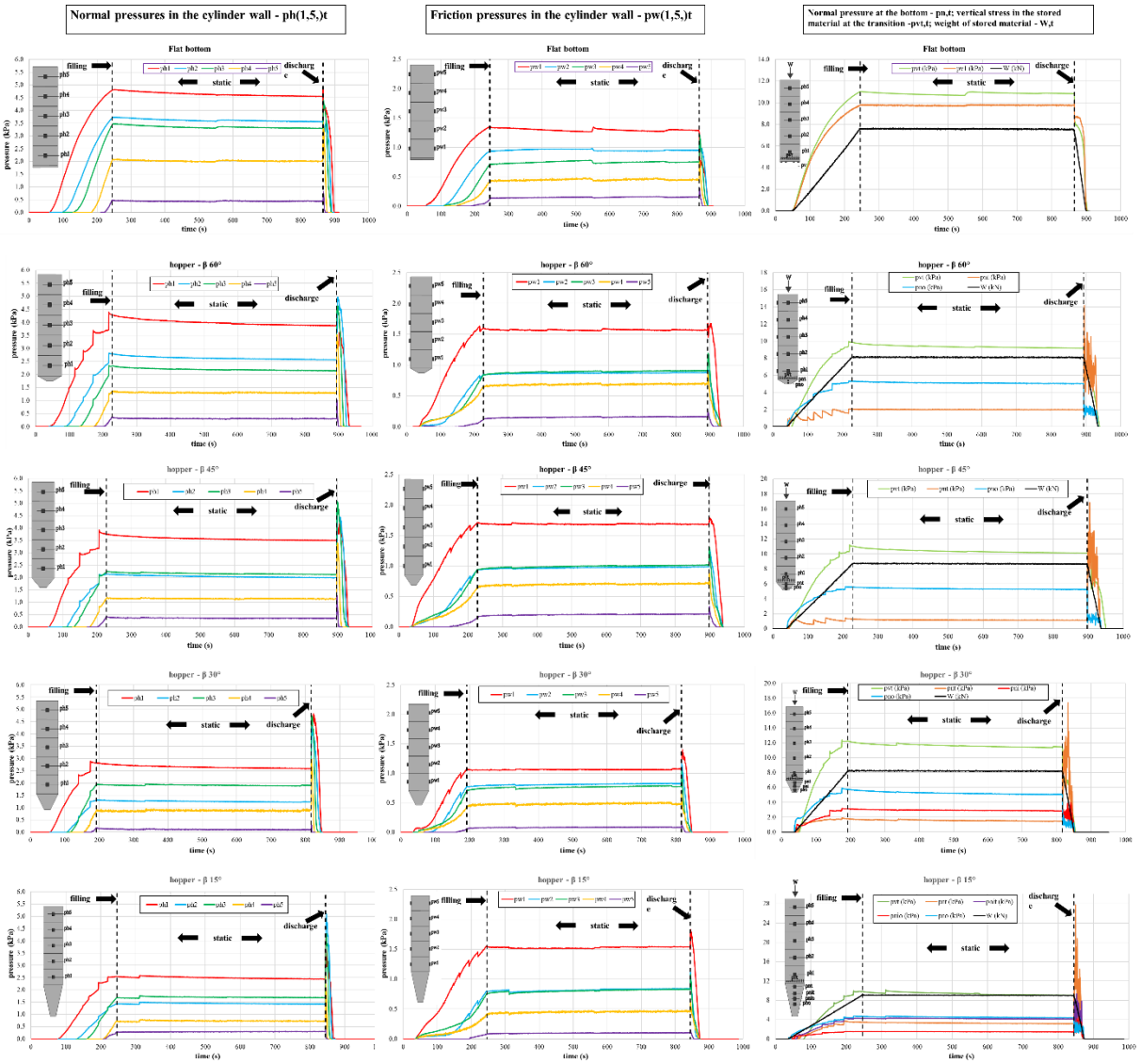


**Figure 5.** Normal silo cylinder wall pressures ($p_{h,t}$), friction silo cylinder wall pressures ($p_{w,t}$), normal hopper wall pressures ($p_{n,t}$), vertical stress in the stored material at the transition ($p_{vt,t}$) and weight of stored material ($W,_t$).

The flat bottom in the filling does not show settling peak due to the right angle (β = 90 °), providing stability of the stored product. Therefore, in the cylinder and bottom of the silo there are no oscillations in friction and normal pressures.

It is observed that between the height 0.75 and 1.25 meters ($p_{h2}$ and $p_{h3}$), as the angle β decreases (β: 90, 60, 45, 30 and 15 °), the normal pressures in the cylinder tend to cross. At β = 45 ° they cross at the end of filling and at β = 30 and 15 ° they cross just after the start of filling. It is believed that the smaller the hopper angle, the greater the formation of mechanical arches

between 0.75 and 1.25 m. Some authors have verified the same finding, however, using other stored products [27,48,50].

The friction pressures clearly show the settling peaks in all configurations, even if the stored product was only 10 minutes static, it is easy to see the peaks provided by the consolidation. This finding was verified for the first time in 2012 [48], however there are still many gaps in the prediction of this behavior.

Normal and friction pressures at discharge have greater magnitude according to the decrease in the hopper angle, in other words $p_h$, $p_n$ and $p_w$ β (90 <60 <45 <30 <15 °). In addition, the maximum normal pressures in the cylinder ($p_{h\,(1.5),\,t}$) are approximately 5 kPa, that is, during filling and static condition, the normal pressures in the cylinder are higher for larger β. However, at discharge the overpressure is greater in β less, but all have an approximate maximum value.

The normal pressures in $p_{h1}$ and $p_{h2}$ showed a significant variation due to the angle of β. It is believed that there is a static zone (flow channel) that changes according to the hopper angles and influences the behavior of pressures at 1/3 the height of the silo cylinder (0.83 m). Therefore we decided to analyze more carefully the temporal behavior of $p_{h1}$ and $p_{h2}$ in the five configurations.

**Normal pressures in the cylinder 0.25 m above the transition ($p_{h1}$)**

The silo-hopper transition presents the maximum overpressures at discharge because the stored product changes from static to dynamic condition and the vertical displacement of the stored product in the geometric transition, for mass flow [5,51]. In the funnel flow there are stored product channels (effective transition), that is, static material forming a passage of the product to the outlet gate of the silo, dampening the pressures [23,45]. These theories and affirmations are seen in Figure 6 in a simple and visual way.

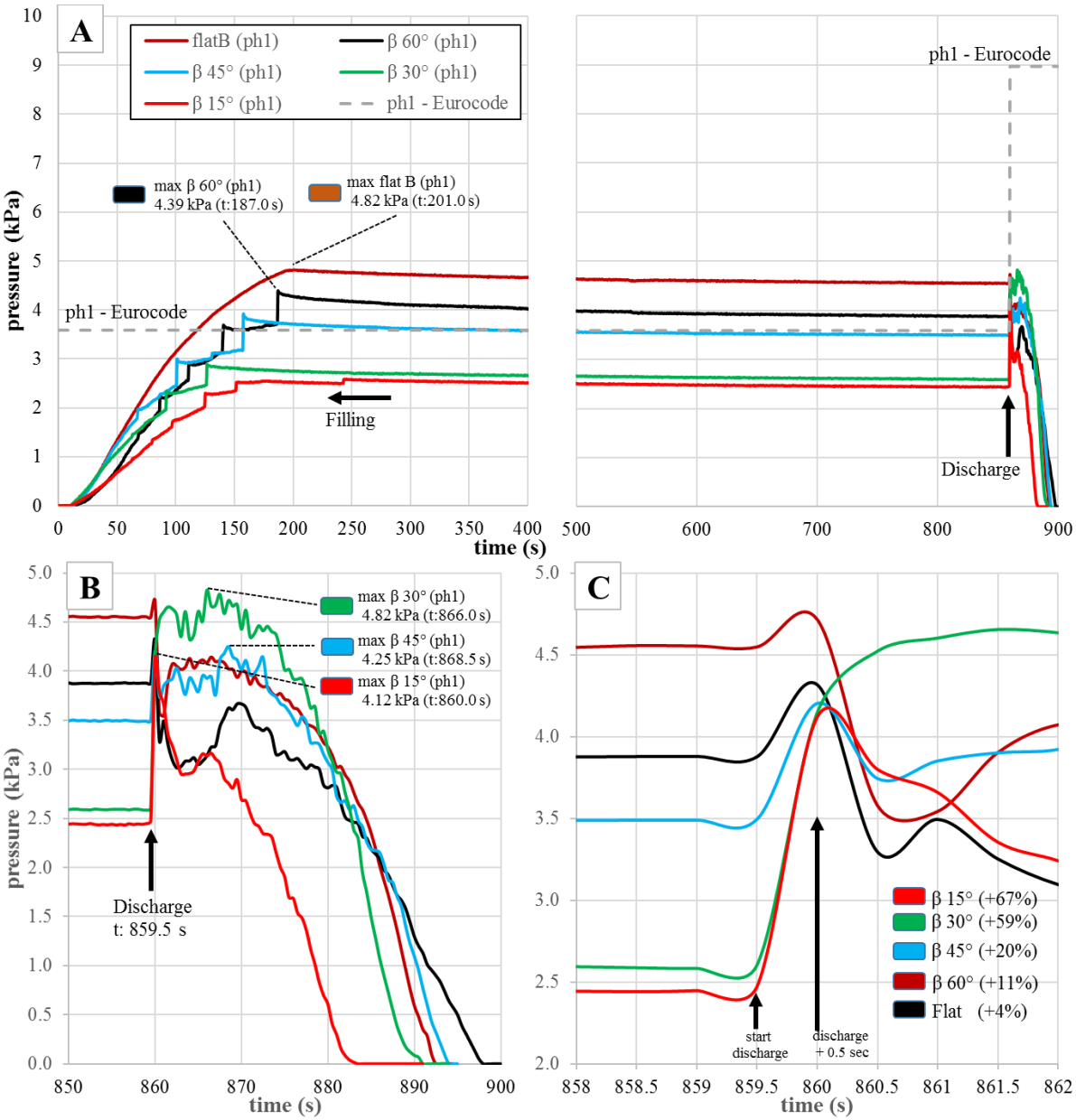


**Figure 6.** Normal pressures in the cylinder ($p_{h1,\,t}$) 0.25 m above the transition.

(A) Complete test; (B) Discharge; (C) Overpressures.

It is observed that in Figure 6A, during filling, the maximum normal pressures in the cylinder occurred for FlatB and β60 ° at height 0.25 m ($p_{h1}$). The flow pattern of the two configurations is funnel flow, and geometrically they are flat bottom (FlatB) and shallow hopper (β60 °) according to Eurocode.

Figure 6B demonstrated that for β45 °, β30 ° and β15 ° the maximum normal pressures in the cylinder occurred at discharge. Although, according to Eurocode, hoppers with funnel flow (β45 °), mixed flow (β30 °) and mass flow (β15 °) are geometrically steep type hoppers.

Another interesting fact is the moment of occurrence after the discharge, first β15 ° followed by β30 ° and β45 °.

Exactly after the start of the discharge and 0.5 seconds before, the overpressure in $p_{h1}$ was calculated for all configurations (Figure 6C). It was found that according to the greater angle in β, the lower the overpressure, that is, $p_{h1}$ (β15 °> β30 °> β45 °> β60 °> FlatB). Figure 6A shows that the maximum experimental pressures are lower than that calculated by Eurocode.

In order to understand if increasing the height of the cylinder (0.75 m, $p_{h2}$) the normal pressures would be influenced by the formation of flow channel and static stored product according to the angle β, the same analysis was conducted.

**Normal pressures in the cylinder 0.75 m above the transition ($p_{h2}$)**

During filling, the occurrence of the maximum normal pressure in the cylinder was verified in FlatB (Figure 7A), presenting values higher than those calculated by Eurocode.

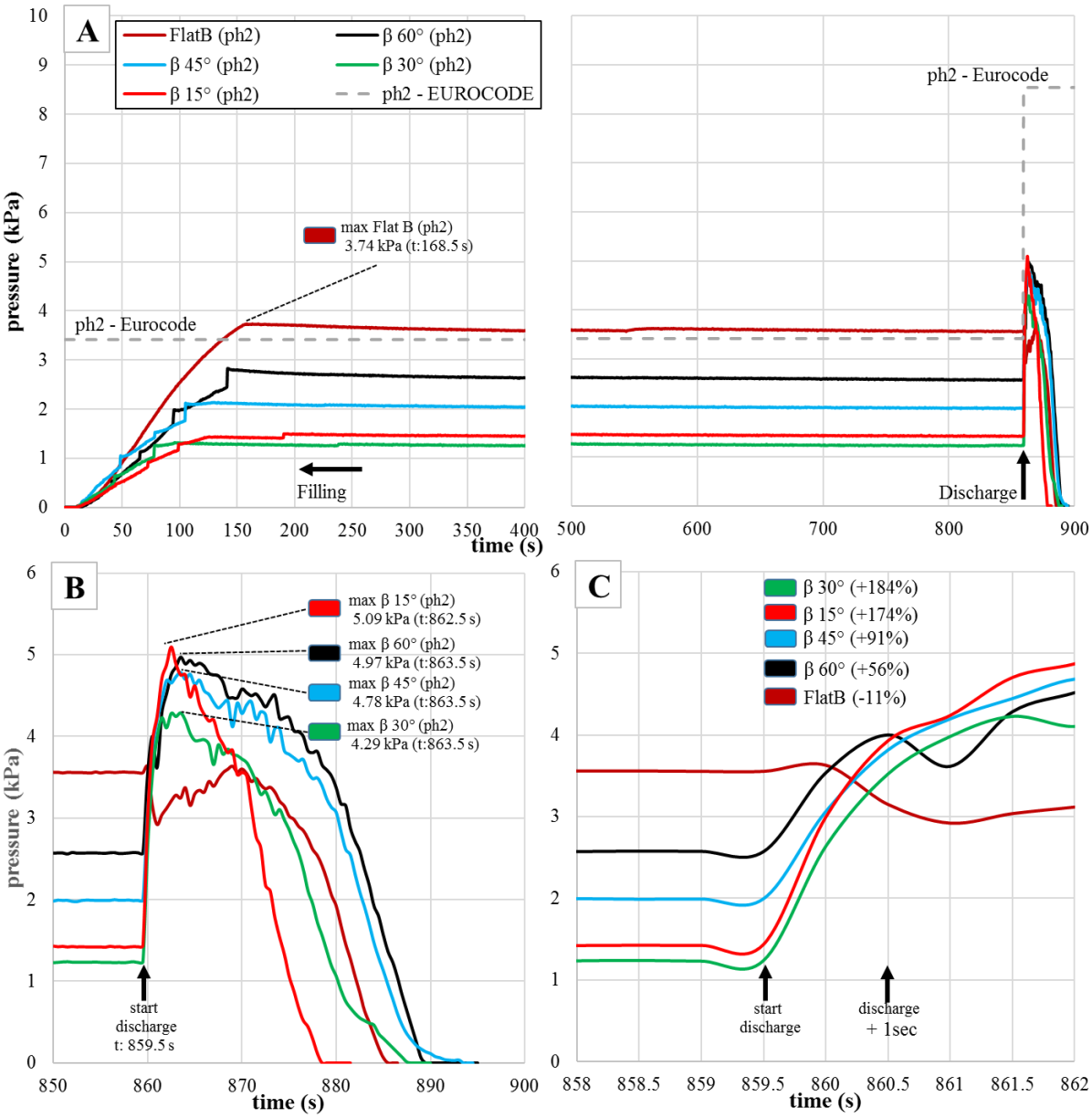


**Figure 7.** Normal pressures in the cylinder ($p_{h2,\,t}$) 0.75 m above the transition.

(A) Complete test; (B) Discharge; (C) Overpressures.

The maximum normal pressures in the cylinder at discharge (Figure 7B), once again, demonstrate that for mass flow (β15 °) it had the highest overpressure and occurred in the shortest time. Subsequently, those with funnel flow (β45 ° and β60 °) and mixed flow (β30 °). Comparing with Figure 6B, it can be seen that the overpressure at β30 ° decreased and for β45 ° and β60 ° increased, due to the greater height of the flow channel and because β30 ° is classified as a transition flow, influenced by the height of the stored product.

The overpressures (Figure 7C) shows that the highest was at β30 °, however, if we compare with Figure 6C ($p_{h1,}$ with 0,25 m) the increase in β45 ° and β60 ° was 3 to 4 times, while β15 ° and β30 ° was less than 2 times and in FlatB there have been no changes. In other words, affirming the pressure damping zones (static product zones) for hoppers with a greater β angle (effective transition). Checking the influence of the hopper type and the type of flow, at height 0.25 m the friction pressure in the cylinder ($p_{w1}$) was also evaluated.

**Friction pressures in the cylinder 0.25 m above the transition ($p_{w1}$)**

As with normal cylinder pressure at 0.25 m ($p_{h1}$) (Figure 6A), the maximum friction pressure in FlatB occurred during filling (Figure 8A).

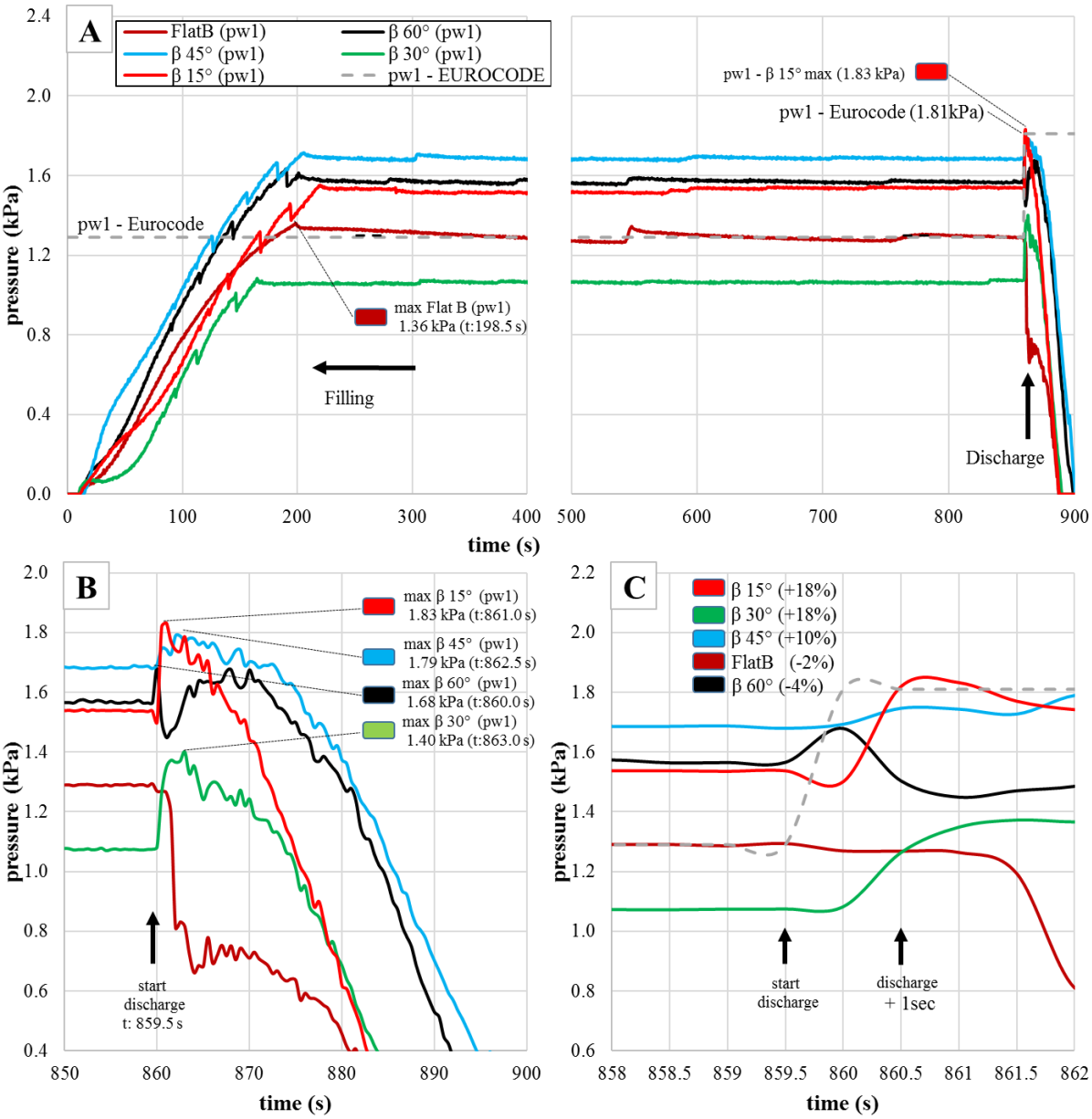


**Figure 8.** Friction pressures in the cylinder ($p_{w1,\,t}$) 0.25 m above the transition.

(A) Complete test; (B) Discharge; (C) Overpressures.

For funnel flow hoppers and classified as flat bottom (FlatB) and shallow hopper (β60 °), in the discharge, after a few seconds there was a sharp drop in pressure (Figure 8B). In FlatB it was due to the static material and at β60 ° possibly when emptying the hopper, the material was accommodated by increasing the pressure in a few seconds. For steep hoppers (β45 °, β30 ° and β15 °) peak pressure occurred at the beginning of the discharge.

The overpressures calculated after 1 second from the beginning of the discharge indicate that the magnitude is directly related to the decrease in β (Figure 8C). Only in FlatB that the stored product was static for two seconds before the pressure drop.

In general, it is observed that almost all configurations exceeded that calculated by Eurocode during filling, however, in the discharge, only at β15 ° was higher than the standard.

**Coefficient of lateral pressures (K)**

The Lateral pressure ratio (K) is obtained by Eurocode [7] in a simple way, only by the type of the stored material, not being influenced by the geometry of the hopper. Figure 10 presents the values during the tests performed in all configurations, being possible to evaluate the behavior of K in each one of them. The significant change in pressures ($p_{vt}$ and $p_{h1}$) results in the values of the lateral pressure ratio (K), which is influenced by the angle β. (Figure 10).

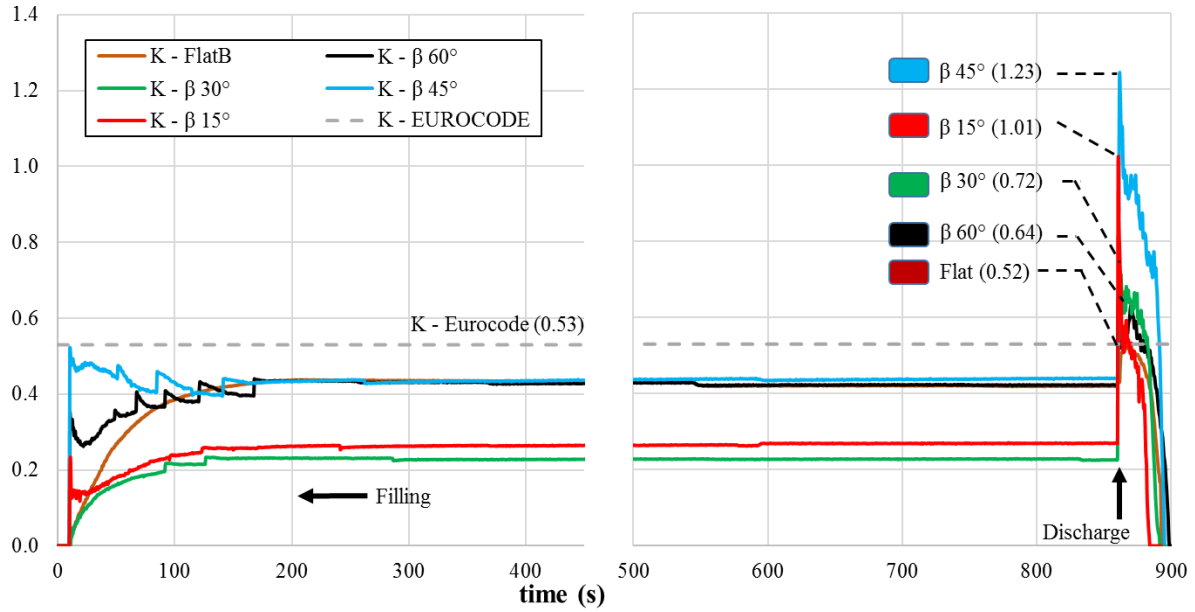


**Figure 9.** Temporal behavior of the coefficient of lateral pressures ($K_{,t}$) at transition.

It is observed that practically all configurations at discharge exceeded the K calculated by Eurocode, except for FlatB (flat bottom and funnel flow). The highest K was in β45 ° (steep hopper and funnel flow), later β15 ° (steep hopper and mass flow) and β30 ° (steep hopper and transition flow). The same was confirmed by some authors who noticed a considerable increase in K during the first seconds of the discharge surpassing Eurocode 1, part 4 [27,48,50].

Obviously, K increases when the discharge occurs, but it is interesting that for β45º it increases a lot, although it is not basic flow. Therefore, it is believed that because it is half the right angle (90 º) and because β45º has the lowest $p_{vt}$ (Figure 5), providing the highest lateral pressures ratio in the transition between the 5 configurations.

**Normal pressure at transition ($p_{nt}$)**

The normal pressures on the silo cylinder wall during discharge are erratic for mass flow [52]. In Figure 11 it is observed in the mass flow (β15 °), the pressures during the discharge oscillate considerably. Oscillations also occur in the funnel flow and transition flow (β60 °; β45 ° and β30 °), but with lesser magnitude and more normalized.

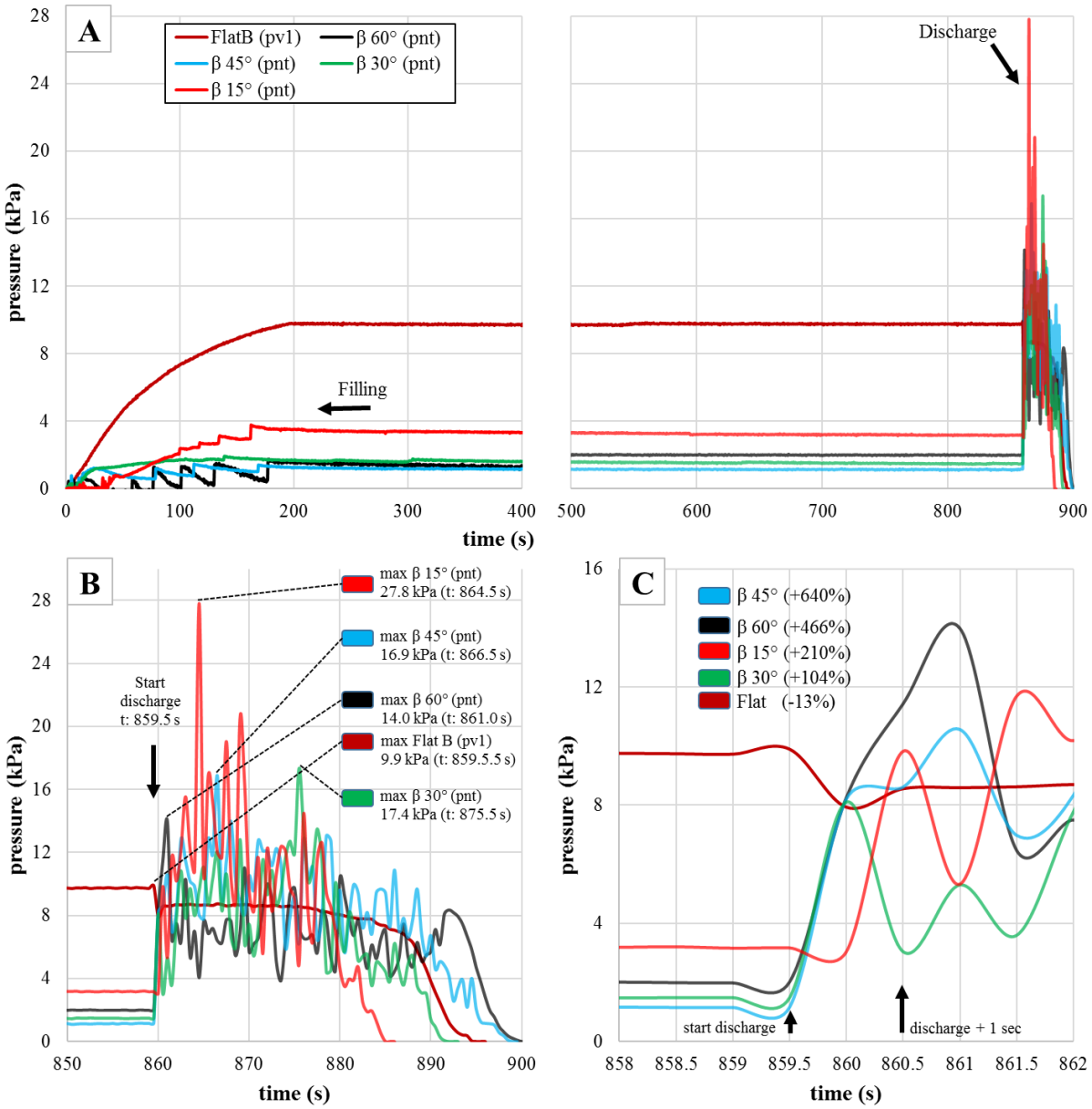


**Figure 10.** Normal pressures in the bottoms (hopper and flat) (pnt,t, pv1,t).

(A) Complete test; (B) Discharge; (C) Overpressures.

During filling, it is observed that (Figure 11A), opposite to the normal pressure in the cylinder above the transition (0.25 m, ph1) (Figure 6), and with the exception of the flat hopper (FlatB) the pressures are higher according to the decrease in β. It is also found that the settling peaks are higher at β60 ° and decrease until β15 °, with the exception of β30 °. Possibly, during filling, this point is a dead zone, where no acting forces are found due to the decrease of the β angle.

## Maximum normal pressures (ph max)

The maximum pressure curves during filling and discharge are shown in Figure 12. The results were compared with those calculated by Eurocode 1, part 4 [7].

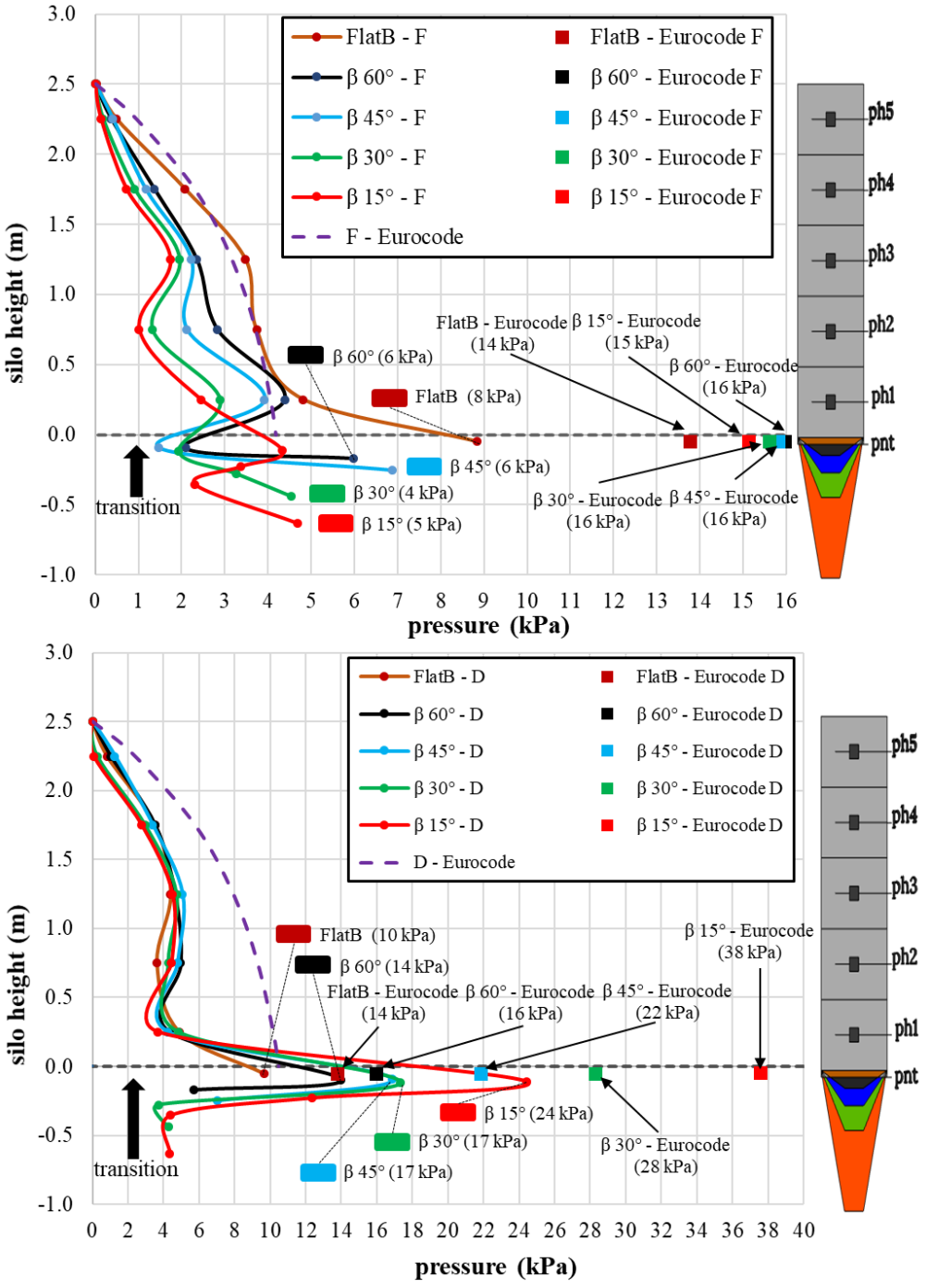


**Figure 11.** Maximum normal pressures on the wall (ph and pn). Comparison with Eurocode 1, part 4.

F: Filling; D: Discharge.

Observing the shapes of the discharge curves (Figure 12), it seems that for an angle of β15º we have a mass flow, however for the rest of the angles we have a channel flow. In the case of funnel flow the horizontal loads are lower just below the hopper, but on the vertical wall it will have a greater load, due to the fact that an interior hopper is formed through which the grain slides. In the funnel flow it is normal that at some point on the vertical wall it has greater pressures than those obtained for mass flow, they are surely located in an area near the transition of the internal hopper. It seems that β30 º, β45 º and β 60º have the maximum pressure on the vertical wall at a height of 1.25 m, but this is not exactly the case, it is because the measurement cells are at that height, is not possible to say what happens below or above. That is, the pressure can be higher between measurement cells. Although the result is not exact, it is very close to reality.

Differences between the filling and discharge curves depending on whether it is mass or funnel flow are also interesting, in the mass flow the pressures are high in $p_{h1}$ for filling, but they do not grow as much as in $p_{h3}$ during the discharge, for the effect we have previously indicated (inner cone). It is also interesting that there is less difference between filling and discharge when the bottom is flat.

The pressures obtained experimentally are lower when compared to the values obtained by Eurocode 1, part 4. Although during filling and near transition ($p_{h1}$) the values for hopper flow hoppers (, β45 º, β 60º and FlatB) are higher than the standard. However, this does not compromise the standard regarding silo design, as design calculations are made with discharge values and not filling values.

**Maximum friction pressures (pw max)**

Figure 13 gives the maximum frictional pressures in the cylinder compared with those given in Eurocode 1, part 4, showing the five configurations divided between the five hopper geometries.

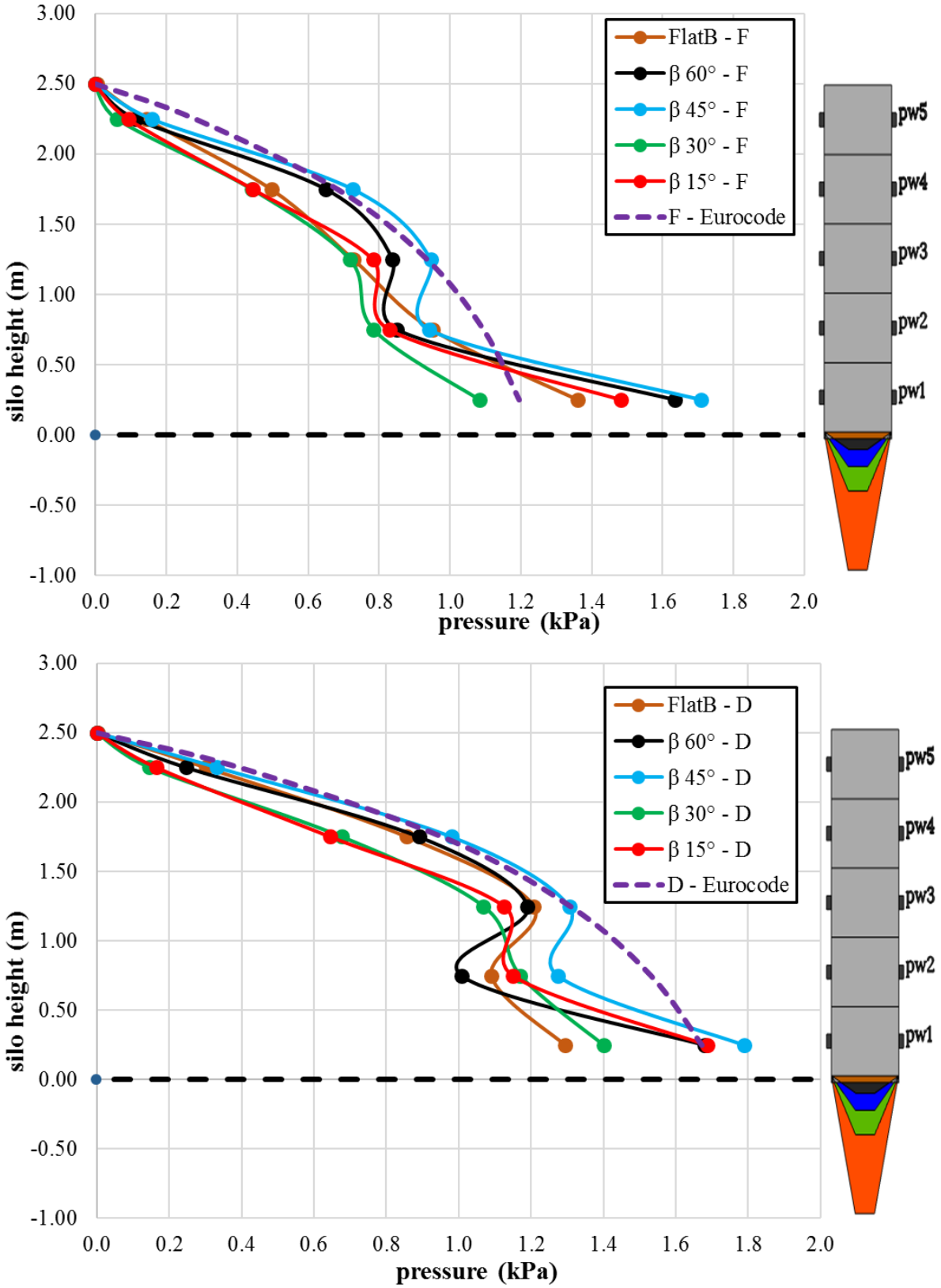


**Figure 12.** Maximum friction pressures on the wall (pw). Comparison with Eurocode 1, part 4.

F: Filling; D: Discharge.

The maximum experimental frictional pressures in the pilot silo exceeded those obtained by Eurocode 1, part 4 at several points. Several failures have occurred related to buckling due to the vertical force exerted on the wall of the silo in Brazil.

It was not possible to understand a pattern related to friction pressures with hopper angles. We observed that the β45 º hopper presented the highest pressure values regardless of the phase (filling or discharging). Furthermore, quantitatively, the values of friction pressures at the time of discharge did not show a significant increase.

It is interesting to say that for all variables (hopper angles and silo phases) a decrease in friction pressure was observed at 0.75 meters, corresponding to 1/3 of the total height of the silo.

We believe that the possible reason is because the Vertical stress in the stored material ($p_{vt,}$) at the transition (Figure 5) is the smallest among the hopper angles, providing the highest coefficient of lateral pressure (K), in other words, half the right angle, β = 45 °, provides the greatest destabilization of the stored product and increases the friction force on the silo wall. Even so, we can see in Figure 5 a, that in discharge, the $p_{vt,}$ for β45 ° presented the greatest drop in the vertical stress.

## 4. Conclusions

Flat bottom hoppers have a discharge flow greater than or equal to shallow hoppers (β = 60 °) when using maize.

During silo filling the flat bottom does not shows settling peaks.

The smaller the angle in β promotes a larger formation of stress arcs close to 1/3 of the height of the silo.

The moment of maximum normal pressures at 0.25 m above the transition is different in relation to the hopper angle. For flat bottom (β = 90 °) and shallow hoppers (β = 60 °) they

occurred at the end of filling, for steep hoppers (β = 45 °; 30 °; 15 °) they occurred at the beginning of discharge.

Also, in relation to the normal pressures at 0.25 m above the transition (or 1/10 of silo height), the magnitude of the overpressures at the beginning of the discharge was directly proportional to the decrease in the hopper angle (β). In other words, the magnitudes of the overpressures were: β15 ° > β30 ° > β45 ° > β60 ° > β90 °.

Friction pressures at 0.25 m above the transition were higher than those obtained by Eurocode 1 part 4 during filling.

The coefficient of lateral pressures (K) at discharge exceeded that calculated by the standard for all hopper bottoms, except for the flat bottom.

Normal pressure between 1/10 to 1/3 of silo height vary considerably according to the hopper angle. The reason is that there is a static zone (flow channel) that varies according to the inclination of the bottoms.

Hoppers with a higher angle (in this case β = 90°) promote greater normal pressures on the cylinder wall during the filling and static phases. However, at discharge, the maximum pressures tended to coincide. Thus, overpressure during discharge using hoppers with a smaller angle (in this case β = 15°) was greater. In addition, the settling peaks and the magnitude of the pressure during settling rose as silo slenderness increased.

It is observed that several factors during discharge are out of the pattern due to the transition flow classification in β30 °, such as: the moment of occurrence of the maximum pressure in the transition, friction pressures 0.25 above the transition, normal pressures 0.25 and 0 .75 above transition, vertical stress in the stored material at the transition.

## 5. Declaration of Competing Interest

The authors declare that they have no known competing financial interests or personal relationships that could have appeared to influence the work reported in this paper.

## 6. Acknowledgements

The authors are very grateful to CAPES (Coordenação de Aperfeiçoamento de Pessoa de Nível Superior) for funding the doctoral scholarship related to the project.

## REFERENCES

[1] H.A. Janssen, Versuche uber getreidedruck in silozellen, Z. Ver. Dtsch. Ing. 39 (1895) 1045–1049.

[2] D. Walker, An approximate theory for pressures and arching in hoppers., Chem. Eng. Sci. 22 (1967) 486. https://doi.org/10.1016/0009-2509(67)80145-3.

[3] J.K. Walters, A theoretical analysis of stresses in axially-symmetric hoppers and bunkers, Chem. Eng. Sci. 28 (1973) 779–789. https://doi.org/10.1016/0009-2509(77)80012-2.

[4] J.K. Walters, A theoretical analysis of stresses in silos with vertical walls, Chem. Sci. 28 (1973) 13–21.

[5] A.W. Jenike, J.R. Johanson, J.W. Carson, Bin loads—part 3: mass-flow bins, J. Manuf. Sci. Eng. Trans. ASME. 95 (1973) 6–12. https://doi.org/10.1115/1.3438163.

[6] DIN, DIN 1055-6: Basis of design and actions on structures – Part 6: design 623 loads for buildings and loads in silo bins, in: Berlin, Verlaz, 2005.

[7] CEN, EN 1991-4:2006. Eurocode 1: Actions on Structures. Part 4: Silos and Tanks, Brussels, 2006.

[8] A.. Jenike, Storage and Flow of Bulk Solids Bull. 123, University of Utah, 1964.

[9] WPMPS, Standart Shear Testing Technique for Particulate Solids Using the Jenike

528 Shear Cell“, England, 1989.

529 [10] A. Dogangun, Z. Karaca, A. Durmus, H. Sezen, Cause of damage and failures in silo
530 structures, J. Perform. Constr. Facil. 23 (2009) 65–71.
531 https://doi.org/10.1061/(ASCE)0887-3828(2009)23:2(65).

532 [11] F. Ayuga, Some unresolved problems in the design of steel cylindrical silos., in: J.G.
533 Chen, J.F., Teng (Ed.), Struct. Granul. Solids From Sci. Princ. to Eng. Appl., CRC
534 Press-Taylor & Francis Group, Boca Raton, USA, 2008: pp. 123–133.

535 [12] J. Nielsen, From silo phenomena to load models, in: J.F. Chen, J.G. Teng (Eds.),
536 Struct. Granul. Solids From Sci. Princ. to Eng. Appl., CRC Press-Taylor & Francis
537 Group, Boca Raton, USA, 2008: pp. 49–57. https://doi.org/10.1201/9780203884447.

538 [13] CONAB - COMPANHIA NACIONAL DE ABASTECIMENTO, Acompanhamento
539 da safra brasileira de grãos, Brasilia, 2022.
540 https://www.conab.gov.br/component/k2/item/download/40788_0ee9dd051572570453
541 55d00863c854b0.

542 [14] DPE - DIRETORIA DE PESQUISA E COORDENAÇÃO AGROPECUÁRIA, IBGE -
543 Pesquisa de Estoques 2º semestre de 2019, 2019.

544 [15] Ministério da Agricultura Pesca y Alimentación, Avances de superficies y
545 producciones agrícolas. Diciembre 2020, 2020.

546 [16] AGRICULTURA Y GANADERIA de Castilla y León, TABLAS DE LA COSECHA
547 DE MAÍZ 2020 EN CASTILLA Y LEÓN, 2020.
548 https://agriculturaganaderia.jcyl.es/web/jcyl/AgriculturaGanaderia/es/Plantilla100Detal
549 le/1246464862173/Noticia/1284998741023/Recurso.

[17] J. Nielsen, Pressures from flowing granular solids in silos, Philos. Trans. R. Soc. A Math. Phys. Eng. Sci. 356 (1998) 2667–2684. https://doi.org/10.1098/rsta.1998.0292.

[18] C. Bywalski, M. Kamiński, A case study of the collapse of the over-chamber reinforced concrete ceiling of a meal silo, Eng. Struct. 192 (2019) 103–112. https://doi.org/10.1016/j.engstruct.2019.04.100.

[19] Y. Sun, Y. Wang, Collapse reasons analysis of a large steel silo, Adv. Mater. Res. 368–373 (2012) 647–650. https://doi.org/10.4028/www.scientific.net/AMR.368-373.647.

[20] G. Gutiérrez, C. Colonnello, P. Boltenhagen, J.R. Darias, R. Peralta-Fabi, F. Brau, E. Clément, Silo collapse under granular discharge, Phys. Rev. Lett. 114 (2015) 5–9. https://doi.org/10.1103/PhysRevLett.114.018001.

[21] B.J. Teng, PLASTIC COLLAPSE AT LAP JOINTS IN PRESSURIZED CYLINDERS UNDER AXIAL LOAD, 120 (1994) 23–45.

[22] J.G. Teng, J.M. Rotter, Plastic collapse of restrained steel silo hoppers, J. Constr. Steel Res. 14 (1989) 139–158. https://doi.org/10.1016/0143-974X(89)90020-5.

[23] A.W. Jenike, J.R. Johanson, J.W. Carson, Bin Loads—Part 4: Funnel-Flow Bins, J. Eng. Ind. 95 (1973) 13–20.

[24] E.J. Benink, Flow and stress analysis of cohesionless bulk materials in silos related to codes, University of Twente, 1989.

[25] Internacional Organization for Standardization, ISO 11697:2012. Bases for design of strutures - Loads due to bulk materials, 2012.

[26] R.M. Gandia, F.C. Gomes, W.C. de Paula, P.J.R. Aguado, Influence of specific weight and wall friction coefficient on normal pressures in silos using the Finite Element

572 Method, Rev. Eng. Na Agric. - Reveng. 29 (2021) 192–203.
573 https://doi.org/10.13083/reveng.v29i1.12336.

574 [27] A. Couto, A. Ruiz, P.J. Aguado, Experimental study of the pressures exerted by wheat
575 stored in slender cylindrical silos, varying the flow rate of material during discharge.
576 Comparison with Eurocode 1 part 4, Powder Technol. 237 (2013) 450–467.
577 https://doi.org/10.1016/j.powtec.2012.12.030.

578 [28] J.F. Chen, J.M. Rotter, J.Y. Ooi, Z. Zhong, Correlation between the flow pattern and
579 wall pressures in a full scale experimental silo, Eng. Struct. 29 (2007) 2308–2320.
580 https://doi.org/10.1016/j.engstruct.2006.11.011.

581 [29] A.J. Sadowski, J.M. Rotter, Structural Behavior of Thin-Walled Metal Silos Subject to
582 Different Flow Channel Sizes under Eccentric Discharge Pressures, J. Struct. Eng. 138
583 (2012) 922–931. https://doi.org/10.1061/(asce)st.1943-541x.0000530.

584 [30] K. PIEPER, M. SCHÜTZ, Bericht Über das Forschungsvorhaben - Norm-Mess-Silo
585 für Schüttguteigenschaften, Technische Universität Braunschweig, 1980.

586 [31] J. Zegzulka, The angle of internal friction as a measure of work loss in granular
587 material flow, Powder Technol. 233 (2013) 347–353.
588 https://doi.org/10.1016/j.powtec.2012.06.047.

589 [32] C.Y. Song, J.G. Teng, Buckling of circular steel silos subject to code-specified
590 eccentric discharge pressures, Eng. Struct. 25 (2003) 1397–1417.
591 https://doi.org/10.1016/S0141-0296(03)00105-6.

592 [33] C.J. Brown, J. Nielsen, Silos: Fundamentals of theory, behaviour and design, London,
593 1998.

[34] J.C. Calil, A.B. Cheung, Silos: pressões, fluxo, recomendações para o projeto e exemplo de cálculo, São Carlos, 2007.

[35] R.M. Gandia, F.C. Gomes, W.C. de Paula, E.A. de Oliveira Junior, P.J. Aguado Rodriguez, Static and dynamic pressure measurements of maize grain in silos under different conditions, Biosyst. Eng. 209 (2021) 180–199. https://doi.org/10.1016/j.biosystemseng.2021.07.001.

[36] J.G. Teng, Y. Zhao, L. Lam, Techniques for buckling experiments on steel silo transition junctions, Thin-Walled Struct. 39 (2001) 685–707. https://doi.org/10.1016/S0263-8231(01)00030-1.

[37] A. Couto, A. Ruiz, P.J. Aguado, Design and instrumentation of a mid-size test station for measuring static and dynamic pressures in silos under different conditions - Part I: Description, Comput. Electron. Agric. 85 (2012) 164–173. https://doi.org/10.1016/j.compag.2012.04.009.

[38] W. Sun, J. Zhu, X. Zhang, C. Wang, L. Wang, J. Feng, Multi-scale experimental study on filling and discharge of squat silos with aboveground conveying channels, J. Stored Prod. Res. 88 (2020) 101679. https://doi.org/10.1016/j.jspr.2020.101679.

[39] C. V Schwab, I.J. Ross, G.M. White, D.G. Colliver, WHEAT LOADS AND VERTICAL PRESSURE, 37 (1994) 1613–1619.

[40] C.J. Brown, E.H. Lahlouh, J.M. Rotter, Experiments on a square planform steel silo, Chem. Eng. Sci. 55 (2000) 4399–4413. https://doi.org/10.1016/S0009-2509(99)00574-6.

[41] T. Schuricht, C. Furll, G.G. Eenstad, Full scale silo tests and numerical simulations of the „cone in cone" concept for mass flow, in: Handb. Powder Technol., Elsevier

617 Science BV, 2001: pp. 175–180.

618 [42] Z. Zhong, J.Y. Ooi, J.M. Rotter, The sensitivity of silo flow and wall stresses to filling
619 method, Eng. Struct. 23 (2001) 756–767. https://doi.org/10.1016/S0141-
620 0296(00)00099-7.

621 [43] Y. Zhao, J.G. Teng, Buckling experiments on steel silo transition junctions. II: Finite
622 element modeling, J. Constr. Steel Res. 60 (2004) 1803–1823.
623 https://doi.org/10.1016/j.jcsr.2004.05.001.

624 [44] J.G. Teng, X. Lin, Fabrication of small models of large cylinders with extensive
625 welding for buckling experiments, Thin-Walled Struct. 43 (2005) 1091–1114.
626 https://doi.org/10.1016/j.tws.2004.11.006.

627 [45] J. Härtl, J.Y. Ooi, J.M. Rotter, M. Wojcik, S. Ding, G.G. Enstad, The influence of a
628 cone-in-cone insert on flow pattern and wall pressure in a full-scale silo, Chem. Eng.
629 Res. Des. 86 (2008) 370–378. https://doi.org/10.1016/j.cherd.2007.07.001.

630 [46] A. Ramírez, J. Nielsen, F. Ayuga, On the use of plate-type normal pressure cells in
631 silos. Part 1: Calibration and evaluation, Comput. Electron. Agric. 71 (2010) 71–76.
632 https://doi.org/10.1016/j.compag.2009.12.004.

633 [47] A. Ramírez, J. Nielsen, F. Ayuga, On the use of plate-type normal pressure cells in
634 silos. Part 2: Validation for pressure measurements, Comput. Electron. Agric. 71
635 (2010) 64–70. https://doi.org/10.1016/j.compag.2009.12.005.

636 [48] A. Ruiz, A. Couto, P.J. Aguado, Design and instrumentation of a mid-size test station
637 for measuring static and dynamic pressures in silos under different conditions - Part II:
638 Construction and validation, Comput. Electron. Agric. 85 (2012) 174–187.
639 https://doi.org/10.1016/j.compag.2012.04.008.

[49] R.M. Gandia, F.C. Gomes, W.C. de Paula, E.A. de O. Junior, P.J.A. Rodriguez, Static and dynamic pressure measurements of maize grain in silos under different conditions, Biosyst. Eng. 209 (2021) 180–199. https://doi.org/10.1016/j.biosystemseng.2021.07.001.

[50] A. Couto, A. Ruiz, L. Herráez, J. Moran, P.J. Aguado, Measuring pressures in a slender cylindrical silo for storing maize. Filling, static state and discharge with different material flow rates and comparison with Eurocode 1 part 4, Comput. Electron. Agric. 96 (2013) 40–56. https://doi.org/10.1016/j.compag.2013.04.011.

[51] M. Wójcik, J. Tejchman, G.G. Enstad, Confined granular flow in silos with inserts - Full-scale experiments, Powder Technol. 222 (2012) 15–36. https://doi.org/10.1016/j.powtec.2012.01.031.

[52] A.J. Sadowski, J.M. Rotter, Buckling of very slender metal silos under eccentric discharge, Eng. Struct. 33 (2011) 1187–1194. https://doi.org/10.1016/j.engstruct.2010.12.040.

**Final considerations**

The experimental station proved to be versatile, allowing numerous configuration possibilities due to its instrumentation and structural independence.

The test station fully complied with the objectives and expectations proposed at the beginning of the investigation, it also obtained new and unprecedented conclusions such as:

- influence of slenderness on consolidation;
- normal pressure and friction relationships with slenderness and consolidation;
- maximum silo pressure time at the beginning of discharge;
- pressure relationships with; consolidation; the discharge time by type of flow; influence of flow type on discharge pressures.
- Influence of slenderness in relation to K and Pvt.

In addition, the numerical simulation showed how the specific weight and the wall friction coefficient are variables that influence the pressures in silos.

**Future research**

It is interesting to note that this thesis composed more than fifteen works for national and international congresses. It is intended to send at least ten more works in the next two years. In addition, it should be noted that two more articles are expected for journals of interest addressing: eccentricity in the hoppers and the effect of the second discharge on pressures and flow.

Considering the rich structure of the experimental station at the Federal University of Lavras and the help of the professionals involved (professors, researchers and national and international collaborators who contributed significantly to this thesis), it is recommended to evaluate the pressures and flows using the other walls (changing the coefficient of friction between the stored product and the silo wall) of the experimental station.

In addition, for future works, it is interesting to use a camera at the top of the silo, enabling (visually) the analysis of the flow and dynamics of the stored product during the phases, especially during discharge. Only a few materials were found in the current literature regarding pressures and flows in very slender silos, so the continuity of this work would be of great value for the studies of pressures in silos.

Another suggestion for future work is the use of a product stored with different moisture, verifying the behavior of pressures and flow. Many stored products are harvested with high moisture content and are often stored without primary processing (pre-cleaning and drying) in silos for short periods.

**Team of researchers**

| Researchers | Title and Institution | Attribution |
|---|---|---|
| Rômulo Marçal Gandia | Doctoral Student in Agricultural Engineering - Federal University of Lavras (UFLA) / Doctoral Student in Biosystems Engineering - Universidad de León (ULe) | Preparation and execution of activities |
| Francisco Carlos Gomes | PhD in Structural Engineering – Full Professor at Federal University of Lavras. | advisor |
| Pedro José Aguado Rodriguez | PhD Agronomic Engineering – Full Professor at University of Léon (ULe) | co-supervisor |
| Wisner Coimbra de Paula | PhD in Dr. Agricultural Engineering – Professor at at Federal University of Lavras | collaborator |
| Estácio Antunes de Oliveira Júnior | Agricultural Engineering - Federal University of Lavras | collaborator |
| Luiz Felipe Souza | Graduating in Agricultural Engineering - Federal University of Lavras | collaborator |